Recycling mine waste to improve the acid resistance of cement-based composites for underground structures

by

Linping Wu

A thesis submitted in partial fulfillment of the requirements for the degree of

Doctor of Philosophy

in

Mining Engineering

Department of Civil and Environmental Engineering
University of Alberta

Abstract

Cement-based composites are widely used in underground structures for various applications, such as tunnel lining, mine backfilling, and grouting. However, cement-based composites are highly susceptible to attack by sulfuric acid that can be naturally generated around underground structures through a biogenetical and chemical process. This sulfuric acid attack not only significantly reduces the service life of cement-based underground structures, but also leads to an extremely high cost for the maintenance and rehabilitation of the structures. Hence, cement-based composites should be made in a way that is more durable against the sulfuric acid attack. Among all the methods in improving the acid resistance of cement-based composites, the use of pozzolanic materials that can be sourced from local mine waste has shown great potential.

The main objective of this thesis is to systematically explore the potential of three types of pozzolanic materials (fly ash, metakaolin and silica fume) that can be recycled from local mine waste in improving the acid resistance of cement-based composites. These three materials were first used as admixtures to replace ordinary Portland cement (OPC) at various dosages. The results showed that the addition of pozzolans in OPC mortar could reasonably improve the acid resistance. In particular, the mixture with 5% silica fume showed the lowest mass loss after sulfuric acid immersion. Then the performance of silica fume and nano-silica was compared. The silica fume was found to be more effective in enhancing the properties of OPC mortar regarding the volume of permeable voids, compressive strength, and acid resistance. After that, the acid resistance of metakaolin-based geopolymers was explored when calcium aluminate cement (CAC) was added. It was found that the addition of CAC drastically improved the acid resistance due to the reduced permeable voids and increased neutralization capacity. Additionally, as fibers are a common component in cement-based materials for underground structures, a green and sustainable nanofiber

(cellulose nanocrystals) was introduced in the OPC system to improve the acid resistance. This nanofiber was found to improve the compressive strength and the acid resistance of OPC mortar. At last, based on previous experimental data, a predictive model was proposed to forecast the deterioration of cement-based materials by considering both mixture design and testing conditions. The proposed Bayesian optimized support vector regression model was able to accurately predict the mass change and compressive strength of mortar samples under a sulfuric acid attack.

Overall, this thesis explores the potential of pozzolanic materials in improving the acid resistance of cement-based composites. The research findings provide an effective way to mitigate the sulfuric acid attack of cement-based underground structures and an innovative way of recycling mine waste.

Preface

This thesis has identified potential applications of pozzolans in cement-based materials to improve the acid resistance. It is extended from 6 papers that have been either published or submitted:

Chapter 2 of this thesis has been published as **L. Wu**, C. Hu, W.V. Liu, (2018). The sustainability of concrete in sewer tunnel—a narrative review of acid corrosion in the City of Edmonton, Canada. *Sustainability*, © MDPI. 10(2): 517.

Chapter 3 of this thesis has been published as **L. Wu**, C. Hu, W.V. Liu, (2019). Effects of pozzolans on acid resistance of shotcrete for sewer tunnel rehabilitation, *Journal of Sustainable Cement-Based Materials*. © Taylor & Francis. 8(1), 55-77.

Chapter 4 of this thesis has been submitted for peer review as **L. Wu**, G. Huang, C. Hu, W.V. Liu, Performance evaluation of nano-silica and silica fume on enhancing the acid resistance of cement-based composites, *Journal of Central South University.* © Elsevier. (under review).

Chapter 5 of this thesis has been submitted for peer review as **L. Wu**, G. Huang, C. Hu, W.V. Liu, Effects of calcium aluminate cement on the acid resistance of metakaolin-based geopolymer. *Advances in Cement Research.* © ICE Virtual Library (under review).

Chapter 6 of this thesis has been submitted for peer review as **L. Wu**, G. Huang, C. Hu, W.V. Liu, (2020). Effects of cellulose nanocrystals on improving the acid resistance of cement-based composites in mining, *International Journal of Minerals, Metallurgy and Materials.* © Springer. (accepted).

Chapter 7 of this thesis has been submitted for peer review as **L. Wu**, C. Hu, W.V. Liu, Forecasting the deterioration of cement-based mixtures under sulfuric acid attack using support vector regression based on Bayesian optimization, *SN Applied Sciences*. © Springer. (under review).

In this thesis, my original work includes experiment design, data collection, and data analysis in Chapter 3 through Chapter 6, model development in Chapter 7, literature review in Chapter 2, as well as concluding analysis in Chapter 8. Dr. Chaoshi Hu assisted in concept formation and field survey, Guangping Huang assisted in data collection in Chapter 4, Chapter 5 and Chapter 6. Dr. Wei Victor Liu was the academic supervisor who was involved in concept formation and contributed to manuscript composition and edits.

This thesis is dedicated

to my love and my family.

Acknowledgment

First, I would like to offer heartfelt thanks to my supervisor, Dr. Wei Victor Liu, for his professional guidance and encouragement throughout my research life at the University of Alberta. It is extremely lucky to have a supervisor who is so patient with all my questions, and who responded my requests promptly.

Next, I would like to express my gratitude to my committee members Dr. Derek Apel, Dr. Mustafa Kumral, Dr. Wenming Zhang, Dr. Yashar Pourrahimian and Dr. Yuxiang Chen, for their insightful comments and suggestions on my research. I also wish to extend my sincere gratitude to Dr. Chaoshi Hu for his support and guidance on field investigation.

Sincere appreciation goes to my colleagues, Guangping Huang, Xincheng Hu, Yunting Guo, Shaosen Ma and Chengkai Fan, who have inspired me in the research, and helped me in daily life.

Nevertheless, I would like to thank Rizaldy Mariano, a concrete lab technician, for his supportive attitudes and guidance on my experiments.

My deepest gratitude dedicates to my wife, who cares about me so much, who encourages and supports me throughout my PhD program. I also extremely grateful for the continuous support and endless love from my parents and mother-in-law.

Table of contents

List of tables

List of figures

List of abbreviations

Abbreviation	Description
AAE	Average absolute error
ACI	American Concrete Institute
ANN	Artificial neural network
ASTM	American Society for Testing and Materials
BET	Brunauer-Emmett-Teller
BO	Bayesian optimization
BOD	Biochemical oxygen demand
CAC	Calcium aluminate cement
C-A-H	Calcium aluminate hydrate
CH	Calcium hydroxide
CIPP	Cured-in-place pipe
CNC	Cellulose nanocrystal
COE	City of Edmonton
C-S-H	Calcium silica hydrate
CSA	Canadian Standards Association
DO	Dissolved oxygen
DTG	Derivative of thermo-gravimetric
EDS	Energy Dispersive X-Ray Spectroscopy
EPA	Environmental Protection Agency
EPR	Evolutionary polynomial regression
FNA	Free nitrous acid
FTIR	Fourier Transform Infrared Spectroscopy
GS	Grid search
GU	General use
ITZ	Interfacial transition zone
MAE	Mean absolute error
MAPE	Mean absolute percent error
MIC	Microbially induced corrosion

MSE	Mean square error
OPC	Ordinary Portland cement
PSO	Particle swarm optimization
PVC	Polyvinyl chloride
RBF	Radial basis function
RH	Relative humidity
RMSE	Root mean square error
RS	Random search
SCM	Supplementary cementitious materials
SEM	Scanning Electron Microscopy
SOB	Sulfur-oxidizing bacteria
SRB	Sulfate-reducing bacteria
SVR	Support vector machine
TGA	Thermo-gravimetric analysis
UCS	Unconfined compressive strength
UPV	Ultrasonic pulse velocity
w/c	Water-cement ratio

List of nomenclatures

A_{CV}	Value of the performance indicators for the *k*-fold cross-validation
b	Offset scalar of SVR function
C	Penalty factor
FM	Test statistic of Friedman's test
F_0	Compressive strength after 28 days of standard curing, MPa
F_n	Compressive strength after acid immersion, MPa
$f(x)$	SVR predicted value
f_c	Change in compressive strength, %
$K(x_i, x_j)$.	Kernel function
k	Number of data fold
k_F	Number of models for comparison
Δm	Mass change, %
m_n	Mass of sample after a certain period of immersion, g
m_0	Mass of sample before immersion, g
N	Number of neurons in a hidden layer
N_F	Number of parameters used for performance evaluation
n	Number of samples
n_1	Number of input parameters
$\Delta \mathrm{p}$	Change in unconfined compressive strength
P_0	Property values after 28 days of standard curing
P_i	Value of performance indicator in each data fold
P_n	Property value after acid immersion
p_c	Change in properties, %
p_N	Unconfined compressive strength of samples immersed in pH6.5 acid, MPa
p_n	Unconfined compressive strength of samples immersed acid with a pH of 1.5 and 3, MPa
R^2	Coefficient of determination

R_F	Sum of the average rank of performance parameters for each model
s_i	Rank of the parameter for performance evaluation for each model.
w	SVR function slope
x_i	Input vector in the training dataset
x'	Standardized data
x_{min}	Minimum value of the input parameter
x_{max}	Maximum value of the input parameter
y_i	Output value in the training dataset
y_i'	Predicted value
α_i, α_i^*	Lagrange multipliers
ϵ	Tolerable error
ξ_i, ξ_i^*	Slack variables
σ	Width of radial basis function

Chapter 1. Introduction

1.1. Research background

Cement-based materials have been extensively used in a variety of structural applications such as civil engineering and mining engineering. The demand for cement and cement-based composites has been increasing for decades (Miller et al., 2018). It is reported that the global cement demand showed an annual growth rate of 7.4% during the period from 2002 to 2012 (Armstrong, 2013). Cement production has grown 4-fold since 1990 (Andrew, 2018). In 2011 alone, approximately 3.6 billion tons of cement were produced worldwide (Gao et al., 2016). However, Portland cement-based composites are highly susceptible to chemical attacks such as sulfate, carbon dioxide, acids, and chloride (Neville, 1995). Among these chemicals, sulfuric acid is particularly aggressive because of the subsequent sulfate attack of gypsum (Attiogbe & Rizkalla, 1988). Due to the alkaline nature, the Portland cement hydrates can be easily decomposed at the presence of H_2SO_4 acid (Reardon, 1990; Zivica & Bajza, 2001). That is, hydration products (i.e., portlandite, calcium aluminate hydrate, ettringite, and calcium silica hydrate) dissolve sequentially when the pH of the solution gradually decreases from 12.5 to below 8.8 (Reardon, 1990). In this attacking process, aggressive ions in sulfuric acid (i.e., H^+ and SO_4^{2-}) first penetrate pore structures of concrete, and then these ions react with hydration products such as calcium hydroxide (CH) and calcium silica hydrate (C-S-H) (see Equation 1-1 and 1-2). One immediate product is gypsum ($CaSO_4$)— it is expansive—the volume increases by 124% (Idriss et al., 2001; Parande et al., 2006).

$$H_2SO_4+CSH\rightarrow CaSO_4+Si(OH)_2+2H_2O \quad (1\text{-}1)$$

$$H_2SO_4+CH\rightarrow CaSO_4+2H_2O \quad (1\text{-}2)$$

Then a subsequent reaction (see Equation 1-3) occurs between gypsum and tricalcium aluminates. This reaction is destructive due to the formation of ettringite ($3CaO\cdot Al_2O_3\cdot 3CaSO_4\cdot 31H_2O$) that expands the volume by ~227%-700% (Idriss et al., 2001; Jiang et al., 2014; Parande et al., 2006).

The continuing generation of ettringite causes internal peeling and cracking. This finally leads to hydration products being removed from the congregate and the loss of concrete integrity.

$$CaSO_4+3CaO.Al_2O_3.6H_2O+25H_2O\rightarrow 3CaO.Al_2O_3.3CaSO_4.31H_2O \quad (1\text{-}3)$$

This sulfuric acid attack occurs in various occasions such as sewer tunnels (U.S. Environmental Protection Agency, 1991) and underground mines (Ercikdi et al., 2009; Tariq & Yanful, 2013; Yin et al., 2017).

The presence of sulfuric acid is very common in underground structures, particularly in sewer tunnels (House & Weiss, 2014). The main mechanism for the corrosion of concrete sewer tunnels is called the microbially induced corrosion (MIC), as shown in Figure 1.1. Under the MIC process, the sulfate content in the wastewater can be converted via a series of bacteria activities into sulfuric acid that reduces the pH of the concrete surface down to 1~2 (House, 2013). In such acidic environments, cement hydration products can be easily decomposed, and the corrosion rate can be as high as 12 mm/year (in thickness) in many sewer systems (Wells & Melchers, 2014). Under such serious corrosion, the service life of sewer tunnels could be significantly reduced. It is reported that the service life of concrete structures in sewer tunnels can be reduced dramatically by MIC from expected 100 years down to 30–50 years (Jensen, 2009), in some extreme cases, even down to 20 years (Wu et al., 2018). To restore the service in transporting water/wastewater, significant maintenance and rehabilitation are required, leading to considerable financial outlays (Ayoub et al., 2004; Grengg et al., 2015; Oualit et al., 2012). For example, in 2009, the U.S. spent more than $50 billion US dollars in water/wastewater systems (Lieser & Stek, 2010). The estimated cost in Germany exceeds $40 billion US dollars to repair the MIC deteriorated wastewater infrastructure (Hewayde et al., 2006). In Australia, the annual cost is at the magnitude of tens of hundreds of million dollars in the rehabilitation of MIC damaged sewer infrastructure.

Beside the great financial outlays, advanced MIC in a sewer tunnel can also result in unexpected catastrophic tunnel collapse interrupting wastewater transportation and ground traffic (Kuliczkowska, 2016; Wells et al., 2009).

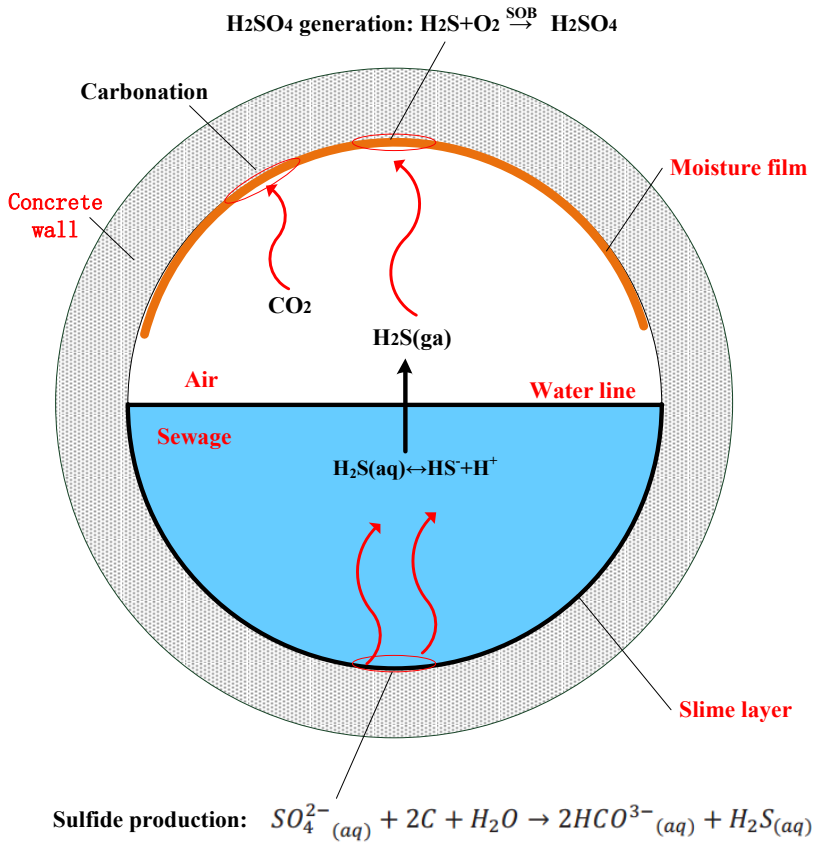

Figure 1.1. Schematic of the MIC process within a sewer tunnel (Wu et al., 2018)

In addition to sewer tunnels, sulfuric acid also commonly exists in underground mines. The primary source of sulfuric acid for mining operations is acid mine drainage. Acid mine drainage refers to the acidic mine water generated from the oxidation and bio-oxidation of sulfidic ores, particularly pyrite (FeS_2 ores) (Kefeni & Mamba, 2020; Vélez-Pérez et al., 2020). Upon exposure to air and water, sulfidic ores can be oxidized, generating sulfuric acid by the following equations (Ergüler, 2015):

$$2FeS_2+7O_2+2H_2O \rightarrow 2Fe^{2+}+4SO_4^{2-}+4H^+ \quad (1\text{-}4)$$

$$4Fe^{2+}+O_2+4H^+\rightarrow 4Fe^{3+}+2H_2O \quad (1\text{-}5)$$

$$4Fe^{3+}+3H_2O\rightarrow Fe(OH)_3+3H^+ \quad (1\text{-}6)$$

$$FeS_2+4Fe^{3+}+8H_2O\rightarrow 15Fe^{2+}+2SO_4^{2-}+16H^+ \quad (1\text{-}7)$$

The oxidation of pyrites releases a large amount of sulfuric acid to groundwater, lowering the pH to as low as 2 (Jones & Cetin, 2017). Under such an acidic environment, the cementitious structures can be easily corroded, damaging their mechanical performances.

This acid attack can cause severe problems in underground mines as cement-based composites are one of the most extensively used materials in mining operations such as shotcreting, grouting, backfilling, shaft sinking, and other infrastructure constructions (Yang & Wang, 2005; Yin et al., 2020). It is reported that as much as one million tonnes of cement can be consumed by a single mining company (Sivakugan et al., 2015). For shotcrete alone, over 700,000 m^3 is consumed annually in North America and Australia (Yu et al., 2018). The cement-based structures in underground mines can be easily corroded at the presence of sulfuric acid. This acid corrosion has been reported in shaft lining (Yang & Ji, 2012), support systems (Kaufmann, 2014), backfill (Ercikdi et al., 2009; Tariq & Yanful, 2013; Yin et al., 2017), and infrastructure in mines (Ekolu et al., 2016).

To mitigate the sulfuric acid attack, the cement-based composites should be made more durable in sulfuric acid environments to ensure structural stability and sufficient service life, and reduce structure maintenance. Among all the options in improving the acid resistance of cement-based composites, the use of pozzolanic materials has shown great potential (Hewayde et al., 2007a; Singh et al., 2015; Zhang et al., 2016). Many researchers have indicated that the pozzolanic materials can be generally used in three ways: 1) pozzolans have been commonly used as admixtures to partially replace ordinary Portland cement (OPC) in mixtures (Berodier & Scrivener,

2014; Duan et al., 2013; Tokyay, 2016); 2) with the development of nanotechnology, the use of nano-pozzolan has attracted great interests in enhancing the performance of cement-based materials (Diab et al., 2019; Mahdikhani et al., 2018); 3) some of the pozzolanic materials (e.g., fly ash and metakaolin) can be used as raw materials for the production of geopolymer cement (De Spot & Wojtarowicz, 2003; Lahoti et al., 2017; Palomo et al., 1999).

A significant source of these mine waste (e.g., fly ash, metakaolin, and silica fume) is from mine waste recycling. Mine waste is defined as materials that have little or no economic value from mineral extraction and processing operations, including waste rock, tailings, slags, and gaseous waste (Das & Choudhury, 2013). For example, fly ash is a by-product from coal combustion (Tokyay, 2016). It is produced by collecting the suspended ash particles in the flue gas with mechanical and electrical precipitators during from coal combustion. Metakaolin can be sourced from superheated kaolin in oil sand tailings (Siddique & Khan, 2011). The production process involves the dispersion and removal of bitumen of oil sand tailings. Then, the kaolin-rich is calcined at temperatures of 600-800℃ to produce metakaolin. Silica fume is a by-product from silicon metal and the ferrosilicon alloys production (Tokyay, 2016). It is produced by collecting the small droplets from flue gases with a series of filter bags during the heating process.

Alberta, Canada, is abundant in these mine waste. For example, around 60% of Canada's fly ash is produced in Alberta, approximately 2.6-3 million tonnes per year (AMEC Earth & Environmental, 2006). The oil sand fields in northern Alberta were found to contain up to 60 million tonnes of kaolin (De Spot & Wojtarowicz, 2003). However, the recycling rate is low for this mine waste with a value of 15-20% for fly ash in Alberta. The unrecycled mine waste is normally stored outdoor or landfilled, which causes serious environmental issues. The toxic compounds in the mine waste can be leached out causing soil and groundwater contamination

(Choi et al., 2002; Haynes, 2009). Thus, exploring the possibility of their use in making more acid-resistant cement-based composites could bring enormous environmental and economic benefits.

1.2. Research objectives

Due to the vast reserve of mine waste in Canada, and strong demand for acid-resistant cement-based composites in civil and mining fields, it is of great significance in developing a mixture using pozzolanic materials with high acid resistance. Thus, the main objective is to systematically explore the potential of three types of pozzolanic materials (fly ash, metakaolin and silica fume) that can be recycled from mine waste in improving the acid resistance of cement-based composites. In order to achieve this overall objective, five sub-objectives have been identified as shown in Figure 1.2.

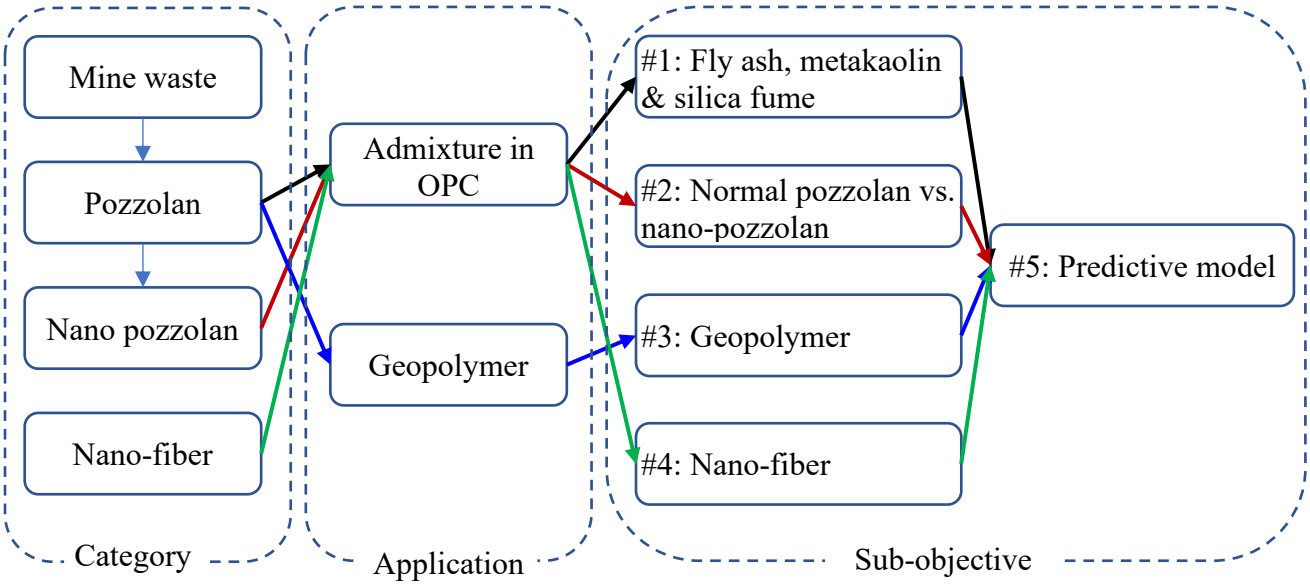

Figure 1.2. Flowchart of thesis research

(1) Despite many studies about the effects of different pozzolans (fly ash, metakaolin, and silica fume) on the acid resistance of OPC concrete, no work has been done to

systematically compare the effects of the three pozzolans under the same acid immersion conditions. Thus, the first sub-objective is to investigate the use of three pozzolanic materials—fly ash, metakaolin, and silica fume—to improve acid resistance of OPC mixtures.

(2) Currently, very few studies have been carried out to compare the effects of silica fume (normal pozzolan) and nano-silica (nano-pozzolan) on the acid resistance of cement-based composites. Among the studies that have been conducted to date, contradictory results have been reported (Hendi et al., 2017; Mahmoud & Bassuoni, 2020). Thus, the second sub-objective is to compare the performance of a normal pozzolan (silica fume) and a nano pozzolan (nano-silica) in enhancing the sulfuric acid resistance of mortar mixtures.

(3) As the production of OPC has been reported to be responsible for about 7% of global carbon dioxide emissions (Voldsund et al., 2019; Worrell et al., 2001), researchers have been trying to find alternatives of the OPC. Among the options, the geopolymer cement is the most promising one because of its superior mechanical strength and chemical resistance. However, the application of metakaolin-based geopolymers is limited due to a lack of a comprehensive understanding of its performance in aggressive environments (Abbas et al., 2020). Thus, the third sub-objective is to investigate the acid resistance of geopolymers activated from metakaolin.

(4) Additionally, fibers are commonly added to mixtures for underground structures to enhance their mechanical performance. There is a need to understand the effects of fibers on the acid resistance of cement-based materials. Besides, cement-based material is a multiscale composite. The use of nano-fiber has the potential to mitigate the propagation of microcracks and inhibit the penetration of acid, thus improve the acid resistance. Herein,

the fourth sub-objective is to explore the effects of a nanofiber (cellulose nanocrystals) on the acid resistance of cement-based composites.

(5) Lastly, as the experimental test investigates the acid resistance of mixtures in a discrete way regarding the pozzolan dosages and testing conditions (e.g., pH). A predictive model is needed to understand the experimental data in a continuous way and provide a preliminary predictive method that considers mixture design and testing conditions. Thus, the fifth sub-objective is to establish a predictive model to forecast the deterioration of mortars under sulfuric acid attack.

1.3. Thesis statement and thesis organization

Thesis statement: *Pozzolanic materials recycled from mine waste can be used to produce more acid-resistant cement-based composites than conventional OPC-based ones for applications in underground structures.*

This thesis is presented in a paper-based format, consisting of seven chapters (as shown in Figure 1.3). The following is a brief description of each chapter.

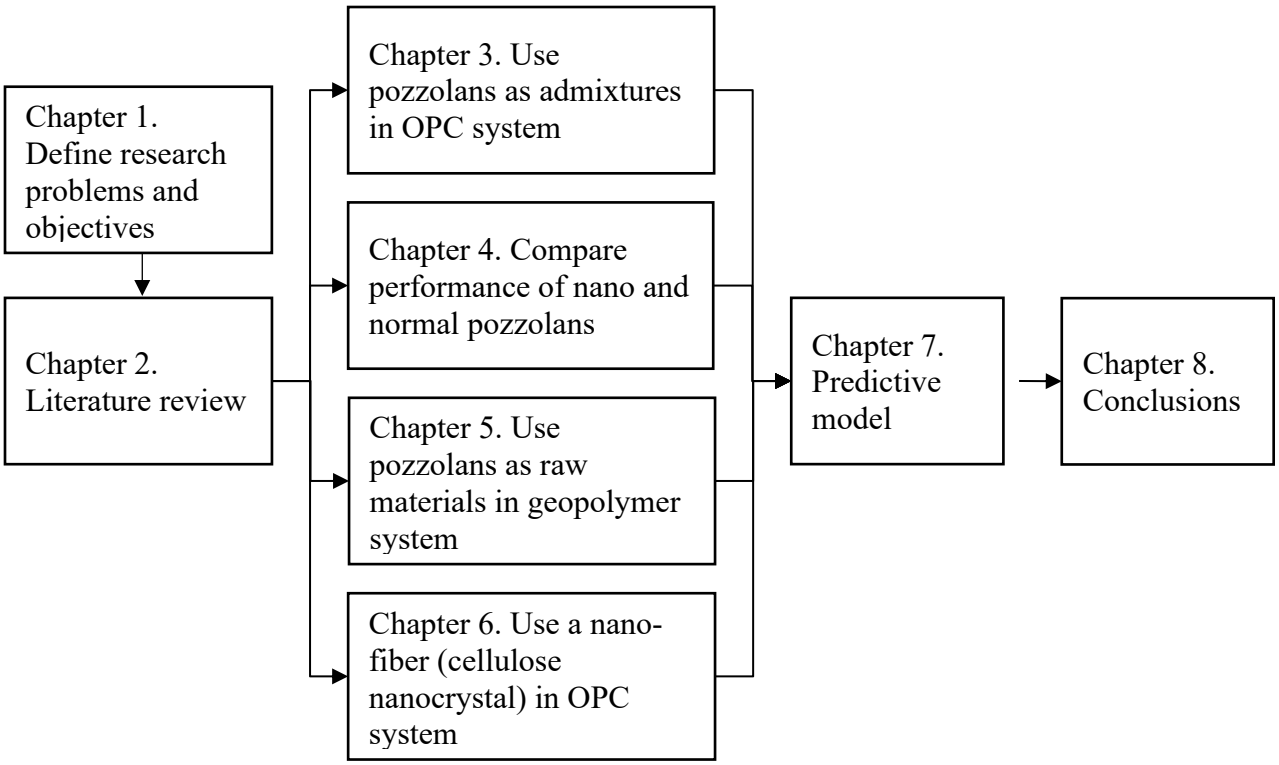

Figure 1.3. Flowchart of thesis outline

Chapter 1 defines the research problems and the main objective of this thesis, which is to systematically explore the potential of three pozzolans in improving the acid resistance of cement-based composites. To achieve this objective, five sub-objectives have been identified and accomplished in Chapter 3 through Chapter 7.

Chapter 2 provides a state-of-art review on the corrosion process in a sewer tunnel. After that, potential methods to control the acid corrosion were summarized, and cement-based rehabilitation techniques were reviewed.

Chapter 3 explores the use of pozzolans—fly ash, metakaolin, and silica fume—which can be sourced from local mine waste to improve acid resistance of rehabilitation shotcrete. In this early

work, a discussion was carried out on the significance of immersion conditions and parameter selections on the evaluation of acid resistance.

After that, in **Chapter 4**, a performance comparison was made between a normal pozzolan (silica fume) and a nano pozzolan (nano-silica) in enhancing the sulfuric acid resistance of mortar mixtures. The nano-silica and silica fume were added as substitutions for cement at various dosages. Their effects on cement hydrations were also investigated in this chapter.

Chapter 5 extends the application of pozzolans in the production of a geopolymer. The performance of metakaolin-based geopolymers was investigated in resisting the sulfuric acid attack. Calcium aluminate cement was added to partially replace metakaolin to accelerate the geopolymerisation. Besides, a discussion was carried out on the mechanism of improvement in the acid resistance of a metakaolin-based geopolymer.

Additionally, as fibers are a common component in cement-based materials for underground structures, **Chapter 6** investigates the effects of a nanofiber (cellulose nanocrystal) on the acid resistance. CNCs were added to the mortar mixtures as additives at cement volume ratios of 0.2%, 0.4%, 1% and 1.5%. Changes in mass and length were monitored during immersion to evaluate the acid resistance of mixtures. The mechanism of improved acid resistance was also discussed.

Based on experimental data collected in previous chapters, **Chapter 7** forecasts the deterioration of mortar mixtures under a sulfuric acid attack using a support vector regression (SVR) algorithm considering both mixture design and immersion conditions. The SVR models were optimized through the Bayesian optimization (BO) technique to find the optimal hyperparameters. The performance of the BO-SVR model was compared with four other predictive models using four evaluation parameters.

Finally, **Chapter 8** summarizes the key conclusions and presents the key contributions of this thesis. Limitations of current research and recommendations for future research are also provided in this chapter.

Chapter 2. Literature review

This chapter has been published as **L. Wu**, C. Hu, W.V. Liu, (2018). The sustainability of concrete in sewer tunnel—a narrative review of acid corrosion in the City of Edmonton, Canada. *Sustainability*, © MDPI. 10(2): 517.

2.1. Introduction

In sewer systems, when hydrogen sulfide gas (H_2S) emitted from sewage meets condensing moisture, the process can form sulfuric acid (H_2SO_4) that corrodes the concrete in sewer tunnel rapidly (Apgar & Witherspoon, 2008; U.S. Environmental Protection Agency, 1991). This is known as the microbially induced corrosion (MIC), which poses a severe threat to the sustainability of concrete in a sewer tunnel. Acid corrosion causes gradual loss of concrete—this significantly reduces the service life of concrete structures in sewer systems and may lead to structural failures such as collapse, threatening public safety. Costs to rehabilitate corroded sanitary sewer tunnels can be extremely high. In the United States (US) alone, it was estimated to cost around $14 billion USD per year to rehabilitate and replace the deteriorated sewers (Brongers et al., 2002). When sanitary structures corrode, several processes coincide as a consequence of excessive chemical content (i.e., sulfate, acids, and chloride) in wastewater. Sulfate and acids react mainly with the cement hydration products, while chloride facilitates the corrosion of reinforcing steels by destroying the protective layer on steel surface (Neville, 1995). Among these chemicals, sulfuric acid is particularly aggressive because of the highly expansive corrosion products (Attiogbe & Rizkalla, 1988).

Currently, concrete MIC issues have emerged throughout the sewer system in the City of Edmonton (COE), Canada. Many sewer tunnels are significantly deteriorated. For example, in Figure 2.1, the chamber and tunnel segment (located under the 127 street and 153 Avenue in Edmonton; constructed in 2001), was found severely deteriorated, showing peeled-off zone and exposed rebar in a walk-through inspection conducted in 2016. As a result, the lifetime of this chamber has been significantly reduced from 75-100 years to less than 20 years. In general, the lifetime of many sewer tunnels built in the 1960s and 1970s has been greatly reduced from 75-100

years to less than 50 years. Severe corrosion (up to 100 mm in depth) was even observed in sewer tunnels built in the late 90s (e.g., Clareview Sanitary Trunk). As shown in Figure 2.2, up to 20% of the sanitary infrastructure was reported to present poor conditions (Stolte, 2015). To repair the deteriorated sewer infrastructure, the COE has been spending a significant portion of its budget on rehabilitation. In 2009, the emergency repair cost was $6.5 million CAD. By 2015, this number had jumped to $16.8 million CAD (City of Edmonton, 2016).

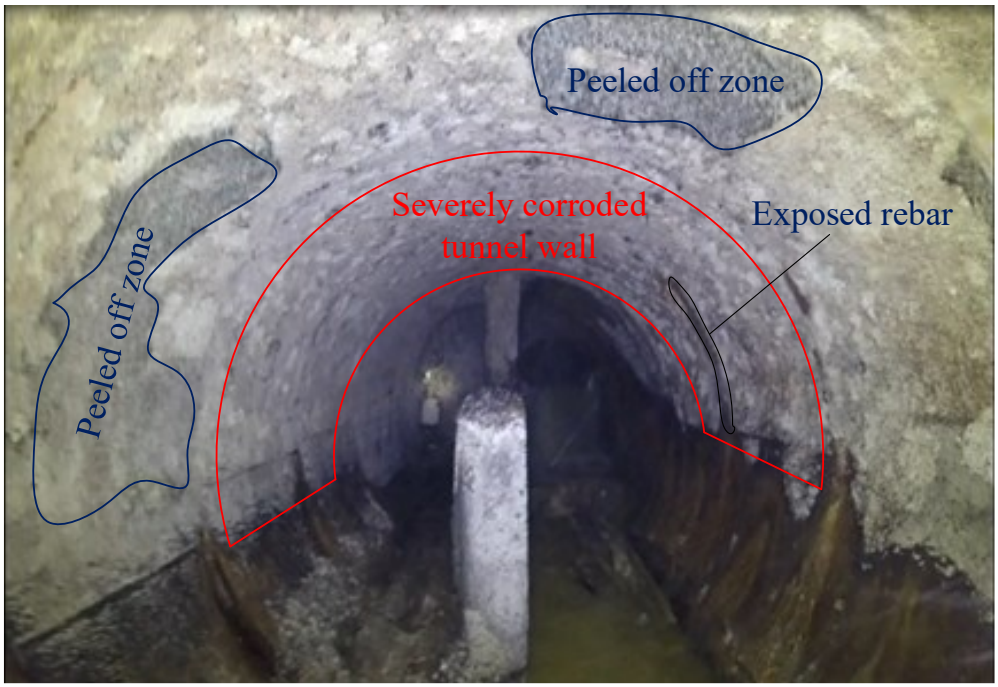

Figure 2.1. Corrosion conditions in a chamber located under the 127 street and 153 Avenue in Edmonton

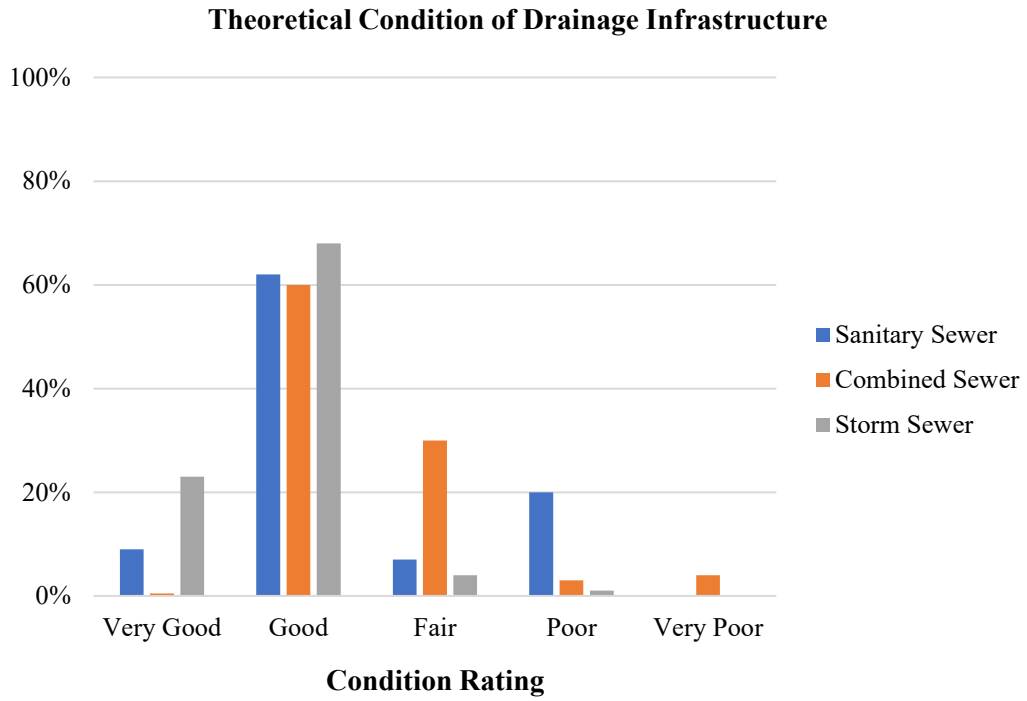

Figure 2.2. Estimated condition of Edmonton's drainage infrastructure (Stolte, 2015). Modified from “Major Edmonton sewer trunk line hanging on by "ribs and lagging".” by E Stolte. (2015) *Edmonton Journal*

But there is a lack of understanding of how MIC occurs and what the options are to control it. To that end, this paper is intended to conduct a narrative review on the acid corrosion of sewer tunnel concrete in the COE. It aims to provide a preliminary investigation of the MIC mechanism and recommendations on how to mitigate MIC issues in Edmonton concerning drainage design, corrosion control methods, rehabilitation techniques and materials.

2.2. Fundamentals for microbially induced corrosion of sewer concrete

In the sanitary sewer systems, the progress of microbially induced corrosion (MIC) often determines the service life of concrete structures (Jiang et al., 2016). Under the MIC process, aqueous H_2S is firstly converted from sulfate by bacteria activities in a slime layer. After that, the gaseous H_2S is released from sewage to the tunnel crown. This gaseous H_2S then dissolves in the

moisture film formed at the tunnel crown. Finally, the dissolved H_2S is converted to sulfuric acid (H_2SO_4) under the reactions of sulfur-oxidizing bacteria (SOB) (i.e., Thiobacillus) (Alexander & Fourie, 2011). The sulfuric acid is the end product that reduces the pH value of the concrete surface down to 1~2 (House, 2013). In such acidic environments, cement hydration products can be easily decomposed. That is, hydration products (i.e., portlandite, calcium aluminate hydrate, ettringite and calcium silica hydrate) dissolve sequentially when the pH of the solution gradually decreases from 12.5 to below 8.8 (Reardon, 1990). In addition, MIC is an active deterioration process in which bacteria provide sustained sulfuric acid in the reaction (House, 2013); as a result, the MIC rate can be as high as 12 mm/year in many sewer systems (Wells & Melchers, 2014) and even 14 mm/year in laboratory setups (Æsøy et al., 2002). The following section provides more detail regarding the MIC process.

As shown in Figure 2.3, there are five sub-processes in MIC—carbonation, H_2S generation in sewage, H_2S buildup at the crown, sulfuric acid generation, and corrosion reaction. These sub-processes are explained in detail below.

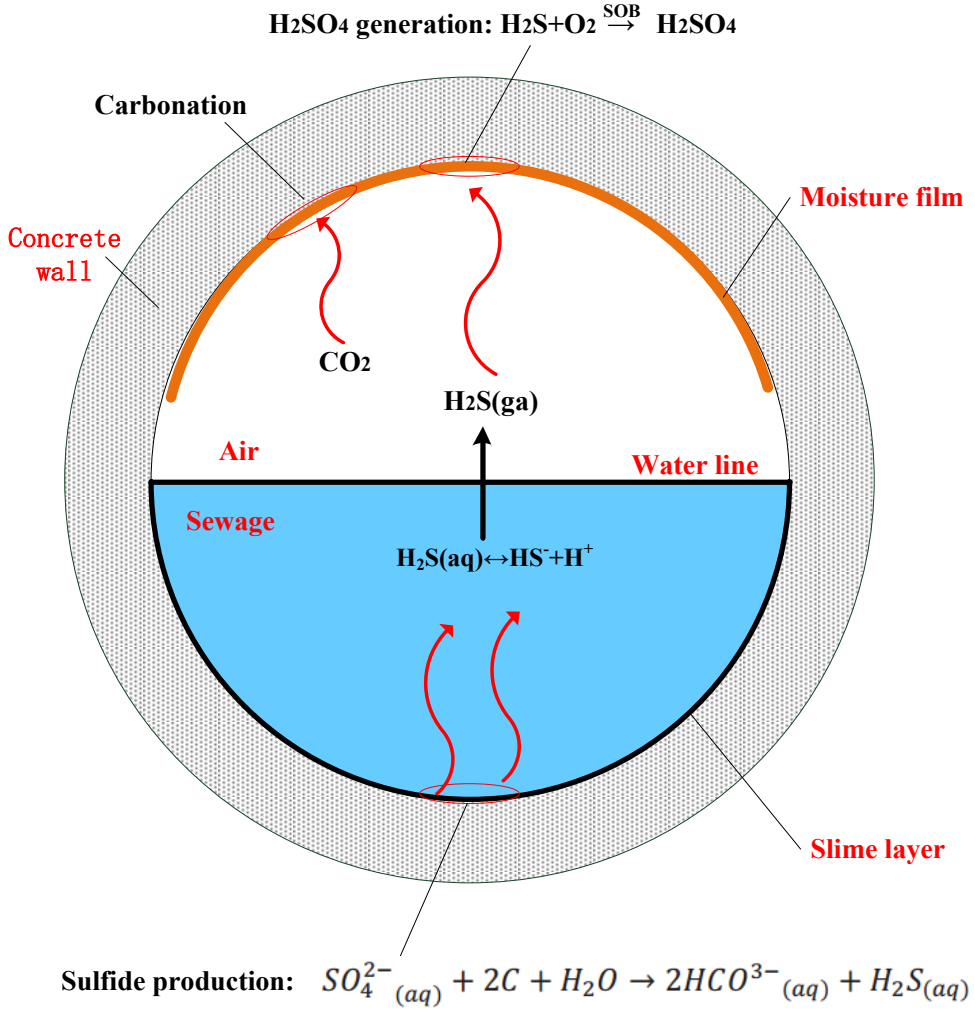

Figure 2.3. Schematic of the MIC process within a sewer

2.2.1. Hydrogen sulfide generation

The root cause of MIC is the formation of aqueous hydrogen sulfide—H_2S (aq). It is produced from sulfate in wastewater under a reaction with sulfate-reducing bacteria (SRB) located in a slime layer. The slime layer is a layer of bacteria and inert solids at the interface between the concrete wall and the sewage—the submerged portion (Okun et al., 2010). The slime layer is typically between 0.3 and 1.0 mm thick, depending on the flow velocity and solids abrasion in the sewage (Bowker & Smith, 1985).

The slime layer often consists of three laminated zones (counting from the sewage toward the concrete wall): an aerobic zone, an anaerobic sulfate-reducing zone, and an inert layer. These zones are presented in Figure 2.4. The aerobic zone has aerobic SOB that consumes the dissolved oxygen (DO) in sewage. The other two zones consist of SRB that requires an anaerobic environment (e.g., DO level < 0.1mg/L). As it penetrates through the slime layer, oxygen in sewage is firstly consumed in the aerobic zone, leading to the second zone—an anaerobic sulfate-reducing zone (House, 2013). The second zone is suitable for the growth of anaerobic SRB. Also, as shown in Equation 2-1, these anaerobic SRB generate H_2S from the nutrients—sulfate and organic matters (org). The nutrients in sewage are gradually consumed by SRB while they diffuse through the slime layer, and nutrients concentration approaches zero near the surface of the concrete wall. At this location, the third zone, the inert layer, is formed. This portion of the slime layer is called the inert layer because it cannot receive enough sulfate and organic matter, and therefore the bacteria become inactive (Bowker & Smith, 1985).

The amount of H_2S that can be emitted from the slime layer is highly dependent on the DO level in sewage (House, 2013). If the DO level is high, H_2S will be oxidized by SOB in the aerobic zone—the first layer. As a result, no H_2S can escape from the slime layer to the sewage, as shown in Figure 2.4(a). On the other hand, when the DO level in sewage is low, and DO is not enough to consume all the H_2S, the H_2S (aq) can diffuse through the aerobic zone—the first layer—and then disperse in the sewage as H_2S (aq), as shown in Figure 2.4(b).

$$SO_4^{2-} + org \rightarrow H_2S + HCO_3^- \quad (2\text{-}1)$$

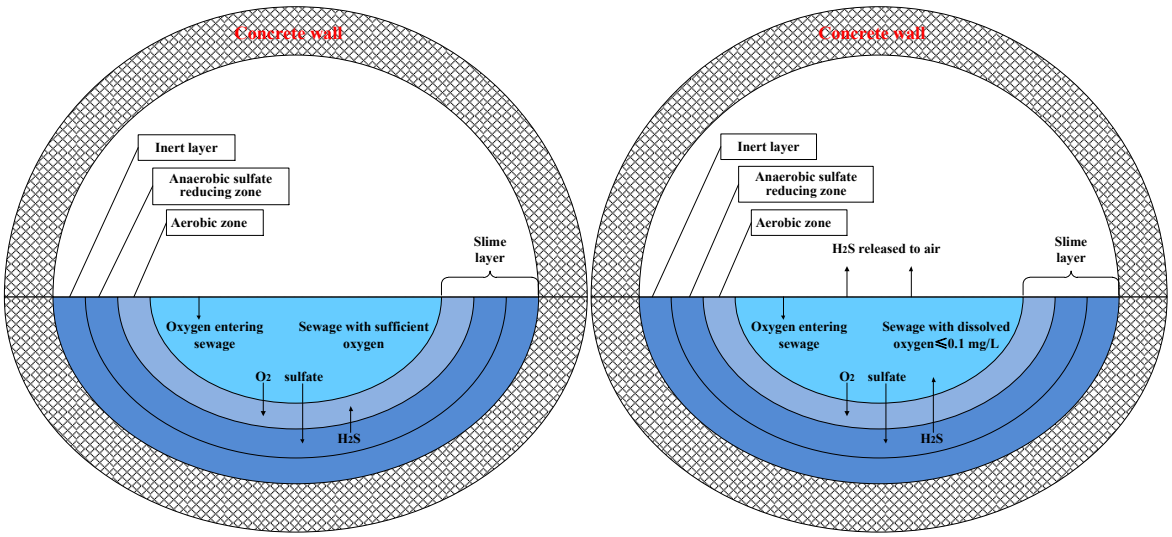

(a) (b)

Figure 2.4. Process occurring in sewage with: (a) sufficient dissolved oxygen (b) insufficient dissolved oxygen

Many factors influence the concentration of dissolved H_2S in sewage, including the DO level, temperature, flow velocity, retention time, and biochemical oxygen demand (BOD). These factors are summarized in Table 2.1. Among these factors, the DO level is the most important (Hewayde, 2005; House, 2013) because other factors mostly affect the H_2S generation by altering the DO level in sewage. For example, temperature changes the oxygen solubility in wastewater; a high flow velocity encourages the aeration of wastewater; and a long retention of sewage gradually depletes DO in wastewater as a result of the relatively slow dissolution of new oxygen from the tunnel atmosphere. Another important parameter is the BOD that indicates the nutrient concentration—a high BOD level means that bacteria are more active in consuming DO in sewage.

Table 2.1. Summary of factors affecting H_2S generation

Factors	Effects on H_2S generation
DO	• High DO enhances the oxidation of H_2S; thus, it reduces the release of H_2S from the slime layer.
BOD	• High BOD accelerates bacteria activities and consumes oxygen.
Wastewater temperature	• High temperature increases the microbial activity level in the slime layer. • High temperature reduces the oxygen solubility in wastewater.
Flow velocity	• High velocity accelerates the aeration of wastewater, so it increases the oxidation of H_2S, resulting in the lowered potential for sulfide build up.
Retention time	• Long retention time depletes the DO in wastewater. • Long retention time results in a loose slime layer that is easy for sulfate to penetrate.

2.2.2. H_2S release from sewage and subsequent sulfide buildup at crown

H_2S dissolves in sewage after it is diffused through the slime layer. The dissolved H_2S can exist as both aqueous H_2S and HS^- in wastewater, depending on the pH value. The reaction equilibrium (Equation 2-2) determines the amount of aqueous H_2S in sewage. On the one hand, at a pH of 6, near 100% sulfur exist as aqueous H_2S in wastewater. On the other hand, when the pH rises to 9, H_2S content decreases significantly, and nearly 100% sulfur exists as HS^- (Bowker & Smith, 1985). The typical pH of sewage is in the range of 6 to 8 (Firer et al., 2008). Thus, a large amount of sulfide exists as aqueous H_2S. The aqueous H_2S then is released in gaseous form from the sewage and disperses throughout the atmosphere in the sewer. This gaseous H_2S is a significant issue because it causes the acid corrosion of concrete during the subsequent process of MIC. Also, gaseous H_2S results in odour problems when released out of the sewer system.

$$H_2S\ (aq) \leftrightarrow HS^- + H^+ \tag{2-2}$$

In addition to wastewater pH, the other two important factors that affect the release of aqueous H_2S are wastewater temperature and turbulence. They are summarized in Table 2.2. The first is the wastewater temperature—a high temperature improves the release of H_2S by reducing the

solubility of H_2S. For example, it is reported that a variation of H_2S concentration at the crown corresponds with a daily variation in temperature (House, 2013). The other factor is the turbulence—a strong turbulence directly exacerbates the release process of H_2S from sewage to the crown of the pipe. For instance, severe acid corrosion is often spotted in turbulent areas such as drop manholes, lift stations, and junction boxes (House & Weiss, 2014). Rather than these designated locations, strong turbulence can also result from high flow velocities, or poor sewer construction.

After the release of gaseous H_2S into the sewer atmosphere, there is a sulfide buildup at the tunnel crown. That is, gaseous H_2S accumulates and dissolves around the tunnel crown. This buildup plays an essential role in MIC of concrete. There is a general idea that a higher gaseous H_2S concentration in the crown causes a higher level of corrosion. However, it still remains unclear for the relationship between H_2S concentration and the MIC rate (Vollertsen et al., 2008; Wells et al., 2009). A wide range of H_2S concentration—from 2 ppm to several hundred ppm—can trigger severe acid corrosion (Sun, 2015). For example, severe corrosion was also reported in a low concentration environment (e.g., 4 ppm) (Æsøy et al., 2002).

Table 2.2. Summary of factors affecting H_2S buildup

Factors	Effects
Wastewater pH	Wastewater pH affects the $H_2S_{(aq)}$ concentration in sewage
Wastewater temperature	Low temperature reduces the H_2S solubility in sewage
Turbulence	Strong turbulence exacerbates the H_2S release by increasing the area of sewage-air interface

2.2.3. Carbonation of concrete surface

Along with sulfide buildup, carbonation co-occurs at the tunnel crown (see Figure 2.3). Carbonation is a reaction between carbon dioxide and one of the concrete compounds (e.g., calcium hydroxide). Carbonation occurs when concrete is exposed to air.

$$Ca(OH)_2+CO_2 \rightarrow CaCO_3+H_2O \quad (2\text{-}3)$$

Carbonation is a very slow process. The rate of carbonation is highly dependent on relative humidity (RH). The highest rates of carbonation occur when RH is in the range of 50% to 75%; CO_2 penetration would be restricted above 75% RH (ACI Committee 201, 2001), thereby inhibiting the carbonation rate. Another factor that affects the carbonation rate is the permeability of the concrete. Low permeability concrete experiences slower carbonation than relatively permeable concrete because of the inhibited CO_2 penetration (Portland Cement Association, 2002). The low permeability usually comes with a low water-to-cement ratio and proper curing, leading to less carbonation (ACI Committee 201, 2001). Table 2.3 summarizes the effects of RH and permeability on the carbonation rate.

Table 2.3. Summary of factors affecting carbonation rate

Factors	Effects
RH	The highest rates of carbonation occur in environments in which the RH of the surrounding atmosphere is kept in the range of 50% to 75% (ACI Committee 201, 2001).
Permeability	Low permeability inhibits the penetration of CO_2, restricting the carbonation to the concrete surface.

Carbonation reduces the concrete surface pH by consuming alkaline calcium hydroxide (Equation 2-3); as a result, the concrete surface pH decreases from 12-13 to as low as 8.5 (Portland Cement Association, 2002). This low pH is suitable to colonize microorganisms at the crown surface of the tunnel, allowing a further microbial process—sulfide oxidation.

2.2.4. Sulfide oxidation

In this process, the H_2S is oxidized into sulfuric acid (H_2SO_4) through bacteria activities. First, moisture in the tunnel atmosphere condenses on the concrete wall, forming a moisture film. Then, due to carbonation, the surface pH of the concrete drops to around ~9, and SOB start to colonize on the crown of the tunnel (Sun, 2015). The H_2S dissolved in the moisture film during the sulfide buildup is then oxidized by SOB, which forms sulfuric acid.

The sulfuric acid formation is mainly affected by two factors (see Table 2.4): atmospheric temperature and RH. Atmospheric temperature is critical for the intensity of microbial activities. High atmospheric temperature increase microbial activities (Huseyin et al., 1987; Joseph et al., 2012), thereby raising the MIC rate. For example, the rate of sulfide oxidation at 25 °C were found 15% higher than those at 20 °C (Sun, 2015). Temperature below 15.6 °C inhibits the bacteria's sulfide oxidizing activity (Sublette et al., 1998). RH is the other influencing factor of the sulfuric acid formation. A minimum value of 87% RH is required for bacteria to be active (Rootsey et al., 2012). In general, high humidity increases the rate at which sulfuric acid forms (Islander et al., 1991). For example, the pH in a concrete surface was reduced more significantly when the RH was 95 to 100% than when the RH was 85 to 95% (Wells et al., 2012). In other words, more sulfuric acid forms when the RH is between 95 to 100%.

Table 2.4. Summary of factors affecting H_2SO_4 generation

Factors	Effects
RH	High RH increases the rate of H_2SO_4 generation
Atmosphere temperature	High temperature accelerates microbial activities at the crown

2.2.5. Acid corrosion reaction

Because of its alkaline nature, concrete decomposes easily after sulfuric acid forms. In this process, aggressive ions in the sulfuric acid (i.e., H^+ and SO_4^{2-}) first penetrate the pore structures of the

concrete, and then these ions react with hydration products such as calcium hydroxide ($Ca(OH)_2$) and calcium silica hydrate ($CaO{\cdot}SiO_2{\cdot}2H_2O$) (see Equation 2-4 and 2-5). One immediate product is gypsum ($CaSO_4$)–it is expansive—the volume increases by 124% (Idriss et al., 2001; Parande et al., 2006).

$$H_2SO_4+CaO.SiO2.2H_2O\rightarrow CaSO_4+Si(OH)_2+2H_2O \quad (2\text{-}4)$$

$$H_2SO_4+Ca(OH)_2\rightarrow CaSO_4+2H_2O \quad (2\text{-}5)$$

Then a subsequent reaction (see Equation 2-6) occurs between gypsum and tricalcium aluminates. This reaction is destructive due to the formation of ettringite ($3CaO.Al_2O_3.3CaSO_4.31H_2O$) which expands the volume by ~227%-700% (Idriss et al., 2001; Jiang et al., 2014; Parande et al., 2006). The continuing generation of ettringite causes internal peeling and cracking, and finally leads to hydration products being removed from the congregate, and the concrete losing its integrity.

$$CaSO_4+3CaO.Al_2O_3.6H_2O+25H_2O\rightarrow 3CaO.Al_2O_3.3CaSO_4.31H_2O \quad (2\text{-}6)$$

The chemical corrosion reaction rate is greatly regulated by the mixture design of concrete. For example, the acid corrosion rate decreased when calcareous aggregates were used in the mixture. This increases the alkalinity of the concrete surface and creates a local buffering environment for cement binder (Hewayde et al., 2007a). This research also observed higher levels of deterioration in concrete samples with higher cement content and lower water/cement ratios. In addition to concrete alkalinity, the porosity/permeability is considered the most important intrinsic property for predicting the durability of hardened concrete (House, 2013). This also applies to the acid corrosion because aggressive sulfuric acid needs to penetrate through pore structures before attacking the inner part of the concrete. Therefore, when the mixture is designed properly, concrete can reach a low porosity that limits the corrosion rate. Another factor that changes the corrosion reaction rate is atmospheric temperature. Higher temperatures raise corrosion reaction rates (Huseyin et al., 1987). Table 2.5 summarizes the factors affecting the corrosion reaction rate.

Table 2.5. Summary of factors affecting the corrosion reaction rate

Factors	Effects
Porosity	High porosity enhances the penetration of aggressive ions
Atmosphere temperature	High temperature accelerates the corrosion reaction rate

2.3. Discussions about potential methods to control microbially induced corrosion

This section focuses on the potential methods to control MIC in the light of the corrosion mechanism. As previously discussed, the rate of the MIC process is affected by many factors (summarized in Table 2.6). When these factors are controlled, the acid corrosion on drainage concrete may be mitigated or even prevented. Generally, these factors can be classified into three categories: environmental factors, sewer hydraulic parameters, and concrete mixture design. Environmental factors include RH, DO, BOD, wastewater temperature, atmospheric temperature, and wastewater pH; sewer hydraulic design parameters include flow velocity, turbulence, and retention; concrete design parameters include porosity/permeability and alkalinity. In general, sewer hydraulic parameters mainly affect the processes of H_2S generation and the buildup process while proper concrete design reduces the corrosion reaction rate. Environmental factors can alter the rate of several subprocesses within the MIC. The control methods falling into these three categories are investigated and summarized in the following section.

Table 2.6. Summary of factors affecting MIC rate

Factors	Effects
RH	• The highest rates of carbonation occur in environments in which the RH of the surrounding atmosphere is between 50% and 75% (ACI Committee 201, 2001). • A high RH increases the rate of H_2SO_4 generation
Porosity/Permeability	• Low permeability inhibits the penetration of CO_2, restricting the carbonation to the concrete surface. • High porosity enhances the penetration of aggressive ions
DO	• A high DO increases the oxidation of H_2S, thereby reducing the release of H_2S from the slime layer
BOD	• A high BOD encourages bacteria activities that consume DO
Wastewater temperature	• A high temperature increases the microbial activity level in the slime layer • A high temperature reduces H_2S and oxygen solubility in sewage
Atmosphere temperature	• A high temperature accelerates the corrosion reaction rate • A high temperature increases the microbial activity level at the crown
Flow Velocity	• A high flow velocity encourages re-aeration resulting in the growth of sulfur-oxidizing bacteria (SOB), hence encourages chemical oxidation resulting in lowered potential for sulfide buildup
Turbulence	• A strong turbulence exacerbates H_2S release by increasing the area of sewage-air interface
Retention time	• A long retention time depletes the DO in wastewater • A long retention time results in a loose slime layer, which is easy for sulfate penetration, hence increasing SRB activities.
Wastewater pH	• Typical sewage pH ranges between 6 and 8 (Firer et al., 2008). It affects the $H_2S_{(aq)}$ concentration in sewage.

2.3.1. Changing sewer tunnel environment

The first category of control methods is achieved by changing the sewer environment. The sewer tunnel environment includes the wastewater (sewage) and the tunnel atmosphere. The available control methods that the author is aware of tend to adjust wastewater conditions by adding chemicals to the wastewater. Many chemicals dosed to the sewage have been effective in reducing sulfide concentrations in sewage. These chemicals include magnesium hydroxide, sodium hydroxide, iron salts, free nitrous acid (FNA), nitrate, oxygen, hydrogen peroxide, ozone, chlorine,

and permanganate. There are three main mechanisms for these chemicals in controlling MIC: 1) raising the pH of sewage and hence reducing the H_2S state sulfide in sewage, such as by using magnesium hydroxide and sodium hydroxide (Ganigue et al., 2011). 2) inhibiting SRB growth, thus reducing the production of sulfide, such as by using iron salt (Sun et al., 2015; Zhang et al., 2009), FNA (Jiang et al., 2011b), nitrate (Jiang et al., 2011a; Mohanakrishnan et al., 2008; Mohanakrishnan et al., 2009), magnesium hydroxide and sodium hydroxide. And 3) oxidizing sulfide directly, such as by using oxygen (Gutierrez et al., 2008), ozone, hydrogen peroxide, chloride and permanganate (Cadena & Peters, 1988).

There are many drawbacks to these chemical-adding methods, beginning with the high cost of the required continuous dosing to the sewage. Also, some chemicals dosed into the sewage can cause environmental problems. For example, unwanted chemicals may be generated as a result of the dosed chemical and the chemicals already in the sewage (Sun, 2015).

2.3.2. Using proper hydraulic parameters in sewer design

The second category of control methods is the use of appropriate hydraulic parameters in design. These parameters include sewage flow velocity, retention, and turbulence (US Environmental Protection Agency, 1985). In general, high velocity in the flow stream increases the DO level and accordingly reduces the aqueous H_2S content in sewage (Hewayde, 2005), while sudden turbulence enhances the release of H_2S which accelerates the MIC process (House, 2013). The DO level of sewage is key to the H_2S generation process. A high flow velocity of sewage enhances the turbulent diffusion of atmospheric oxygen into water, so it increases the DO level in wastewater. This high DO intensifies the oxidation of H_2S during its diffusion back to sewage; hence, it reduces the aqueous H_2S content in wastewater. Above a certain flow velocity, there will be no generation of H_2S (Pomeroy & Bowlus, 1946; Subcommittee on paints and protective coatings, 1969). In

other words, low velocity and long retention time should be avoided in sewer system design to prevent DO depletion under such conditions. In practice, wastewater storage in pump stations and debris and sediment buildup in sewers are common sources for the long retention of wastewater in sewer systems. These locations tend to trap sulfate and organic matters, leading to more active SRB. This causes the high content of aqueous H_2S in wastewater. In this case, when H_2S has already appeared in sewage, high velocity/turbulence accelerates the release of H_2S from wastewater to the tunnel crown. There are many potential sources of turbulence in sewer systems—a hydraulic drop in a manhole, discharge from force mains, sharp bends, junctions, and sections with steep slopes (Hewayde, 2005).

Accordingly, some locations are particularly susceptible to MIC. These include locations with high turbulence where upstream have long retention or low velocity (US Environmental Protection Agency, 1985). One example of such a location is a force main from which water is discharged. Wastewater, stored in the wet well of a pump station, is pumped through the force main and released to the sewer tunnels at the discharge. Long retention in wet well provides the perfect condition for the H_2S generation, while the high turbulence at the discharge of force main enhances the release of H_2S. Note that full flow in the force main will also increase the H_2S generation since no atmospheric oxygen is available to oxygenate the wastewater (Churchill & Elmer, 1999). This further increases the potential for corrosion at the discharge.

In the authors' opinion, high velocity in the flow stream is recommended in sewer design, while sudden turbulence like hydraulic jump should be reduced. When long retention and undue turbulence are impossible to avoid, proper supplementary measures should be taken to control concrete corrosion:

1. When debris and sediment buildup cause long retention or low flow velocity, a good maintenance plan is more efficient than proper tunnel design to minimize the buildup of hydrogen sulfide.

2. When the long retention is caused by the storage of wastewater—at locations such as pump stations—chemical dosing to the wastewater in a wet well will greatly reduce the chance of H_2S generation (Clidence & Shissler, 2008).

3. When sudden turbulence is inevitable, the quality of wastewater upstream of the turbulence should be carefully evaluated before selecting the pipe material.

2.3.3. Improving concrete mixture design

The third category of control methods has to do with improving the concrete mixture design. Note that acid corrosion is unavoidable because the cement-based concrete is alkaline in nature, and decomposes under an acid environment (ACI Committee 201, 2001). But improving the concrete mixture design is still a viable method because it changes the rate of the corrosion reaction process. Here, two additives are taken as examples in the concrete mixture design: one is the addition of pozzolans, and the other is the introduction of biocides.

The first type of additives are pozzolans, some researchers partially replaced cement with pozzolans (e.g., ground granulated blast furnace slag, rice husk ash, pulverized fuel ash, palm oil fuel ash, silica fume, fly ash and metakaolin) (Hossain et al., 2016). The incorporation of pozzolans generally changes the acid resistance of concrete in two aspects: the change of chemical compositions and the reduction of porosity. The first aspect is the change of the chemical compositions due to pozzolanic reaction. When added in the mixture, pozzolans chemically reacts with calcium hydrate $Ca(OH)_2$ in the concrete matrix forming extra calcium-silicate-hydrate

(CSH) which possess cementitious properties (Sabir et al., 2001). This reaction is called the pozzolanic reaction, which consumes the $Ca(OH)_2$that is believed to be the primary reason for the poor acid resistance of plain concrete (Mehta, 1977). The reduced content of $Ca(OH)_2$ in concrete through pozzolanic reaction results in the lesser formation of expansive corrosion products in acid attack (Torii & Kawamura, 1994a). This mitigates the corrosion rate of concrete under acidic environment. Furthermore, the extra calcium-silicate-hydrate (CSH) from pozzolanic reaction, is more stable than $Ca(OH)_2$ under an acidic environment (Roy et al., 2001). In addition to the chemical compositions, the second aspect is the reduction of porosity. The addition of pozzolans refines the pore structures of concrete and reduces its porosity. This is due to the CSH produced from pozzolanic reactions and the filling of small pozzolans particles (Duan et al., 2013; Dunster et al., 1993). The porosity is crucial to the acid resistance of concrete because it affects the penetration of aggressive ions from acids into concrete (Gruyaert et al., 2012). A higher porosity causes a larger diffusion of the aggressive ions into concrete, which increases the contact area between cement hydrates and the aggressive ions (Monteny et al., 2003). In other words, a lower corrosion could be expected in concrete with a lower porosity—this has been supported by many studies. For example, Chatveera et al, (Chatveera et al., 2006) found that a more porous concrete tends to show more negative effect from the acid attack. Also, some other literature (Sabir et al., 2001) reported the improvement in resistance to harmful solutions due to the refined concrete pore structure. However, the reduced porosity does not guarantee a better acid resistance of concrete. Under severe sulfuric acid attack, Senhadji et al, (Senhadji et al., 2014) found that refining the porosity had little effect on the improvement of the acid resistance. They observed that the addition of silica fume reduced the porosity of concrete, but the acid deterioration of concrete was not effectively prevented. Besides that, some controversial results were also reported regarding the

effectiveness of pozzolan addition. Some studies observed opposite results (Hewayde et al., 2007d; Kannan & Ganesan, 2014; Tamimi, 1997) of pozzolan addition on acid resistance owing to variations in experimental conditions and the chemical composition of differently sourced pozzolans. Therefore, the chemical compositions of pozzolans should be individually examined, and experimental conditions should be mimiced as close as possible to the real sewer conditions before using it in an actual sewer. In this way, a better determination can be made whether they are effective at improving corrosion resistance.

In addition, researchers have been trying to use some pozzolans (e.g., fly ash and metakaolin) in producing a new type of cement—geopolymer, which has shown superior mechanical strength, low permeability and excellent chemical resistance. (Singh et al., 2015; Zhang et al., 2016). Geopolymer is an 'inorganic polymer' produced by activating aluminosilicate source materials (fly ash, metakaolin, and slag) with alkali solutions (Bajpai et al., 2020; Duxson et al., 2007). A variety of aluminosilicate materials have been used as raw materials for the production of geopolymer cement including fly ash, metakaolin, slag and natural pozzolan (Kani et al., 2017; Perná & Hanzlíček, 2016; Rovnaník et al., 2018; Zhang et al., 2020). Under the alkaline condition, the raw materials are rapidly dissolved into free $[SiO_4]^-$ and $[AlO_4]^-$. Then, the free $[SiO_4]^-$ and $[AlO_4]^-$ are linked in the geopolymerisation process, forming Si-O-Al-O bonds. These bonds have more stable cross-linked polymer structures, improved homogeneity, more ordered and denser geopolymer binding gel (Karthik et al., 2017), compared with C-S-H of OPC. This makes geopolymer a promising product for application in an acidic environment. In addition, geopolymer is a sustainable and green material because of its low carbon dioxide emission in production. The production of OPC was reported to be responsible for about 7% of global carbon dioxide emission (Voldsund et al., 2019; Worrell et al., 2001), while the production of geopolymer generates little

or zero emission of carbon dioxide (Faisal & Muhammad, 2016). The use of geopolymers could reduce the emission of greenhouse gas, which is more environmentally friendly.

Apart from the pozzolanic materials, the innovative addition of biocides into concrete mixture provides another possibility in combating MIC in sewer tunnels. For example, the addition of Conshield to concrete mixes inhibits SOB (e.g. Thiobacillus) colonies on the concrete surface (Caicedo-Ramirez, 2018). Different from pozzolans, Conshield is a highly charged cationic polymer that kills the gram-negative Thiobacillus on a concrete surface. As previously mentioned, the Thiobacillus on the tunnel crown converts the H_2S into sulfuric acid. The elimination of bacteria could prevent the generation of aggressive acid, which cuts off the MIC process fundamentally. However, this material has not been widely used due to the concerns from industry that the cationic polymer is consumptive, and the SOB may finally colonize the concrete surface when it is depleted. Besides Conshield, some literature has investigated many other materials for their use as biocidal additives in concrete. For instance, Park et al, (Park et al., 2009) examined the effectiveness of Zeolite and Zeocarbon microcapsules on the prevention of fungi growth in concrete. In their study, no fungus growth was observed on the surface of concrete. Freed (Freed, 2000) patented reinforced concrete containing antimicrobial-enhanced fibers, which aimed to reduce the susceptibility of concrete against biogenetic attack. Although the addition of these materials has been verified to be effective for some microorganisms, their biocidal effect towards SOB have not been examined. More research is needed specifically for combatting MIC in sewer tunnels.

2.3.4. Other methods

In addition to the previous three categories of control methods, there are more options to control MIC, and the number is still increasing. One of these methods is surface treatment on concrete. As

the name suggests, surface treatment is a technology that uses physical or chemical additives sprayed on the surface of a concrete liner, so the SOB can be inhibited or deactivated. For example, coating with a sacrificial layer, such as magnesium, increases the surface pH, which inhibits bacterial colonization (James, 2003); coating with incorrodible materials, such as epoxy (Valix et al., 2012), prevents concrete from coming into contact with the corrosive environment. Additionally, recent research reported that high-pressure washing increases the concrete surface pH by removing the corrosion layer and consequently decreasing the bacteria. However, it only took 60-140 days for SOB to recover to its pre-washing level (Sun et al., 2016). The disadvantages of these methods are summarized in Table 2.7.

Table 2.7. Disadvantages of coating and surface wash

Methods	Disadvantages
Coating with sacrificial layer	• Applying the sacrificial layer requires regular treatment and preparation of the concrete surface. • The sacrificial material is costly.
Coating with incorrodible materials	• Some coating chemicals are not environmentally friendly. • It requires reliable adhesion.
Surface wash	• It is effective only in the short term. • Must frequently be repeated.
Using polyvinyl chloride (PVC) pipe	• Not suitable for deep sewer tunnels (City of San Diego, 2015).

2.4. Rehabilitation

In addition to the control methods, another important aspect in combatting MIC is the approach to make deteriorated structure functional again—this is called rehabilitation. In rehabilitating sewers deteriorated by MIC, there are three categories of techniques: repair, renewal, and replacement. The progression from repair to renewal to replacement requires increasing investment, targeting at decreasing level of concrete integrity (Water Environment Federation, 2009). As summarized

in Figure 2.5, many rehabilitation methods are currently available, including point repair, shotcrete, cured-in-place pipe (CIPP), slip lining, fold-and-form pipe, and epoxy coating. Each method may be capable of one or more categories of rehabilitation. Renewal or replacement is often required to rehabilitate sewer infrastructure severely corroded by MIC, and there are many technologies available for this, as shown in Figure 2.5. However, this paper will only investigate the advantages and limitations of cement-based renewal technologies and materials. Note that the term "renewal" is interchangeable with "rehabilitation" in the sewer industry. This paper follows the same convention.

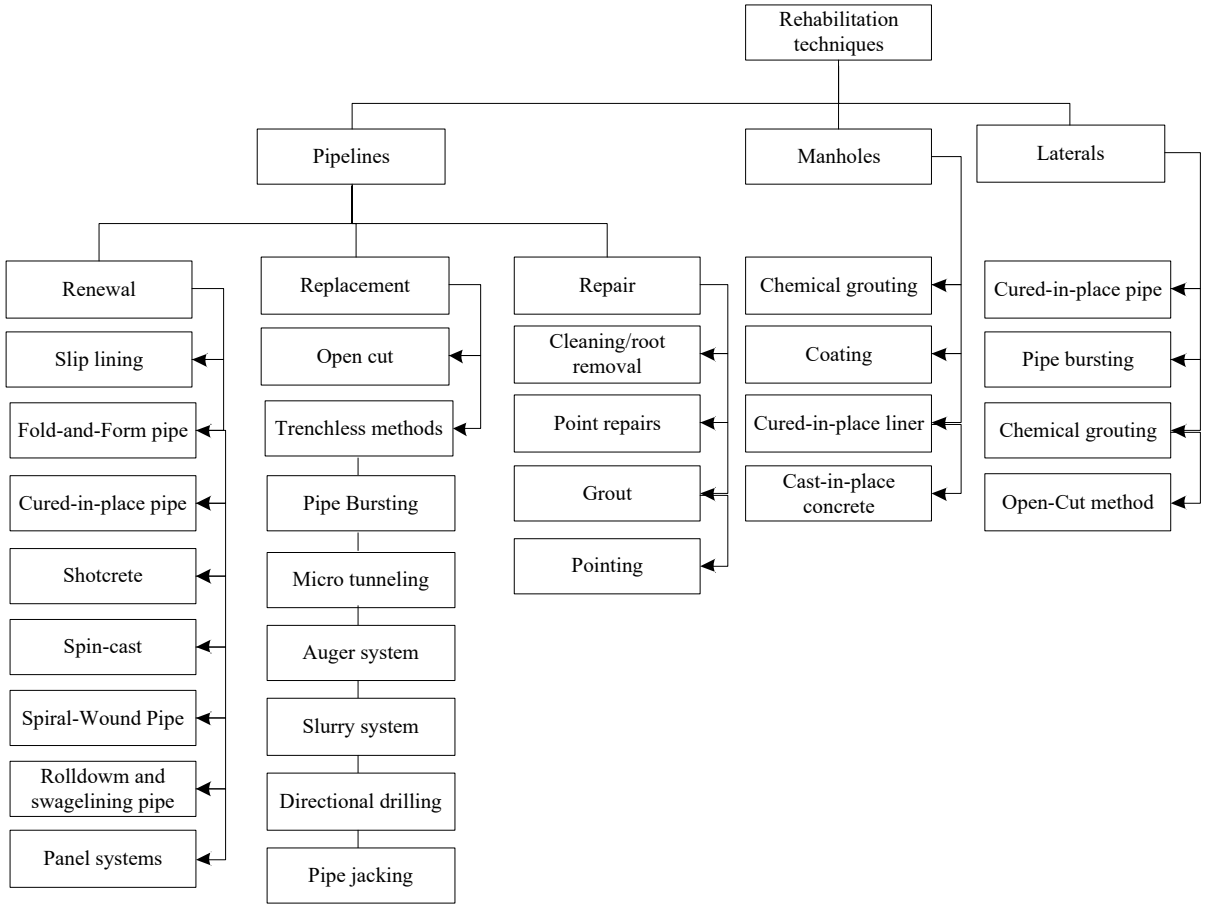

Figure 2.5. Rehabilitation techniques

2.4.1. Cement-based rehabilitation techniques

Cement-based rehabilitation methods are actively used in severely deteriorated sanitary sewer tunnels because of their excellent mechanical and bonding performance on damp surfaces. They can provide structural rehabilitation to deteriorated sanitary tunnels, where the existing pipe acts merely as a right-of-way in the liner installation (Morrison et al., 2013). Cement-based materials can be sprayed (shotcrete), pumped (cast-in-place concrete), and spin cast. More details are explained in the following section.

2.4.1.1. Shotcrete

Shotcrete is the method of pneumatically spraying fresh cement-based mixtures onto a surface through a hose at a high velocity (ACI Committee 506, 2016). There are two types of processes—wet-mix and dry-mix. In the dry-mix process, water is added at the nozzle, while in the wet-mix process, all ingredients are mixed with water before being introduced to the delivery hose and the nozzle. As shown in Figure 2.6, shotcrete mixture is conveyed through a hosepipe and then sprayed via a nozzle onto the corroded tunnel wall. Mesh is often incorporated in the operation to limit cracking and provide structural support.

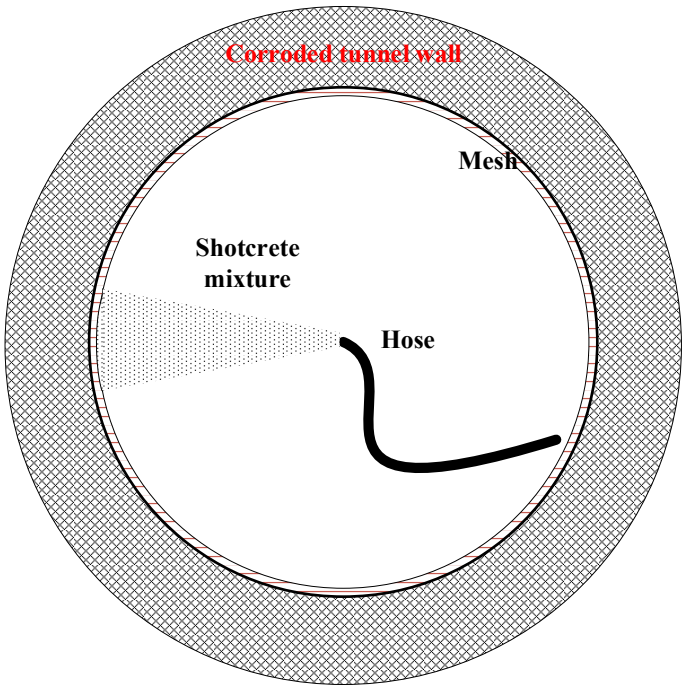

Figure 2.6. A schematic showing the shotcrete rehabilitation process

Shotcrete has been actively used as a flexible and economic rehabilitation technique for sewer tunnels, providing better performance than conventional concrete. Shotcrete's high-speed pneumatic projection provides enhanced compaction, resulting in superior bonding characteristics and strength, increased density, and reduced permeability. The high density and low permeability reduce the penetration of the aggressive solution into the concrete pore structures (Schrader & Kaden, 1987). As a consequence, shotcrete demonstrates more improved acid resistance than ordinary cast concrete (Water Environment Federation, 2009). In addition, shotcrete eliminates the necessity of formwork or an assembly system; thus, it can be applied at a faster rate and lower cost than conventional concrete placement methods.

But there are limitations to using shotcrete in sewer tunnel rehabilitation. The first limitation is rebound, in which large aggregates with cement and sand bounce off the receiving wall. The second limitation is that shotcrete has a relatively rough surface, which increases the Manning's value and causes an accumulation of sediment and organic matter. This could, directly and

indirectly, accelerate the MIC progress. Thus, after shotcrete is applied in a sewer tunnel, troweling is highly recommended to make the surface smooth. In addition, in-situ shotcrete is not applicable in small diameter sewers, manholes and other structures because it requires personnel entry, and equipment and material handling. The preferred diameter for shotcreting is approximately 122 cm and larger (Water Environment Federation, 2009).

2.4.1.2. Cast-in-Place method

Cast-in-place concrete is an effective rehabilitation method for a variety of sewer shapes. The designed steel mesh is affixed to the existing pipe as reinforcement. As shown in Figure 2.7, formwork (slip-forms or fixed-forms) are set up to provide the finished wall section prior to concrete placement (Water Environment Federation, 2009). The space between the tunnel wall and the formwork is the annular space that will be filled later. A venting or overflow hole is required at the highest point of the formwork that not only provides a path for air to escape when fresh concrete is injected. This venting hole also informs the worker to stop grouting when it is overflowed (Dietrich Stein & Robert Stein, 2004; McAlpine & Anderson, 2005). After the formwork, a grouting pipe can be laid in the crown of the sewer tunnel. Then concrete ingredients are introduced and mixed in the grout plant on the ground. The readily mixed fresh mixture is next pumped to the grouting location through the pipe laid on the crown of formwork. When the venting hole is overflowed, the grout operation stops, and then the venting hole is sealed with a plug.

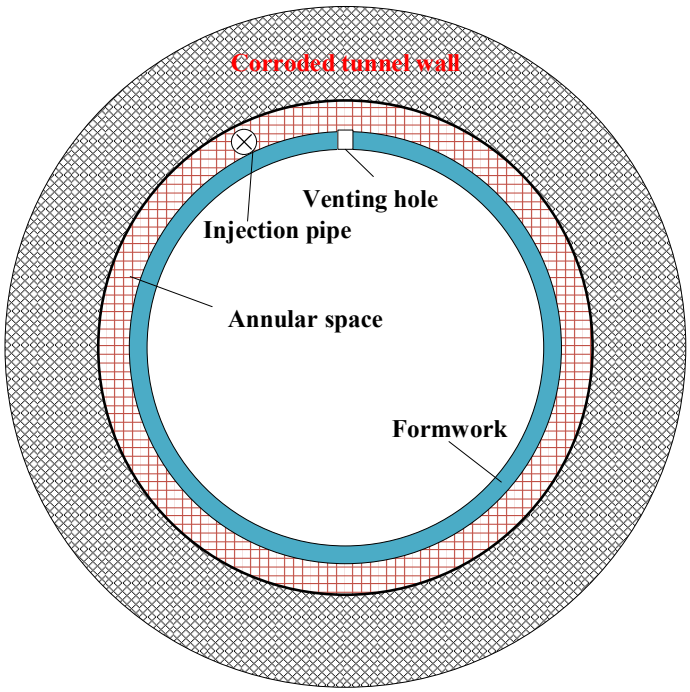

Figure 2.7. A schematic showing the cast-in-place rehabilitation process

Studies reviewed for this paper showed that the cast-in-place method is seldom used in sewer rehabilitation. A recent literature review revealed only two documents (McAlpine & Anderson, 2005; Water Environment Federation, 2009) indicating such a use of the cast-in-place method. Possible reasons that this method is not widely used are that it requires extensive formwork and a minimum sewer diameter (approximately 122 or larger), and the material handling is labor-intensive.

2.4.1.3. Spin-cast method

The spin-cast is an automated process that uses centrifugal force to spin cementitious materials onto the tunnel wall; it is an effective rehabilitation method for circular or near-circular sewers. First, a pumping plant is set up on the ground. Similar to the cast-in-place method, all ingredients are introduced and mixed here. However, no coarse aggregates are introduced in spin-cast method. Then the readily mixed paste is transported to a spincaster (see Figure 2.8) that is located in the tunnel. During rehabilitation, the spincaster rotates and sprays cementitious materials onto the old,

corroded structure. This centrifugal projection produces a densely packed lining with little rebound (Norman E, 2016). As the projection proceeds, the spincaster moves along the tunnel axis. Theoretically, a thickness of one inch (25 mm) or more can be reached per pass (Kurt W. Koehn, 1994). Unlike the cast-in-place method, there is no need for man-entry in the confined sewer space; this makes spin-cast a safer technique that can be used in smaller sewer pipes. The major limitation is the difficulty in ensuring that the rehabilitation materials are distributed properly. In circular tunnels, spin-casting can provide uniform thickness if the spinning head is guided at a constant rate. However, for non-circular shapes, particularly shapes with sharp edges, it becomes almost impossible to achieve a uniform thickness of rehabilitation materials on the tunnel surface.

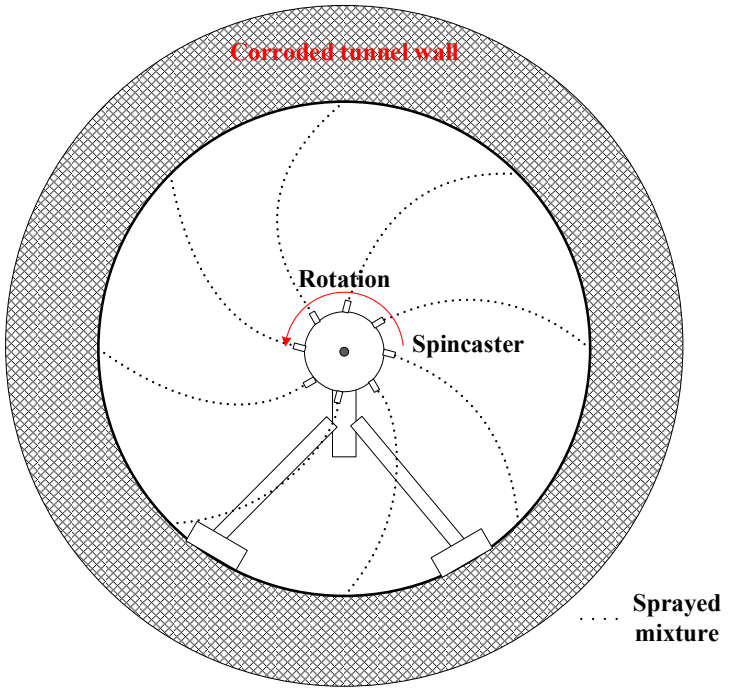

Figure 2.8. A schematic showing the Spin-cast rehabilitation process

2.4.2. Cement-based rehabilitation—method selection

Rehabilitation methods and materials should be selected using criteria such as cost, inflow and infiltration (I & I), pipe cleaning, corrosion resistance, by-pass possibility, level of deterioration (structural or non-structural), access, above-ground conditions (i.e., access and traffic limitations), and underground conditions (i.e., depth of the pipe, groundwater, and crossing utilities). Table 2.8 compares the three cement-based rehabilitation methods using some of these criteria.

As mature techniques, the three aforementioned cement-based methods have several advantages. First, they can rehabilitate sewers with various levels of deteriorations, because the thickness of the rehabilitation layer is adjustable. Second, fiber or wire mesh can be incorporated into cement-based mixtures to enhance the mechanical performance and structural support. Third, cementitious material bonds well to damp surfaces, providing excellent integrity to the rehabilitated structure. Finally, the mixture design is adjustable, so its chemical resistance can be improved through optimized mixture design.

But cement-based methods also have their disadvantages. First, tunnel surfaces have to undergo intense preparation, and infiltration and inflow must be removed to ensure proper bonding with the old pipe. Second, a flow by-pass plan is needed, which greatly increases the cost. Third, because cement-based rehabilitation techniques reduce the cross-sectional area in all repaired tunnels, the sewage transport capacity of sewer tunnel will be reduced after rehabilitation. Finally, cement-based materials are subject to acid corrosion: all hydraulic-cement concretes, regardless of the composition, are unable to withstand for long in an acid with a pH below 3 (ACI Committee 201, 2001). Precautions must be taken to ensure the acid resistance of these cement-based materials.

Table 2.8. Summary of advantages and limitations of cement-based rehabilitation techniques

Techniques	Advantages	Limitations
Spin-cast	• Cost-effective • Can be done without confined space entry • Can be used in small diameter pipes	• Limited acid resistance • Flow by-pass required • High level of cleaning required • Removal of I & I required • Decreased cross-sectional area
Shotcrete	• Fiber-reinforced shotcrete shows excellent mechanical properties • Improved compaction resulting in enhanced chemical resistance • Applicable in most sewer shapes	• Limited acid resistance • Flow by-pass required • High level of cleaning required • Removal of I & I required • Decreased cross-sectional area • Applicable for tunnels with ≥35” in diameter • Pumping length <500m • Rebound impact
Cast-in-place concrete	• Effective for a variety of sewer shapes	• Limited acid resistance • Flow by-pass required • High level of cleaning required • Removal of I & I required • Decreased cross-sectional area • Applicable for tunnels with ≥48” in diameter • Formwork or assembly system required

2.4.3. Cement-based rehabilitation—material selection based on the acid resistance

Acid resistance is the most important criterion to consider when selecting what kind of concrete/cementitious material to use in cement-based rehabilitation. Acid resistance is the term used to describe a material's ability to combat deterioration caused by acid (Alexander & Fourie, 2011). However, it is not easy to evaluate acid resistance due to: 1) the lack of standard testing procedure and 2) controversial results of acid resistance from various indicators. The first reason is the lack of standard specifying the testing procedure. This may lead to totally different results in different experiments for the same mix. The commonly used test procedure of assessment is to immerse concrete samples in an acid solution (known as the immersion method), which directly investigates the resistance of concrete to acid. Many researches (Chindaprasirt et al., 2004; Dinakar

et al., 2008; Durning & Hicks, 1991; Ekolu et al., 2016; Hossain et al., 2016; Newman & Choo, 2003; Pavel & Jiří, 2016; Shetti & Das, 2015; Torii & Kawamura, 1994a) have used this method to evaluate the effectiveness of supplementary cementitious materials (SCMs) in improving the acid resistance of the concrete. But there are many drawbacks regarding the immersion method. First of all, this method requires long immersion time, often several months to several years. In order that the test duration can be shortened, acceleration is commonly required, such as increasing the testing temperature, using a high concentration of acid, a surface brush, and dry and wet cycling. Second, there is currently no standard specifying the detailed testing procedure, which may lead to totally different results in different experiments for the same mix. Variations in testing procedures and environmental conditions (e.g., temperature, concrete surface area-to-acid volume ratio, the frequency of acid replenishment, acid strength) can significantly alter the results. For example, improved acid resistance was found for silica fume concrete immersed in 1% sulfuric acid. However, Hewayde and Nehdi et al. (Hewayde et al., 2007c) found little difference between the reference sample and silica fume samples with up to 15% replacement ratio after 61 days of immersion in 3% and 7% sulfuric acid. They concluded that this was attributed to the excessive acid concentration. Third, for the microbially induced corrosion (MIC) process, a simple acid immersion of samples cannot reflect the corrosion resistance of the mix as some mixes may inhibit the growth of bacteria instead of improving the chemical acid resistance. For example, Conshield, an additive to concrete mixes, was reported to be able to kill the sulfide oxidizing bacteria (SOB) in the moisture film (Caicedo-Ramirez, 2018), but the chemical acid resistance was not improved. Thus, some researcher also tried to establish a test method that incorporates the microbial process occurred in sewer tunnels. For example, Mori et al. (Mori et al., 1992) and Sand et al. (Sand, 1987) built simulation chambers mimicking the sewer environment to test the biological corrosion of

concrete. In these tests, specific conditions such as temperature, nutrients and humidity can be controlled. Furthermore, some researchers (Wells & Melchers, 2014) mounted the concrete coupons in a real sewer tunnel to observe the physico-chemical process of MIC. But the duration is even longer for these tests incorporating the microbial process than the immersing method, normally on the magnitude of years. More research is needed to develop a test method that is not only time-efficient but also able to simulate the real sewer condition as close as possible.

In addition to the lack of testing procedure, the second difficulty comes from the controversial results of acid resistance from various indicators. Acid resistance itself is not a parameter that can be characterized by a single test; instead, it needs to be assessed by many different parameters. Some parameters are mass loss (Alexander & Fourie, 2011; Breit, 2002; Fernando & Said, 2011; Koenig & Dehn, 2016; Roy et al., 2001; Shing et al., 2012), strength loss (Ariffin et al., 2013; Aydın et al., 2007; Jerlin Regin et al., 2017), dimensional changes (De Belie et al., 2002; Koenig & Dehn, 2016; Shing et al., 2012), corrosion depth (Koenig & Dehn, 2016; Macías et al., 1999; Yuan et al., 2013), hydrogen ion consumption, and mineralogical changes (Yuan et al., 2013). Despite the frequent use of these parameters in the assessment of the acid resistance of concrete, low correlation between these parameters were reported in these researches. For example, Vlasta et al (Ondrejka Harbulakova et al., 2017) measured the concrete pH and the concentrations of Ca^{2+} and Si^{4+} in immersion solution as the indicators of the deterioration. They conducted analytical and statistical methods to correlate these parameters, and they found low correlations of Si/concrete pH and Ca/concrete pH and an inverse correlation of Si/concrete pH for samples immersed in a pH 3 sulfuric acid solution. In another research conducted by Chang et al, (Chang et al., 2005), a lack of correlation was also reported between mass change and strength change. This low correlation between assessing parameters may be due to the complex links between

parameters and various processes. For example, among these parameters, mass loss which is the most commonly used one, is convenient to measure, and directly indicates the corrosion rate. But the result of mass loss is greatly influenced by the sample density (Alexander et al., 2013). Strength is also not reliable because it is affected by three processes (Alexander et al., 2013): 1) corrosion reaction, which lowers the strength; 2) hydration reaction, which improves the strength; and 3) pore filling by corrosion products (e.g., gypsum), which improves the mechanical performance. Dimensional change and hydrogen ion consumption are not sensitive enough when acid used is at low concentrations. Thus, a combination of these indicators will be required to assess the acid resistance of concrete more accurately. But there is very limited research focusing on this topic. The analytical and statistical models will be required to combine those assessing parameters.

2.5. Drainage design standards

A design standard would define requirements for planning, designing, constructing and maintaining drainage systems. Some standards (Government of the Hong Kong-Special Administrative Region, 2013) even include rehabilitating deteriorated sewer infrastructure. The review of microbially induced corrosion (MIC) fundamentals and rehabilitation showed that the progress of MIC is greatly related to the sewer design (hydraulic) and concrete mixture design. Proper design of drainage may be able to ease the MIC rate and extend the service life of concrete structures. This section is aiming to find out if the current municipal sewer design standards consider the MIC. Eight municipals design standards will be reviewed. Possible gaps will be identified, and recommendations will be made for further modifications to Edmonton's design standards. Building on the previous literature investigation of the MIC mechanism, design factors that can affect the MIC rate include flow velocity, concrete mix design, and retention time. The review will focus on these three aspects.

2.5.1. Flow velocity

As mentioned in Section 2.1, flow velocity substantially affects the rate of MIC process. In total, eight municipal design standards were reviewed including those from Edmonton (City of Edmonton, 2015), London (Canada) (City of London (Canada), 2015), Hong Kong (Government of the Hong Kong-Special Administrative Region, 2013), Toronto (City of Toronto, 2009), Saskatoon (City of Saskatoon, 2017), Kamloops (City of Kamloops, 2012), Dallas (City of Dallas, 2015), and Singapore (Singapore, 2004). Commonly, the flow velocity is calculated mainly to ensure that sewage is self-cleansing, and to minimize erosion and scouring. The effect of velocity on the progress of MIC is merely considered in the design standards. Table 2.9 lists the flow velocity specifications from various cities. Most cities use 0.6 m/s as the minimum velocity to ensure particle suspension in the flow. However, there is a wide range of the maximum velocity. A velocity of 3.0 m/s is adopted by most cities as the maximum value to prevent scouring and abrasion of the tunnel wall. This value is increased to 6 m/s in Hong Kong when abrasion resistant pipe is used. Singapore and Kamloops use lower values of 2.4 and 2.5 m/s respectively. London (Canada) sets 4.5 m/s as the maximum allowable velocity.

A procedure to calculate velocity to prevent MIC was outlined in the United States (US) Environmental Protection Agency (EPA) design manual (Bowker & Smith, 1985). The change in flow velocity alters the dissolved oxygen (DO) level in sewage. Since the required DO level in sewage is related to temperature and the concentration of organic matter (or biochemical oxygen demand (BOD)), the EPA combined these two factors into effective BOD (EBOD) (Bowker & Smith, 1985). The required velocity to prevent MIC differs significantly depending on location. The EPA design manual (Bowker & Smith, 1985) provides a detailed estimation of minimum pipe slope.

Table 2.9. Specifications for flow velocity

City	MIC/odour issues	Min velocity (m/s)	Max velocity (m/s)	Comments
Edmonton	Yes	0.6	3.0	0.9-1.5 m/s (force main) Prevents undue turbulence, minimizes odours due to sulfide generation
London (Canada)	N/A	0.6	4.5	Ensures self-cleansing and minimizes erosion
Hongkong	Yes (Larsen et al., 2013)	0.7	3.0	Max velocity can be relaxed to 6 m/s for abrasion-resistant pipe Higher minimum velocities for larger sewers
Toronto	Yes (Hewayde, 2005)	0.6	3.0	Self-cleansing and minimizes erosion
Saskatoon	N/A	0.61	3.0	Reduces turbulence and scouring 1.0-1.6 m/s (force main)
Kamloops	Yes (Klassen, 2013)	0.6	2.5	Self-cleansing and minimizes erosion
Dallas	Yes (Wodetzki & Kaakaty, 2013)	0.6	3.0	Self-cleansing and minimizes erosion
Singapore	Yes (Jenkins, 2013)	0.8-0.9	2.4	Self-cleansing and minimizes erosion

2.5.2. Retention time

As previously discussed, a long retention of sewage enhances the generation of H_2S. Common causes for the long retention time are debris and sediment buildup, low flow velocity, and wastewater storage. Most city standards that were reviewed specified that sewers should be free of debris, and proper maintenance should be conducted to avoid grit and sediment buildup. The differences lie in the regulations concerning retention time in pump stations. Except Edmonton and Hong Kong, the cities reviewed do not specify the shortest retention time for pump stations (see Table 2.10). In Edmonton, the maximum retention in a pump station is not to exceed 30 minutes; the total retention in a wet well and the force main should be less than four hours.

However, such short retention times mean that the storage capacity is very low, which does not meet the high demand of pump capacity in wet seasons. Consequently, the actual design of many pump stations in Edmonton did not follow this design specification (10.10.1.IV); instead, a higher value was often used. For example, at the Duggan Lift station near Southgate Centre, Edmonton, the retention time is designed to be as long as 24 hours. In this case, severe corrosion was observed at the discharge of the force main.

Table 2.10. Requirements of retention time in pump stations

City	Retention time
Edmonton	30 min in wet well 4 hrs in wet well and force main
Hong Kong	2 hrs

2.5.3. Mixture design in the concrete liner

Material used in a liner is critical for extending the service life of concrete drainage structures under the MIC process. Most Canadian cities use Canadian Standards Association (CSA) standards for concrete mixture design and manufacturing, as listed in Table 2.11. In CSA standards, requirements for concrete are determined by the exposure level to the aggressive environment. Sewer concrete structures are subject to a class A exposure. For different classes of exposure, the CSA specifies various requirements for concrete. In an environment with more severe exposure, a lower water-to-cement ratio and higher strength are required. In class A-XL and A-1, concrete is expected to experience severe acid corrosion. Extra requirements for permeability are specified to extend the service life of a concrete structure subjected to class A-XL and A-1 exposure. For example, chloride penetrability should be less than<1000 coulombs within 91 d in class A-XL exposure (CSA, 2014a). In short, CSA standards have relatively comprehensive requirements for drainage structure concrete design.

Table 2.11. CSA standards for concrete manufacture

Construction	Standards
Precast concrete pipe (reinforced)	CSA/CAN A257.2-14 (CSA, 2014c)
Precast concrete pipe (non-reinforced)	CSA/CAN A257.1-14 (CSA, 2014b)
Precast concrete segment	CSA A23.4-16 (CSA, 2000)
Grouting	CSA-A23.1-14 (CSA, 2014a) and ASTM C404-11 (ASTM, 2011)
Cement	CSA-A3000 (CSA, 2013)
Shotcrete	CSA A23.2-14 (CSA, 2014a)

But since acid corrosion on concrete is unavoidable, acid-resistant materials are preferred for sewer construction when possible. There is still a lack of regulations for commonly used non-cement materials in sewer systems. These materials include polyvinyl chloride (PVC), resin, and epoxy. Based on the findings in this paper, it is recommended to include a list of approved materials in the COE standards. The list should specify the characteristics of the materials such as the bonding strength with a substrate, acid corrosion resistance, correspondent rehabilitation techniques, and costs.

2.6. Concluding remarks

Microbially induced corrosion (MIC) has been recognized as a destructive process posing a severe threat to the sustainability of concrete in a sewer tunnel. To address this, this paper conducted a narrative review of acid corrosion regarding corrosion mechanism, control methods, cement-based rehabilitation techniques and materials, and drainage design standards. The main findings are summarized in the following:

(1) Three categories of main influencing factors were identified for the rate of MIC: hydraulic parameters, environmental factors, and concrete mixture design.

(2) Many chemicals dosed to the sewage have been effective in reducing sulfide concentrations in sewage such as magnesium hydroxide, sodium hydroxide, iron salts, free nitrous acid (FNA), nitrate, oxygen, hydrogen peroxide, ozone, chlorine, and permanganate.

(3) A proper sewer tunnel design is an efficient and cost-efficient method to control MIC. It is recommended to consider MIC during the hydraulic design phase. However, the current COE standards do not include any related regulations.

(4) All hydraulic-cement concretes, regardless of the composition, are unable to withstand for long in an acid with a pH below 3. However, improving the concrete mixture design is still a viable method for controlling MIC rate because it changes the rate of the corrosion reaction process.

(5) Cement-based rehabilitation methods can be used in severely deteriorated tunnels to provide structural restoration. However, supplementary measures (e.g., coating, chemical dosing) should be taken to prevent future corrosion, due to the alkaline nature of the cement-based material.

(6) No available testing standard was found that guides the acid resistance test of cement-based material at present.

(7) There is a lack of regulations on commonly used non-cement materials in COE standards. It is recommended to include a list of approved materials in the COE standards specifying the characteristics of the materials such as the bonding strength with a substrate, acid corrosion resistance, correspondent rehabilitation techniques, and costs.

Chapter 3. Effects of pozzolans on acid resistance of shotcrete for sewer tunnel rehabilitation

This chapter has been published as **L. Wu**, C. Hu, W.V. Liu, (2019). Effects of pozzolans on acid resistance of shotcrete for sewer tunnel rehabilitation, *Journal of Sustainable Cement-Based Materials*. © Taylor & Francis. 8(1), 55-77.

3.1. Introduction

Microbially induced corrosion (MIC) on concrete-based sewer tunnels is a severe issue that occurs in North America and worldwide (House & Weiss, 2014). Under the MIC process, the sewer tunnels experience a gradual concrete loss, which damages structural integrity and reduces the service life of the tunnel. The service life of concrete structures in sewer tunnels can be reduced significantly by MIC from the expected 100 years down to 30–50 years (Jensen, 2009), and in some extreme cases, even down to 20 years (Wu et al., 2018). In order that the service of transporting water/wastewater is restored, significant maintenance and rehabilitation are required, leading to great financial outlays (Ayoub et al., 2004; Grengg et al., 2015; Oualit et al., 2012). For example, in 2009, the U.S. spent more than $50 billion in water/wastewater systems (Lieser & Stek, 2010). The estimated cost in Germany exceeds $40 billion to repair the MIC deteriorated wastewater infrastructure (Hewayde et al., 2006). In 2015, the City of Edmonton spent C$16.8 million for the emergency repair of corroded sewer infrastructure (City of Edmonton, 2016). Besides the great financial outlays, the advancing of MIC in sewer tunnels can result in unexpected catastrophic tunnel collapse interrupting wastewater transportation and ground traffic (Kuliczkowska, 2016; Wells et al., 2009).

In the MIC process, the hydrogen sulfide (H_2S) emitted from wastewater is converted to sulfuric acid (H_2SO_4) by bacteria (i.e., Thiobacillus) colonized on the crown of the tunnel (Alexander & Fourie, 2011). Due to their alkaline nature, the cement hydrates can be easily decomposed in the presence of H_2SO_4 acid (Reardon, 1990; Zivica & Bajza, 2001). As the pH increases from the surface towards the inner part of concrete (Bakharev et al., 2003), different decomposition processes occur at various depths (Allahverdi & Škvára, 2000; Shi & Stegemann, 2000) (see Figure 3.1). Under the sustained supply of H_2SO_4 acid from microbial activities, the pH on a

concrete surface can be reduced to as low as 1-2 (House, 2013), and the corrosion rate can reach as high as 12 mm/year (Wells & Melchers, 2014).

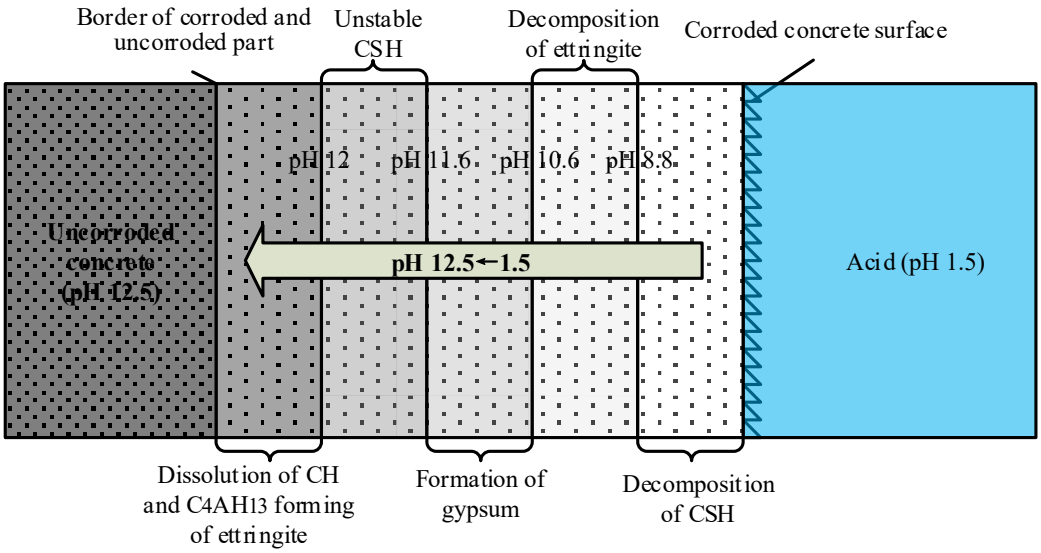

Figure 3.1. Decomposition of hydrates at various depths

In order that corroded sewer tunnels are restored, shotcrete is one of the actively used rehabilitation techniques that provide watertight structural repair (Zhao, 1998; Zhao & Rajani, 2002). The high-speed pneumatic projection of shotcrete mixtures offers superior bonding to the corroded tunnel wall, which can integrate the new structure (shotcrete) with the corroded structure. Shotcrete often shows more improved chemical resistance when compared to ordinary cast concrete due to the low permeability caused by compaction during projection (Schrader & Kaden, 1987; Wu et al., 2018).

Under the MIC process, the shotcrete mixture must have good acid resistance to ensure a reasonable lifespan for the rehabilitated structure. For precast concrete, supplementary cementitious materials (i.e., pozzolans) are highly favored because they can offer both improved durabilities against chemical attack and enhanced mechanical properties (Mardani-Aghabaglou et al., 2014; Tsubone et al., 2016). Pozzolans are defined as amorphous siliceous materials that will chemically react with CH to form the compound C-S-H (Thomas, 2007). The product of the

pozzolanic reaction, being C-S-H, is more stable than CH under an acidic environment (Roy et al., 2001). Moreover, as the acid attack is a water-induced reaction, another beneficial effect of pozzolans is to fill pores in the concrete and minimize its hydraulic permeability. This is because pozzolan particles have smaller diameters than cement, which can fill the voids in the interfacial transition zone (ITZ) (Duan et al., 2013).

But the effectiveness of pozzolans—fly ash, silica fume, and metakaolin—in improving the acid resistance of concrete is controversial. On the one hand, much research (Chindaprasirt et al., 2004; Dinakar et al., 2008; Durning & Hicks, 1991; Ekolu et al., 2016; Hossain et al., 2016; Newman & Choo, 2003; Pavel & Jiří, 2016; Shetti & Das, 2015; Torii & Kawamura, 1994a) have confirmed that these three pozzolans could provide improved resistance to acid attack. Supporting evidence can be found with regard to each of them. First, regarding the fly ash, Torii and Kawamura (Torii & Kawamura, 1994a) found improved durability of fly ash samples in 2% H_2SO_4 acid. In their study, cement was replaced by more than 10% of fly ash, and they found no mass loss within 36 months of exposure to sulfuric acid. On the contrary, the control mixture that has no fly ash had a complete decomposition after seven months. Also, Dinakar et al. (Dinakar et al., 2008) reported that the mass loss of self-compacting concrete, when exposed to 5% H_2SO_4 acid for 60 days, decreased as the fly ash percentage increased (for levels of replacement >30%). Second, in terms of the silica fume, many researchers (Chindaprasirt et al., 2004; Ekolu et al., 2016; Hossain et al., 2016; Shetti & Das, 2015) confirmed that the addition of silica fume would significantly increase the acid resistance of concrete. For example, Torii and Kawamura (Torii & Kawamura, 1994a) investigated the effectiveness of silica fume replacement on resistance to H_2SO_4 acid. It was found that the progress of deterioration largely depended on the replacement ratio, and no mass loss was observed on the samples with more than 5% silica fume replacement. Lastly, in regards to the

metakaolin, Pavel and Jiří (Pavel & Jiří, 2016) replaced cement with metakaolin from 10 wt.% up to 30 wt.% Then cubic samples were inserted in H_2SO_4 acid of various concentrations (e.g., 0.25, 0.5, 1.0, 2.0 %) for 28 days. They concluded that the addition of metakaolin positively influenced the resistance of samples to the acidic environment. Another study (Newman & Choo, 2003) indicated that the concrete produced by replacing 10% of OPC with metakaolin provided more significant resistance to acid attack in comparison with OPC concrete. Pavel and Jiří (Pavel & Jiří, 2016) also noted that the addition of metakaolin generally improved the compressive strength and reduced mass loss of concrete under 2% H_2SO_4 acid.

On the other hand, other researchers reported negligible effects of pozzolans on the improvement of acid resistance. For example, Kannan and Ganesan (Kannan & Ganesan, 2014) observed a higher mass loss when samples with metakaolin were immersed in 5% H_2SO_4 acid for up to 12 weeks. Tamimi (Tamimi, 1997) reported a mass loss reduction of less than 2% when samples with 10% silica fume were exposed to 1% H_2SO_4 acid for 15 weeks. Hewayde and Nehdi et al. (Hewayde et al., 2007b) found no reduction in mass loss of samples containing a 6-15% of silica fume after being exposed to 3% or 7% H_2SO_4 acid for 60 days. Furthermore, House (House, 2013) summarized that the positive effects of fly ash inclusion are less apparent as the concentration of acid increases.

Until now, despite much literature on the acid resistance of pozzolan materials, no work has been done to systematically compare the effects of the three pozzolans (fly ash, metakaolin, and silica fume) under the same acid immersion conditions. It is economically significant to conduct this research because all these three pozzolans can be locally sourced from the local mining industry—the mine waste from Alberta, Canada. Among the abovementioned pozzolans, fly ash is the by-product of coal combustion (Tokyay, 2016), metakaolin can be produced from oil sands operation

(Siddique & Khan, 2011), and silica fume is the by-product of silicon metal and the ferrosilicon alloys production (Tokyay, 2016). Alberta is abundant in these mine waste. For example, around 60% of Canada's fly ash is produced in Alberta, which amounts to approximately 2.6-3 million tonnes per year (AMEC Earth & Environmental, 2006). Currently, the oil sands fields in northern Alberta contain up to 60 million tonnes of kaolin (De Spot & Wojtarowicz, 2003). Exploring the possibility of their use in the making of more acid-resistant cement-based composites could bring enormous social and economic benefits.

In this regard, this paper aims to investigate the performance of pozzolanic materials (i.e., fly ash, silica fume, and metakaolin) that can be sourced from local mine waste in the shotcrete application, and to provide a comparison of the effectiveness of these three pozzolans. During the investigation, both mass loss and strength loss were selected to measure corrosion deterioration in the research. The effectiveness of these two parameters was discussed regarding the evaluation of acid resistance. Furthermore, the influence of acid concentration on corrosion was studied as the pH values in sewer tunnels vary spatially and tend to change over time.

3.2. Methodology

3.2.1. Materials and mix design

All the materials used in the research were locally sourced in Alberta, Canada. To investigate the effects of pozzolans, Type GU (general use) Portland cement was replaced with silica fume /fly ash/metakaolin at ratios of 5%, 10%, 20%, and 30 wt.%, as shown in Table 3.1. According to ACI 506R-16 (ACI Committee 506, 2016), a typical shotcrete water to cement ratio (w/c) of 0.45 was used for all mixtures in this study. Typical concrete sand was used as fine aggregates for sample preparation. Sieve analysis of fine aggregate was conducted as per ASTM C136/C136M-14

(ASTM, 2014) using a mechanical shaker. As shown in Figure 3.2, the grain size distribution of the sand falls in the Grade I zone specified in ACI 506R-16 (ACI Committee 506, 2016). The oven-dry bulk density of the sand is 1,575 kg/m^3, and saturated surface dry state water content is 3% by weight. Also, a maximum of 0.35 wt.% of powder superplasticizer of a modified polycarboxylic was added to the silica fume mixtures and the metakaolin mixtures to ensure required slump for shotcreting (between 75 and 150 mm (ACI Committee 506, 2009)). Note that no water reducer was needed for fly ash mixtures, as slump tests showed increased slump from 114 to 123 mm as a result of fly ash addition. Slump tests were conducted for all mixtures, according to ASTM C143/C143M-15a (ASTM, 2015). The slump was kept in the range of 11.3-12.3 cm.

Table 3.1. Mix proportions of experimental samples

Mixtures	Cement (kg/m^3)	Water (kg/m^3)	Sand (kg/m^3)	Pozzolan (kg/m^3)	Pozzolan ratios, %	Water reducer (%)	Slump (mm)	W/C
Reference	493.25	221.96	1541.40	0.00	0	0	114	0.45
SF-5	468.59	221.96	1541.40	24.66	5	0.044	119	0.45
SF-10	443.92	221.96	1541.40	49.32	10	0.088	121	0.45
SF-20	394.60	221.96	1541.40	98.65	20	0.22	119	0.45
SF-30	345.27	221.96	1541.40	147.97	30	0.35	113	0.45
FA-5	468.59	221.96	1541.40	24.66	5	0	114	0.45
FA-10	443.92	221.96	1541.40	49.32	10	0	116	0.45
FA-20	394.60	221.96	1541.40	98.65	20	0	120	0.45
FA-30	345.27	221.96	1541.40	147.97	30	0	123	0.45
MK-5	468.59	221.96	1541.40	24.66	5	0.044	117	0.45
MK-10	443.92	221.96	1541.40	49.32	10	0.088	119	0.45
MK-20	394.60	221.96	1541.40	98.65	20	0.22	120	0.45
MK-30	345.27	221.96	1541.40	147.97	30	0.35	121	0.45

*Note: FA means fly ash; MK means metakaolin; SF means Silica fume

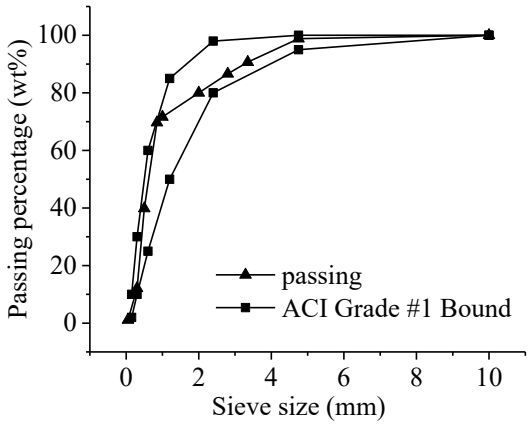

Figure 3.2. Sieve analysis of aggregates

3.2.2. Sample preparation

Cylinder samples were made according to ASTM C192-16a (ASTM, 2016b). Cement, sand, and pozzolans were mixed using a concrete drum mixer. The freshly mixed slurry was cast in cylinder molds (50 mm in diameter × 100 mm in height). A table vibrator was used to compact the mix into the cylinder molds. After 24 hours of casting, samples were de-molded, stored, and then cured in a standard moisture room (with a temperature of 25 ± 2 °C and relative humidity of 100%) until the 28th day. Next, samples were cut using a rock saw to ensure flat ends and the same contact area with acid.

3.2.3. Tests procedures and specifications

In total, there were five groups of samples made for different tests, which will be explained in detail in this section. The sample numbers are summarized in Table 3.2.

Table 3.2. Sample numbers

	Group 1	Group 2	Group 3	Group 4	Group 5
Test procedure	Tested for density, water absorption and the volume of permeable voids	Immersed in pH1.5 acid for strength tests at ages of 0^{th}, 7^{th}, 21^{st}, 56^{th}, 91^{st} day*	Immersed in pH3 acid for strength tests at ages of 7^{th}, 21^{st}, 56^{th}, 91^{st} day*	Immersed in pH6.5 acid for strength tests at ages of 7^{th}, 21^{st}, 56^{th}, 91^{st} day*	Immersed in pH4.5 acid for strength tests at ages of 91^{st} day*
Number of sample	13×2 = 26	13×3×5 = 195	13×3×4 = 156	13×3×4 = 156	13×3 = 39

***Note:** The immersion age is counted from the first day of insertion in acids on the 28^{th} day of curing in moisture room (e.g., the 0^{th} day of immersion age is equal to the 28^{th} day of curing age).

3.2.3.1. Density, water absorption, and volume of permeable voids tests

The first group with two samples for each mixture was tested for water absorption and the volume of permeable voids that can be used to indirectly reflect the durability of concrete samples (Hossain et al., 2016; Supit & Shaikh, 2015; Wang et al., 2015). These physical properties of concrete were determined following the test method described in ASTM C642 (ASTM, 2013), on the 7^{th} day of curing as required for shotcrete in ACI 506.5R-09 (ACI Committee 506, 2009).

3.2.3.2. Sulfuric acid resistance tests

The rest of the four groups of samples were exposed to H_2SO_4 acid immersion after 28 days of curing in a standard moisture room. Two groups of cylindrical samples were inserted into controlled H_2SO_4 acid at a pH of 1.5 and 3.0, respectively, to examine the degradation process. The pH values of 1.5 and 3.0 were selected based on the field measurement of concrete surface in Edmonton's sewer system, where a range of 1.7 to 2.8 was found. The fourth group of samples acts as references, which were immersed in H_2SO_4 acid with a pH of 6.5 because the pH of wastewater was found to be 6.83 in Edmonton (Stantec Consulting Ltd., 2015). In addition, the

fifth group of samples was made to be immersed in pH 4.5 acid to investigate the influence of acid concentration on the deterioration.

As mentioned in the introduction section, the corrosion of concrete structures in sewer tunnels is caused by H_2SO_4 acid. Thus, the immersion acid was made using tap water to dilute 98% H_2SO_4 acid. In this study, the pH values of the immersing acid were recorded using pH meters or pH papers. Regarding the acid renewal frequency, the immersion acid was replaced every week to maintain acidity.

To test the resistance of concrete against H_2SO_4 acid, the choice of degradation measurement is of great importance. Commonly used parameters include mass loss, dimension change, strength change, and hydrogen ion consumption. One single parameter can hardly suffice to characterize concrete deterioration sufficiently. Therefore, a combination of these parameters is commonly used in the evaluation of acid resistance. Among these parameters, mass loss is so far the mostly measured parameter in the evaluation of acid resistance due to its simplicity to measure and a direct reflection of deterioration level (Joorabchian, 2010), while unconfined compressive strength (UCS) is one of the most important structural design parameters for concrete. Thus, both mass loss and UCS change were selected for this research as the indicators of degradation level.

(1) Mass change due to acid corrosion.

Mass change of the samples was monitored every seven days as a possible indicator of degradation. Samples were taken out from H_2SO_4 acid and air-dried under the normal indoor condition (20 °C) for 2 hours (see Figure 3.3(a)). Then the mass of samples before (m_0) and after (m_n) the immersion cycle was measured using an electronic scale with an accuracy of 0.01 gram (see Figure 3.3(b)).

Consequently, the mass change (Δm %) was calculated as Equation 3-1, where the negative Δm indicates a mass loss, while the positive value indicates a mass gain.

$$\Delta m = \frac{m_n - m_0}{m_0} \times 100\% \quad (3\text{-}1)$$

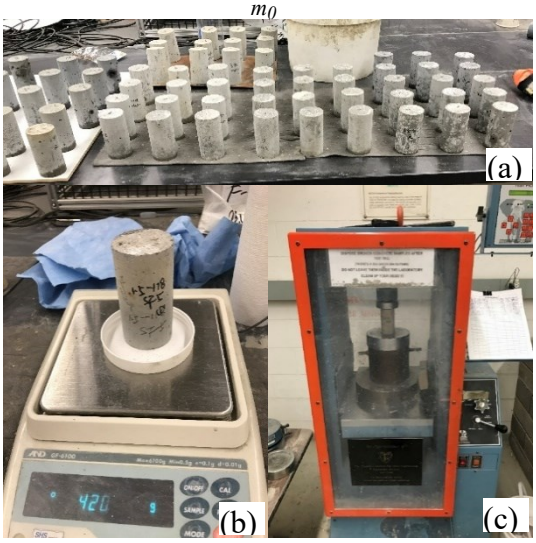

Figure 3.3. Tests performed: (a) sample drying; (b) mass measurement; (c) compression testing

(2) Change of compressive strength due to acid corrosion.

The UCS was tested per ASTM C42-16 (ASTM, 2016a) on the 0th (28th day of curing), 7th, 21st, 56th, and 91st day of immersion to monitor the UCS change (see Figure 3.3(c)). It was reported that the sulfuric acid immersion leads to a dissolution of cement hydrates and peeling off of aggregates. The UCS calculated by dividing the peak load with the actual cross-sectional area only represents the strength of the uncorroded area. Thus, Change et al. (Chang et al., 2005) proposed to measure the loading capacity to evaluate the sample deterioration. The loading capacity was calculated by dividing the peak load with the original cross-sectional area. In this thesis, the loading capacity was adopted as a parameter for acid resistance evaluation. And the change in loading capacity was termed as UCS change in this thesis for convenience.

The UCS change of samples immersed in pH3 and pH1.5 acids was calculated using sample strength in pH6.5 acid as references (Chang et al., 2005; Fan et al., 2010; Kristiawan & Tyas, 2016;

Pacheco-Torgal & Jalali, 2009), as shown in Equation 3-2. The UCS development of samples in pH6.5 acid can be considered mainly due to the continued cement hydration, while the sample UCS in pH1.5/3 acids is attributed to a combined effect of acid corrosion and continued cement hydration (Tsubone et al., 2016). These two effects had the opposite influence on the sample UCS that often leads to uncertain UCS change with time. The proposed calculation on UCS change helps to distinguish the two opposite effects and to understand the corrosion mechanism.

$$\Delta p = \frac{p_n - p_N}{p_N} \times 100\% \tag{3-2}$$

where, Δp is the UCS change, %.

p_N is the UCS of samples immersed in pH6.5 acid, MPa;

p_n is the UCS of samples immersed in pH of n acid, MPa.

3.3. Results and Discussion

3.3.1. Density, absorption, and permeable voids on the 7th day of curing

The water absorption and volume of permeable voids are of great importance for evaluating the acid resistance of concrete since the intrusion of aggressive ions into the concrete matrix occurs with the penetration of water (Papadakis et al., 1991). To address this, the water absorption, volume of permeable voids, and density of samples were measured on the 7th day of curing, and the results are plotted in Figure 3.4. Figure 3.4 (a) presents that, from 5% to 20% replacement ratios, mixtures with silica fume and fly ash had a similar water absorption of ~9.5% with the reference mixture (at 0% replacement ratio). However, when the replacement ratio reached 30%, the water absorption of mixtures with silica fume and fly ash showed an increase to 11.78% and 10.68%, respectively. Contradictorily, the addition of metakaolin continuously reduced the water

absorption of samples from ~9.5% down to 7.39% while the replacement ratio increased from 0% to 30%. The results of shotcrete samples with metakaolin and silica fume are consistent with previous research (Khatib & Clay, 2004; Valipour et al., 2013), but the water absorption of shotcrete samples with fly ash varies in different research. Khatib (Khatib, 2008) observed insignificantly higher absorption of shotcrete samples with fly ash than reference samples on the 28th day, while Chahal et al. (Chahal et al., 2012) reported a reduction of water absorption after the incorporation of fly ash. The large variation in water absorption could be due to the broad range of particle size of fly ash, which greatly depends on their sources. A larger particle size leads to a slower pozzolanic reaction (Joshi, 1973; Watt & Thorne, 1965), leaving a large amount of unreacted fly ash particles. These unreacted fly ash particles in samples increased porosity and enhanced water absorption (Davis, 1954). As reported, the particle size of fly ash in Khatib's research (with a specific area of 356 m^2/kg) (Khatib, 2008) is significantly larger than that in Chahal's research (with a specific area of 19,000 m^2/kg) (Chahal et al., 2012).

Next, Figure 3.4 (b) shows the relationship between the volume of permeable voids with various pozzolan replacement ratios. The trends were generally similar to that in Figure 3.4 (a): the permeable void volume of fly ash mixtures remained at the same level when compared with the reference mixture, whereas the metakaolin mixtures had decreased void volumes when replacement ratios increased. However, in comparison with Figure 3.4 (a), the trend of silica fume in Figure 3.4 (b) was different at replacement ratios from 0% to 20%, showing a linear decrease from 21.81% to 17.08%. In Figure 3.4 (b), silica fume mixtures presented a similar declining trend with metakaolin mixtures until the replacement ratio reached 20%. However, after this, there was a sudden increase to 24.94% regarding the permeable voids of silica fume mixtures. These results could indicate that, in general, the addition of metakaolin and silica fume reduces the volume of

pores in samples, while the addition of fly ash has little effect on the volume of pores. Two effects can explain the reduced permeable voids of metakaolin and silica fume samples: 1) the pore-filling effect and 2) the pozzolanic effect (Duan et al., 2013; Hossain et al., 2016). Both of the effects refine the pore structure of the concrete matrix, which makes the concrete denser (Shih et al., 2006). The negligible effect of fly ash addition was due to the deficiencies in samples resulting from delayed pozzolanic reaction (Fraay et al., 1989), which compensates for the pore-filling effect. It is reported that fly ash is unreactive when the pH of a pore solution is below 13.2, and it takes one or more weeks for the pH of a pore solution to reach this value (Fraay et al., 1989; Pietersen et al., 1989).

Figure 3.4 (c) shows the relationship between bulk density and the pozzolan replacement ratio. It can be seen that the addition of pozzolan lowers the density of shotcrete mixtures. This can be attributed to a lower specific gravity of pozzolans (e.g., 1.9-2.8 for fly ash, 2.2-2.5 for metakaolin, 2.2-2.5 for silica fume) than that of OPC (~3.15) (Al-Akhras, 2006; Demirboğa & Gül, 2003; Li, 2004). In general, the oven-dry bulk density of fly ash and silica fume mixtures decreased with the rising replacement ratio. Compared to the reference mixture, the largest density differences of shotcrete samples were 134.17 kg/m^3 and 83.62 kg/m^3 for silica fume mixtures and fly ash mixtures, respectively. Regarding the metakaolin addition, it showed a limited effect on the sample density with the lowest value of 2007.43 kg/m^3 for the mixture with 10% of metakaolin—it is only slightly lower than the density of the reference mixture (2039.41 kg/m^3).

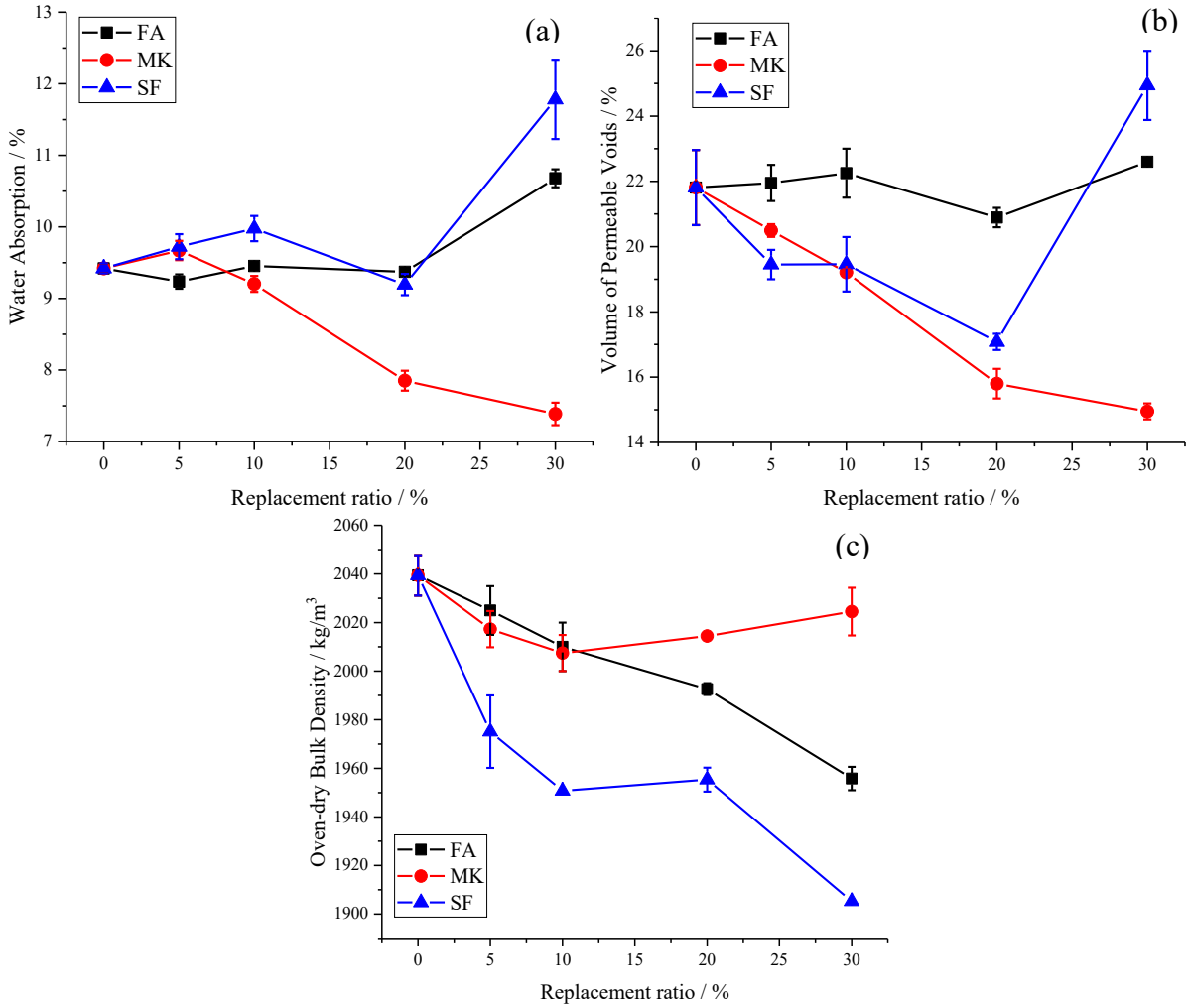

Figure 3.4. Mixture properties: (a) water absorption; (b) volume of permeable voids; (c) oven-dry density

3.3.2. The compressive strength at 28 days

The compressive strength on the 28th day is critical to the performance of underground shotcrete (ACI Committee 506, 2009). It is important to understand the influences of pozzolan addition on the compressive strength of shotcrete. The UCS of all mixtures was tested after 28 days of curing in a standard moisture room, and the results are presented in Figure 3.5. Compared with the reference mixture, the results indicate that the partial replacement of cement with silica fume and metakaolin improved the UCS of samples on the 28th day, whereas the partial replacement of fly

ash reduced the 28th day UCS of samples. On the one hand, the improved UCS of metakaolin and silica fume shotcrete samples can be explained by three effects (Duan et al., 2013; Hossain et al., 2016; Khatib & Hibbert, 2005; Madandoust & Mousavi, 2012; Said-Mansour et al., 2011; Wild et al., 1996): (1) the filling effect of smaller metakaolin/silica fume particles which fill the voids in the interfacial transition zone, (2) the nucleation effect which accelerates cement hydration, and (3) the pozzolanic reaction between metakaolin/silica fume and CH which generates extra binding C-S-H. These three effects all refine the pore structure of the concrete matrix (Dunster et al., 1993), making the concrete denser (Duan et al., 2013; Hewayde et al., 2007b). This is confirmed by the reduced water absorption and permeable voids in Section 2.3.1. On the other hand, the abovementioned effects were not reflected in the fly ash mixtures since their UCS values decreased with the fly ash additions. This could be due to the delayed pozzolanic reaction of fly ash. That is, fly ash is not reactive when the pH of a pore solution is below 13.2, and it takes one or more weeks for a pore solution pH to reach this value (Fraay et al., 1989). Hence, the UCS development of fly ash shotcrete samples is relatively long in comparison with the reference mixture, and a higher fly ash percentage results in a slower UCS development (Gopalan & Haque, 1986). Despite this, the long-term UCS of the fly ash shotcrete sample is expected to be improved, compared with the reference mixture; therefore, the final strength gain should be proportional to silica content in fly ash (Papadakis, 1999). This will be further discussed in Section 2.3.3 in this paper.

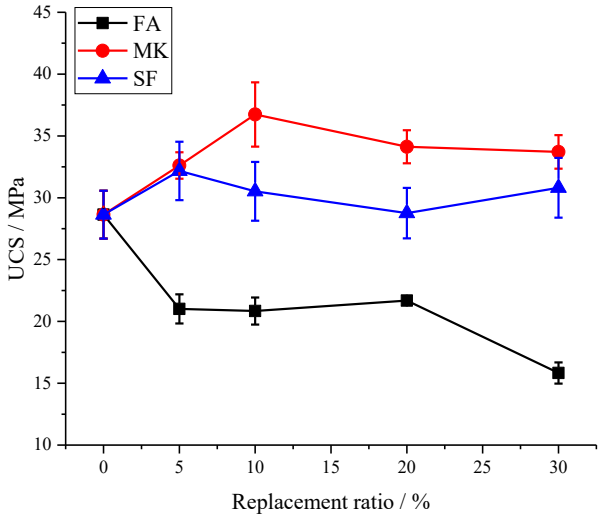

Figure 3.5. The UCS of samples after 28 days of curing in a standard moisture room

3.3.3. Change of compressive strength under acid immersion

3.3.3.1. Compressive strength development under pH6.5 acid

Table 3.3 lists the UCS of samples under pH6.5 acid, and Figure 3.6 presents the UCS change relative to the UCS before immersion. In general, all 13 mixtures showed a gradual increase of UCS with immersion time in the pH6.5 H_2SO_4 acid. Also, the final UCS increase varied depending on the pozzolan types and replacement ratio. Shotcrete mixtures with fly ash addition had greater UCS changes than the reference mixture (with 0% of pozzolans), while the UCS change of metakaolin mixtures was comparable to that of the reference mixture. First, the greater UCS change of fly ash mixtures could be due to the accelerated pozzolanic reaction between fly ash and cement hydrates (i.e., calcium hydroxide, calcium aluminate hydrate, ettringite and calcium silica hydrate) after 28 days (Fraay et al., 1989; Papadakis, 1999). Also, as noted in Figure 3.6 (a), a higher fly ash percentage leads to a higher UCS increase after 28 days—the curve moved up when the percentage of fly ash increased. This could be explained as follows: a higher fly ash percentage in samples consumes CH faster, which reduces the pH of the pore solution. This slows the reaction

between fly ash particles and the CH. Second, regarding the shotcrete mixtures containing metakaolin, the replacement of metakaolin only enhanced the UCS development rate from 7 to 14 days of curing, and it had little effect on the UCS development after 28 days of curing (Wild et al., 1996). That is, all metakaolin shotcrete samples showed comparable UCS changes with the reference mixture. Third, for silica fume mixtures, most of them showed a lower UCS change than the reference throughout the immersion period. This could be caused by the fast pozzolanic reaction of silica fume at early ages; a previous study (Wild et al., 1995) found that the replacement of silica fume enhanced the UCS at the end of the first week of curing, but after that, the development of UCS was relatively slow. Hence, most silica fume shotcrete samples showed a lower UCS increase after immersion compared to the reference mixture. In summary, the influence of pozzolan replacement on the UCS change under pH6.5 H_2SO_4 acid was in the order: fly ash> silica fume > metakaolin.

Table 3.3. The UCS of samples under pH6.5 acid (MPa)

Immersion age, day	Ref	FA-5	FA-10	FA-20	FA-30	MK-5	MK-10	MK-20	MK-30	SF-5	SF-10	SF-20	SF-30
0	28.64	21.01	20.84	21.68	15.83	32.61	36.74	34.12	33.71	32.17	30.52	28.76	30.81
7	27.19	25.19	23.93	21.52	18.87	23.35	27.89	29.98	32.07	27.55	27.11	30.37	30.01
21	30.73	27.41	30.45	25.72	23.15	29.03	41.38	36.03	37.99	31.35	32.34	32.27	33.32
56	34.97	28.14	36.03	31.16	32.99	43.06	43.77	43.18	44.43	35.02	31.29	33.87	38.3
91	31.75	32.76	35.29	33.04	31.39	41.05	42.24	42.36	41.65	34.16	30.88	32.61	37.3

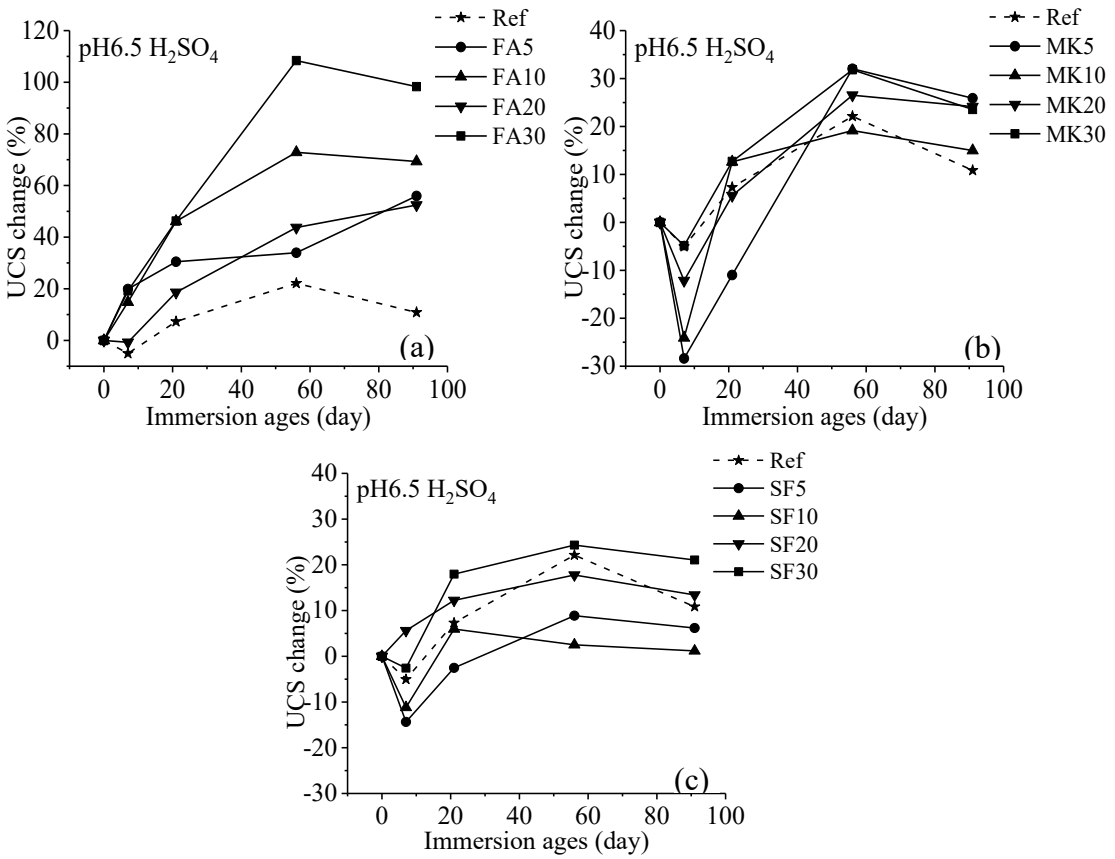

Figure 3.6. The UCS development under pH6.5 acid: (a) mixtures with fly ash; (b) mixtures with metakaolin; (c) mixtures with silica fume

3.3.3.2. Strength change with immersion time under pH3 and pH1.5 acids

Table 3.4 and Table 3.5 list the UCS of samples under pH1.5 and pH3 acids, respectively. The UCS change was presented in Figure 3.7, wherein a positive value indicates a higher UCS in comparison with the reference (in pH6.5 acid). As can be seen in Figure 3.7, most samples experienced higher UCS gain than those immersed in the pH6.5 H_2SO_4 acid at early ages (1-3 weeks) regardless of acidity. This initial UCS increase was also reported in the literature (Fan et al., 2010), where the strength slightly increased at the initial stages (within one month). This indicated that the acid immersion enhanced the UCS development of shotcrete samples. The phenomena could be caused by the pore filling of corrosion products (e.g., gypsum and ettringite),

which made the sample denser and mechanically stronger. The pore filling of concrete by corrosion products was observed in research conducted by Tsubone et al. (Tsubone et al., 2016). After the initial increase, the UCS change started to decrease significantly. The reason for this dominant reduction could be explained as follows: as the corrosion products accumulate in the pores of the samples, they cause an internal stress concentration (Fan et al., 2010; Israel et al., 1997). This results in micro-cracks and finally leads to the peel off of the sample constituents (e.g., corrosion products, hydrates, and aggregates) (Yang et al., 2018). Among all the pozzolan shotcrete samples, the samples with fly ash showed a slower drop of UCS change than that of samples with metakaolin and silica fume. This could be attributed to the delayed pozzolanic reaction of fly ash with CH. This delayed reaction leads to a slower strength development within 28 days of curing. After 28 days, the strength continues to grow, which somehow compensates for the strength reduction caused by acid corrosion.

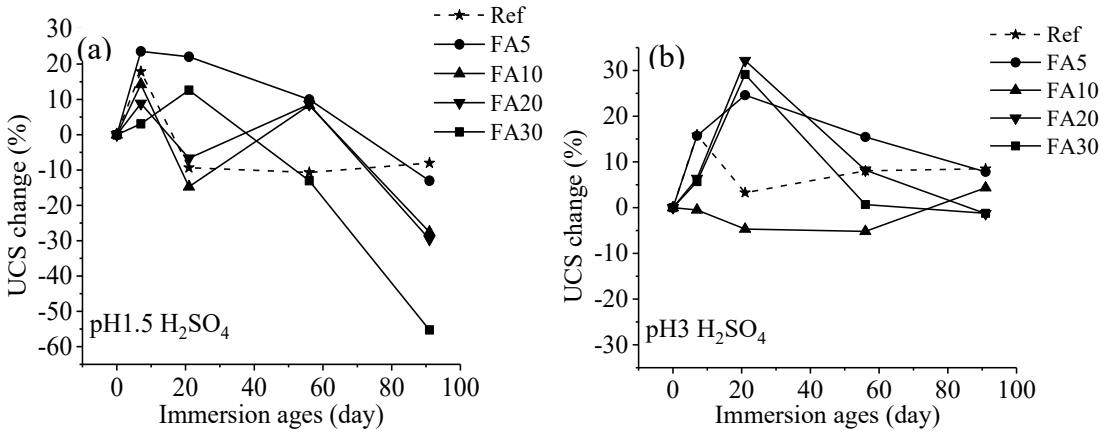

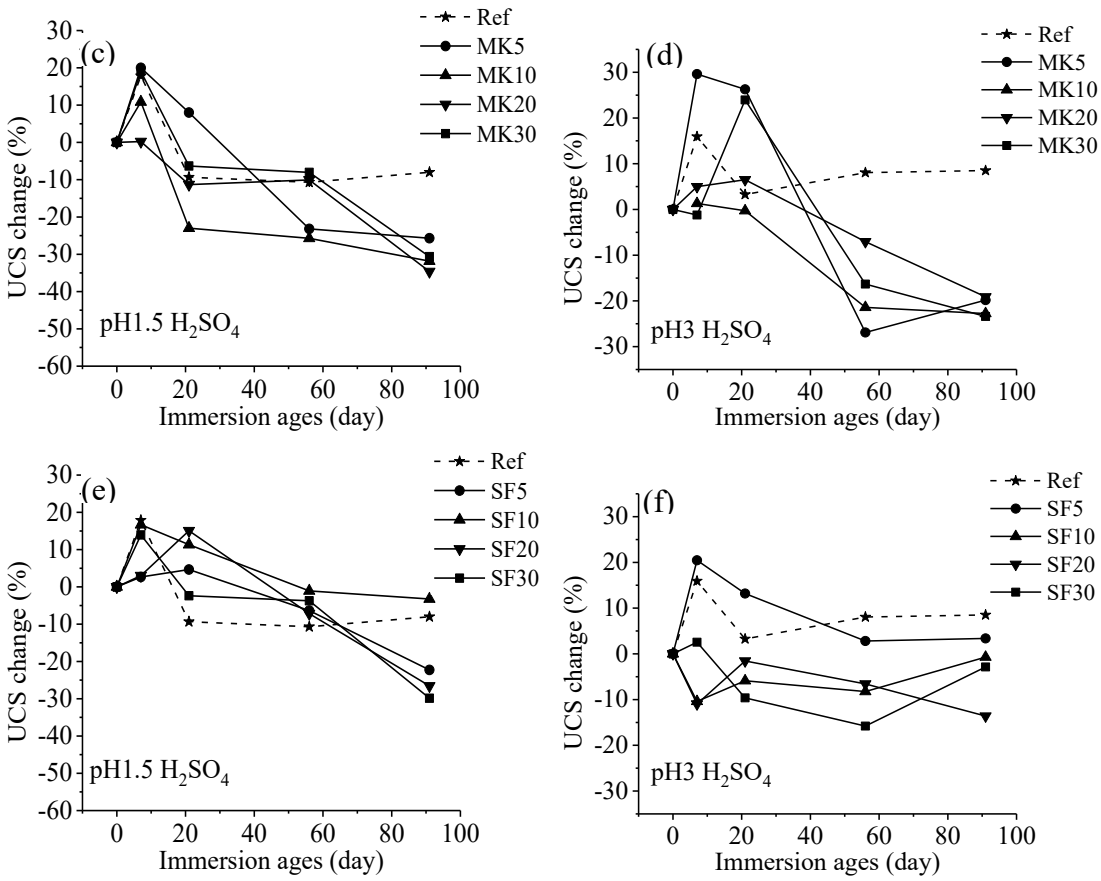

Figure 3.7. UCS change with immersion time under various immersion pH: (a),(b) FA mixtures; (c), (d) MK mixtures; (e),(f) SF mixtures

Table 3.4.The UCS of samples under pH1.5 acid (MPa)

Immersion age, day	Ref	FA-5	FA-10	FA-20	FA-30	MK-5	MK-10	MK-20	MK-30	SF-5	SF-10	SF-20	SF-30
0	28.64	21.01	20.84	21.68	15.83	32.61	36.74	34.12	33.71	32.17	30.52	28.76	30.81
7	32.05	31.13	27.35	23.42	19.45	28.03	30.91	30.05	38.17	28.28	29.84	31.29	34.19
21	27.86	33.46	25.97	24	26.07	31.35	31.86	31.95	35.58	32.82	36	37.13	35.48
56	31.24	30.95	39.03	33.83	28.69	33.07	32.51	38.83	40.87	32.8	30.95	31.44	36.87
91	29.2	28.5	25.55	23.26	14.05	30.51	28.79	27.69	28.89	26.55	29.88	23.95	26.16

Table 3.5. The UCS of samples under pH3 acid (MPa)

Immersion age, day	Ref	FA-5	FA-10	FA-20	FA-30	MK-5	MK-10	MK-20	MK-30	SF-5	SF-10	SF-20	SF-30
0	28.64	21.01	20.84	21.68	15.83	32.61	36.74	34.12	33.71	32.17	30.52	28.76	30.81
7	31.52	29.15	23.81	22.9	19.94	30.27	28.25	31.47	31.68	33.19	24.29	27.04	30.78
21	31.73	34.16	29.03	33.99	29.89	36.65	41.26	38.37	47.08	35.49	30.44	31.77	30.11
56	37.79	32.49	34.16	33.72	33.21	31.47	34.39	40.14	37.18	36.01	28.7	31.64	32.25
91	34.45	35.33	36.82	32.61	31	32.92	32.63	34.27	31.9	35.31	30.66	28.18	36.23

3.3.3.3. Optimum replacement ratio under different pH values

Figure 3.8 shows the relationship between the final UCS change and the pH of acids on the 91st day of immersion. It can be seen that acid concentration and the replacement ratio were found to have a significant influence on the final strength change. First, regarding the fly ash shotcrete mixtures, it can be seen that the fly ash shotcrete samples inserted in acid with pH3 and above presented comparable UCS change, which means the addition of fly ash showed little effect on UCS change under low acidity. However, the percentage of fly ash in the sample had a great influence on the UCS change when the pH was less than three. Among all the replacement levels, the samples with 5% fly ash showed the lowest UCS change in pH1.5 H_2SO_4 acid, with a value of -13.01% (see Table 3.6). Differently, the percentages of metakaolin showed little influence on the UCS change at all acidity levels. That is, all metakaolin shotcrete samples showed comparable UCS change. Lower pH leads to a higher difference in UCS change between the reference mixture and metakaolin mixtures. Contradictory to metakaolin shotcrete samples, the silica fume percentages demonstrated a significant influence on the UCS change at all pH levels. But the optimal silica fume percentages varied depending on the pH level. As shown in Table 3.6 and Figure 3.8 (c), under pH1.5 H_2SO_4 acid condition, samples with 10% silica fume had the lowest UCS change after three months of immersion, with a value of -3.25%. However, when pH

increased to 3, samples with 5% silica fume demonstrated the lowest UCS change with a value of 3.38%. A similar conclusion can also be drawn from fly ash and metakaolin shotcrete samples. This means that the optimal percentages for the lowest UCS change depend on the acidity of immersing acid.

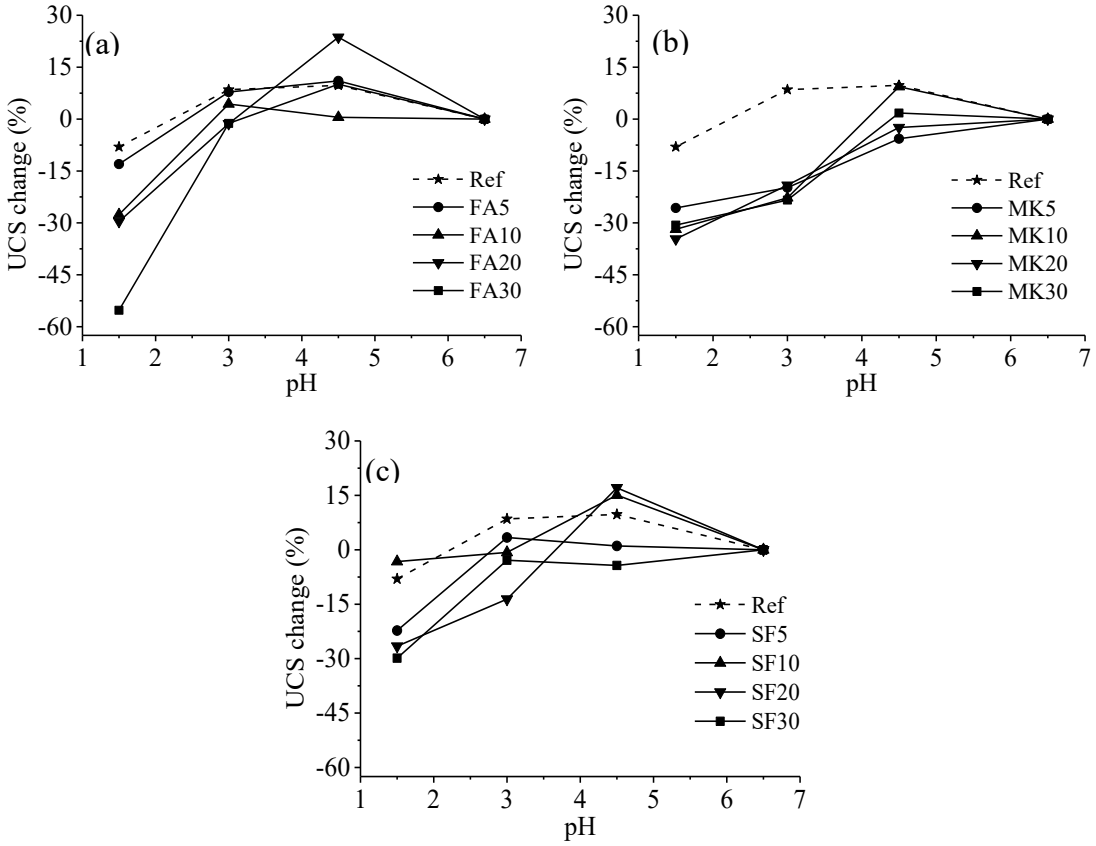

Figure 3.8. UCS change with pH of immersion acids on the 91st day of immersion: (a) mixtures with fly ash; (b) mixtures with metakaolin; (c) mixtures with silica fume

Table 3.6. The optimum replacement with the lowest UCS change

pH	FA		MK		SF	
	Replacement, %	UCS change, %	Replacement, %	UCS change, %	Replacement, %	UCS change, %
1.5	5%	-13.01%	5%	-25.69%	10%	-3.25%
3	5%	7.83%	20%	-19.11%	5%	3.38%
4.5	20%	23.67%	10%	9.35%	20%	17.08%

3.3.4. Mass change under acid immersion

3.3.4.1. The trend of mass change with pH values

Figure 3.9 presents the relationship between mass change and immersion times (1 to 91 days) under various acidic conditions. It can be seen that the relationship between mass change and immersion time was highly affected by the pH values of immersion acids. That is, when the pH of immersion acids was 4.5 or 6.5, all 13 mixtures were gradually gaining mass with the immersion time. However, when the pH of immersing acid was reduced to 3, all mixtures presented mass loss, and the mass loss was kept at certain levels after 21 days of immersion. When the pH of the immersing acid was further reduced to 1.5, all mixtures started to lose mass at nearly a constant rate after the 7^{th} day. The difference in the trend of mass change could be attributed to the interaction between two effects: 1) cement hydration and pozzolanic reaction, and 2) corrosion reaction (between cement hydrates and acids) (Tsubone et al., 2016) under various pH levels. When the pH of the immersing acid is high (4.5 or 6.5), hydration reaction plays a dominant role in mass gain, particularly for fly ash concrete where the pozzolanic reaction is delayed (Fraay et al., 1989). The limited amount of corrosion products from the hydrates' decomposition, being expansive gypsum, could be dissolved in the immersing acid (Bock, 1961). This explains the phenomenon that the samples immersed in pH4.5 H_2SO_4 acid generally experienced a lower mass gain than those in pH6.5 H_2SO_4 acid. Under low pH conditions (i.e., pH1.5), the corrosion reaction overwhelmed the hydration reaction. The generated gypsum cannot all be dissolved by the immersing acid, and the solid gypsum fills the pores in samples (pore-filling effect) (Tsubone et al., 2016). This leads to a mass gain at the early stage of immersion (0-7 days), as shown in Figure 3.9 (d), (h), (l). Similar results were also reported in the research conducted by Kannan et al. (Kannan & Ganesan, 2014). They observed a mass gain of metakaolin concrete immersed in 5%

H_2SO_4 acid between 7 and 14 days. Then, as the corrosion proceeded, samples started to lose aggregates due to the loss of C-S-H and corresponding binding forces (Reardon, 1990; Zivica & Bajza, 2001). This contributed to the mass loss of samples at the later stage (after 7 days). In the case of pH3, the mass gain resulting from the hydration reaction comes to a balance with the mass loss caused by the loss of sample constituents. This keeps the mass change of samples in pH3 acid at the same level.

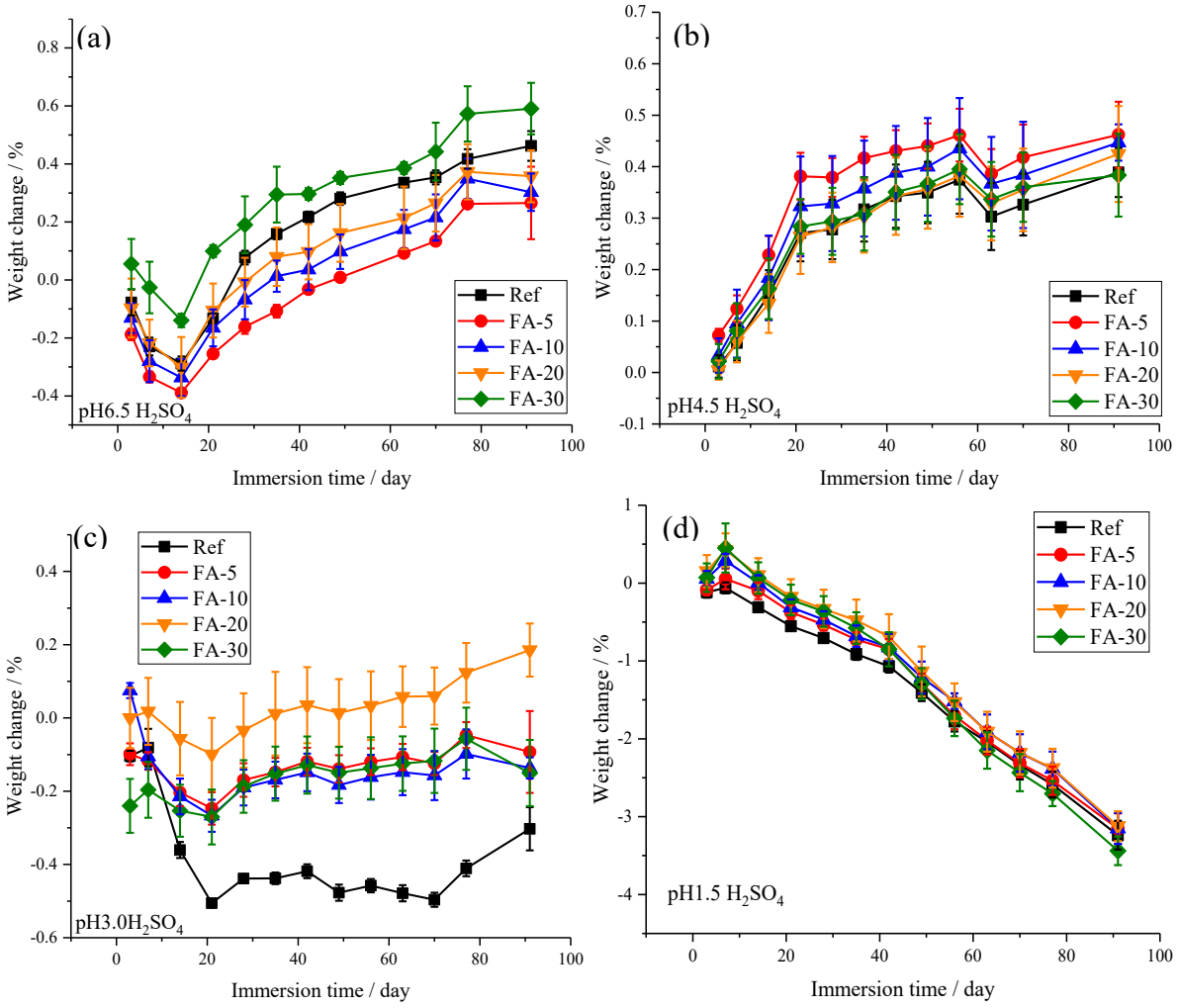

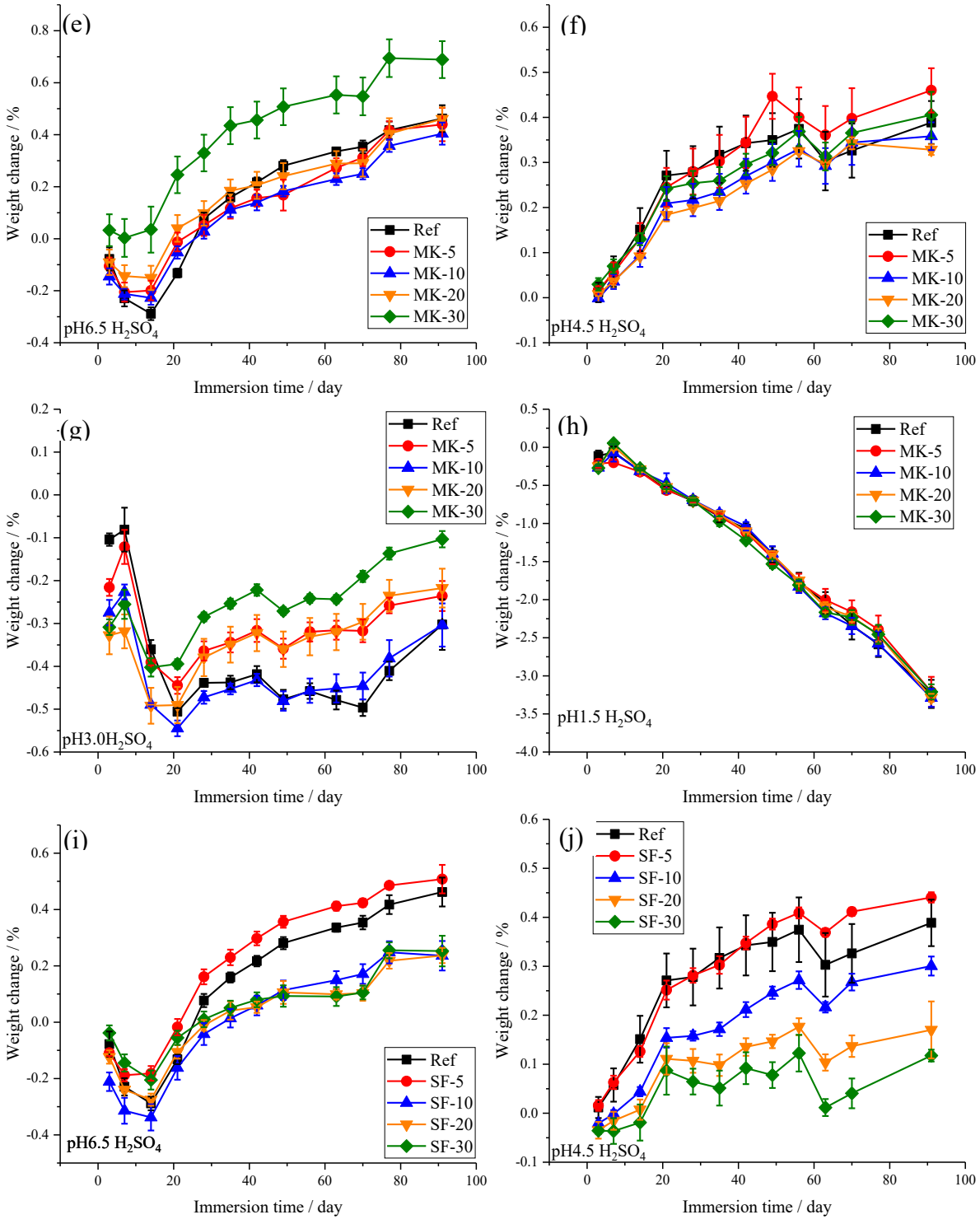
(e)
Weight change / %
Immersion time / day
pH6.5 H2SO4
Ref
MK-5
MK-10
MK-20
MK-30
(f)
Weight change / %
Immersion time / day
pH4.5 H2SO4
Ref
MK-5
MK-10
MK-20
MK-30
(g)
Weight change / %
Immersion time / day
pH3.0H2SO4
Ref
MK-5
MK-10
MK-20
MK-30
(h)
Weight change / %
Immersion time / day
pH1.5 H2SO4
Ref
MK-5
MK-10
MK-20
MK-30
(i)
Weight change / %
Immersion time / day
pH6.5 H2SO4
Ref
SF-5
SF-10
SF-20
SF-30
(j)
Weight change / %
Immersion time / day
pH4.5 H2SO4
Ref
SF-5
SF-10
SF-20
SF-30

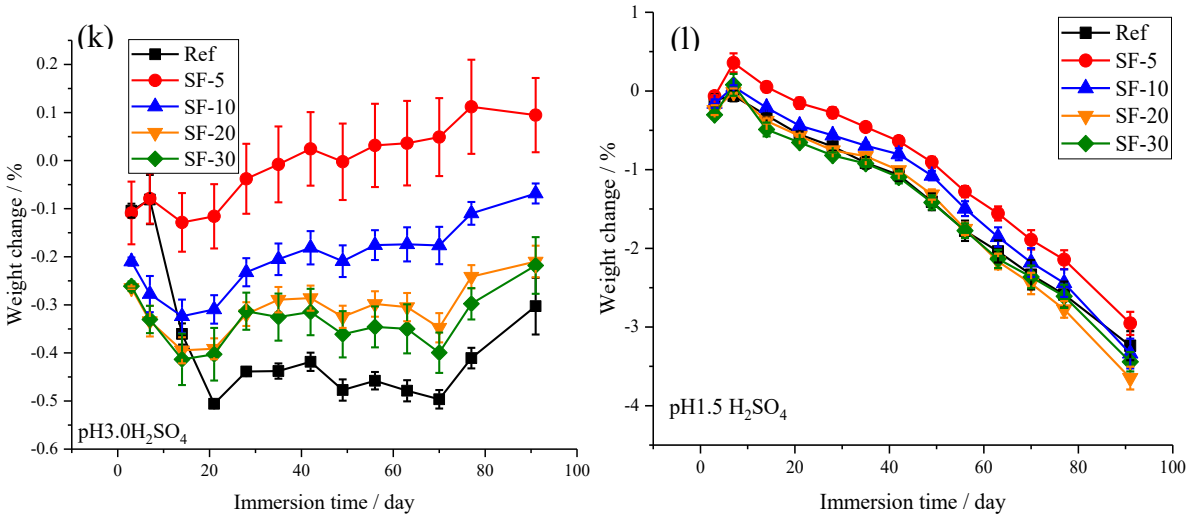

Figure 3.9. Mass changes of samples with immersion time under various immersion pH: (a)~(d) mixtures with fly ash; (e)~(h) mixtures with metakaolin; (i)~(l) mixtures with silica fume

3.3.4.2. The relationship between mass change and replacement ratios under pH1.5 acid

Apart from the acidity of H_2SO_4 acid, the pozzolan type and percentage in the mixture also had a great influence on the mass change of samples. Here, the samples immersed in pH1.5 acid were taken as an example because it has a near-linear trend and pH1.5 represents the most severe corrosion condition. Figure 3.10 demonstrates the relation of the pozzolan replacement ratio with the total mass loss after three months of immersion in pH1.5 H_2SO_4 acid. First, as the replacement ratio increased, the fly ash sample had a decreased mass change and peaked at the replacement of 20% with a value of -3.12%. However, the optimal replacement ratio varies in various literature. On the one hand, Torri et al. (Torii & Kawamura, 1994a) found that 50% replacement of fly ash resulted in the lowest mass change after 36 months of immersion in a 2% H_2SO_4 acid. On the other hand, Aydın et al. (Aydın et al., 2007) observed that mass loss decreased with the replacement ratio (≤70%) after 60 days of immersion in a 5% H_2SO_4 acid. The reason for the varied optimal fly ash replacement could be due to: 1) the difference in the acidity of immersing acid—this is discussed in Section 2.3.4.3; 2) the variation in compositions and reactivity of the fly ash,

depending on the source (Carette & Malhotra, 1987). Second, the replacement of metakaolin showed little effect on the mass change since the value only ranged from -3.21% to -3.29%. In particular, the mixture with 5% metakaolin had the lowest mass change, showing only about 0.03% less mass loss than the reference mixture. This conforms to the findings in the research by Kannan and Ganesan (Kannan & Ganesan, 2014), where a negligible improvement in the mass loss was revealed from metakaolin shotcrete samples when immersed in 5% H_2SO_4 acid for up to 12 weeks. The insignificant effect of the metakaolin addition on the mass loss was attributed to a high proportion of alumina in metakaolin (~40% of Al_2O_3) (Siddique & Khan, 2011). When immersed in H_2SO_4 acid, the high alumina content enhanced the generation of expansive ettringite, leading to internal cracking and severe deteriorations. This deterioration compensates for the positive effect against acid corrosion from the refined pore structure of metakaolin shotcrete samples (Kannan & Ganesan, 2014), leading to the negligible effect of metakaolin replacement on mass loss. Third, among all three pozzolanic materials, silica fume showed the most significant effect on the mass change of samples (see Figure 3.10). The mixture SF-5 demonstrated the lowest mass change among all 13 mixtures, with a value of -2.95%. This result is consistent with the research by Torii and Kawamura (Torii & Kawamura, 1994a) wherein the mass loss dramatically increased when the replacement ratio of silica fume rose from 5% to 20%. In summary, the addition of pozzolans can be beneficial or detrimental to the mass change of cement-based samples, depending on the replacement ratio. Also, it was found that the effect of pozzolan addition on mass change decreases in the order from silica fume to fly ash to metakaolin, which is consistent with the results from research by Bakharev et al. (Roy et al., 2001).

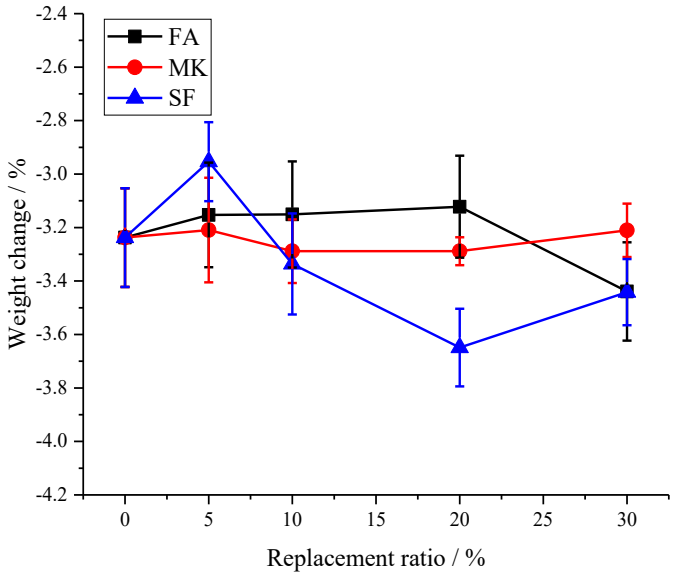

Figure 3.10. Total mass change with replacement ratio in pH 1.5 H_2SO_4 acid

3.3.4.3. Optimum replacement ratio with pH values

Figure 3.11 shows the relationship between final mass change and the pH of acids on the 91st day of immersion. It can be concluded that the optimum replacement ratio (the one with the lowest mass change), varied with pH values. The optimum replacement ratios under different pH are summarized in Table 3.7. Among the three tested pozzolanic materials, only silica fume gives a consistent optimal replacement ratio of 5% regardless of acidity of the immersing acid, due to its lowest mass loss. The optimal replacement of metakaolin and fly ash was dependent on the acidity of immersing, as shown in Table 3.7. For example, as the pH decreased from 6.5 to 1.5, the optimal replacement of fly ash with the lowest mass change varied from 30% to 20%. This phenomenon suggests that the selection of acid concentration should be undertaken with caution during the design of experiments.

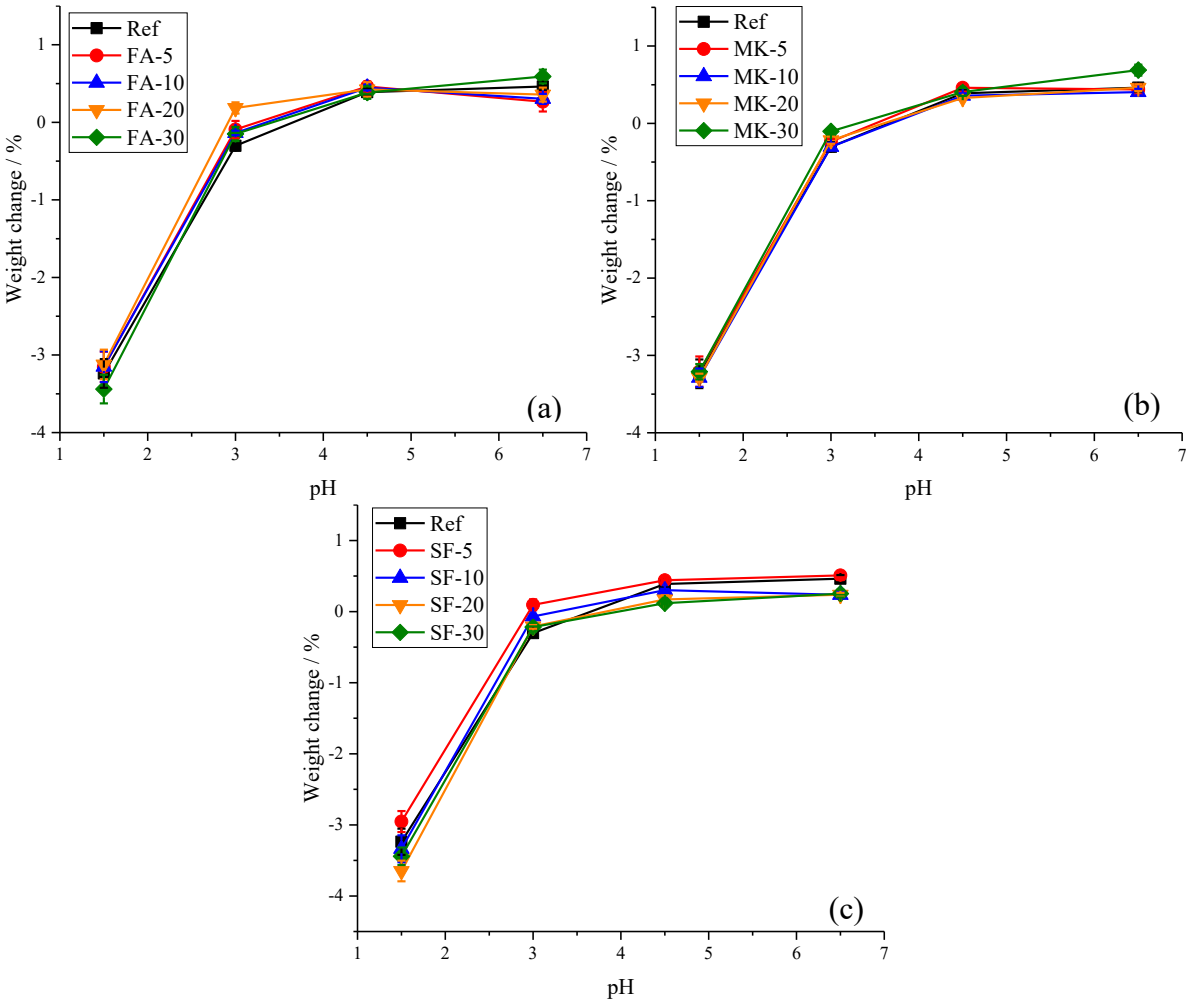

Figure 3.11. Total mass change with the acidity of immersion acid: (a) mixtures with fly ash; (b) mixtures with metakaolin; (c) mixtures with silica fume

Table 3.7. The optimum replacement with the lowest mass change

pH	FA		MK		SF	
	Replacement, %	Mass change, %	Replacement, %	Mass change, %	Replacement, %	Mass change, %
1.5	20%	-3.12%	5%	-3.21%	5%	-2.95%
3	20%	0.19%	30%	-0.10%	5%	0.09%
4.5	5%	0.46%	5%	0.46%	5%	0.44%
6.5	30%	0.59%	30%	0.69%	5%	0.51%

3.3.5. Correlation between mass change and UCS change under acid immersion

As discussed in the previous sections, the addition of pozzolan to the shotcrete mixtures improves acid resistance of shotcrete, regarding mass change and UCS change. However, the results from mass change and UCS change could be very different. Figure 3.12 shows the linear correlation between UCS change and mass change. It can be seen that the correlation between UCS change and mass change was relatively low with a Pearson's correlation coefficient of 0.76, as shown in Figure 3.12. The lack of correlation between mass change and strength change was also reported in research conducted by Chang et al. (Chang et al., 2005). The inconsistent results from mass change and UCS change indicated that neither mass change nor UCS change alone could reflect acid resistance accurately. First, mass change alone is not suggested because the precipitation of corrosion products in the pores could largely influence the results. As discussed in Section 2.3.4.1, the mass gain was observed during immersion, which could be misleading for acid resistance evaluation. In addition, some research suggests that the mass change of samples is greatly dependent on the sample density (Alexander et al., 2013), which is highly affected by the mixture design. Second, the UCS change alone is also not a good indicator because it is affected not only by acid corrosion but also by the continued cement hydration and pore filling by corrosion products (Tsubone et al., 2016). Hence, further research is ongoing to develop a better parameter or evaluation system for the assessment of acid resistance.

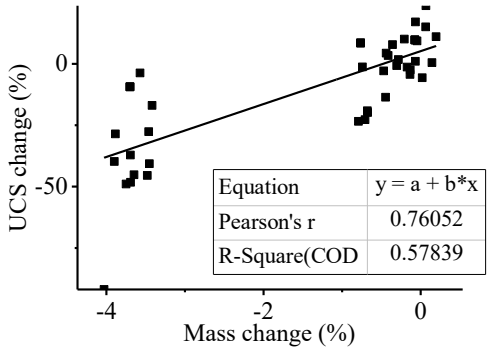

Figure 3.12. Low correlation between UCS change and mass change

3.4. Conclusions

The following are the conclusions drawn from this study:

(1) The substitution of metakaolin and silica fume reduces the volume of permeable voids of samples, while the replacement of fly ash has little effect on the water absorption and volume of permeable voids. Among all the mixtures, the one with 30% metakaolin had the lowest water absorption and permeable voids.

(2) From the unconfined compressive strength (UCS) results, it is concluded that, after 28 days of curing, a partial replacement of cement with silica fume and metakaolin improved the UCS of shotcrete samples, whereas the incorporation of fly ash reduced the UCS of the samples.

(3) There was a significant UCS gain in the early ages (0-21 days) of acid immersion. A lower pH of immersion acid leads to a higher UCS at earlier ages. There is an optimal percentage at which the sample has the lowest UCS change. Also, the optimal percentages for the lowest UCS change depend on the acidity of the immersing acid.

(4) The immersion of shotcrete samples in H_2SO_4 acid can lead to a mass gain. After 91 days of immersion in pH1.5 H_2SO_4 acid, a total moss loss between 2.95% and 3.7% (wt.) was

measured for all mixtures. The mixture with 5% silica fume demonstrated the lowest mass change, with a value of -2.95%, among all 13 mixtures.

(5) Higher acidity results in higher mass change, indicating that the increase of the acid concentration can drastically accelerate the corrosion rate. Therefore, the selection of acid concentration should be performed with caution.

(6) The correlation between mass change and UCS change is relatively low (Pearson's r of 0.76). The difference in acid resistance from mass change and UCS change may indicate that neither mass change nor UCS change alone can reflect acid resistance.

Chapter 4. Effects of nano-silica and silica fume on improving the acid resistance of cement-based composites

*This chapter has been submitted for peer review as **L. Wu**, G. Huang, C. Hu, W.V. Liu, Performance evaluation of nano-silica and silica fume on enhancing the acid resistance of cement-based composites, *Journal of Central South University.* © Elsevier. (under review)

4.1. Introduction

MIC has been recognized as one of the main deterioration mechanisms of concrete sewer tunnels worldwide (Erbektas et al., 2019). The estimated annual cost was €450 million in Germany for the rehabilitation of deteriorated sewer tunnels (Grengg et al., 2018), and around $390 billion is required in the next 20 years for their repair in the United States (Gutiérrez-Padilla et al., 2010). In the MIC process, the abundant sulfate content in wastewater can be converted to hydrogen sulfite (H_2S) via anaerobic biological activities. Then, the H_2S is released from wastewater and converted into sulfuric acid at the tunnel crown through a series of aerobic bacterial activities (Li et al., 2019). Owning to the alkaline nature of CH and C-S-H, cement-based composites can be easily corroded by sulfuric acid through the following reactions (Jeon et al., 2020).

$$CH + H_2SO_4 \rightarrow C\overline{S}H \quad (4\text{-}1)$$

$$CSH + H_2SO_4 \rightarrow C\overline{S}H + SiO_2 + H_2O \quad (4\text{-}2)$$

where $C\overline{S}H$ is gypsum ($CaSO_4 \cdot 2H_2O$).

The generated gypsum is expansive (two times larger than cement hydrates) and has no binding capacity (Khan et al., 2019). Under sulfuric acid attack, cementitious structures can be corroded at rates as high as 12 mm/year (in thickness), leading to a gradual loss of their bearing capacity and, finally, structural failure (Wu et al., 2018). This structural failure increases the risk of many public safety issues and reduces the service life of sewer tunnels substantially. First, wastewater leaked from the failed sewer tunnels can contaminate groundwater and waterways, which may result in adverse environmental and public health issues (Davies et al., 2001). Second, since sewer systems operate continuously and mostly out of view, the structural failures may not be identified until sudden surface subsidence (Read & Vickridge, 1997). This sudden subsidence of ground surface

(sinkhole) threatens public safety, blocks ground traffic, and damages other infrastructure (e.g. buildings and cables) and vital services (Bao et al., 2018). Third, the service life of sewer tunnels can be drastically reduced from more than 70 years down to less than 20 years under the sulfuric acid attack (Sun et al., 2016).

In order that the service life of cementitious structures can be extended, one of the approaches is to develop a more acid-resistant concrete mixture. By partially replacing cement with silica fume, much research has indicated that the acid resistance of concrete can be noticeably enhanced (Mehta, 1985; Torii & Kawamura, 1994a; Wu et al., 2019). Torri et al. (Torii & Kawamura, 1994a) investigated the acid resistance of mortar samples and found that the 10% substitution of cement with silica fume inhibited deterioration after 36 months of immersion in 2% H_2SO_4 solution. Mehta et al. (Mehta, 1985) explored the chemical resistance of concrete mixtures and concluded that a 15% substitution of cement with silica fume demonstrated enhanced performance under 1% HCl, 1% H_2SO_4, 1% lactic acid and 5% acetic acid. Wu et al. (Wu et al., 2019) investigated the acid resistance of shotcrete samples and observed that a 5% cement substitution with silica fume showed the lowest mass loss and strength change after three months of exposure to sulfuric acid. The improved acid resistance has been attributed to the following effects: (1) the pozzolanic reaction between CH and silica fume consumes CH. CH was considered the main component leading to the low acid resistance of cement-based composite (Mehta, 1977). In addition, the pozzolanic reaction generates more C-S-H, which densifies the cement-based composites and inhibits the penetration of aggressive chemicals (Amin & Bassuoni, 2017; Bassuoni & Nehdi, 2007; Gutberlet et al., 2015). (2) The silica fume of a smaller size is reported to fill small pores such as those in the interfacial transition zone in the cement-based composites, which also makes the cement-based composites denser (Duan et al., 2013).

Furthermore, nanoparticles have been increasingly used in cement-based composites. Since nano-silica has a smaller particle size (1–100 nm) and higher reactivity, the pozzolanic reaction could be faster and the filler effect could be more significant. Thus, nano-silica could have better performance than silica fume in improving the acid resistance of cement-based composites. Research has been conducted to investigate the acid resistance of cement-based composites incorporating nano-silica. For instance, Diab et al. (Diab et al., 2019) immersed three grades of concrete (55 MPa, 80 MPa and 90 MPa) in nitric acid and sulfuric acid for 360 days. They found that the inclusion of nano-silica enhanced acid resistance in terms of strength loss, weight loss, and UPV loss. Mahdikhani et al. (Mahdikhani et al., 2018) investigated the durability of concrete samples under sulfuric acid rain leaching. It was found that the incorporation of nano-silica reduced weight loss at all ages of leaching. In other words, acid resistance was improved by the addition of nano-silica.

However, commercial nano-silica is much more expensive than silica fume (Biricik & Sarier, 2014). The price of commercial nano-silica can be more than 8800 US dollars per tonne (Quercia Bianchi, 2014), compared with 640 US dollars per tonne for silica fume (Assi, 2017). Thus, it is economically important to compare the efficiency of nano-silica and silica fume in improving acid resistance. This can help end-users in their decision-making regarding the selection of admixtures. However, very few studies have been carried out to compare the effects of silica fume and nano-silica on the acid resistance of cement-based composites. Among the studies that have been conducted to date, contradictory results have been reported. For example, Hendi et al. (Hendi et al., 2017) and Amin et al. (Amin & Bassuoni, 2017) found that the substitution of silica fume performed better than nano-silica in resisting sulfuric acid. However, Mahmoud et al. (Mahmoud & Bassuoni, 2020) conducted three phases of sulfuric acid immersion tests (Phase #1: pH 4.5 for

12 weeks; Phase #2: pH 1 for 12 weeks; and Phase #3: pH 0.5 for 12 weeks) on concrete samples with silica fume and nano-silica. They found that only the mixtures with nano-silica demonstrated enhanced acid resistance during Phase #2 immersion. Furthermore, contradictory results were also reported on acid resistance of silica fume containing mixtures. For example, Hewayde et al. (Hewayde et al., 2003) found that concrete with silica fume exhibited no improvement in sulfuric acid resistance, which is contrary to the previous research (Mehta, 1985; Torii & Kawamura, 1994a). More specifically, Rahmani et al. (Rahmani et al.) found that the sulfuric acid resistance of silica fume mixtures depended on the acidity of the immersion solution. Furthermore, other testing conditions such as wetting-drying cycles, immersion time, and the ratio of sample surface to acid volume were also reported to affect concrete deterioration drastically (Attiogbe & Rizkalla, 1988; Rombén, 1980; Wafa, 1994). Since there is currently no standard testing procedure in acid resistance evaluation, these immersion conditions could be significantly different in various studies. Thus, it is crucial to compare the effects of silica fume and nano-silica on the acid resistance of cement-based composites under the same testing procedure. In addition, it is environmentally significant to carry out this research as the silica fume is the waste from the metal and alloy production industry, while nano-silica can be extracted by processing silica fume (Tokyay, 2016). Exploring the use of silica fume and nano-silica can help with the recycling of this industry waste.

In this regard, this study aims to compare the performance of silica fume and nano-silica in enhancing the acid resistance of mortar mixtures. The silica fume was added to substitute for cement in mixtures at ratios of 5%, 10% and 15%, while the nano-silica was used as a cement substitution at ratios of 0.5%, 1%, 1.5% and 2%. The samples were exposed to a sulfuric acid

solution with a pH of 2 for 75 days. Acid resistance was evaluated by monitoring the change in mechanical strength, mass, and length.

4.2. Methodology

4.2.1. Materials and mix proportions

In this research, the general use (GU) type of Portland cement was used as the binding material. Table 4.1 lists the chemical compositions of the cement. The fine aggregate used in the mixtures was the typical sand for concrete making, with a bulk density of 1575 kg/m^3 and water absorption of 1.5%. Figure 4.1 presents the sieve analysis of the aggregates. The particle-size distribution of the sand was in the American Concrete Institute (ACI) grade zone #1 (ACI Committee 506, 2016). The silica fume, sourced from a local supplier, was added to the mortar mixture to partially replace cement at ratios of 5%, 10% and 15%. The silica fume had a Brunauer-Emmett-Teller (BET) surface area of 2.808 m^2/g; its primary chemical composition is listed in Table 4.2. The nano-silica was sourced from a local supplier, and the main physical and chemical properties of it are presented in Table 4.3. Nano-silica was added to the mixtures as a substitution for Portland cement at ratios of 0.5%, 1.0%, 1.5% and 2.0%. In this study, the dosage selection for nano-silica and silica fume was generally based on the following reasons. First, the dosage with the best mechanical strength is included because strength is a critical parameter for the design of underground structures. Studies have reported that the optimum dosage with high strength was in the range of 0.5-1% for nano-silica (Berra et al., 2012), and 5-10% for silica fume (Siddique, 2011; Wu et al., 2019). Second, excessive nano-silica leads to particle agglomeration that acts as defects in samples. Significant agglomeration has been reported at dosages of $\geqslant$1.5% (Khaloo et al., 2016). Thus, the max dosage of nano-silica was set at a relatively low value of 2%. Third, excessive dosage (>10%)

of silica fume could lead to a reduced cement content and a significant amount of unreacted silica fume in the sample that reduces the mechanical strength (Wong & Abdul Razak, 2005; Wu et al., 2019). The mixture proportions are presented in Table 4.4.

Table 4.1. Main composition of type GU cement

Oxide	MgO	Al_2O_3	SiO_2	SO_3	CaO	Fe_2O_3
w.t%	4.6	3.8	19.9	2.9	62.2	3.50

Table 4.2. Primary composition of silica fume

Oxide	MgO	Al_2O_3	SiO_2	P_2O_5	SO_3	K_2O	CaO	Na_2O	Fe_2O_3
w.t%	0.29	0.14	95.6	0.1	0.26	0.53	0.38	0.15	0.07

Table 4.3. Physical and chemical properties of nano-silica

Properties	Nano-silica
Surface area, m^2/g	295 (BET)
Tamped density, g/L	50
Loss on drying, %	<1.5
pH value, %	3.7-4.5
Al_2O_3, %	< 0.03
Fe_2O_3, %	< 0.003
TiO_2, %	< 0.03
HCl, %	< 0.020
SiO_2 content, %	> 99.8

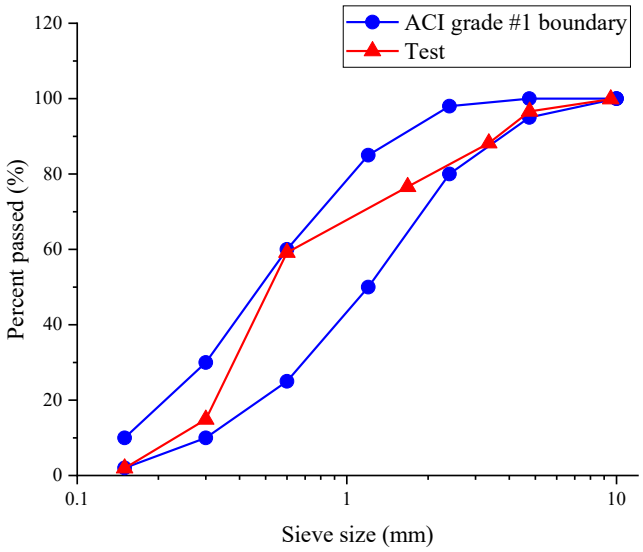

Figure 4.1. Sieve analysis of fine aggregates

Table 4.4. Proportioning of mixtures with silica fume and nano-silica

No.	Mixture ID	Cement kg/m^3	Water kg/m^3	Sand kg/m^3	Admixtures kg/m^3	Admixture content, %		w/c
1	Reference	493.25	221.96	1541.4	0	0		0.45
2	SF5	468.59	221.96	1541.4	24.66	5		0.45
3	SF10	443.93	221.96	1541.4	49.33	10		0.45
4	SF15	419.26	221.96	1541.4	73.99	15		0.45
5	NS0.5	490.78	221.96	1541.4	2.47	0.5		0.45
6	NS1.0	488.32	221.96	1541.4	4.93	1		0.45
7	NS1.5	485.85	221.96	1541.4	7.41	1.5		0.45
8	NS2.0	483.39	221.96	1541.4	9.88	2		0.45

4.2.2. Sample preparation

Cylindrical mortar samples were cast as per ASTM C192-16a (ASTM, 2016b). For mixtures with silica fume, the cement, fine aggregate and silica fume were mixed in a mixing drum for 3 minutes, then water was added to the mixture and mixed for another 3 minutes. For mixtures with nano-silica, only the cement and fine aggregate were dry mixed in the mixing drum. The nano-silica was added and stirred in the water to make a suspension. Then, the suspension was added to the mixing

drum for another 3 minutes of mixing. The fully mixed wet mixture was cast into Φ50×100 mm cylinder molds and stored under an ambient environment for 24 hours. Then the cylindrical samples were de-molded and stored in a moisture room with a temperature of 25 ± 2 °C and relative humidity of 100% for 28 days.

4.2.3. Testing procedure

Prior to sulfuric acid immersion, some basic properties were tested on the hardened samples. First, the density, absorption, and volume of permeable voids were tested as per ASTM C642-13 (ASTM, 2013). For each mixture, three samples were used in the test, and then an averaged value was calculated. Second, a thermo-gravimetric analysis (TGA) was conducted to examine the hydration degree and hydration products of each mixture. In order that the effects of aggregate on the TGA results are eliminated, cylindrical paste samples were made for each mixture (without fine aggregate). After 28 days of standard curing, two thin slices of the paste samples were cut and ground into small particles. Then, the particles were immersed in acetone for 48 hours to extract free water and therefore stop the hydration reaction. After the acetone immersion, the particles were oven-dried at 60 °C for 24 hours and further ground into powder smaller than <63 μm for the TGA test. For each test, 1.2 ± 0.05 g of a sample was heated under a nitrogen atmosphere from 20 °C to 980 °C at a heating rate of 10 °C per minute. Third, the unconfined compressive strength (UCS) was monitored based on ASTM C39 / C39M – 18 (ASTM, 2018). Three samples were tested to calculate the average values.

Then, the samples were soaked in the sulfuric acid solution with a pH of 2. The ratio between acid volume to sample surface area was kept constant with a value of 5.09 (one liter of acid per sample). Concentrated sulfuric acid was regularly (every five days) added to the immersing solution to

maintain the acidity. During immersion, the ultrasonic pulse velocity (UPV), mass, and length of samples were monitored every 15 days. Prior to the tests, the samples were dried in the ambient environment for 24 hours to eliminate the effects of moisture on mass and UPV.

After 75 days of immersion, the samples were moved out from the immersing acid for further evaluation. One sample of each mixture was cut from the middle for visual observation. The cross-section was dyed with phenolphthalein to assess the degree of corrosion visually. Then the rest of the samples were dried and tested for final mass, length, and UPV. After that, the samples were brushed with a steel brush to remove the corrosion layer, and the mass and length were remeasured to obtain the values after brushing. Finally, the UCS test was carried out to evaluate mechanical performance after sulfuric acid immersion.

4.3. Results and discussion

4.3.1. Properties before sulfuric acid immersion

4.3.1.1. Density, water absorption and permeable voids

The durability of concrete against sulfuric acid is closely related to the water absorption and volume of permeable voids of cement-based composites (Hossain et al., 2016; Supit & Shaikh, 2015; Wang et al., 2015). Thus, the tests for density, water absorption, and volume of permeable voids were conducted for all mixtures. The results are plotted in Figure 4.2 and Figure 4.3 for silica fume mixtures and nano-silica mixtures, respectively. It can be seen from Figure 4.2 (a) that the incorporation of silica fume increased the bulk density from 2045.7 kg/m^3 for the reference mixture to 2071.3 kg/m^3 for the mixture with 5% silica fume. Then the bulk density decreased with the increase of silica fume content, reaching 2030.5 kg/m^3 for the mixture with 15% silica fume. The increased bulk density at 5% silica fume could have been due to the reduced porosity that resulted

from the generation of secondary C-S-H from pozzolanic reaction (Poon et al., 2006) and from the pore-filling effects of silica particles (Abbass et al., 2019). The reduced bulk density at higher silica fume content could have been caused by the lower specific gravity of silica fume (2.2-2.3 compared with 3.15 for Portland cement). The reduced bulk density at higher silica fume content could have been caused by the lower specific gravity of silica fume (2.2-2.3 compared with 3.15 for Portland cement). The increase in silica fume dosage reduces the availability of CH for pozzolanic reaction, thus leads to a higher content of unreacted silica fume. The unreacted particles acted as either inert filler or defects in the matrix (Yajun & Cahyadi, 2004) that reduced the bulk density of samples. The existence of unreacted silica fume can be confirmed from the TGA results in this study by comparing the actual and theoretical CH content which can be calculated based on the method proposed by Rupasinghe et al. (Rupasinghe et al., 2017) and Dodson et al. (Dodson, 1990), respectively. It was found that the actual CH content was around 23%, 20% and 18% for the mixture with 5%, 10% and 15%, respectively, while the corresponding theoretical values were around 20%, 16% and 13%. Higher actual CH contents than the theoretical values suggest that only part of the silica fume was reacted. Another contributing reason for the reduced bulk density is the generated low Ca/Si CSH. The CSH generated from the pozzolanic reaction has a lower Ca/Si ratio than that of CSH from cement hydration reaction (Bassuoni & Nehdi, 2007; Richardson, 1999). It is reported that the density of CSH is linearly proportional to the Ca/Si. A lower Ca/Si ratio leads to a lower density of CSH (Bahafid et al., 2017; Pelisser et al., 2012). The apparent density generally decreased with the increase of silica fume content. It reduced from 2500.4 kg/m^3 for the reference mixture to 2353 kg/m^3 for the mixture with 15% silica fume. The reduction in apparent density suggests that the volume of impermeable voids is increased (ASTM, 2013). It was found that the silica fume addition led to an increase in pores smaller than 40 nm for

mortar samples (Torii & Kawamura, 1994b), which are more impermeable (Mehta & Monteiro, 2014). The increased C-S-H gel from the pozzolanic reaction may be responsible for the increase in the impermeable voids, as gel pores <20 nm coexist with C-S-H gel (Quercia et al., 2014; Zhang et al., 2012). Figure 4.2 (b) illustrates the water absorption and volume of permeable voids. Both the water absorption and volume of permeable voids were decreasing with the increase of silica fume content. Water absorption decreased from 8.55% for the reference mixture to 6.67% for the mixture with 15% silica fume, while the volume of permeable voids reduced from 18.19% to 13.71%. This finding is in good agreement with previous research. Wu et al. (Wu et al., 2019) found that the volume of permeable voids was decreasing with silica fume content until it reached 20%. The reduced water absorption and volume of permeable voids suggests a reduction in large pores. This finding coincides with previous studies. Torii et al. (Torii & Kawamura, 1994b) found through a mercury intrusion test that the silica fume addition reduced the pores larger than 100 nm, which are water-permeable pores. Similarly, Yajuun et al. (Yajuun & Cahyadi, 2002) observed that the pores larger than 10 nm decreased significantly from 19.38% for the reference mixture to 15.06% for the mixture with 15% silica fume.

Figure 4.3 (a) shows the results of bulk density and the apparent density of mixtures containing nano-silica. The bulk density generally increased with nano-silica content from 2045.7 kg/m^3 for the reference mixture to 2056.6 kg/m^3 for the mixture with 1% nano-silica. This can be attributed to the pore filling effect and the enhanced cement hydration that made the mortar denser (see Section 3.1.2). Then, the bulk density was reduced when more cement was replaced with nano-silica, reaching 2039.1 kg/m^3 for the mixture with 2% nano-silica. The particle agglomeration could be responsible for this reduction. It was found that ≥1.5% nano-silica led to significant agglomeration which acted as defects in mortar samples (Khaloo et al., 2016). The agglomerated

particles acted as defects in mortar samples that reduced the bulk density. The apparent density, however, was reduced with the increase of nano-silica content. The mixture with higher nano-silica content showed lower apparent density. The reference mixture had an apparent density of 2500.4 kg/m^3, and the apparent density was reduced to 2454.6 kg/m^3 for the mixture with 2% nano-silica. The decrease in apparent density suggests that the volume of impermeable voids was increased with the nano-silica addition. This is in good agreement with the research of others. Li et al. (Li et al., 2016) found that the addition of nano-silica up to 4% increased pores smaller than 20 nm, while Wu et al. (Wu et al., 2016) observed an increase in pores smaller than 50 nm with nano-silica content up to 2.0%.

Figure 4.3 (b) illustrates the water absorption and volume of permeable voids for nano-silica mixtures. The water absorption decreased slightly from 8.55% for the reference mixture to 7.89% for the mixture with 1.0% nano-silica. The further addition of nano-silica increased the water absorption to 8.03% for the mixture with 2.0% nano-silica. This coincides with the findings by Wu et al. (Wu et al., 2016), which revealed that the mixture with 1% nano-silica showed the lowest porosity. A similar trend was observed for the volume of permeable voids, except the lowest value was found at 1.5% nano-silica content. The increase in water absorption at dosage>1% could be due to the particle agglomeration that act as defects in mortar samples (Khaloo et al., 2016).

Compared with nano-silica, silica fume showed a more significant influence on density and microstructure. For example, the water absorption was reduced from 8.55% to 6.67% by a 15% silica fume addition, while the lowest water absorption was 7.89% at a 1% nano-silica addition. Similar findings on the microstructure of mixtures with silica fume and nano-silica were reported in previous research. Jalal et al. (Jalal et al., 2015) found the capillary water absorption and chloride ion penetration of a mixture with 10% silica fume was lower than that with 2% nano-silica. A

possible reason for this is that the extremely fine particle size of nano-silica can only affect a narrow range of pores. Kong et al. (Kong et al., 2012) found that silica fume with a large particle size was more effective in reducing macropores, while nano-silica was found to be more efficient in refining micropores. Forood et al. (Forood et al., 2016) found a nano-silica addition to mixtures with a water-to-binder ratio of 0.65 significantly reduced porosity for pores between 20-50 nm, but only a marginal reduction in porosity was found for pores larger than 50 nm.

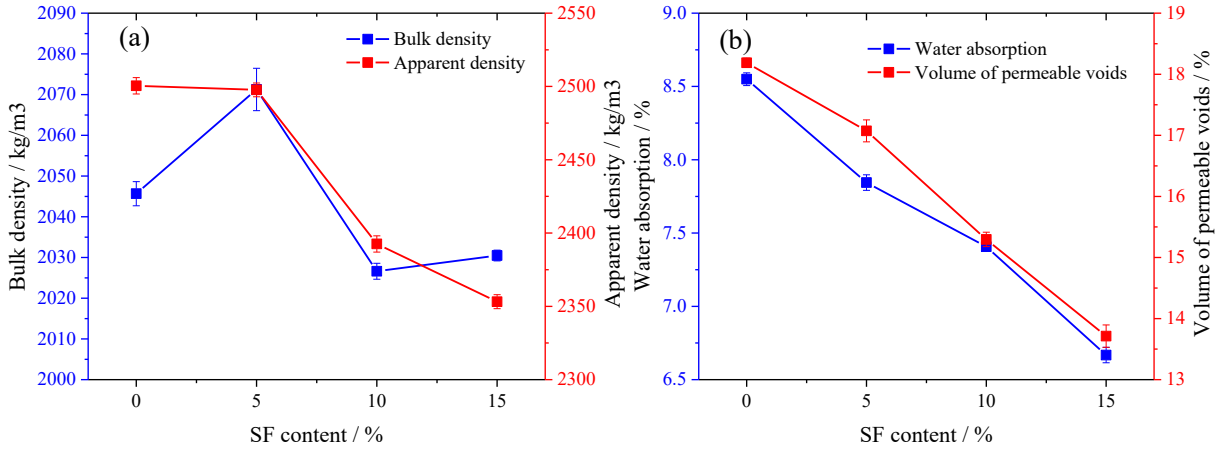

Figure 4.2. Density, water absorption and volume of permeable voids of SF mixtures: (a) bulk density and apparent density; (b) water absorption and volume of permeable voids

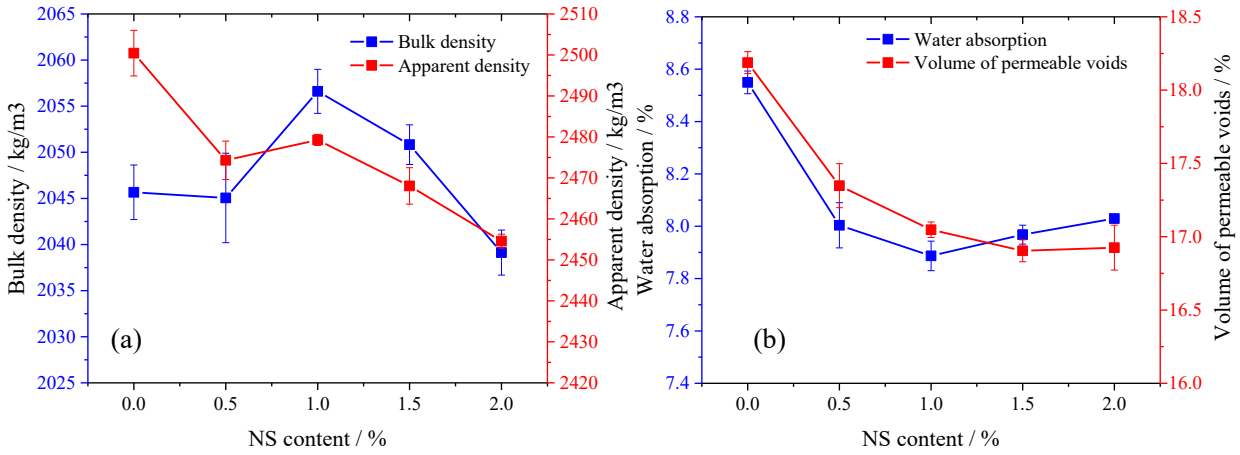

Figure 4.3. Density, water absorption and volume of permeable voids of NS mixtures: (a) bulk density and apparent density; (b) water absorption and volume of permeable voids

4.3.1.2. Thermo-gravimetric analysis

A thermo-gravimetric analysis (TGA) was conducted to evaluate the influence of silica fume and nano-silica on the hydration of cement-based composites. The results are shown in Figure 4.4. There are three main phases of weight loss. The first phase of weight loss starts from room temperature (~20 ℃) to 400 ℃, which results from the dehydration of C-S-H gel and ettringite (Lim & Mondal, 2015). The second phase of weight loss ends at around 560 ℃ (Rupasinghe et al., 2017). The dehydration of CH is responsible for the weight loss at this phase. The last phase of weight loss starting from 560 ℃ to 840 ℃ is caused by the decarbonization of $CaCO_3$ (Rupasinghe et al., 2017).

Figure 4.4 (a) shows the thermo-gravimetric (TG) and derivative of thermo-gravimetric (DTG) curves of mixtures with silica fume. It is noticed that the peak of CH on the DTG curves reduced with the increase of silica fume content, while the peak of C-S-H was increased with the silica fume content. This is attributed to the pozzolanic reaction between CH and silica fume, which consumes CH and generates secondary C-S-H gel (Sargent, 2015). With the increase in silica fume content, more CH is consumed, generating more C-S-H gel, which caused the reduction of the CH peak and the increase of the C-S-H peak on the DTG curves.

Compared with the mixtures with silica fume, the addition of nano-silica showed less pozzolanic reaction as negligible reduction of CH peak was observed for mixtures with nano-silica. This may be caused by the lower dosage of nano-silica than that of silica fume. Despite the low pozzolanic reaction, the substitution of cement with nano-silica increased the final weight loss. The reference mixture had a final weight loss of 22.15%, while a weight loss of 22.17%, 22.95%, 23.22% and 23.44% was found for mixtures with 0.5%, 1.0%, 1.5% and 2.0% of nano-silica, respectively. The

increase in the final weight loss could be caused by the improved hydration caused by the nucleation effect (Abid et al., 2018) and secondary C-S-H generated from the pozzolanic reaction. It can be seen from the residual weight results that the mixtures with nano-silica showed less residual weight at a temperature of 400 ℃ than that of the reference mixture, which suggests that there was more C-S-H gel in the mixtures with nano-silica.

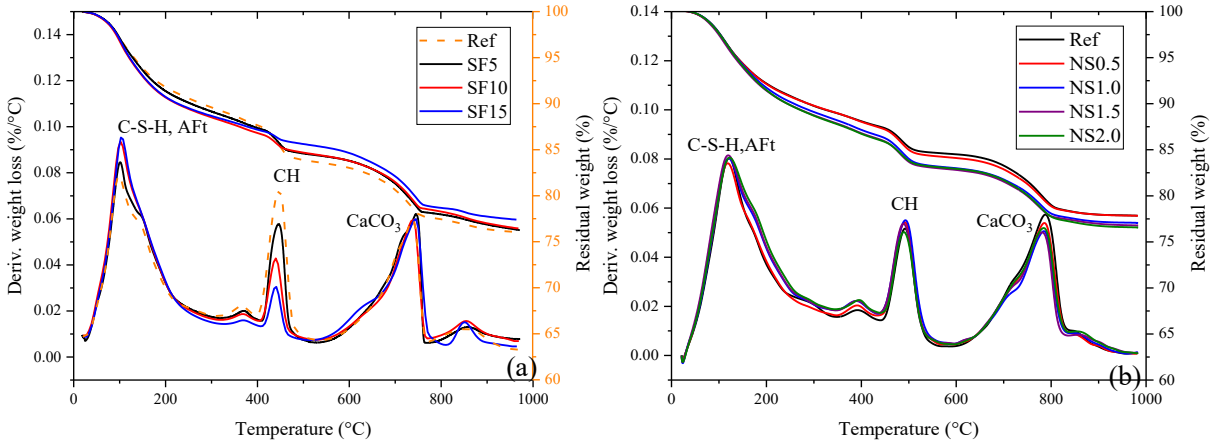

Figure 4.4. TG/DTG curves of mortar mixtures: a) silica fume; b) nano-silica

4.3.1.3. Mechanical strength

Mechanical strength is critical for underground structure performance as it indicates the bearing capacity of the structure. In this study, the UCS was tested after 28 days of standard curing. The results are plotted in Figure 4.5. The addition of nano-silica and silica fume enhanced the UCS of mortar samples. The UCS increased from 34.429 MPa for the reference mixture to 40.159 MPa for the mixture with 1.0% of nano-silica, which accounts for a 16.64% improvement. Then, it dropped back to 35.524 MPa at 2.0% nano-silica. Improved compressive strength has also been reported in previous research (Aydın et al., 2018; Du et al., 2014; Mahdikhani et al., 2018). For example, an improvement of 9% and 12% in UCS was observed by Du et al. (Du et al., 2014) for concrete mixtures with 0.3% and 0.9% nano-silica, respectively. The enhanced UCS may be attributed to the reduced porosity, which is confirmed by the results of water absorption and the

volume of permeable voids. Compared with the nano-silica mixtures, silica fume incorporation showed more significant enhancement of UCS. The UCS increased to 52.7 MPa at 10% silica fume, accounting for a 47% improvement. Then, the UCS reduced to 48.9 MPa at 15% silica fume. This finding has also been reported in previous research. Al-Swaidani et al. (Sadrmomtazi et al., 2009) found that a mixture with a nano-silica content of less than 3% showed lower compressive strength than a mixture with 10% silica fume. This more drastic improvement in UCS by silica fume could be due to the lower volume of water-permeable voids of mixtures with silica fume. It was observed that the silica fume is more effective at refining the pores size distribution, as discussed in Section 3.3.1.1. In addition, the TGA results illustrated that the pozzolanic reaction in mixtures with silica fume was more significant than that in mixtures with nano-silica. This may also be one of the reasons for the more drastic improvement in UCS by silica fume (Aggarwal et al., 2015).

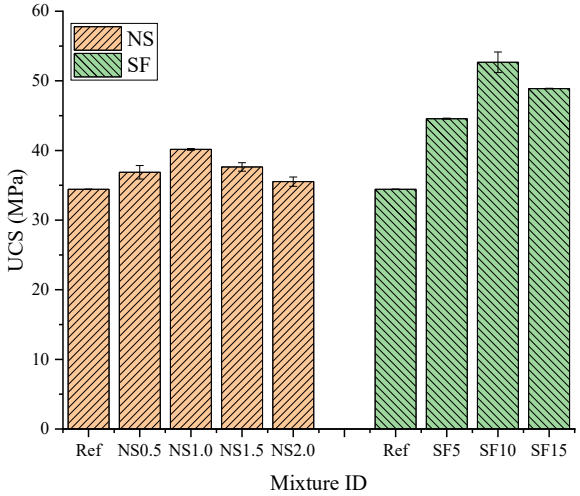

Figure 4.5. UCS of mixtures after 28 days of curing

4.3.2. Properties after sulfuric acid immersion

4.3.2.1. Visual observation

Visual observation was conducted as one of the evaluation methods of sample deterioration. Figure 4.6 shows the cross-section of samples after phenolphthalein spray. The purple area indicates the unneutralized area, while the white/grey area is the neutralized area. From Figure 4.6, the reference sample was severely corroded because a ~1.5mm thick neutralized layer was clearly observed at the surface of the reference sample. With the substitution of 5% silica fume, the thickness of the neutralized layer was significantly reduced. As shown in Figure 4.6 (b), the neutralized layer is noticeably thinner. By adding more silica fume, the neutralized layer became thicker. A neutralized layer of about 2 mm thick was observed for mixtures with 10% and 15% of silica fume. It is also noted that a lower volume of permeable voids did not necessarily lead to a thinner neutralized layer. This is because the addition of silica fume affects a group of mortar properties that influences the acid resistance including porosity, neutralization capability, and chemical stability. First, the addition of silica fume reduced the volume of permeable voids due to the pozzolanic reaction (Poon et al., 2006) and pore-filling effect (Abbass et al., 2019). The reduced volume of permeable voids hindered the acid penetration thus reduced the corrosion degree. Second, the chemical stability of samples was increased due to consumption of CH and the generation of CSH from the pozzolanic reaction. It is reported that the CSH from the pozzolanic reaction has a low Ca/Si ratio, which leads to a more stable structure (Bassuoni & Nehdi, 2007; Richardson, 1999). Third, the replacement of cement by silica fume reduced the content of cement hydration products, thus reduced the neutralization capability. It has been reported that higher neutralization capability could lead to a higher acid resistance (Dyer, 2017; Lin-ping et al.). This reduced neutralization capability led to a thick neutralized layer of about 2 mm at 10% and 15% of silica fume.

For mixtures with nano-silica, inhibited corrosion can be observed compared with the reference mixture as the neutralized layers are relatively thin. But it is difficult to tell which sample showed better performance as the boundary between the neutralized area and unneutralized area is not clear. Thus, more indicators (e.g., mass change and length change) should be used to evaluate the acid resistance.

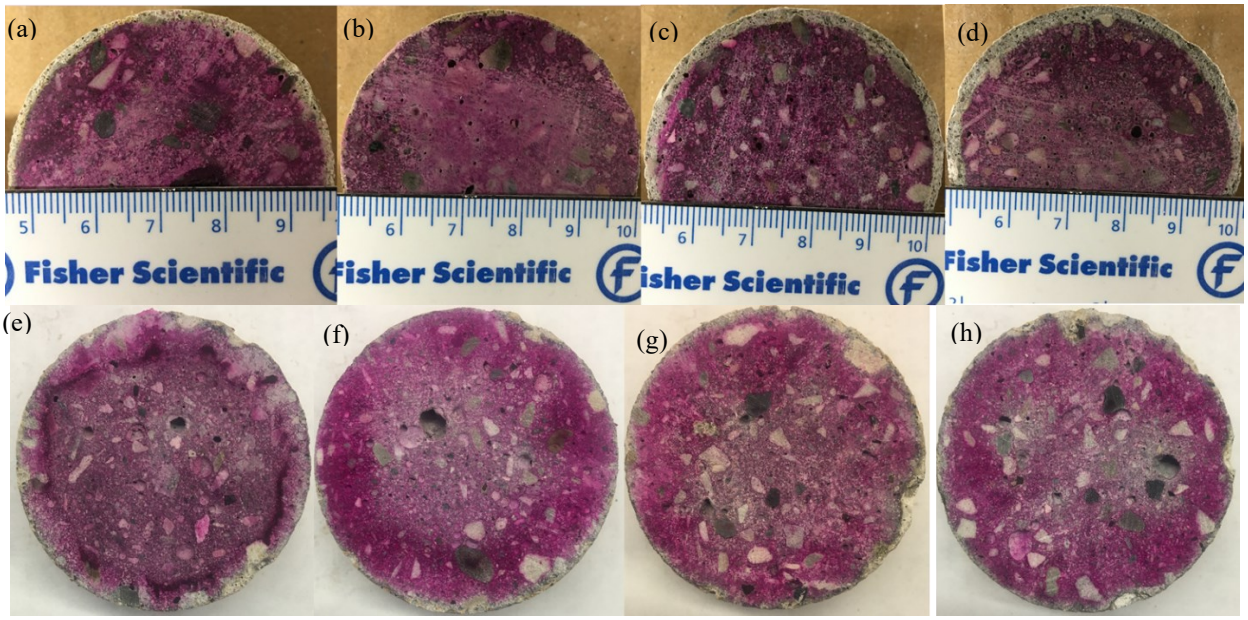

Figure 4.6. Visual observation: a) Ref; b) SF5; c) SF10; d) SF15; e) NS0.5; f) NS1.0; g) NS1.5; h) NS2.0

4.3.2.2. Mechanical strength

The UCS and UCS change after 75 days of acid immersion are illustrated in Figure 4.7. The positive UCS change means a UCS increase, while the negative UCS change indicates a UCS loss. For mixtures with nano-silica, all mixtures showed a positive UCS change. The reference mixture had a UCS change of 21%. The UCS change dropped with the increase of nano-silica content, reaching 4.6% at 1% nano-silica. Then, the UCS change increased again to 13.69% at 2% nano-silica. After the 75 days of sulfuric acid immersion, all mixtures showed a similar UCS of ~42

MPa. A UCS increase during sulfuric acid immersion was also reported in previous research. For example, Makhloufi et al. (Makhloufi et al., 2014) investigated the compressive development of mortars with blended cement during sulfuric acid immersion. It was found that all Portland cement mixtures demonstrated a compressive strength increase during immersion, with the highest strength increase of 30% at the age of 180 days of immersion. They attributed the increase in compressive strength to the continuous hydration of cement. Similarly, Rahmani et al. (Rahmani & Ramzanianpour, 2008) investigated the strength development of Portland-cement-based concrete mixtures under sulfuric acid attack. A strength increase of up to 11.2% was observed after 28 days of sulfuric acid immersion. They attributed the strength increase to the continuous hydration and the filler effect of generated gypsum and ettringite. The continuous hydration has been confirmed in previous research. For example, Feng et al. (Feng et al., 2018) found that the CH content in Portland cement paste increased from 18.36% after 28 days of curing to 21.2% after 90 days of curing. In addition, Al-Swaidani et al. (al-Swaidani et al., 2016) observed a UCS increase of 10-15 MPa from 28 days to 90 days of standard curing. In terms of the filler effect of corrosion product, Tsubone et al., (Tsubone et al., 2016) found that the total pore volume near the boundary between the corroded part and uncorroded part was smaller than that in the inner uncorroded part. This suggests that the pores may be filled by the produced gypsum.

Contrary to mixtures with nano-silica, all mixtures with silica fume showed negative UCS change. The mixture with a higher content of silica fume showed a higher UCS loss. The reference mixture had a UCS change of 21%, while the mixture with 15% silica fume showed a UCS change of -17.5%. After 75 days of sulfuric acid immersion, the mixture with 10% silica fume showed the highest UCS with a value of 46.47 MPa. The other three mixtures showed a similar UCS of 42 MPa. The negative UCS change of silica fume mixtures may be caused by the enhanced hydration

before sulfuric acid immersion. Huang et al. (Cheng-yi & Feldman, 1985) observed that the silica fume particles acted as nucleation sites during cement hydration, which accelerates the cement hydration reaction. More specifically, Kadri et al. (Kadri et al., 2011) observed a higher heat release rate of silica fume mixtures at earlier stages compared with the reference mixture. This accelerated hydration mitigated the effect of continuous hydration on strength development during sulfuric acid immersion.

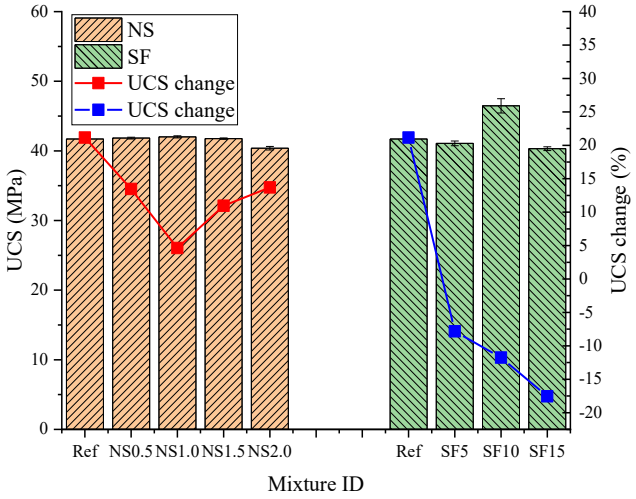

Figure 4.7. UCS and UCS change after 75 days of sulfuric acid immersion

4.3.2.3. Ultrasonic pulse velocity

The test of UPV is increasingly adopted as a non-destructive method to assess the deterioration of cement-based composites (Diab et al., 2019; Jeon et al., 2020; Nematzadeh & Fallah-Valukolaee, 2017; Siad et al., 2016). In this research, the UPV was monitored during sulfuric acid immersion as a possible indicator of sample deterioration. A high UPV indicates a dense microstructure and fewer cracks (Jeon et al., 2020). Figure 4.8 presents the UPV results of mixtures with silica fume and mixtures with nano-silica. Before sulfuric acid immersion, the UPV of mixtures with nano-silica ranged from 4070-4193 m/s, which can be classified as being of good quality (3600-4500 m/s) (Feldman, 1977; Leslie & Cheesman, 1949). The addition of nano-silica and silica fume

enhanced the UPV of mortar samples. For example, the addition of nano-silica increased the UPV from 4070 m/s for the reference mixture to 4193 m/s for the mixture with 0.5% nano-silica. This can be attributed to the reduced porosity which has been confirmed in Section 3.1.1. Compared with the nano-silica mixtures, the silica fume addition showed a more significant enhancement in the UPV. The mixture with a 5% silica fume showed the highest UPV of 4343.3 m/s.

During sulfuric acid immersion, the UPV of all mixtures was decreasing with the immersion time. This can be attributed to the formation of the corrosion layer on the sample surface (see Section 3.2.1), which has a porous structure. As shown in Figure 4.8 (a), the addition of nano-silica showed a limited effect on the UPV throughout the immersion period as mixtures with nano-silica showed similar UPV values at all ages. After 75 days of immersion, the UPV of mixtures with nano-silica ranged from 3710 to 3800 m/s, which indicates the samples were still of good quality. However, the mixtures with nano-silica had a lower UPV than the reference mixture. Compared with mixtures with nano-silica, the mixtures with silica fume showed a higher UPV. It ranged from 3690 m/s to 3906 m/s after sulfuric acid immersion. The highest UPV was found on the mixture with 5% of silica fume.

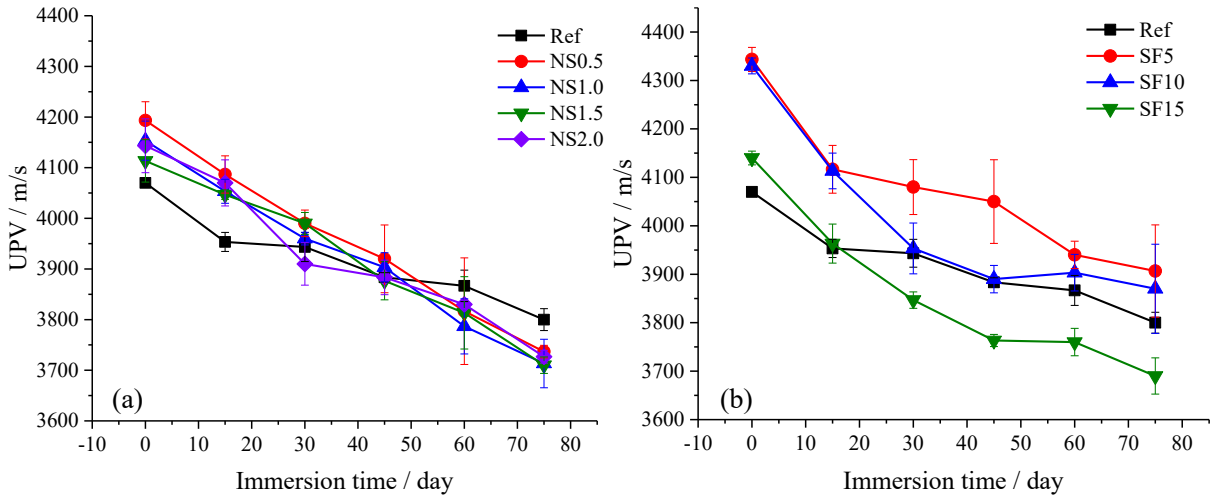

Figure 4.8. UPV with immersion time: 1) NS mixtures; 2) SF mixtures

4.3.2.4. Length change

The sulfuric acid corrosion can result in a length change due to the dissolution of cement hydrates and the peeling off of aggregates. Thus, the change in length was monitored as one of the indicators to evaluate sample deterioration. The length change of mixtures with nano-silica is demonstrated in Figure 4.9. A positive value implies that the sample length was increased. As shown in Figure 4.9 (a), all samples showed a positive length change throughout the immersion period, and the length change increased with immersion time. The reference mixture had the lowest length increase throughout the immersion period. It is also noticed that the nano-silica dosage showed a negligible effect on the length change since the length change of mixtures with nano-silica was similar at all immersion ages. The length change after 75 days of immersion is plotted in Figure 4.9 (b). Before sample brushing, the reference mixture had a length change of 0.12%. The greatest length change of 0.47% was found for the mixture with 2% nano-silica. This positive length change may be caused by the generation of gypsum, which is two times larger compared with cement hydration products (Khan et al., 2019). The length of samples was also measured after removing the corrosion layer on the sample surface, and the results are shown in Figure 4.9 (b) with a blue line. All samples showed a negative length change after removing the corrosion layer. The reference mixture showed a length change of -1.34%. The nano-silica addition slightly reduced the length change to -0.93% for the mixture with 1 % nano-silica. With nano-silica content higher than 1%, a higher length change was observed, with a value of -1.22% for the mixture with 2% nano-silica. The higher length loss at nano-silica>1% could be due to the increased water absorption caused by the agglomeration of nano-silica, which has been confirmed in Section 3.1.1. The increased water absorption enhanced the acid penetration and led to a higher length loss.

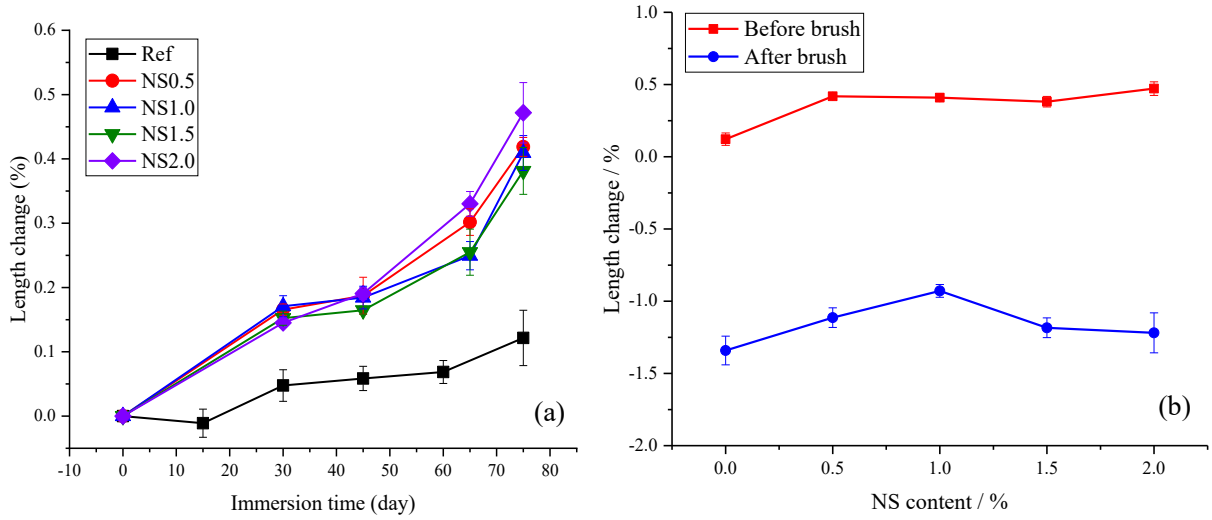

Figure 4.9. Length change of NS mixtures a) with immersion time; b) with NS content after sulfuric acid immersion

The length change of silica fume mixtures is presented in Figure 4.10. Similarly, the mixtures with silica fume also showed a positive length change during immersion. The length change also increased with immersion time. The reference mixture had the lowest length change, while the mixture with 5% silica fume showed the greatest length change in the entire immersion period. The length change after 75 days of sulfuric acid immersion is plotted in Figure 4.10 (b). The mixture with 5% silica fume showed the greatest length change of 0.43%. After sample brushing, the corrosion layer on the sample surface was removed. The length change after sample brushing is plotted in Figure 4.10 (b) with a blue line. All mixtures showed a negative length change. The lowest length change of -0.57% was observed on the mixture with 5% silica fume. This may suggest that the mixture with 5% silica fume has the highest acid resistance. The reduced volume of permeable voids and the increased chemical stability were responsible (as discussed in Section 3.2.1) for the reduced length change for the mixture with 5% of silica fume.

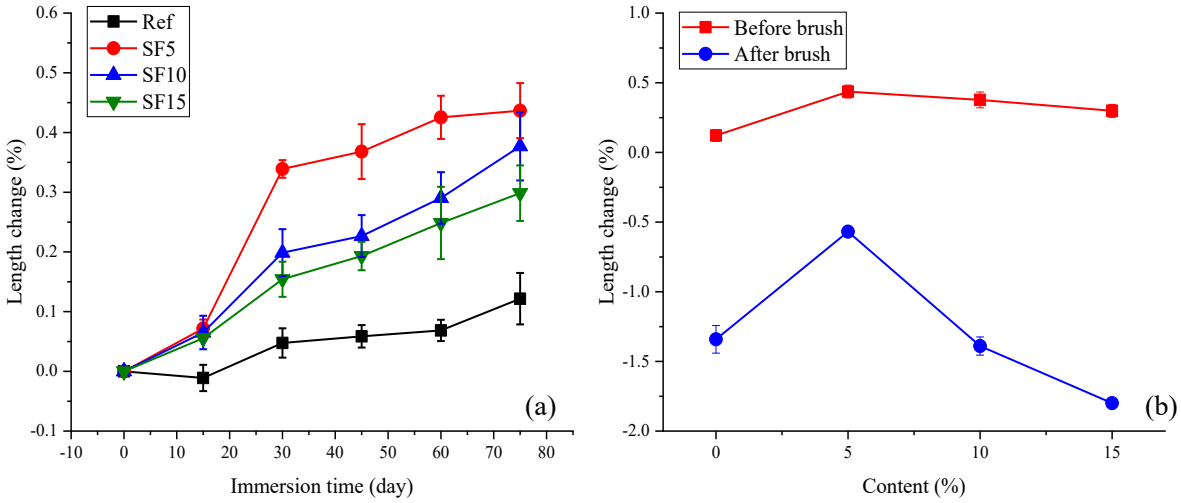

Figure 4.10. Length change of SF mixtures a) with immersion time; b) with SF content after sulfuric acid immersion

4.3.2.5. Mass change

Sulfuric acid corrosion can lead to a loss of sample due to the dissolution of cement hydrates and the peeling off of aggregates. Thus, the change in mass was monitored as another parameter to assess sample deterioration during sulfuric acid immersion. Figure 4.11 illustrates the mass change of mixtures with nano-silica. A positive value indicates mass gain, while a negative value indicates a mass loss. In general, the mass change of all mixtures increased with immersion time for all mixtures. After 75 days of immersion, the mixtures had a mass change ranging from 0.835% to 1.383%, with the mixture with 0.5% nano-silica having the lowest mass change. The increased mass during acid immersion was due to the generation of gypsum that attached to the sample surface (as shown in the visual observation results). To better understand the sample deterioration, the corrosion layer was removed by brushing the samples with a steel brush. The mass change after sample brushing is shown in Figure 4.11 (b). All mixtures showed a negative mass change after brushing. The mass loss reduced from -5.48% for the reference mixture to -4.06% for the mixture with 1% nano-silica, and then the mass loss increased to -4.9% for the mixture with 2%

nano-silica. This suggests that the addition of 1% of nano-silica mitigated the deterioration in terms of mass change.

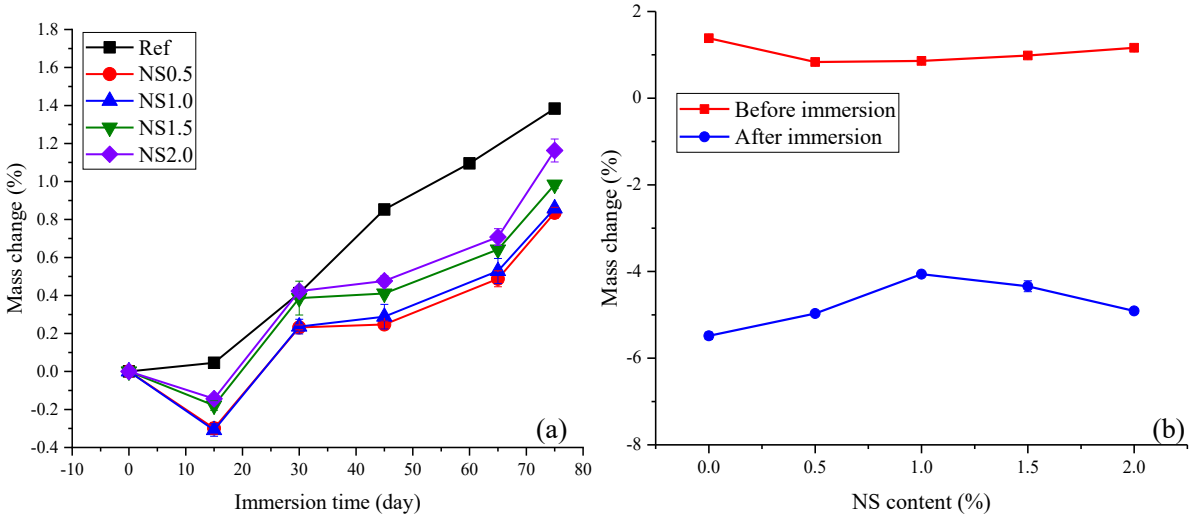

Figure 4.11. Mass change of NS mixtures a) with immersion time; b) with NS content after sulfuric acid immersion

The mass change of silica fume mixtures is plotted in Figure 4.12. Similarly, all mixtures illustrated positive mass change during the immersion period. The mass change after 75 days of immersion ranged from 1.12% for the mixture with 15% silica fume to 1.56% for the mixture with 5% silica fume. After the corrosion layer was removed by brushing, all samples illustrated mass loss. Among the mixtures, the one with 5% silica fume showed the lowest mass loss with a value of -4.15%, compared with -5.48% for the reference mixture. Adding more than 5% silica fume increased the mass loss to -6.63% for the mixture with 15% silica fume. This suggests that the mixture with 5% silica fume showed the best acid resistance in terms of mass change. Compared with nano-silica mixtures, the silica fume mixtures generally showed a higher mass change. The mass change of nano-silica mixtures ranged from -5.48% to -4.06%, while the mass change of silica fume mixtures ranged from -6.63% to -4.15%. This can be attributed to the differences in neutralization ability between these mixtures. As observed in the TGA results, the addition of 15% silica fume reduced

the final weight loss (1.35%), while the addition of 2% of nano-silica increased the final weight loss (1.29%). This suggests that the mixtures with nano-silica had a higher content of cement hydration products, which led to a higher neutralization.

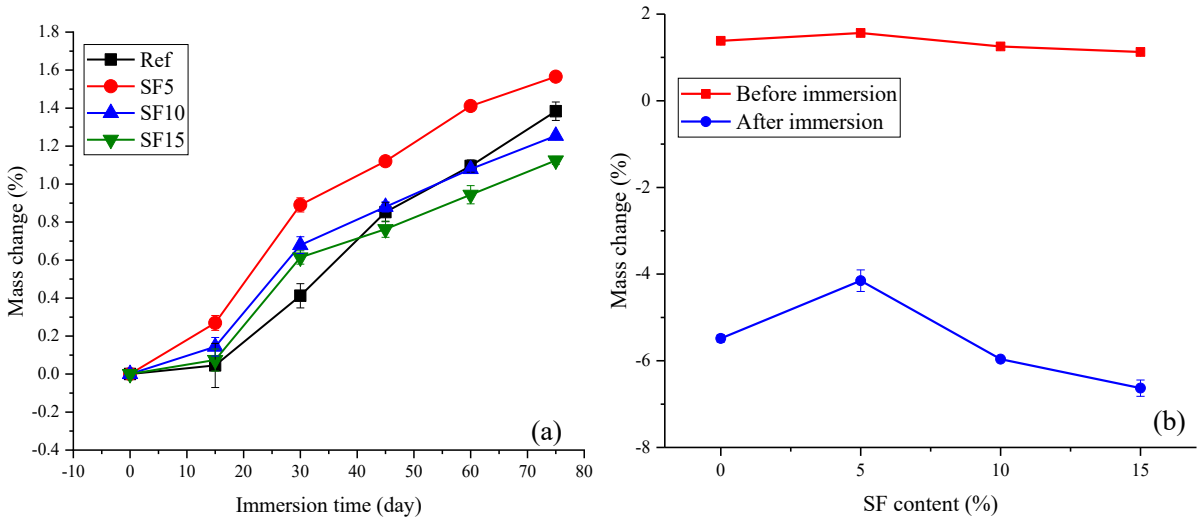

Figure 4.12. Mass change of SF mixtures a) with immersion time; b) with SF content after sulfuric acid immersion

4.3.3. Evaluation of acid resistance

During the sulfuric acid immersion, several tests were conducted to evaluate the acid resistance of mixtures with nano-silica and silica fume. Due to the generation of a corrosion layer on the samples' surface, both mass and length increased during sulfuric acid immersion. The mass change and length change had a good correlation with R^2 of 0.86 and 0.83 for mixtures with nano-silica and silica fume, respectively, as shown in Figure 4.13. However, the positive mass change and length change made the evaluation of sample deterioration difficult because of the complexity of the mechanism of the mass change and length change during immersion. On the one hand, when samples are immersed in sulfuric acid, the CH and C-S-H is decalcified at the presence of H^+ in the pore solution (Grandclerc et al., 2018). This reduces the mass and length of samples. On the

other hand, the chemical reaction between cement hydration products (e.g. CH and C-S-H) and the sulfuric acid generates swelling gypsum that will lead to the formation of a corrosion layer on the sample surface. This causes the mass and length increase during immersion. Thus, to remove the effect of gypsum generation on the mass change and length change, sample brushing with a steel brusher was carried out on samples after 75 days of immersion. The results after brushing showed that the mixture with 5% silica fume and 1% nano-silica had the lowest mass change and length change for silica fume mixtures and nano-silica mixtures, respectively. This reduced deterioration on samples can be attributed to the reduced volume of permeable voids, enhanced chemical stability and cement hydration as discussed in Section 3.1.1 and 3.1.2. Beyond these dosages, higher mass loss and length loss were observed. For mixtures with nano-silica, a possible reason for this is the nano-silica agglomeration that became weak zones in the mortar sample; for mixtures with silica fume, the reduced neutralization capacity was responsible for the high deterioration at high dosage.

However, the UCS and UPV results suggest that other mixtures may have better performances after sulfuric acid immersion. For example, the reference mixture showed a positive UCS change, while all the silica fume mixtures showed negative UCS change after sulfuric acid exposure. In addition, the UPV results indicated that the mixture with nano-silica was of lower quality compared with the reference mixture after 75 days of sulfuric acid immersion. These contradictory results from various indicators may suggest that there is no single indicator that can comprehensively describe the deterioration (Gu et al., 2019). Gu et al. (Gu et al., 2019) compared test methodologies regarding the assessment of deterioration. They concluded that each test method has the following disadvantages: 1) visual observation is a subjective judgment and can be significantly influenced by sample spalling; 2) mass change is highly variable because of the

peeling off of the aggregates; 3) the length is too sensitive to pH change, and may have a high error on rough surfaces. The change in UCS, however, was found in this research to be highly affected by the hydration degree of samples before immersion. At a low hydration degree, such as for the reference mixture, the UCS could be increased during sulfuric acid immersion due to the continuous hydration. This makes the UCS change a poor indicator of sample deterioration. Thus, a combination of indicators should be used to assess the acid resistance of mixtures.

Among all the silica fume mixtures, the one with 5% silica fume showed the best performance in resisting sulfuric acid attack because it had the lowest mass change and length change. In addition, the mixture showed a reasonably high UCS and UPV after sulfuric acid immersion. Similarly, for mixtures with nano-silica, the mixture with 1% nano-silica presented the lowest mass change and length change and a reasonably high UCS. This suggests that for the mixtures with nano-silica, a 1% addition has the best potential with regard to resisting sulfuric acid.

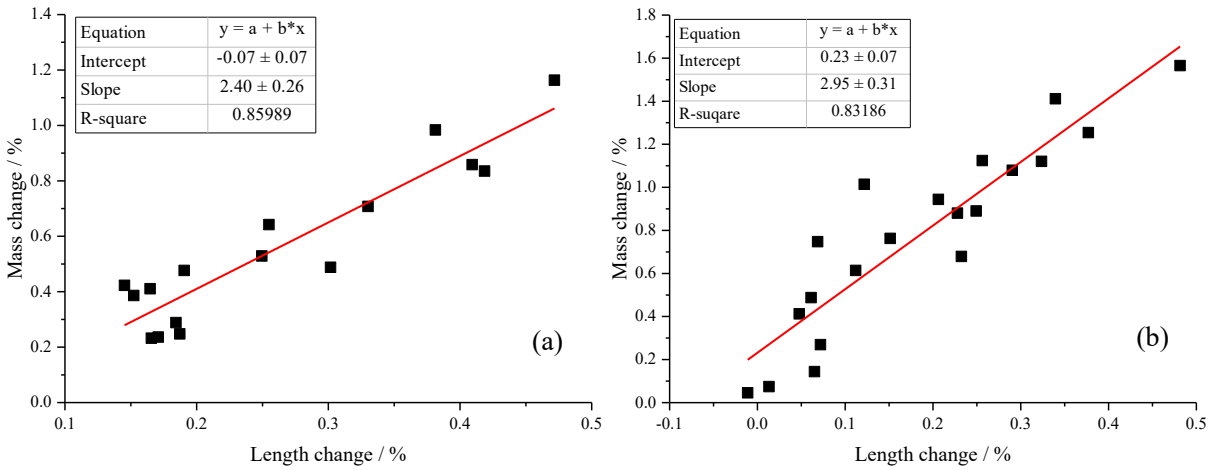

Figure 4.13. Correlation between length change and mass change (before brush): a) NS mixtures; b) SF mixtures

4.4. Conclusions

The mortar samples with silica fume and nano-silica were immersed in sulfuric acid (pH=2) for 75 days to investigate acid resistance. From the test results, the following conclusions can be drawn:

(1) From the density, water absorption, and permeable voids results, the addition of silica fume and nano-silica reduced the water absorption and volume of permeable voids. In addition, the silica fume showed a more drastic influence on the water absorption and volume of permeable voids compared with nano-silica.

(2) From the thermo-gravimetric analysis result, the addition of silica fume significantly reduced calcium hydroxide and increased calcium silicate hydrates in the hardened samples. This is attributed to the pozzolanic reaction between calcium hydroxide and silica fume. The addition of nano-silica showed a negligible effect on cement hydration as there was no significant change in the amount of calcium hydroxide and calcium silicate hydrates.

(3) The addition of nano-silica and nano-silica improved the unconfined compressive strength after 28 days of curing. However, the silica fume showed more significant improvement than that of nano-silica, with the greatest improvement of 16.7% and 47% for nano-silica mixtures and silica fume mixtures, respectively.

(4) The sulfuric acid immersion test illustrated that the silica fume was more effective than nano-silica in improving the acid resistance of cement mortars. The optimal dosages with best acid resistance were 1% and 5% for nano-silica and silica fume, respectively. However, the mixture with 5% silica fume illustrated noticeably better performance than

the one with 1% nano-silica as it had less length change, and higher compressive strength and ultrasonic pulse velocity after 75 days of immersion.

(5) The selection of indicators for deterioration evaluation could significantly affect the evaluation of acid resistance because contradictory results were found from different test methods. This suggests there is no single indicator that is able to describe the deterioration comprehensively.

Chapter 5. Effects of calcium aluminate cement on the acid resistance of metakaolin-based geopolymer

This chapter has been submitted for peer review as **L. Wu**, G. Huang, C. Hu, W.V. Liu, Effects of calcium aluminate cement on the acid resistance of metakaolin-based geopolymer. *Advances in cement research.* © ICE Virtual Library (under review)

5.1. Introduction

Geopolymer is an "inorganic polymer" produced by activating aluminosilicate source materials (e.g., fly ash, metakaolin, and slag) with alkali solutions (Bajpai et al., 2020; Duxson et al., 2007). It has been recognized as a sustainable and green material to substitute for the ordinary Portland cement (OPC) due to its low carbon footprint. The production of OPC has been reported to be responsible for about 7% of global carbon dioxide emissions (Voldsund et al., 2019; Worrell et al., 2001), while the production of geopolymer generates a small or no amount of carbon dioxide emissions (Faisal & Muhammad, 2016). A variety of materials can be used for the production of geopolymers including fly ash, metakaolin, slag and natural pozzolan (Kani et al., 2017; Perná & Hanzlíček, 2016; Rovnaník et al., 2018; Zhang et al., 2020). Many of these materials can be sourced from industrial waste. For example, the metakaolin can be sourced from oil sands tailings (De Spot & Wojtarowicz, 2003). Metakaolin-based geopolymer has attracted increasing interest because of its superior mechanical strength and chemical resistance. Karatas et al. (Karatas et al., 2019) explored the compressive strength development of a metakaolin-based geopolymer, having compressive strength as high as 100 MPa after 28 days of curing. By tuning mixture design, Lahoti et al. (Lahoti et al., 2017) obtained a high compressive strength of 78.96 MPa. Furthermore, Palomo et al. (Palomo et al., 1999) investigated the chemical resistance of a metakaolin-based geopolymer under seawater and sodium sulfate; they found that the samples showed negligible changes in microstructure and strength after 270 days of immersion.

Despite these advantages, the application of metakaolin-based geopolymers is limited due to the lack of a comprehensive understanding of its performance in aggressive environments (Abbas et al., 2020). Among the attacks by aggressive environments, the sulfuric acid attack has been recognized as one of the most common and serious reasons for the deterioration of cementitious

materials (Grengg, 2018). For example, in a sewer system, the sulfur content in the wastewater can be converted to sulfuric acid through a series of bacterial activities, reducing the pH on the concrete surface down to as low as 1 (House, 2013). The sulfuric acid attack has also been a common issue in industrial areas, mines, and areas of acid rains (Barbhuiya & Kumala, 2017; Janfeshan Araghi et al., 2015). In these areas, the pH of the attacking acid could be as low as 1-2 (House, 2013; Jones & Cetin, 2017). In such acidic environments, acid resistance is crucial for the durability and sustainability of cementitious structures. However, limited research has been reported on the acid resistance of metakaolin-based geopolymers. Among these studies, metakaolin-based geopolymers showed insufficient resistance against acid attack. For example, Gao et al. (Gao et al., 2013) investigated the acid resistance of a metakaolin-based geopolymers in a mildly acidic environment (HCl solution with a pH of 2), and a high compressive strength reduction of 37% was found after 28 days of immersion. Bouguermouh et al. (Bouguermouh et al., 2017) immersed the geopolymers activated from three different metakaolin into an HCl solution with a pH of 1.5 for 28 days. However, a high mass loss (up to 9.65%) was observed after 28 days of acid immersion. This insufficient acid resistance could constraint the further application of metakaolin-based geopolymers in aggressive environments.

Thus, it is of great interest to improve the acid resistance of the metakaolin-based geopolymer in acidic environments. One potential method is to blend calcium aluminate cement (CAC) with metakaolin. It has been reported that the addition of CAC was able to accelerate the dissolution of reactive contents in raw materials and facilitate the geopolymerisation process (Fernández-Jiménez et al., 2008; Vafaei & Allahverdi, 2016). Facilitated geopolymerisation is beneficial to the strength development of geopolymer-based materials. Alanazi et al. (Alanazi et al., 2017) observed an enhanced early compressive strength of a metakaolin-based geopolymer in the

presence of CAC. In addition, the incorporation of CAC in geopolymers activated from other raw materials has shown high resistance against sulfuric acid attack. For example, Vafaei et al. (Vafaei & Allahverdi, 2018; Vafaei et al., 2018) investigated the acid resistance of waste glass-based and fly ash-based geopolymers incorporating CAC. They found that these geopolymers with CAC showed superior durability against acid attack by HCl and H_2SO_4. However, no research has explored the effects of CAC on the acid resistance of a metakaolin-based geopolymer. This is of great significance because of the following three-fold benefit. First, the potentially improved acid resistance can enhance the durability of metakaolin-based geopolymers in acidic environments such as industrial areas, sewer tunnels and underground mines. Second, metakaolin can be sourced from oil sands tailings (a mine waste) (Siddique & Khan, 2011). Canada is abundant in this mine waste; in northern Alberta alone, the oil sands fields contain up to 60 million tonnes of kaolin (De Spot & Wojtarowicz, 2003). The use of metakaolin in geopolymer production could help recycle the waste from oil sands operations. Third, the application of metakaolin-based geopolymers emits little carbon dioxide compared with OPC (Bai et al., 2019). The substitution of OPC by metakaolin-based geopolymer could reduce the emission of greenhouse gas, a result which would be more environmentally friendly.

To this end, the main objective of this research is to explore the acid resistance of a metakaolin-based geopolymer with the addition of CAC. The CAC was added to replace the metakaolin at weight ratios of 5% and 10%. The blended raw materials were activated with NaOH and Na_2SiO_3 solutions. The cured geopolymer mortars were immersed in sulfuric acid with a pH of 2 for 75 days. Changes in unconfined compressive strength (UCS), ultrasonic pulse velocity (UPV) and mass and length were monitored to assess sample deterioration.

5.2. Methodology

5.2.1. Materials and mix proportions

All raw materials (metakaolin and CAC) were locally sourced in Alberta, Canada. The chemical compositions of the raw materials are listed in Table 4.2. The fine aggregate used in the mixtures had an oven-dry bulk density of 1575 kg/m^3 and a water absorption of 1.5%. The particle distribution of the fine aggregate fell in the American Concrete Institute (ACI) grade zone #1 (ACI Committee 506, 2016), as shown in Figure 5.1. The liquid alkaline activator was a mixture of NaOH solution and 45% Na_2SiO_3 solution. In order that high mechanical strength can be achieved, a Si-to-Al ratio of 2.5, a water to solids ratio of 0.5, and an Al to Na ratio of 1 were adopted during the mixture design (Lahoti et al., 2017; Rowles & O'connor, 2003). The CAC was added to geopolymer mixtures to substitute metakaolin at weight ratios of 5% and 10%. Mix proportions of geopolymer mortars are listed in Table 5.2.

Table 5.1. Main compositions of raw materials

Constituent (%)	MgO	Al_2O_3	SiO_2	P_2O_5	SO_3	K_2O	CaO	Na_2O	Fe_2O_3
Metakaolin	0.04	45.2	52.3	0.08	/	0.15	0.04	0.22	0.42
Calcium aluminate cement	/	30.10	4.01	/	0.52	0.14	43.58	/	17.28

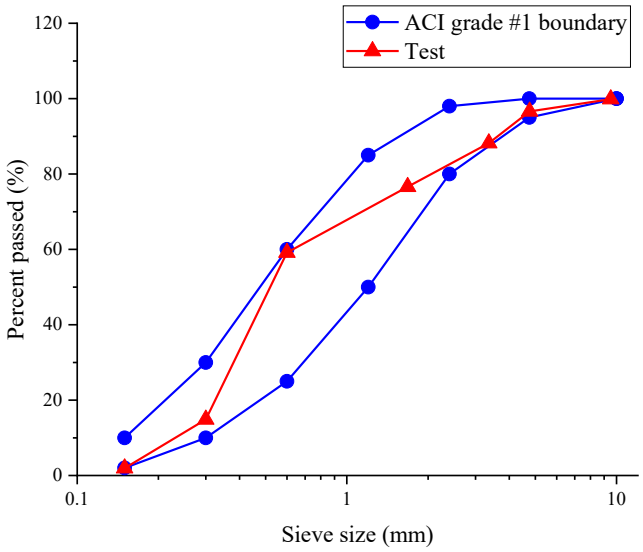

Figure 5.1. Sieve analysis of fine aggregate

Table 5.2. Mix proportions of metakaolin-based geopolymer mortars

Mixture ID	Raw materials, g		Sand, g	Alkali activator, g		
	Metakaolin	CAC		NaOH	Na_2SiO_3	Water
GM	504	0	1512	66.1	179.2	374.36
MC5	478.8	25.2	1512	66.1	179.2	374.36
MC10	453.6	50.4	1512	66.1	179.2	374.36

5.2.2. Sample preparation

The alkali solutions were first prepared by mixing sodium hydroxide and sodium metasilicate pellets with tap water separately. The raw materials were mixed with fine aggregates using a mixing drum for three minutes. When cooled down to room temperature, the alkali solutions were added to the drum and mixed for another three minutes. The readily mixed mixtures were then cast into Φ50×100 mm cylinder molds and stored in an oven at a temperature of 40 °C for 24 hours to accelerate the geopolymerisation process (Atiş et al., 2015). After that, the samples were de-molded and sealed in a plastic container to prevent moisture loss and surface carbonization (Guo

et al., 2010). The sealed container was stored in an ambient environment with a temperature of 25 ± 2 °C for 28 days.

5.2.3. Test procedures

After 28 days of curing, the geopolymer mortar samples were taken out from the sealed container for further tests. The geopolymer mortar samples were divided into two groups. One group of samples was tested before sulfuric acid immersion to investigate the basic properties of geopolymer mortars. These tested properties include the volume of permeable voids, unconfined compressive strength (UCS), thermogravimetric analysis (TGA) and Fourier-transform infrared spectroscopy (FTIR). First, the volume of permeable voids was measured according to the ASTM C642-13 (ASTM, 2013), while the UCS test was conducted based on ASTM C39 / C39M–18 (ASTM, 2018). Second, TGA tests were carried out to identify the geopolymerisation products and geopolymerisation degree. Three thin slices were first cut from a mortar sample of each mixture. These thin slices were then ground into particles, and the large aggregates and particles were sieved out. After that, the sieved particles were soaked in acetone for 48 hours to remove free water and cease the geopolymerisation process. Then, the immersed particles were oven-dried at a temperature of 60 °C for 24 hours to remove the acetone. The oven-dried particles were further ground into powders and sieved with a sieve size of 63 μm. Lastly, 1.2 ± 0.05 g of sieved powders were heated from 20 °C to approximately 980 °C with a heating rate of 10 °C per minute during the TGA test. Third, an FTIR test was conducted for each mixture to investigate geopolymerisation products by distinguishing chemical bonds. A potassium bromide (KBr) pellet was produced for each mixture using 3 mg of geopolymer powder (<63 μm) and 150 mg of KBr. Then, the KBr pellets were used for the FTIR test.

The other group of geopolymer samples was immersed in sulfuric acid with a pH of 2 for 75 days. Concentrated sulfuric acid was added to the immersion solution at an interval of every five days to maintain the acidity. An FTIR test was conducted to examine the change in chemical structures of geopolymer gel after sulfuric acid immersion. In order that sample deterioration can be assessed, UPV, mass, and length of samples were monitored every 15 days during sulfuric acid immersion. Prior to testing, samples were dried in an ambient environment for 24 hours. The UCS of samples was also measured after 75 days of sulfuric acid immersion. Changes in these properties were calculated with the following equation:

$$p_c = \frac{P_0 - P_n}{P_0} \tag{5-1}$$

where p_c is the change in properties (e.g., mass, length, UCS and UPV), P_0 is the property after 28 days of standard curing, and P_n is the property after acid immersion.

5.3. Results and discussion

5.3.1. Density, absorption and permeable voids

Water absorption and permeable voids reflect the ability of aggressive ions to penetrate cementitious materials (Zhang & Zong, 2014). The tests for density, absorption, and permeable voids were carried out on all mortar mixtures, and the results are presented in Figure 5.2. As shown in Figure 5.2 (a), the addition of CAC in a metakaolin-based geopolymer increased the bulk density. The bulk density was raised from 1890.43 kg/m^3 for the mixture GM to 1911.79 kg/m^3 for the mixture with 10% CAC. The increased bulk density can be attributed to a reduced porosity, which is reflected by the results of water absorption and volume of permeable voids. As shown in

Figure 5.2 (c) and (d), water absorption was reduced from 11.38% for the mixture with no CAC addition to 10.15% for the mixture with 10% CAC addition, and the volume of permeable voids decreased from 23.62% for the mixture GM to 20.51% when 10% CAC was added. The reduced water absorption and volume of permeable voids can be attributed to the improved geopolymerisation process that generated more geopolymer gel, which is a process that will be discussed in Section 4.3.4. Contradictory to the results for bulk density, the apparent density was reduced when CAC was added to the metakaolin-based geopolymer. The mixture GM had an apparent density of 2475.2 kg/m^3. The addition of 5% and 10% CAC decreased the apparent density of the metakaolin-based geopolymer to 2458.78 kg/m^3 and 2404.98 kg/m^3, respectively. The reduced apparent density indicates more water-impermeable voids in a mortar sample (ASTM, 2013). A possible reason for the increase of impermeable voids could have been the generation of extra geopolymer gel at the CAC addition; more geopolymer gels lead to more gel pores (<4.5 nm), which are less permeable (Alehyen et al., 2017).

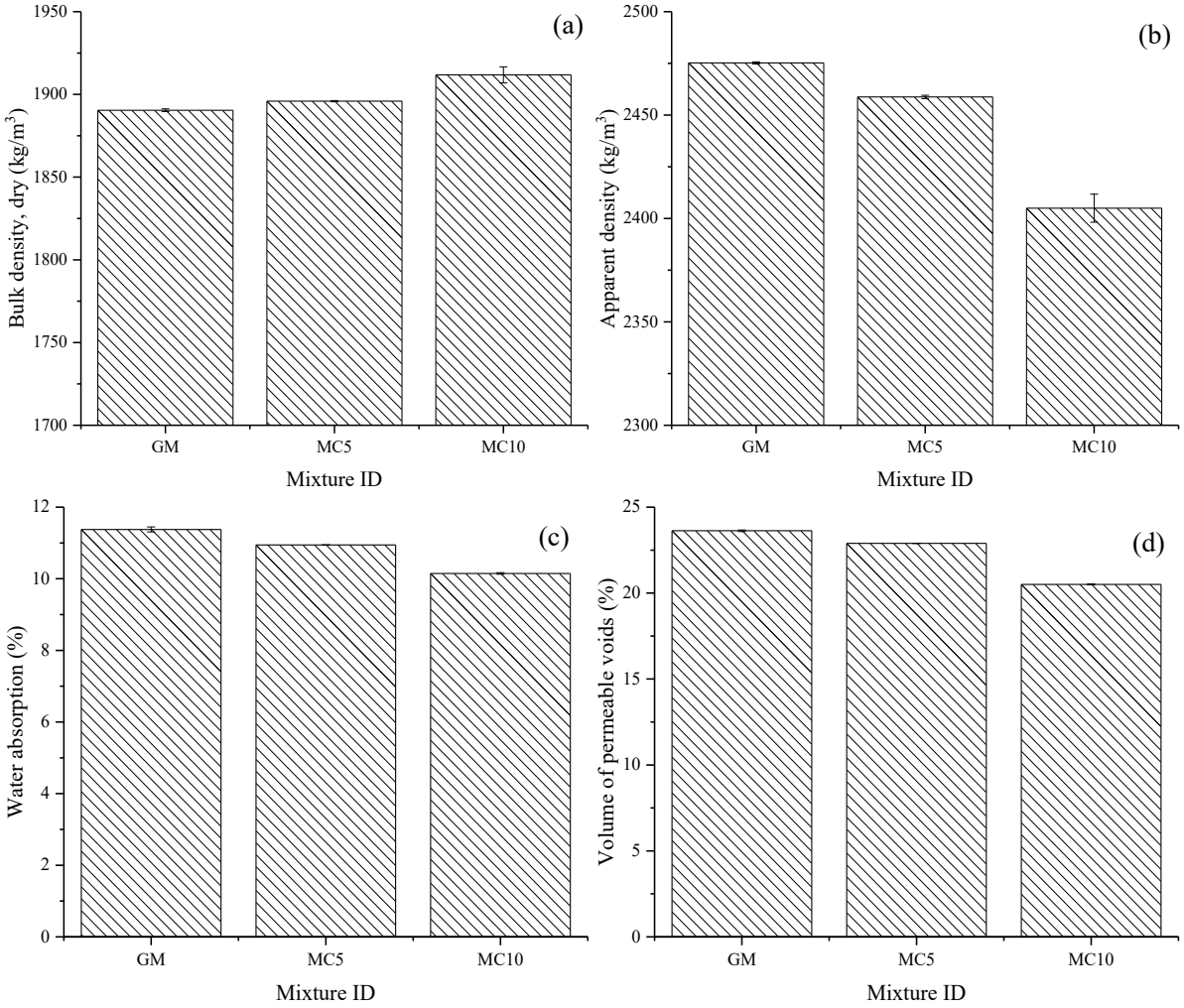

Figure 5.2. Density, absorption and permeable voids for metakaolin-based geopolymers a) bulk density, b) apparent density, c) water absorption, d) volume of permeable voids, where the mixture GM, MC5 and MC10 denote the metakaolin-based geopolymers with no CAC, 5% CAC and 10% CAC, respectively

5.3.2. Unconfined compressive strength

Mechanical strength is crucial when evaluating the mechanical performance of cementitious structures. In this study, the UCS was monitored before sulfuric acid immersion. The results are plotted in Figure 5.3. The mixture GM had a UCS of 56.5 MPa. The addition of CAC reduced the UCS of the metakaolin-based geopolymer to 40.5 MPa when 10% CAC was added. However, the

effect of CAC addition on the compressive strength of metakaolin-based geopolymers varied in different research. For example, Alanazi et al. (Alanazi et al., 2017) investigated the early strength of metakaolin-based geopolymer concrete (activated by NaOH and Na_2SiO_3 solutions); they found that the addition of 20% CAC reduced the compressive strength from 58.01 MPa to 43.38 MPa after 24 hours of curing. Adversely, Fernández-Jiménez et al. (Fernández-Jiménez et al., 2008) found that the addition of 10% CAC in a metakaolin-based geopolymer (activated by a sodium hydroxide solution) showed a compressive strength improvement of 40% after 20 hours of curing. They attributed the strength improvement to the facilitated geopolymerisation reaction with the addition of CAC, which generates more sodium aluminosilicate hydrate (N-A-S-H) and calcium aluminosilicate hydrate (C–A–S–H) gels (Fernández-Jiménez et al., 2008; Fernández-Jiménez et al., 2011). One of the possible reasons for the strength reduction in this study and the study by Alanazi et al. (Alanazi et al., 2017) was the generation of strätlingite (C_2ASH_8). This strätlingite was found to have a low bulk modulus of approximately 23 GPa compared with 34 GPa for geopolymer gel (Jackson et al., 2014). The strätlingite was reported to be one of the main hydrates of CAC when reactive silica was presented (Fernández-Jiménez et al., 2011; Scrivener & Capmas, 1998). The inclusion of Na_2SiO_3 in the alkaline activators may act as a reactive silica source for the formation of strätlingite. In this current study and the study by Alanazi et al. (Alanazi et al., 2017), Na_2SiO_3 was used as one of the activator solutions.

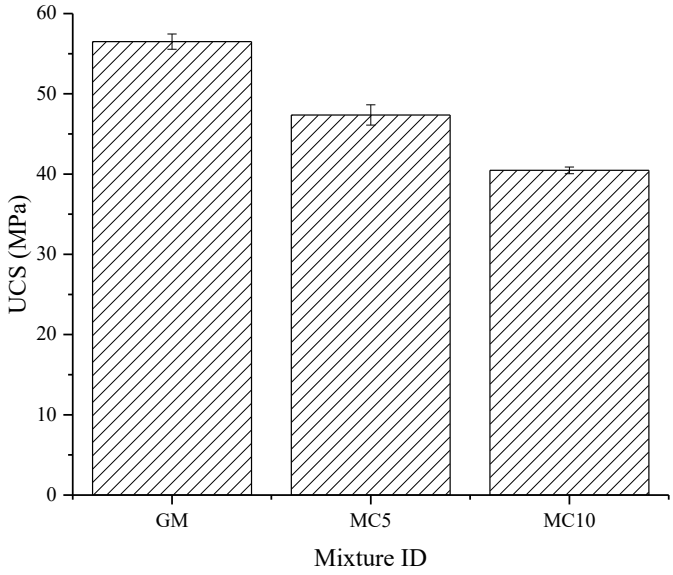

Figure 5.3. Compressive strength of metakaolin-based geopolymers

5.3.3. Thermogravimetric analysis

TGA tests were carried out to investigate geopolymerisation products of metakaolin-based geopolymers. The thermo-gravimetric (TG) and derivative of thermo-gravimetric (DTG) curves are plotted in Figure 5.4. There were two main phases of weight loss. The first phase of weight loss occurred from room temperature to around 400 ℃. The weight loss in this phase could be attributed to the evaporation of bonded water in geopolymer gel (Nath et al., 2016; Zhao et al., 2019). The second phase of weight loss started at around 700 ℃ and ended at 800 ℃. The decarbonization of sodium carbonate was responsible for the weight loss in this phase (Pasupathy et al., 2016; Pouhet & Cyr, 2016). After the heating process, the pure metakaolin-based geopolymer had a residual weight of 84.04%. The addition of 5% and 10% CAC in the metakaolin-based geopolymer led to a lower residual weight of 83.58% and 80.7%, respectively. This result suggests that more products were generated during the geopolymerisation process. It is also noted that the mixtures with CAC showed a broader temperature range of weight loss in the first phase. In particular, the peak on the DTG curve of the mixture with 10% CAC shifted to around 200 ℃

with a shoulder at around 150 ℃. A possible reason for this change could have been the existence of C_2ASH_8 (strätlingite), which dehydrated in the temperature range of 180 ℃ to 220 ℃ (Aggelakopoulou et al., 2011; Pacewska et al., 2011). It has been reported that in the presence of reactive silica, the strätlingite can be formed via Equation 5-2 as one of the hydrates of CAC (Fernández-Jiménez et al., 2011; Scrivener & Capmas, 1998). In the current study, this reactive silica can be provided by the dissolution of metakaolin and the sodium silicate solution. It is also interesting to note that the peak of decarbonization on DTG curves reduced with the increase of CAC content. This reduction may be attributed to the increased uptake of hydroxyl into the strätlingite (L'Hôpital et al., 2016), which reduced the concentration of alkalis in the pore solution. The carbonation of alkalis in pore solution has been reported to be the main cause of the carbonation of geopolymer materials (Babaee et al., 2018; Li & Li, 2018). The reduced alkali concentration in the pore solution mitigated the carbonation degree of samples.

$$CA+H_2O \rightarrow CAH_{10} \text{ or } C_2AH_8+Silicate\ anion \xrightarrow[H_2O]{} C_2ASH_8 \quad (5\text{-}2)$$

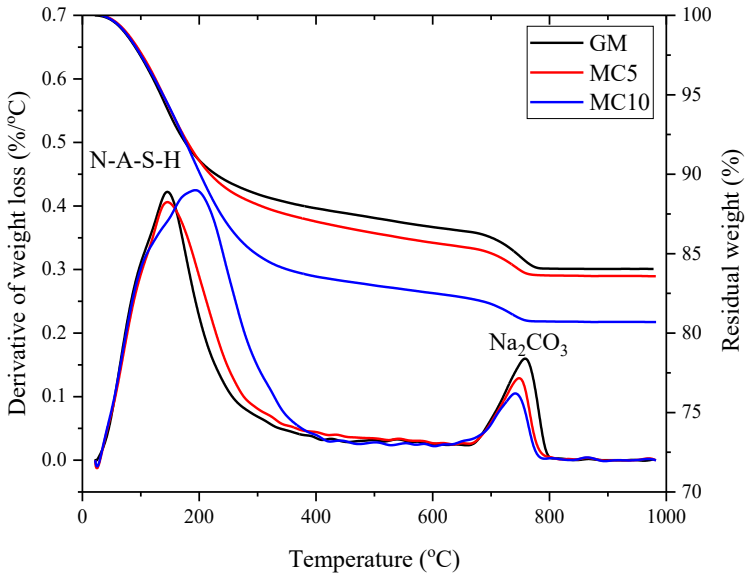

Figure 5.4. TG/DTG curves of metakaolin-based geopolymers

5.3.4. Fourier-transform infrared spectroscopy

The FTIR test can provide information about the vibration energy of different chemical bonds. Therefore, the FTIR tests were carried out to distinguish geopolymerisation products of mixtures. The transmittance of the three metakaolin-based geopolymer mixtures is plotted in Figure 5.5. For the mixture GM (without CAC), the absorption band at 3441 cm^{-1} is attributed to the stretching vibration of chemically bonded hydroxyl (Karthik et al., 2019), while the absorption band at 1653 cm^{-1} is the bending vibration of O-H of adsorbed water (Karthik et al., 2019; Song et al., 2005; Tiffo et al., 2020; Wan et al., 2017). The main peak at 997 cm^{-1} is attributed to the vibration of Si-O-T (T is the tetrahedral Si or Al) in geopolymer gel (N-A-S-H or C-A-S-H) (Madavarapu, 2014; Villaquirán-Caicedo, 2019). With the addition of CAC, the peak position of this chemical bond shifted to lower values of 975 cm^{-1} for the mixture with 5% CAC and 968 cm^{-1} for the mixture with 10% CAC. This may suggest that an obvious change in chemical bonds took place when CAC was presented during the geopolymerisation reaction, leading to the generation of new products. A possible reason is that the addition of CAC facilitated Al incorporation in the geopolymer chains (Wang et al., 2020). The geopolymer chains primarily consist of SiO_4 and AlO_4 tetrahedra units with various Si/Al ratios. When Si/Al=4, 3, 2, 1, 0, the IR absorption bands centered at around 1200, 1100, 950, 900 and 850 cm^{-1}, respectively. Due to the weaker Al-O bond, a higher degree of Si substitution by Al in the geopolymer chain results in a lower wavenumber (Zhang et al., 2008). The absorption band positioned at 1400 cm^{-1} could be caused by the C-O vibration of Na_2CO_3 (Ozer & Soyer-Uzun, 2015), while the band at 693 could be assigned to the Si-O bond of quartz from aggregates (Tiffo et al., 2020). It is also noted that the mixture with CAC showed an additional absorption band at 567 cm^{-1}. This absorption band could be assigned to the Fe-O bond

(Al-Zeer & MacKenzie, 2019). The ferrite content of these two mixtures was introduced from CAC.

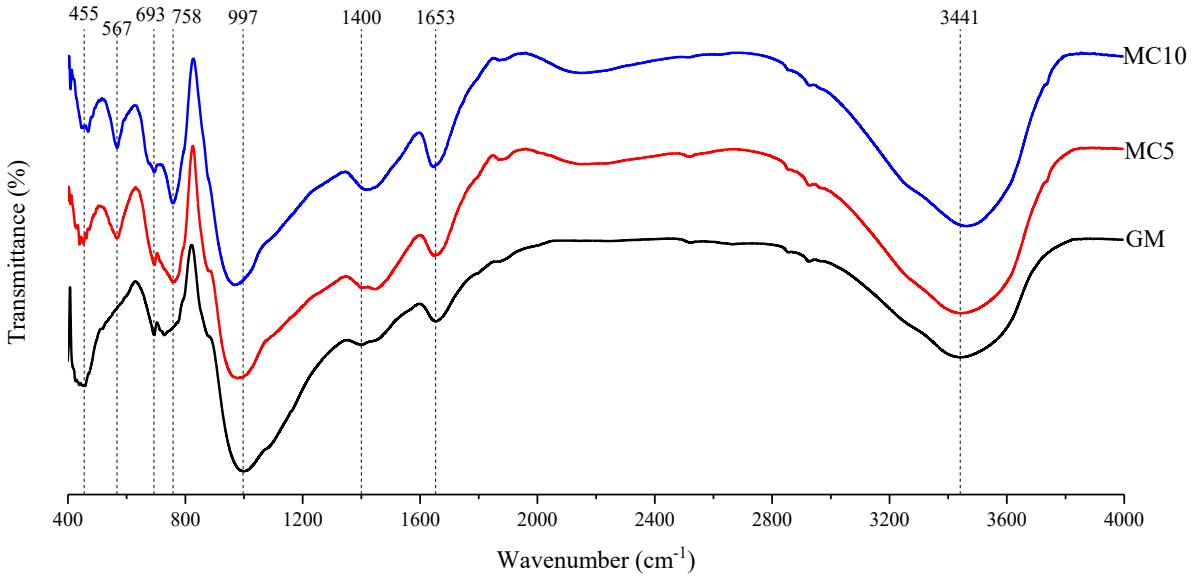

Figure 5.5. FTIR spectra of metakaolin-based geopolymers

5.3.5. Properties after sulfuric acid immersion

5.3.5.1. Fourier-transform infrared spectroscopy

An FTIR test was conducted after sulfuric acid immersion to investigate the change in chemical bonds. The powder samples were prepared from the corroded surface of mortar samples. The IR spectrum of samples after sulfuric acid immersion is presented in Figure 5.6. It can be seen that the vibration peak for Si-O-T bonds from geopolymer gel shifted to a higher value of 1031 cm^{-1} for the mixture GM, compared with the wavenumber before sulfuric acid immersion (997 cm^{-1}). A similar pattern of FTIR change was reported by Bakharev (Bakharev, 2005). He found that the Si-O-Al vibration of fly ash-based geopolymers shifted from 960 cm^{-1} to 986 cm^{-1} after 2 months of immersion in 5% acetic acid and shifted from 960 cm^{-1} to 1022 cm^{-1} after 2 months of immersion in 5% sulfuric acid. This change in vibration bands suggests the leaching out of Al from Si-O-T bonds during sulfuric acid immersion (Zhang et al., 2016). The mixtures with CAC showed more

significant shifting of the Si-O-T bonds: the peak shifted from 975 cm^{-1} to 1041 cm^{-1} for the mixture with 5% CAC and from 968 cm^{-1} to 1042 cm^{-1} for the mixture with 10% CAC. This result suggests that a higher amount of Al leached out during the sulfuric acid immersion of mixtures with CAC, and it also indicates that more acids were consumed to leach out Al in mixtures with CAC. This enhanced neutralization capacity could be one of the reasons for the improved acid resistance of metakaolin-based geopolymers with a CAC addition. It is also noted that the mixtures with CAC showed a higher wavenumber of ~1041 cm^{-1} (compared with 1031 cm^{-1} for the mixture GM) after immersion, implying a higher silicate content of samples. The vibration band of C-O at around 1400 cm^{-1} before immersion disappeared after sulfuric acid immersion. This was caused by the neutralization reaction between Na_2CO_3 and sulfuric acid, which dissolved the Na_2CO_3.

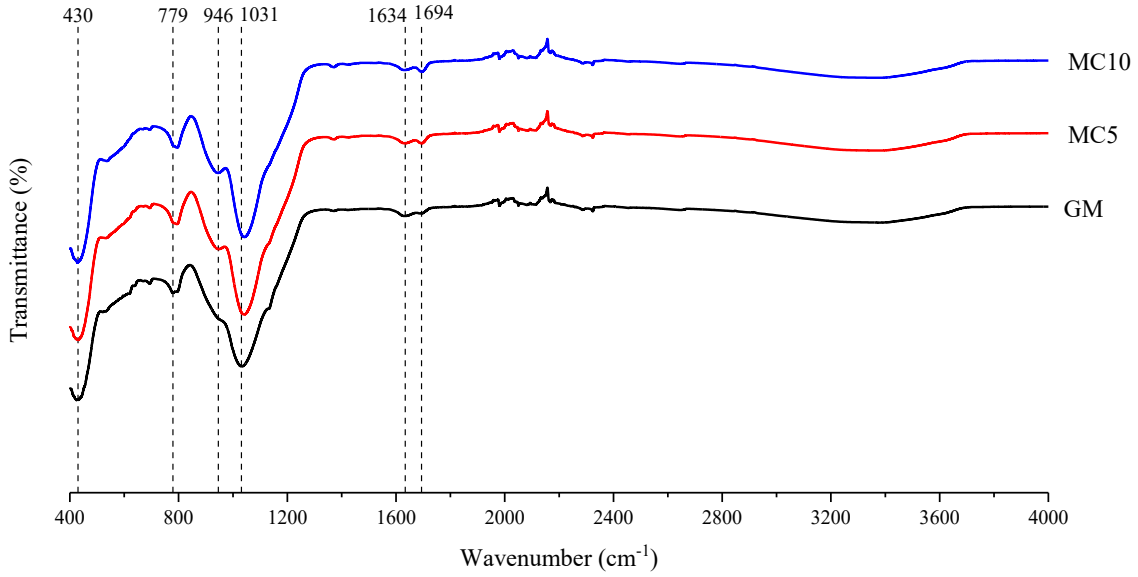

Figure 5.6. FTIR spectra of metakaolin-based geopolymers after 75 days of sulfuric acid immersion

5.3.5.2. Unconfined compressive strength

The UCS results after 75 days of sulfuric acid immersion are presented in Figure 5.7, and the UCS changes are listed in Table 5.3. A negative value indicates a UCS reduction. All metakaolin-based

geopolymers showed negative UCS changes that ranged from -23.47% to -65.66%. This strength reduction after sulfuric acid immersion was caused by the dealumination of geopolymer gel (Zhang et al., 2016). The dealumination of geopolymers is confirmed in this research by the FTIR results, which showed significant leaching of Al from geopolymer gel (see Section 4.3.5.1). The greatest UCS change was observed with the mixture GM (without CAC) with a value of -65.66%. The addition of CAC drastically reduced the UCS change to -25.81% and -23.47% for the mixtures with 5% and 10% CAC, respectively. After the 75 days of sulfuric acid immersion, the mixture with 5% CAC showed the highest UCS of 35.14 MPa among metakaolin-based geopolymer mixtures. The reduced UCS loss by CAC addition could have been caused by the reduced permeable voids (as discussed in Section 4.3.1) that hindered the penetration of sulfuric acid into the mortar samples (Korucu et al., 2019; Rahmani et al.). This mitigated sulfuric acid attack on the inner part of samples. Another possible attributing factor was the increased neutralization capacity of the samples caused by the facilitated geopolymerisation process and the generation of strätlingite. It has been reported that higher neutralization capacity often leads to higher acid resistance of cementitious materials due to the reduced local acidity at the sample surface (Ehrich et al., 1999; Joorabchian, 2010).

Table 5.3. UCS change of mixtures after 75 days of sulfuric acid immersion

Mixture ID	GM	MC5	MC10
UCS change, %	-65.66	-25.81	-23.47

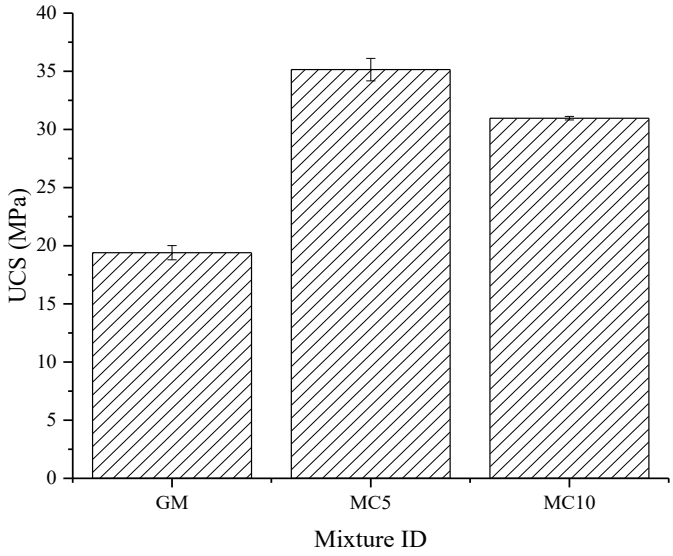

Figure 5.7. UCS of mixtures after 75 days of sulfuric acid immersion

5.3.5.3. Ultrasonic pulse velocity change

The UPV test was carried out in this research as one of the methods to evaluate the deterioration of the metakaolin-based geopolymer under sulfuric acid attack. Table 5.4 lists the UPV of mixtures before and after sulfuric acid immersion. The UPV ranged from 3335-3835 m/s before immersion, a result which can be classified as medium/good quality (medium: 3000-3500; good: 3500-4500) (Singh & Siddique, 2015). The addition of CAC increased the UPV of the metakaolin-based geopolymer. The addition of 5% and 10% CAC increased the UPV of the metakaolin-based geopolymer from 3440 m/s to 3835 m/s and 3640 m/s, respectively. The increased UPV suggests a denser microstructure, which is confirmed by the results of the volume of permeable voids. The mixture with a higher UPV showed a lower volume of permeable voids.

Figure 5.8 demonstrates the UPV change during sulfuric acid immersion, and the final UPV changes after 75 days of sulfuric acid immersion are listed in Table 5.5. With the increase in immersion age, the UPV loss increased gradually. The UPV change of the metakaolin-based geopolymer ranged from -9.76% to -15.84%. This reduced UPV after sulfuric acid immersion

suggests an increase in porosity caused by the leaching of Na^+, Ca^{2+} and dealumination (Medpelli, 2015). The addition of CAC was observed to reduce the UPV change. Among the geopolymer mixtures, the one with 10% CAC showed the lowest UPV change throughout the immersion period with a final UPV change of -9.76%. After 75 days of sulfuric acid immersion, the metakaolin-based geopolymer with 5% and 10% CAC showed higher UPVs of 3260 m/s and 3285 m/s, respectively, compared with the mixture GM (2895 m/s).

Table 5.4. UPV of mixtures before and after sulfuric acid immersion

Mixture ID	Before immersion	After immersion
GM	3440	2895
MC5	3835	3260
MC10	3640	3285

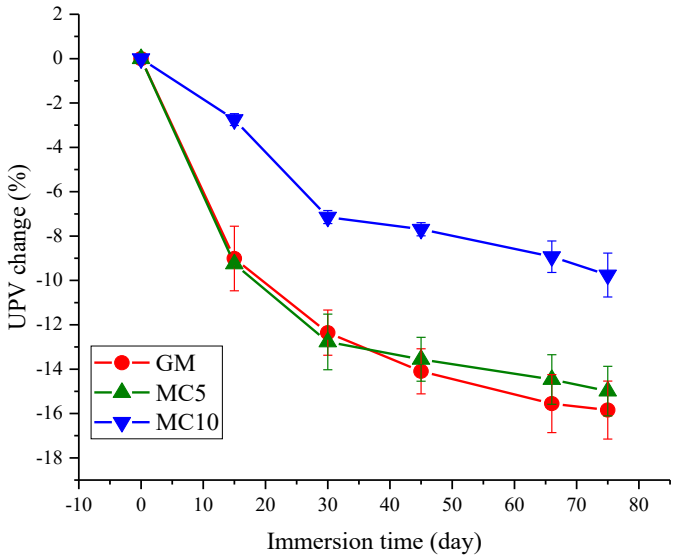

Figure 5.8. UPV change during sulfuric acid immersion

Table 5.5. UPV change of mixtures after 75 days of sulfuric acid immersion

Mixture ID	GM	MC5	MC10
UPV change, %	-15.84	-14.99	-9.76

5.3.5.4. Mass change

Mass change during sulfuric acid immersion was monitored as another indicator of geopolymer deterioration. The results of mass change with immersion time are plotted in Figure 5.9, and the final mass changes are listed in Table 5.6. As shown in Figure 5.9, the geopolymer mortar samples were losing weight as the immersion time increased. Under the sulfuric acid attack, the Na^+ and Ca^{2+} could be replaced by hydrogen ion, and the Al in the geopolymer chain could be leached out (Allahverdi & Skvara, 2001). This leaching of Na^+ and Ca^{2+} and dealumination leads to a loss of the binding ability of geopolymer gel, which further results in the spalling of aggregates. The leaching of soluble contents and the spalling of aggregates were responsible for the mass loss during sulfuric acid immersion. Among the three mixtures, the mixture GM showed the greatest mass change throughout the immersion period, with a final mass change of -13.88%. The inclusion of CAC was found to reduce mass loss. Among the mixtures, the one with 10% CAC showed the lowest mass loss with a final mass change of -10.85%.

Table 5.6. Mass change of mixtures after 75 days of sulfuric acid immersion

Mixture ID	GM	MC5	MC10
Mass change, %	-13.87	-11.46	-10.86

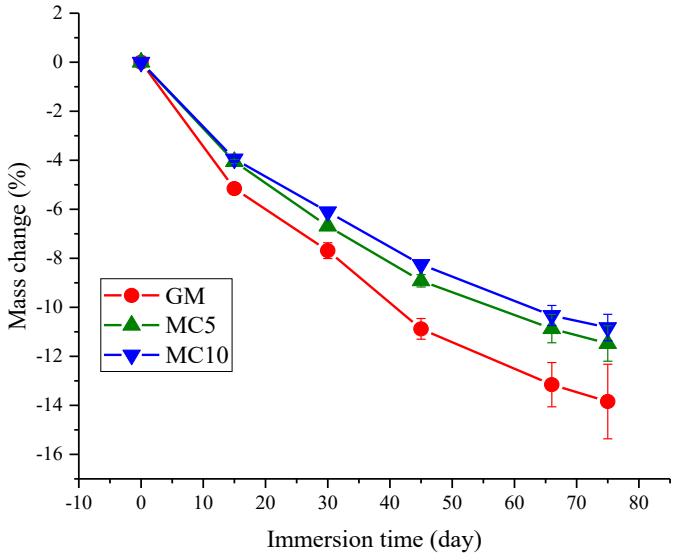

Figure 5.9. Mass change with sulfuric acid immersion time

5.3.5.5. Length change

Length change was monitored as the last indicator of geopolymer sample deterioration. The results of length change with immersion time are illustrated in Figure 5.10. The final length changes after 75 days of sulfuric acid immersion are listed in Table 5.7. A negative value indicates a length reduction. All metakaolin-based geopolymers showed negative length changes within the immersion period. As the immersion time increased, the length of geopolymer samples reduced. After 75 days of sulfuric acid immersion, the mixture GM showed a length change of -2.34%. A significant reduction in length change was observed for metakaolin-based geopolymers when CAC was added. As shown in Figure 5.10, the mixtures with 5% and 10% CAC showed a final length change of -1.19% and -1.27%, respectively.

Table 5.7. Length change of mixtures after 75 days of sulfuric acid immersion

Mixture ID	GM	MC5	MC10
Length change, %	-2.34	-1.19	-1.27

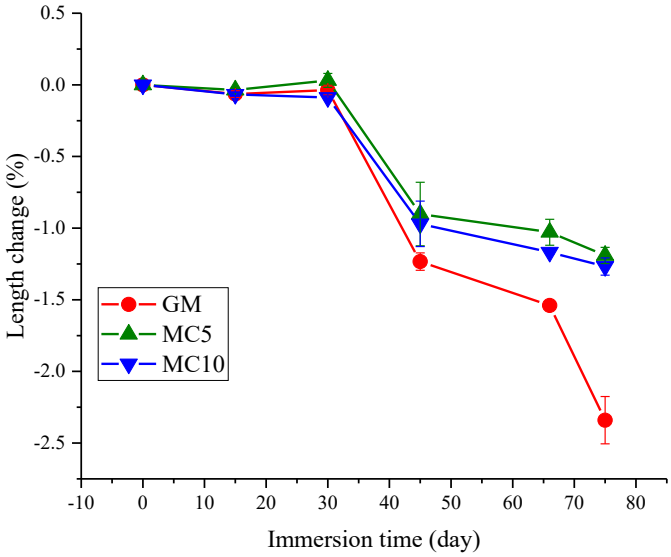

Figure 5.10. Length change with sulfuric acid immersion time

5.3.6. Evaluation of acid resistance

In the presence of sulfuric acid, geopolymer materials deteriorate in three steps (Bakharev, 2005; Sturm et al., 2018). 1) The alkali cations Na^+ in the geopolymer gel can be replaced by hydrogen ions in acidic environments. 2) A strong acid can break the Si-O-Al bonds, ejecting Al from the geopolymer gel. This process leads to a mass loss of geopolymer materials. 3) Si-O-Si bonds hydrolyze in an acidic environment. This deterioration process can result in a change in macro-properties such as UCS, UPV, and mass. In this study, four indicators were monitored to evaluate the deterioration of metakaolin-based geopolymers during sulfuric acid immersion. These indicators were UCS change, UPV change, mass change, and length change. The addition of CAC was found to significantly improve the acid resistance of the metakaolin-based geopolymer because reduced values were observed on the four selected indicators of mixtures with CAC. For instance, the UCS change was significantly reduced from -65.66% to -23.47% when 10% of CAC was added. In general, the mixture with 10% CAC showed the highest acid resistance among the geopolymer mixtures as the mixture showed the lowest UCS change, UPV change, and mass

change. The improved acid resistance from CAC inclusion could be attributed to the facilitated geopolymerisation. It has been reported that the calcium and aluminium in CAC can accelerate the dissolution of reactive contents in raw materials and facilitate the formation of aluminosilicate gels (Fernández-Jiménez et al., 2008; Vafaei & Allahverdi, 2016). A facilitated geopolymerisation was also observed from the FTIR results in this research, where the absorption band for Si-O-Al bonds shifted to a lower wavenumber in the presence of CAC. This facilitated geopolymerisation resulted in the generation of more geopolymer gel that led to the densified microstructure (which has been confirmed by the results of water absorption and volume of permeable voids). The densified microstructure of geopolymers inhibited the penetration of sulfuric acid and further mitigated the attack of acid on the inner part of samples. Another possible contributing factor for improved acid resistance was the increased neutralization capacity results from the generation of strätlingite. It was found that when CAC hydrates in highly alkaline solutions (NaOH and Na_2SiO_3), strätlingite could be one of the hydration products (Fernández-Jiménez et al., 2011). The reaction between strätlingite and sulfuric acid reduced the local acidity at the sample surface, which hindered the attack on the geopolymer structures.

5.4. Conclusions

This study aimed at improving the sulfuric acid resistance of metakaolin-based geopolymer mortars by adding calcium aluminate cement to partially substitute metakaolin. The following conclusions can be drawn from the testing results:

(1) From the test of density, absorption, and permeable voids, the addition of calcium aluminate cement noticeably reduced the water absorption and permeable voids of the metakaolin-based geopolymer. According to the results of Fourier-transform infrared

spectroscopy (FTIR), the reduced permeable voids could be attributed to the improved geopolymerisation.

(2) Based on the thermogravimetric analysis (TGA), the addition of calcium aluminate cement resulted in the generation of strätlingite when Na_2SiO_3 was presented in the activator solution. The low bulk modulus of strätlingite caused the compressive strength reduction of mixtures with calcium aluminate cement before sulfuric acid immersion.

(3) According to the FTIR results after sulfuric acid immersion, the sulfuric acid immersion resulted in the leaching of Al from geopolymer gel. The leaching of Al was responsible for the strength reduction during sulfuric acid immersion.

(4) The addition of calcium aluminate cement drastically improved the acid resistance of the metakaolin-based geopolymer due to the reduced UCS change, UPV change, mass change and length change. Among the mixtures, the one with 10% calcium aluminate cement showed the highest resistance with a UCS change of -23.47%, a UPV change of -9.76% and a mass change of -10.86% after 75 days of sulfuric acid immersion. The improvement in acid resistance from the calcium aluminate cement addition was found to be caused by the enhanced geopolymerisation that reduced permeable voids and by the generation of C_2ASH_8 (strätlingite) that increased the neutralization capacity.

Chapter 6. Effects of cellulose nanocrystals on improving the acid resistance of cement-based composites

This chapter has been submitted for peer review as **L. Wu**, G. Huang, C. Hu, W.V. Liu, (2020). Effects of cellulose nanocrystals on improving the acid resistance of cement-based composites in mining, *International Journal of Minerals, Metallurgy and Materials.* © Springer. (accepted)

6.1. Introduction

Cement-based composites are one of the most extensively used materials in mining operations such as shotcreting, grouting, backfilling, shaft sinking, and other infrastructure constructions (Yang & Wang, 2005; Yin et al., 2020). It is reported that as much as 100,000 tonnes of cement can be consumed by a mining company (Sivakugan et al., 2015). For shotcrete alone, over 700,000 m^3 is consumed annually in North America and Australia (Yu et al., 2018). However, cementitious composites can be easily corroded in the presence of sulfuric acid due to its alkaline nature (Reardon, 1990; Zivica & Bajza, 2001). The primary source of sulfuric acid for mining operations is acid mine drainage. Acid mine drainage refers to the acidic mine water generated from the oxidation and bio-oxidation of sulfidic ores, particularly pyrite (FeS_2 ores) (Kefeni & Mamba, 2020; Vélez-Pérez et al., 2020). Upon exposure to air and water, sulfidic ores can be oxidized generating sulfuric acid by the following equations (Ergüler, 2015):

$$2FeS_2+7O_2+2H_2O\rightarrow 2Fe^{2+}+4SO_4^{2-}+4H^+ \quad (6\text{-}1)$$

$$4Fe^{2+}+O_2+4H^+\rightarrow 4Fe^{3+}+2H_2O \quad (6\text{-}2)$$

$$4Fe^{3+}+3H_2O\rightarrow Fe(OH)_3+3H^+ \quad (6\text{-}3)$$

$$FeS_2+4Fe^{3+}+8H_2O\rightarrow 15Fe^{2+}+2SO_4^{2-}+16H^+ \quad (6\text{-}4)$$

The oxidation of pyrites releases a large amount of sulfuric acid to groundwater, lowering the pH to as low as 2 (Jones & Cetin, 2017). In such an acidic environment, the alkaline cementitious composites (pH ~ 12.5-13 (Reardon, 1990)) can be easily corroded. When exposed to acidic media, the cement hydration product, calcium hydroxide (CH), would first be decomposed, reducing the pH of pore solution in the cementitious composites (Yuan et al., 2015). This facilitates the decalcification of the calcium-silicate hydrates (C-S-H) (Joorabchian, 2010), which is the main compound that binds concrete together (Tajuelo Rodriguez et al., 2017). The process can be summarized in the following chemical reactions (Jeon et al., 2020):

$$CH + H_2SO_4 \rightarrow C\bar{S}H \quad (6\text{-}5)$$

$$C\text{-}S\text{-}H + H_2SO_4 \rightarrow C\bar{S}H + SiO_2 + H_2O \quad (6\text{-}6)$$

where $C\bar{S}H$ is the gypsum ($CaSO_4 \cdot 2H_2O$). As the generated gypsum has no binding capability (Amin, 2016; Gutberlet et al., 2015), the corroded cement composites gradually lose integrity (Wu et al., 2018), damaging the mechanical performance of cementitious structures (Aydın et al., 2007; Mahdikhani et al., 2018).

Therefore, the cement-based materials used in underground mines should be made with high acid-resistance. In recent years, nano additives and nano admixtures are drawing increasing attention to the improvement of acid resistance. For example, Mahdikhani et al. (Mahdikhani et al., 2018) investigated the performance of concrete mixtures with the nano-silica addition under acid rain conditions, and less deterioration was observed with mixtures incorporating nano-silica. Fan et al. (Fan et al., 2016) claimed that the addition of nano-calcined kaolinite substantially increased the resistance of mortars to nitric acid due to the filling effect and the pozzolanic effect. The addition of 3% of nano-calcined kaolinite reduced the compressive strength loss by 17% after 60 days of acid immersion. Diab et al. (Diab et al., 2019) investigated the resistance of concrete mixtures with nano-silica and nano metakaolin to nitric acid and sulfuric acid. They reported that the addition of both nano-silica and nano metakaolin improved the acid resistance of concrete mixtures.

Among the nanomaterials, cellulose nanocrystal (CNC), the crystalline part of cellulose extracted from plants and trees, is another promising additive. First, CNCs have a high aspect ratio of 10-60 and stiffness of >200GPa (comparable to that of steel) (Dufresne, 2013; Khan, 2015). This makes it an excellent reinforcing material from nanoscale for cement-based composites. For example, Dousti et al. (Dousti et al., 2019) found that the porosity of cement pastes with CNC reduced by

33% for pores smaller than 100 nm. Second, the CNC addition can enhance the mechanical strength of cement-based composites. It was reported that the addition of 0.2% CNC increases the flexural strength of cement paste by 30% (Cao et al., 2015). This enhanced mechanical strength is crucial for underground structures in resisting ground motions (Kaiser et al., 2010) and structure deformation (Høien et al., 2019). Third, the addition of CNC in cement-based composites was found to improve the durability of cement-based composites (e.g. resistance to freezing-thawing cycles, resistance to wetting-drying cycles and sulfate resistance). For example, Barnat-Hunek (Barnat-Hunek et al., 2019) examined the effect of CNC on the resistance to the freezing and thawing of concrete mixtures, and improved resistance was observed. Balea et al. (Balea et al., 2019) observed that the addition of cellulose nanofibrils and micro cellulose crystals bridges the microcracks and improves wet-dry durability. Goncalves et al. (Goncalves et al., 2019) investigated sulfate penetration in pastes with the addition of cellulose nanofibrils and reported that the addition of cellulose nanofibrils noticeably reduced the penetration depth of sulfate.

Although the CNC addition showed excellent reinforcing performance and durability in cement-based composites, no research has been conducted in exploring the effect of CNC on the acid resistance of cement-based composites. This investigation is of great importance because improved acid resistance can enhance the durability of cement-based composites in an acid mine drainage environment. In addition, the use of CNC extracted from trees and plants can benefit the forest industry economically. To this end, the main aim of this study is to investigate the acid resistance of mortar mixtures with the CNC addition. In this research, CNCs were added to mortar mixtures as an additive at volume ratios of cement up to 1.5%. The mortar samples were immersed in pH 2 sulfuric acid for 75 days. Acid resistance was evaluated by monitoring the change in mass, length, ultrasonic pulse velocity, and strength.

6.2. Methodology

6.2.1. Materials and mix proportions

The cement used in this study was Portland Type General Use (GU) cement. The main composition of the cement was tested through an X-ray fluorescence test, and the results are listed in Table 6.1. For all mixtures, typical sand with water absorption of 1.5% for concrete-making was used as the fine aggregates. Sieve analysis was conducted per ASTM C136 / C136M – 14 (ASTM, 2014), and the result is illustrated in Figure 6.1. The figure shows that the sand falls in the American Concrete Institute (ACI) grade zone #1 (ACI Committee 506, 2016). The CNC was sourced locally from a manufacturing plant in Edmonton, Canada. The typical properties of the CNCs are listed in Table 6.2. The CNCs were added to the mixture as an additive at ratios of 0.2%, 0.4%, 1.0% and 1.5% of cement volume. The mixture proportions are presented in Table 6.3.

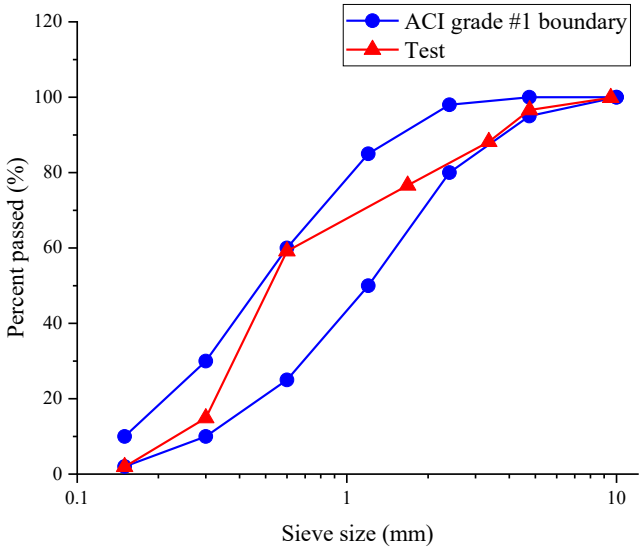

Figure 6.1. Sieve analysis of fine aggregate

Table 6.1. X-ray fluorescence main composition of type GU cement

Oxide	MgO	Al_2O_3	SiO_2	Y_2O_3	SO_3	K_2O	CaO	TiO_2	Cr_2O_3	Fe_2O_3
w.t%	3.07	2.14	14.49	2.57	7.16	0.72	66.01	0.16	0.04	3.50

Table 6.2. Physical and chemical properties of CNC provided by the manufacturer

Appearance	White crystalline powder
Odor	Odorless
pH	6-7
Particle size	100-230 nm in length, 3-5nm in diameter
Specific surface area	1.846 m^2/g
Sulfur content	0.5-2 w.t%
Composition	100% crystalline nano cellulose
Thermal stability	240-275 ºC

Table 6.3. Mixture proportioning of mixtures

No.	Mixture ID	Cement	Water	Sand	CNC content	w/c
		kg/m^3	kg/m^3	kg/m^3	kg/m^3	
1	Reference	493.25	221.96	1541.4	0	0.45
2	C-0.2	493.25	221.96	1541.4	0.49	0.45
3	C-0.4	493.25	221.96	1541.4	0.97	0.45
4	C-1	493.25	221.96	1541.4	2.43	0.45
5	C-1.5	493.25	221.96	1541.4	3.64	0.45

6.2.2. Sample preparation

Samples were prepared according to the ASTM C192-16a (ASTM, 2016b). Fine aggregates and cement were first mixed with a mixing drum for three minutes. The CNC additives were added and stirred in the tap water for three minutes, making a CNC-water suspension. Then, the suspension was added to the dry-mixed fine aggregates and cement mixture, and mixed for another three minutes. The readily mixed mixture was cast to Φ50×100mm cylinder molds and sealed with caps under room temperature for 24 hours. After 24 hours, the samples were de-molded and transferred to a standard curing room (25 ± 2 °C and relative humidity of 100%) for 28 days.

6.2.3. Testing procedure

After 28 days of standard curing, the samples were moved out from the moisture room for further tests. Figure 6.2 shows the setup of these tests. Prior to sulfuric acid immersion, density, absorption and voids tests, thermogravimetric analysis (TGA) tests, and unconfined compressive strength (UCS) tests were conducted to investigate the effects of CNC on the microstructure, cement hydration and mechanical strength of mortar mixtures. Then the readily cured samples were immersed in sulfuric acid with a pH of 2 for 75 days. The ratio of sample surface area to acid solution volume was kept at 0.196 (one liter of acid solution/sample) throughout the immersion period. To maintain the acidity of the acid solution, concentrated sulfuric acid (95%) was added to the solution every five days. During the immersion, changes in ultrasonic pulse velocity (UPV), mass, and length of the samples were monitored every 15 days to observe the deterioration of the samples. Tests for density, mechanical properties, and TGA were also conducted after 75 days of immersion. Detailed test procedures are provided in the following sections.

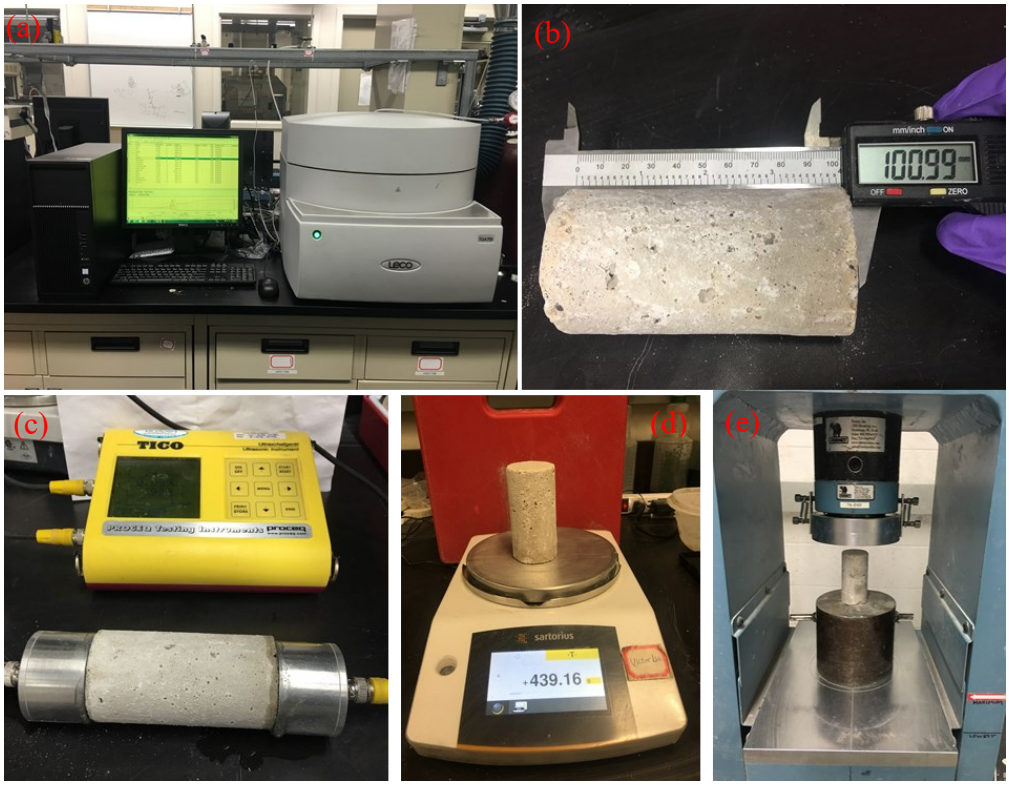

Figure 6.2. Experimental setup: a) TGA test; b) length measuring; c); UPV test; d) weighing; e) UCS test

6.2.3.1. Visual observation

Visual observation is the most straightforward way to evaluate the degree of deterioration. In this research, a phenolphthalein solution was used to identify the boundary between the corroded and uncorroded parts of specimens. The pH of the uncorroded cement-based composite is around 12.5-13 (Mignon et al., 2017), under which point the phenolphthalein solution turns purple in color (Kim et al., 2017). Under the sulfuric acid attack, the neutralization reaction between CH, C-S-H and acid ions reduces the pH of the pore solution. When the pH is reduced to below 8, the phenolphthalein solution is colorless (Khalafi et al., 2015). Thus, in this research, phenolphthalein is used to identify the boundary between the corroded part and the uncorroded part of a sample. A cylinder sample was first cut from the middle, and then the phenolphthalein solution was sprayed

on the cross-section. The part that is purple is uncorroded, while the part that is colorless is corroded. After that, an image-processing technique was adopted to extract the pixel number of the sample cross-section area and the colorless area. The percent of the corrosion area in the cross-section was calculated by dividing the pixels numbers of the corrosion area by pixel number of cross-section area.

6.2.3.2. Density, water absorption and volume of permeable voids test

Since water absorption and permeable voids reflect the penetration capability of aggressive ions into the samples, it is critical to understand the effects of CNC on these properties. Thus, the density, water absorption, and volume of permeable voids tests were carried out according to ASTM C642-13 (ASTM, 2013) after 28 days of standard curing. For each mixture, three samples were prepared and tested. The bulk density, apparent density, water absorption, and volume of permeable voids were calculated by averaging the results of the three samples. This test was also performed on samples after acid immersion to investigate the effects of acid immersion on the microstructure of mortar samples.

6.2.3.3. Thermogravimetric analysis

TGA is a common tool to identify cement hydration products and the degree of cement hydration (Huang et al., 2019). Thus, the TGA test was conducted in this study to investigate the effects of CNC on the hydration of cement particles after 28 days of curing. To prepare the powder sample for the TGA test, a cylindrical paste sample was prepared for each mixture. A slice of the paste sample was cut from the cylinder sample. The slice was then ground into small particles and immersed in acetone for 48 hours to remove the free water and cease the hydration reaction. Then the acetone-immersed samples were oven-dried at 60 °C for 24 hours to remove the acetone. After

that, the particle samples were further ground into powders with a diameter of <63 μm. Finally, powder samples with a weight of 1.2 ± 0.05 g were tested through a Leco TGA 7011, which has a weighing accuracy of ±0.02%. The powder samples were heated from 20 °C to 980 °C with a heating rate of 5 °C per minute under a nitrogen atmosphere. To better understand strength development after sulfuric acid immersion, the above test procedure was also performed on the samples after 75 days of sulfuric acid immersion.

6.2.3.4. Mechanical strength test

To investigate the effect of CNC on the mechanical properties of mortar mixtures, the UCS was tested for all mixtures after 28 days of curing, according to the ASTM C39 / C39M – 18 (ASTM, 2018). Three samples were tested for each mixture to obtain the averaged strength. In order to measure the deterioration of sulfuric acid attack, the UCS was also monitored after 75 days of sulfuric acid immersion. The change in strength was calculated as follows:

$$f_c = \frac{F_0 - F_n}{F_0} \tag{6-7}$$

where f_c is the change in strength, %, F_0 is the strength after 28 days of standard curing, MPa, and F_n is the strength after acid immersion, MPa.

6.2.3.5. Ultrasonic pulse velocity test

The UPV test is a widely adopted non-destructive method to evaluate the quality of cement-based composites by measuring the transmission velocity of ultrasonic pulses (Nematzadeh & Fallah-Valukolaee, 2017). A higher value often indicates a higher strength and denser microstructure (Jeon et al., 2020). In recent years, the UPV test has been increasingly used in the evaluation of

acid resistance of cement-based composites (Diab et al., 2019; Jeon et al., 2020; Nematzadeh & Fallah-Valukolaee, 2017; Siad et al., 2016). In this research, the UPV was measured according to ASTM C597-16 (ASTM, 2016c) every 15 days of immersion until the end of the immersion test. Prior to measurement, the samples were taken out from the immersion container and dried under room temperature for 24 hours to eliminate the effect of moisture on the UPV result.

6.2.3.6. Changes in mass and length

As two of the most widely adopted parameters for deterioration evaluation of cement-based composites, change in mass and change in length are easy to test and directly reflect the deterioration of samples (Wu et al., 2019). Thus, the changes in mass and length were employed as indicators of sample deterioration. The samples were extracted from acid and dried at room temperature for 24 hours prior to measurement. Three samples were tested each time for each mixture, and the averaged value was calculated as the mass change or length change. The change in mass/length was calculated as follows:

$$p_c = \frac{P_0 - P_n}{P_0} \tag{6-8}$$

where p_c is the change in mass/length, P_0 is the mass/length after 28 days of standard curing, and P_n is the mass/length after acid immersion.

6.3. Results and discussion

6.3.1. Visual observation

To visually assess the performance of CNC on sulfuric acid resistance of mortar mixtures, phenolphthalein solution was sprayed on the cross-section of the cylinder sample. The

unneutralized part showed as purple; the neutralized area presented as white/yellow. The dyed cross-section of each mixture sample is presented in Figure 6.3. The reference sample was severely corroded with a thickness of a neutralized layer of around 2 mm. The addition of 0.2% and 0.4% CNC noticeably reduced the corrosion degree as the thickness of the neutralized layer reduced significantly. When the CNC ratios increased to 1% and 1.5%, the corrosion became severe again as the thickness of the neutralized layer increased to a similar level of reference mixture. In order that the neutralized area is quantified, the pixel numbers of both the purple part and the cross-section area were calculated through an image-processing technique. The ratio of the neutralized area to the cross-section was calculated to quantify the degree of deterioration. The results are plotted in Figure 6.4. It can be seen that 9.5% of the cross-section in the reference sample was corroded; the neutralized area reduced to 3.1% at a CNC ratio of 0.4%, then it increased back to 9.3% at 1.5% of CNC addition.

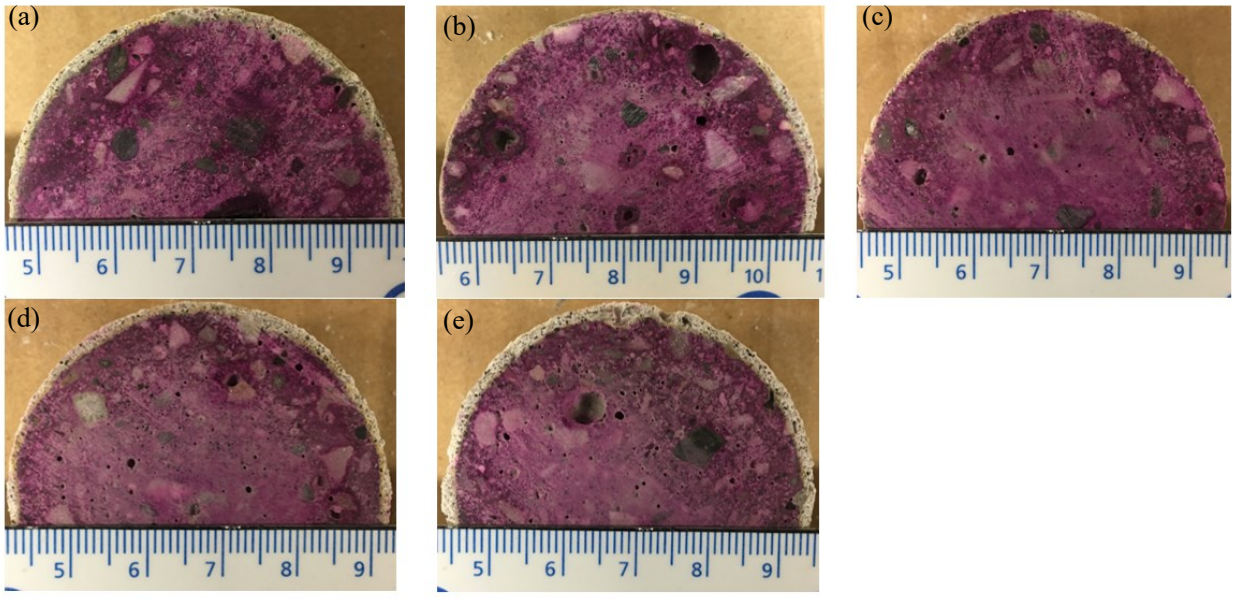

Figure 6.3. Cross-section of CNC mixtures after acid immersion: a) Ref; b) C0.2; c) C0.4; d) C1.0; e) C1.5

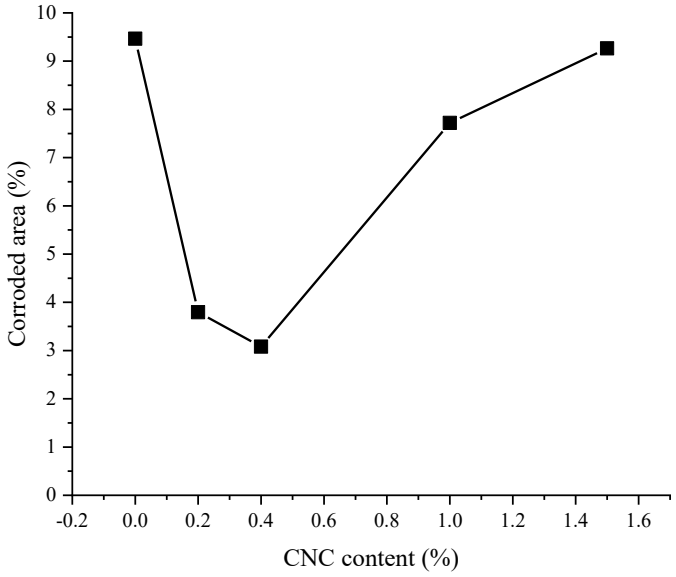

Figure 6.4. Percentage of the neutralized area in cross-section of samples

A Scanning Electron Microscopy / Energy Dispersive X-Ray Spectroscopy (SEM/EDS) test was also carried out to identify the composition of the corrosion layer. A sample of the reference mixture was cut from the edge of the cross-section to about 1 cm deep. Two spots were selected for scanning: one at the inner part of the sample (within the unneutralized area) and the other at the edge of the sample (within the neutralized area). The SEM/EDS results are plotted in Figure 6.5. The SEM image shows that the uncorroded part has a dense structure, and much of the C-S-H can be identified. No sulfur was found in this area, as shown in the EDS spectrum. On the contrary, a loose microstructure was observed in the corrosion layer, and a large amount of sulfur was identified in the EDS spectrum, which suggests the formation of gypsum.

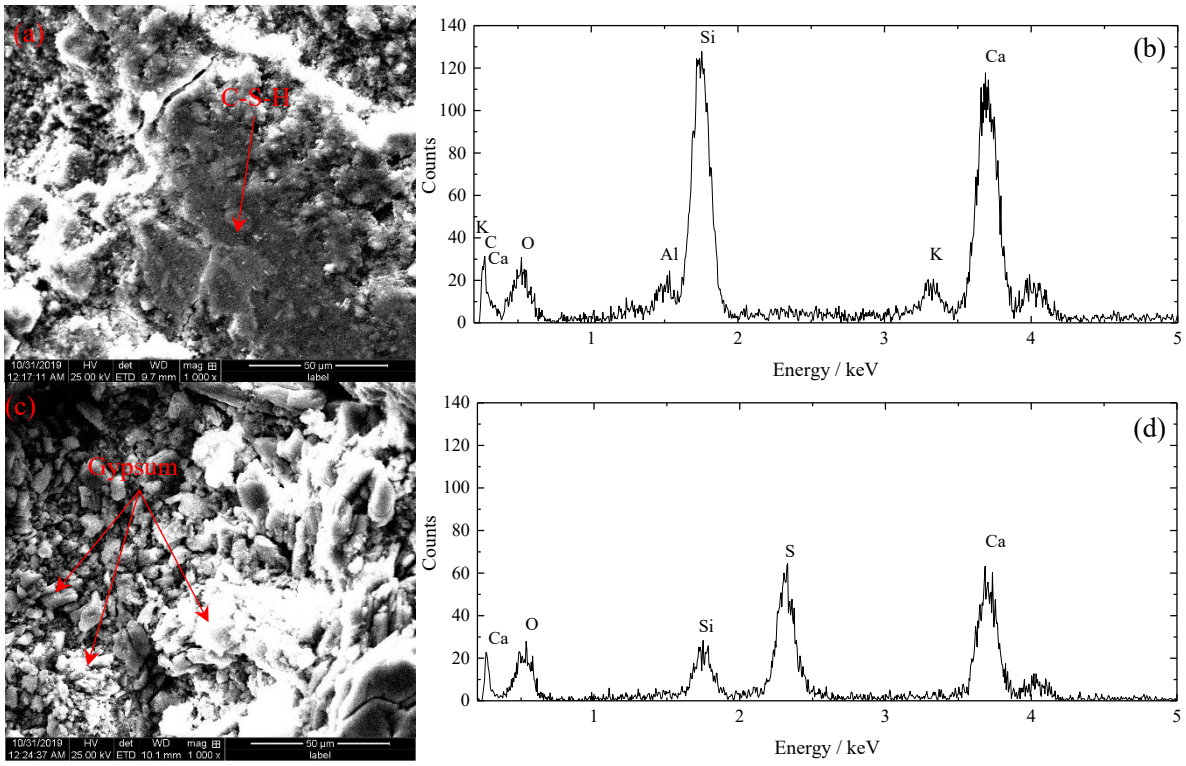

Figure 6.5. SEM results: a) SEM image of the uncorroded part; b) EDS spectrum; c) SEM image of the corroded layer; d) EDS spectrum

6.3.2. Density, water absorption and volume of permeable voids

6.3.2.1. Before sulfuric acid immersion

The durability of concrete against sulfuric acid is closely related to the water absorption and volume of permeable voids of cement-based composites (Papadakis et al., 1991). Thus, the tests for density, water absorption, and volume of permeable voids were conducted before sulfuric acid exposure. The results are plotted in Figure 6.6. Figure 6.6 (a) shows the results of bulk density and apparent density for CNC mixtures. Bulk density depicts the density of all voids and the solids, while the apparent density describes the density, including solids and impermeable voids; a higher apparent density indicates a lower volume of impermeable voids (ASTM, 2013). As can be seen from Figure 6.6 (a), the addition of CNC increased bulk density when the CNC content was lower

than 0.4%. The reference mixture had a bulk density of 2,045 kg/m^3. The value was increased to 2,077 kg/m^3 for the mixture with 0.4% CNC. The increased bulk density can be attributed to reduced porosity, which is confirmed by the water absorption results (which will be discussed later). Reduced porosity has also been reported in previous research. Barnat-Hunek et al. (Barnat-Hunek et al., 2019) found that the addition of 0.5% and 1% of CNC significantly reduced the volume of pores larger than 100 nm. With the further increase in CNC content, bulk density reduced to 2,049 kg/m^3 at 1.5% of CNC content. A possible reason for this reduction in bulk density is the agglomeration of CNC, which forms defects in the cement-based composites (Cao et al., 2016).

Similarly, the addition of CNC slightly raised the apparent density. It increased gradually from 2,500 kg/m^3 for the reference mixture to 2,508 kg/m^3 for the mixture with 1% CNC, and then it fell back to 2,481 kg/m^3 for the mixture with 1.5% CNC. This suggests that the addition of CNC<1% reduced the water-impermeable voids, which is in good agreement with the research of Dousti et al. (Dousti et al., 2019). It was reported that a CNC addition of 1% significantly reduced the pores smaller than 30 nm, and the porosity of pores <100nm was reduced by 40% (Dousti et al., 2019).

Figure 6.6 (b)) shows the water absorption and volume of permeable voids of CNC mixtures. A similar trend can be observed between water absorption and the volume of permeable voids. By adding 0.4% CNC, water absorption and volume of permeable voids were reduced from 8.55% and 18.19%, respectively, for the reference mixture to 8.04% and 17.10%. Then, the water absorption and volume of permeable voids showed an increasing trend with CNC content. The mixture with 1.5% of CNC had a water absorption of 8.17% and a volume of permeable voids of 17.41%. The decrease in water absorption and volume of permeable voids with CNC content

smaller than 0.4% may be caused by improved cement hydration (Cao et al., 2015), which will be further discussed in Section 5.3.3. The increasing trend at CNC>0.4% may be caused by the CNC agglomeration that forms defects in the composites. The agglomeration of CNC has been investigated by Cao et al. (Cao et al., 2015) where a significant agglomeration was found in deionized water when 1.35% of CNC was added. This agglomeration was reported to slightly increase the porosity of cement pastes (Cao et al., 2016).

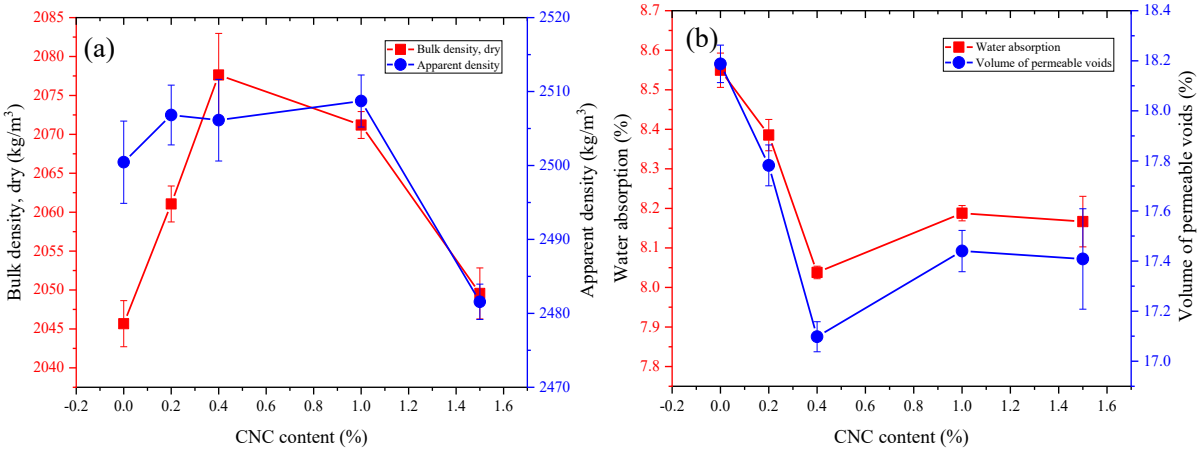

Figure 6.6. Density, water absorption and volume of permeable voids of CNC mixtures: (a) bulk density and apparent density; (b) water absorption and volume of permeable voids

6.3.2.2. After sulfuric acid immersion

Tests for density, water absorption and permeable voids after sulfuric acid immersion were conducted to explore the change in microstructure. The bulk density and apparent density are shown in Figure 6.7 (a). Both the bulk density and the apparent density peaked at 0.4% of CNC with values of 2,056 kg/m^3 and 2,518 kg/m^3 for bulk density and apparent density, respectively. A CNC content of more or less than 0.4% reduced the bulk density and the apparent density. In addition, the 75 days of acid exposure were found to reduce bulk density. The bulk density of samples before immersion was in the range of 2,045-2,077 kg/m^3, while the bulk density ranged in 2,008-2,056 kg/m^3 after exposure to sulfuric acid for 75 days. The reduced bulk density suggests

that the samples become more porous after acid immersion. This can be confirmed by the results of water absorption and permeable voids. As plotted in Figure 6.7 (b), water absorption was raised from the range of 8.04%-8.55% (before immersion) to the range of 8.84%-9.51% (after immersion), while the volume of permeable voids was increased from the range of 17.1%-18.19% (before immersion) to the range of 18.35%-19.47% (after immersion). The increased water absorption and volume of permeable voids may be attributed to the formation of a gypsum layer, which is swelling and porous (Barbhuiya & Kumala, 2017) on the sample surface. Contrary to the bulk density, the apparent density increased from the range of 2,481-2,508 kg/m^3 (before acid immersion) to the range of 2,494-2,518 kg/m^3 after sulfuric acid immersion. This indicates that there are fewer water-impermeable voids in the samples. The reduced water-impermeable voids could be caused by the continued cement hydration (which will be discussed in Section 5.3.3) and the filling effect of generated gypsum. It was observed that the generated gypsum due to sulfuric acid attack could fill the pores in the transition zone of the corroded area and uncorroded area (Tsubone et al., 2016).

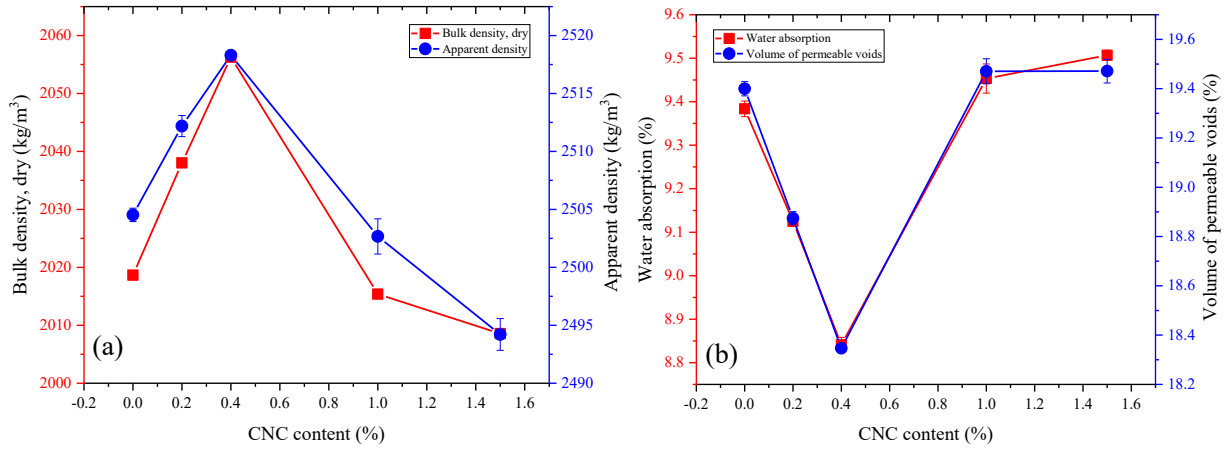

Figure 6.7. Density, water absorption and volume of permeable voids of CNC mixtures: (a) bulk density and apparent density; (b) water absorption and volume of permeable voids

6.3.3. Thermo-gravimetric analysis

6.3.3.1. Before sulfuric acid immersion

To assess the effect of CNCs on the hydration of cement-based composites, the powder samples of paste mixtures were heated up to 985 ℃ at a rate of 5 ℃/min for thermo-gravimetric analysis (TGA). The evolution of residual weight with temperature is presented in Figure 6.8 in solid lines for samples before sulfuric acid immersion. The powder samples experienced three main stages of weight loss. The first stage occurred from room temperature to 400 ℃. The weight loss at this stage was mainly caused by the dehydration of ettringite and C-S-H gel (Lim & Mondal, 2015). The second stage of weight loss occurred from 400 ℃ to 600 ℃, which can be attributed to the dehydration of CH (Rupasinghe et al., 2017). The last stage of weight loss was caused by the decarbonization of $CaCO_3$ from around 600 ℃ to 840 ℃ (Lim & Mondal, 2015; Rupasinghe et al., 2017). Calcium carbonate can be formed through the carbonization of CH when in contact with air. As can be seen from Figure 6.8, the addition of CNC reduced the residual weight of mortar mixtures, which indicates more dehydration during heating. The reference mixture had a final weight of 77.85%. The final residual weight was reduced to 75.54% for the mixture with 0.4% CNC, then increased slightly to 76.95% for the mixture with 1.5% CNC. This suggests that the CNC addition improved the hydration degree of the mortar mixture, and facilitated the generation of C-S-H and CH. As can be seen in Figure 6.8, all mixtures with CNC showed lower residual weight at temperature 400℃, which suggests that there was more C-S-H content in CNC mixtures. As for the CH content, it was directly calculated based on the method proposed by Rupasinghe et al. (Rupasinghe et al., 2017). The results are listed in Table 6.4. It can be seen from Table 6.4 that all CNC mixtures showed higher CH content than the reference mixture. The reference mixture had a CH content of 22.2%, while the highest CH content was 26.5% for the mixture with 0.4%

CNC. This indicates that the mixture with 0.4% of CNC had the highest degree of hydration. These results are in good agreement with previous research. Cao et al. (Cao et al., 2015) found the addition of up to 1.5% CNC enhanced the degree of hydration of cement paste on 7, 14 and 28 days of curing. They suggested two effects were responsible for the increase in hydration degree. First, the CNCs act as a water reducer, which helps the dispersion of cement particles. Second, the CNCs act as channels for water transportation to unreacted cement particles. These two effects improve the hydration reaction between cement particles and water.

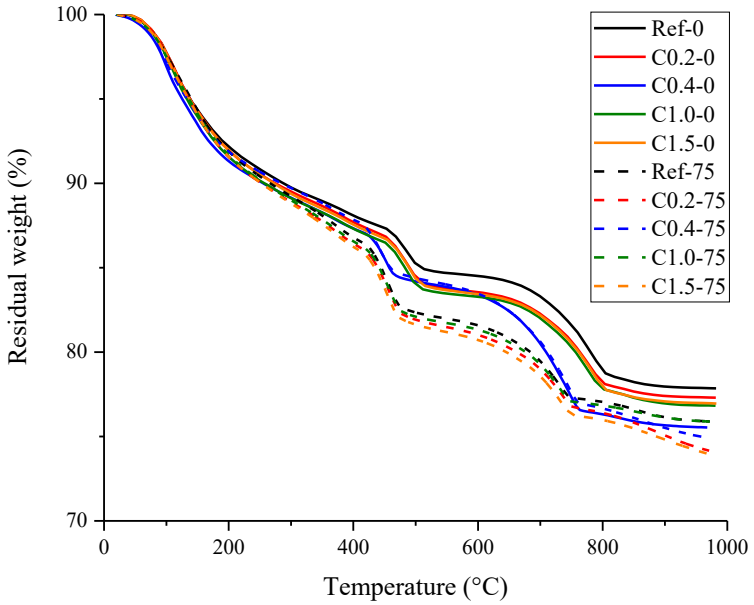

Figure 6.8. TGA curves of mortar mixtures

Table 6.4. CH content calculated from TGA results

Mixture ID	Ref	C-0.2	C-0.4	C-1.0	C-1.5
CH content, wt.%	22.2%	24.2%	26.5%	24%	22.7%

6.3.3.2. After sulfuric acid immersion

The TGA test was also conducted after the 75 days of sulfuric acid immersion. The inner uncorroded part was cut from the paste sample and further prepared into a powder sample smaller than 63 μm. The results are demonstrated in Figure 6.8 in dash lines. No gypsum dehydration was

found during the heating process. In general, all mixtures showed lower residual weight compared with that before immersion. For example, the residual weight reduced from 77.85% to 75.89% for the reference mixture, and a 0.64% drop in the residual weight was found in the mixture with 0.4% CNC. In addition, it can be seen from Figure 6.8 that the weight loss at each phase was lower than that before immersion. This suggests that after 75 days of immersion under sulfuric acid, more C-S-H and CH were formed in the uncorroded part due to the continuous hydration of cement.

6.3.4. Unconfined compressive strength

6.3.4.1. Before sulfuric acid immersion

Mechanical strength is critical for the performance of cementitious structures as they indicate the load capacity of the structure. In this study, the UCS was tested after 28 days of standard curing. The results are plotted in Figure 6.9. The addition of CNC enhanced the UCS of mortar mixtures. The reference mixture had a UCS of 34.43 MPa. The UCS increased with CNC content and peaked at the 0.4% CNC addition with a value of 43.546 MPa. This accounts for a 26.48% improvement compared with the reference mixture. Then the UCS gradually decreased with CNC content, reaching 43.09 MPa at a CNC ratio of 1.5%. The improvement of mechanical properties was also observed by other studies on cement paste (Cao et al., 2015; Dousti et al., 2019; Fu et al., 2017). Danuta et al. (Barnat-Hunek et al., 2019) found a 23.4% improvement in the bending strength of concrete mixture at 1% of CNC addition. Cao et al. (Cao et al., 2015) found the ball-on-three-ball (B3B) flexural strength peaked at 0.2% of CNC at curing ages of older than 3 days, while Fu et al. (Fu et al., 2017) suggested that the mixture with 0.5% of CNC content had the best B3B flexural strength at 28 days. The improved strength was likely due to the increased degree of hydration and

the reduced porosity, which is confirmed by the TGA results and water absorption tests, respectively.

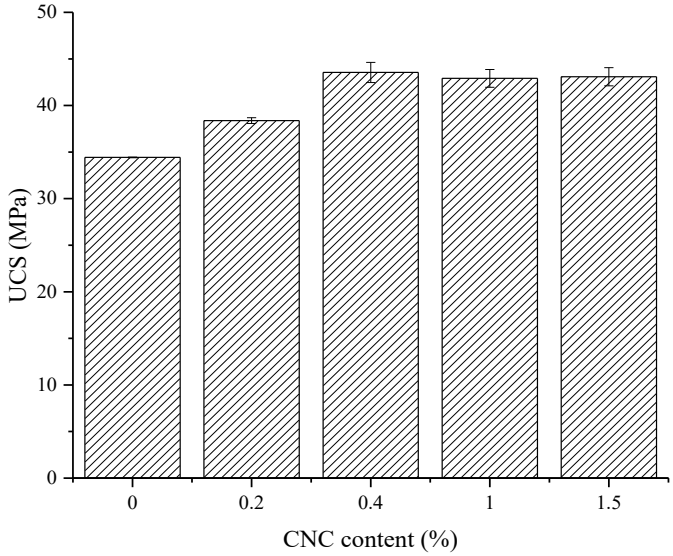

Figure 6.9. UCS of CNC mixtures before sulfuric acid immersion

6.3.4.2. After sulfuric acid immersion

The strength and strength change after 75 days of acid immersion is illustrated in Figure 6.10. The mixtures with CNC contents of less than 0.4% showed a positive UCS change, and the UCS change decreased with CNC content. Compared with the UCS before immersion, the UCS of the reference mixture increased by 21.15%, reaching 41.71 MPa, while the mixture with 0.4% CNC showed a UCS increase of 6.78% with a final UCS of 46.5 MPa. When the CNC content was beyond 0.4%, the mixtures presented a negative UCS change after immersion, with values of -3.03% and -3.84% for mixtures of 1% and 1.5% CNC, respectively. After the 75 days of sulfuric acid immersion, the highest UCS was observed from the mixture with 0.4% CNC. Adding more or less than 0.4% of CNC led to a reduced UCS. The change in UCS during sulfuric acid immersion could be caused by two adverse processes. First, the continued hydration reaction of cement (which is confirmed by the TGA results) leads to an increase of UCS. This continued cement hydration during sulfuric

acid immersion was also reported in previous research (Siad et al., 2016; Wu et al., 2019). Second, the sulfuric acid attack on the sample surface decomposes cement hydration products (CH and C-S-H), damaging the mechanical strength of samples (Yang et al., 2018). Since the reference mixture had a lower degree of hydration after 28 days of standard curing, the cement hydration could be more dominant than the corrosion process. This leads to a positive UCS change. With the increase in CNC content, the hydration degree was increased for samples before acid exposure. Therefore, the corrosion process becomes more dominant during immersion. In addition, when excessive CNC (more than 0.4%) was added, agglomeration may occur, which facilitates the penetration of sulfuric acid during immersion. This could result in severer corrosion (a thicker corrosion layer in visual observation) and a negative strength change at high CNC content.

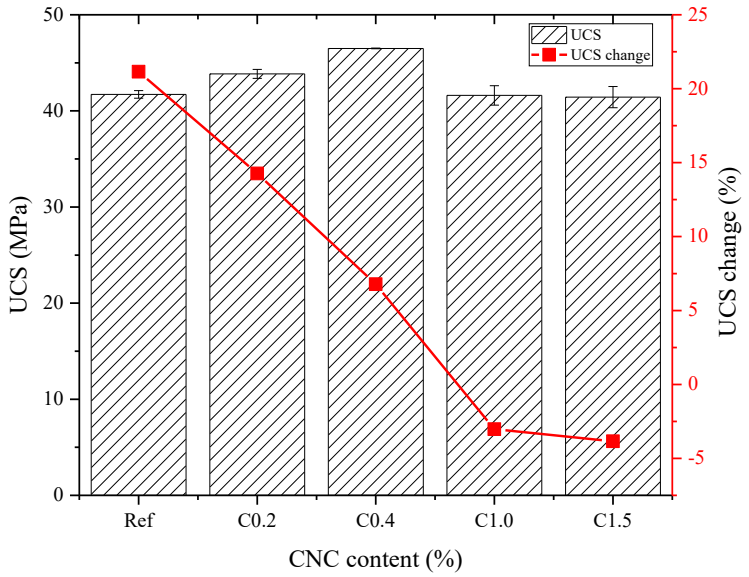

Figure 6.10. UCS and UCS change after sulfuric acid immersion

6.3.5. Ultrasonic pulse velocity

The UPV test is a non-destructive method to evaluate the quality of the concrete samples. A higher UPV indicates a denser microstructure of the samples. In this research, the UPV was monitored during the sulfuric acid immersion, and the results were plotted in Figure 6.11. Figure 6.11 (a)

shows the UPV at different immersion ages. In general, the UPV was decreasing with immersion time for all mixtures, indicating that acid immersion damages the integrity of the samples. As shown in Figure 6.11 (b), the UPV of all the mixtures was in the range of 4070-4307 m/s before sulfuric acid immersion. This suggests that the samples were of good quality (3600-4500 m/s) (Feldman, 1977; Leslie & Cheesman, 1949). It is noticed that the addition of CNC increased the UPV of the mortar mixtures. The UPV increased with CNC content from 4070 m/s for the reference mixture to 4307 m/s for the mixture with 0.4% of CNC. Then, further CNC addition reduced the UPV to 4156 m/s at a CNC content of 1.5%. The increased UPV by CNC addition coincides with the results of the previous study. Mazlan et al. (Mazlan et al., 2016) tested the UPV of cement mortars with up to 0.6% of CNC, and they found the UPV was increased from 4000 m/s to 4310 m/s. The increased UPV could be due to the reduced porosity, as discussed in Section 5.3.2.

After 75 days of sulfuric exposure, the UPV dropped to the range of 3800-3920 m/s, which remained in the range of good quality. The reference mixture showed the lowest UPV of 3800 m/s. Compared with the reference mixture, all mixtures with CNC showed higher UPV after acid exposure. Among the mixtures, the mixture with 0.4% CNC remained the highest UPV of 3920 m/s. This indicates that the mixture with CNC was of higher quality after sulfuric acid immersion. A possible reason for the UPV change after acid immersion was the increased volume of voids. To confirm this hypothesis, a correlation was carried out between the volume of permeable voids and the UPV. The results were plotted in Figure 6.12. A high R^2 of 0.92 was observed, which suggests that the UPV is highly affected by the volume of permeable voids.

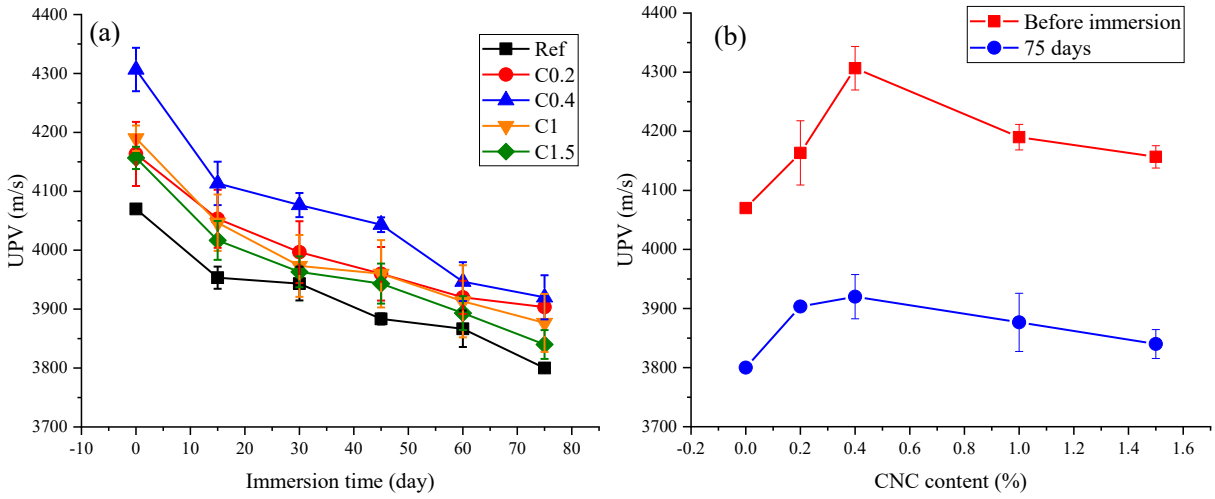

Figure 6.11. UPV results of CNC mixtures: a) with immersion time; b) with CNC content before immersion and after 75 days of immersion

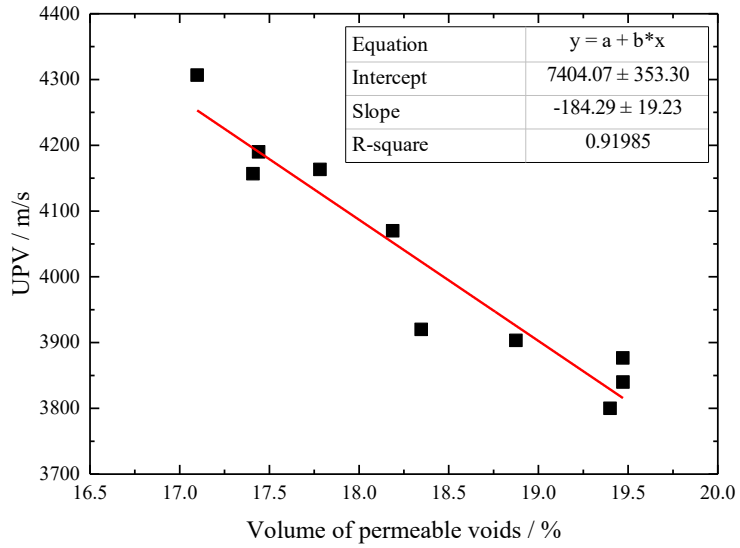

Figure 6.12. Correlation between the volume of permeable voids and the UPV

6.3.6. Mass change

The results of mass change are given in Figure 6.13. Figure 6.13 (a) shows the mass change with immersion time. The positive value indicates the samples were gaining mass. It is demonstrated from Figure 6.13 (a) that all the mixtures were gaining mass, and the mass change was increasing with immersion age. The reference sample gained 1.01% of mass after 75 days of acid immersion.

Figure 6.13 (b) demonstrates that the mass gain was increasing with CNC content after 75 days of immersion. The final mass gain was 1.91% for the mixture with 1.5% CNC. The mass increment during sulfuric acid immersion can be attributed to two processes: 1) the continued cement hydration and 2) the corrosion reaction between cement hydration products (CH, C-S-H) and sulfuric acid. First, during immersion, the absorbed water reacts with the unreacted cement particles, resulting in denser structure and increased mass. Siad et al. (Siad et al., 2016) observed 0.7% of mass gain after 12 weeks of water immersion for the reference mixture. Second, the corrosion reaction, on the one hand, decalcifies the CH and C-S-H and releases calcium cations and water (Yuan et al., 2015), which reduces the mass of the sample. On the other hand, the reaction between cement hydration products (CH, C-S-H) and sulfuric acid generates gypsum (Yang et al., 2018). The retention of gypsum can result in mass increase. The combination of the above-mentioned adverse processes brings uncertainty towards the mass change. To eliminate the effect from gypsum generation, the samples were brushed after 75 days of immersion to remove the gypsum layer on the sample surface. The mass change was calculated, and the results were plotted in Figure 6.13 (b). After removing the gypsum layer, the reference mixture had a mass change of -5.48%; the mixtures with 0.2%, 0.4% and 1% of CNC showed less mass change, with values of -4.97%, -4.82% and -4.98%, respectively. This suggests that the addition of CNC slightly reduced the mass loss of mortar mixtures. The lower mass change after brushing could be due to the reduced volume of permeable voids, which inhibited the penetration of sulfuric acid and thus mitigated the sulfuric acid corrosion (Rahmani et al., 2009).

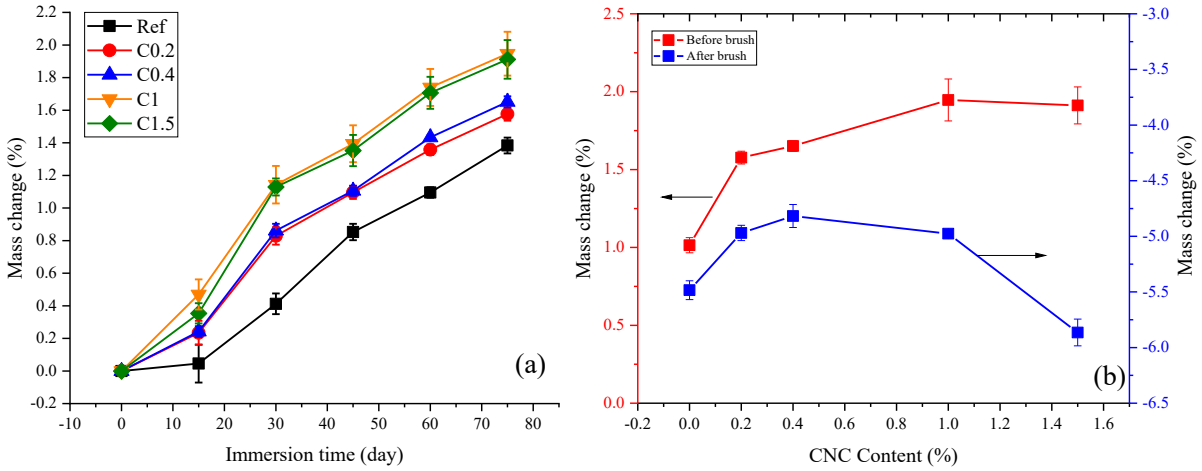

Figure 6.13. Mass change of CNC mixtures: a) with immersion time; b) with CNC content after immersion

6.3.7. Length change

Change in length was monitored as one of the indicators of sample deterioration. The results are demonstrated in Figure 6.14. A positive length change means the length of the sample is increased. As shown in Figure 6.14 (a), all samples were exhibiting positive length change. The reference sample showed a length increase of 0.12% after 75 days of sulfuric acid immersion. It is interesting to notice that the addition of CNC increased the length change of mortar samples. A peak length change of 0.31% was observed for the mixture with 0.2% of CNC. Adding more CNC reduced the length change, reaching 0.196% at a CNC content of 1.5%. This length increment could be attributed to the generation of gypsum, which is twice as large as cement hydration products (Yuan et al., 2015), on the sample surface. To better understand the corrosion degree of the samples, the gypsum layer on the surface was brushed with a steel brusher. The length change after sample brushing was demonstrated in Figure 6.14 (b). It was observed that all samples showed a negative length change after brushing. The reference mixture showed a length change of -1.34%. The length change decreased with CNC content until 0.4%, where the smallest length change was observed

with a value of -0.86%. With the CNC content further increased to 1.5%, the change in length increased to -1.39%. The reduction in length change of mixtures with CNC may suggest that CNC has the potential to mitigate the sulfuric acid attack on cementitious mortars.

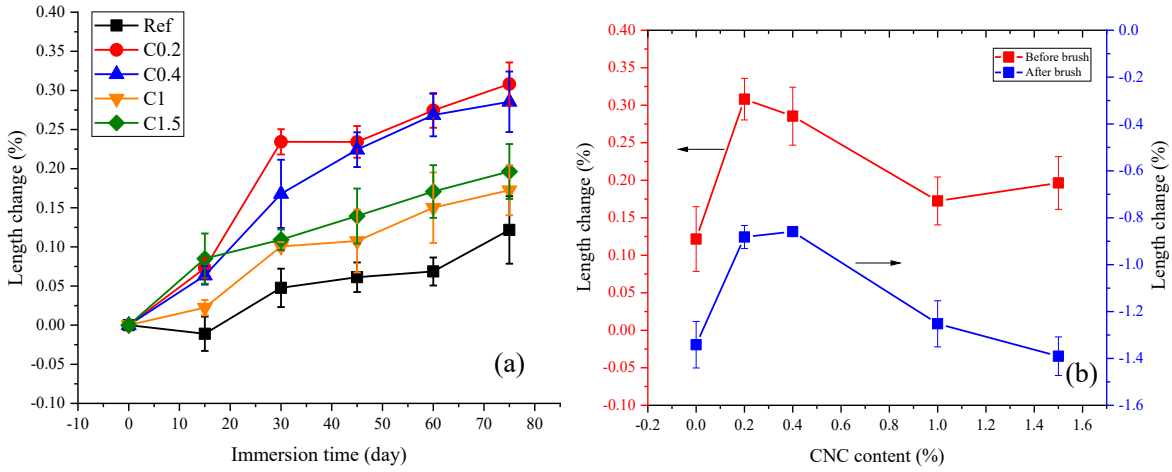

Figure 6.14. Length change of CNC mixtures: a) with immersion time; b) with CNC content after immersion

6.3.8. Evaluation of acid resistance of CNC mixtures

To evaluate the performance of mixtures in resisting sulfuric acid attack, mortar samples were immersed in sulfuric acid with a pH of 2.0 for 75 days. Changes in properties such as UCS, UPV, mass, and length were monitored during immersion to assess the acid resistance of each mixture. These changes in properties were considered indicators of acid resistance. However, the results from different indicators were different. For example, the reference mixture showed the lowest UCS loss after immersion, while the mixture with 0.4% CNC had the lowest mass change (after brushing). In addition, a weak correlation was observed between mass change and length change (before brushing). As shown in Figure 6.15, the R^2 was 0.5023 for the linear correlation. This low correlation between indicators of acid resistance is not uncommon; it has also been reported in previous research. For example, Huber et al. (Huber et al., 2017) found that mass loss and

neutralization depth were weakly correlated for Portland-cement based concrete. Wu et al. (Wu et al., 2019) reported that the correlation between mass change and UCS change was low. This may suggest that each of the indicators may only reflect partial information of sample deterioration. A combination of these indicators may be required to evaluate the acid resistance of samples comprehensively.

From the test results, the mixture with 0.4% CNC showed the best potential in resisting sulfuric acid attack. First, the mixture with 0.4% CNC demonstrated the lowest porosity, highest quality (UPV) and highest UCS before and after sulfuric acid immersion. Second, the mixture illustrated the lowest mass change and length change after sample brushing. The improved acid resistance of CNC mixtures may be attributed to the following two effects. First, the addition of CNC enhanced the hydration of cement, which reduced the porosity of cement-based composites. The reduced porosity inhibited the penetration of aggressive hydrogen ions and sulfate, and thus mitigated the sulfuric acid corrosion. The improved acid resistance by the reduced porosity was also reported in previous research. For example, Mahdikhani et al. (Mahdikhani et al., 2018) investigated the durability of concrete mixtures with nano-silica and concluded that easier deterioration could be observed with mixtures of higher porosity. Bhogayata (Bhogayata & Arora, 2018) found that the addition of short metalized plastic waste fiber improved acid resistance of concrete mixtures due to the densified interfacial transition zone. Korucu et al. (Korucu et al., 2019) observed that the reduced progression of water improved the resistance of cement-based composites reinforced by carbon-based materials. More specifically, Rahmani et al. (Rahmani et al.) found that when the sulfuric acid solution had a pH of higher than 2, lower porosity could reduce the corrosion level of cement-based composites. Second, the addition of CNC improved the hydration degree of cement. The increased amounts of hydration products (e.g. CH and C-S-H) can raise acid

neutralization capability. It has been reported in many studies that the materials with increased neutralization capacity are more acid-resistant. Joorabchian et al. (Joorabchian, 2010) claimed that the higher neutralization capacity of the outer surface prevents acids from penetrating into the inner part. Thus, a higher amount of hydration products CH and C-S-H can provide better resistance to sulfuric acid attack. Ehrich et al. (Ehrich et al., 1999) investigated the acid resistance of Portland cement mortar and calcium aluminate cement mortar. They found that the calcium aluminate cement-based mortars were more resistant to sulfuric acid attack due to their higher neutralization capacity. Xiao et al. (Xiao et al., 2016) stated that a high neutralization capacity reduces the local acidity, which slows the rate of acid attack.

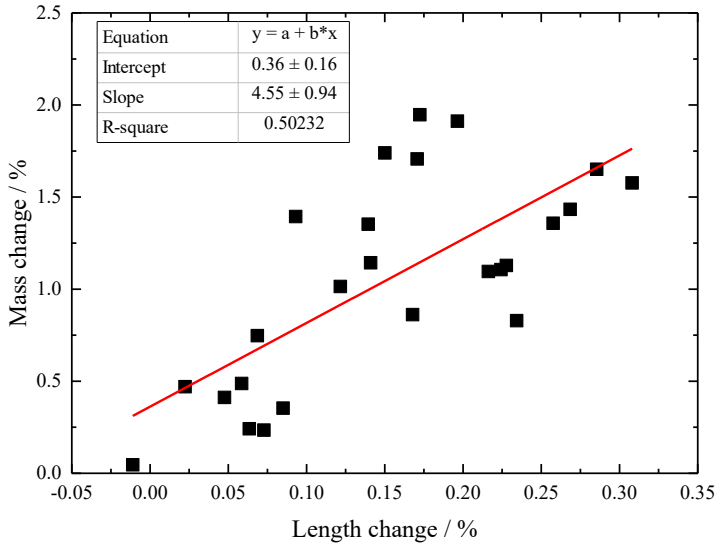

Figure 6.15. Correlation between length change and mass change

6.4. Conclusions

This study aims to explore the potential of cellulose nanocrystals (CNC) to improve the acid resistance of cement mortar. The following conclusions can be drawn based on the test results:

(1) From the density and water absorption tests, the addition of CNC refined the microstructures of mortars by reducing the water absorption and volume of permeable

voids. The mixture with 0.4% CNC showed the lowest water absorption and volume of permeable voids. Acid exposure increased the water absorption and volume of permeable voids due to the generation of a gypsum layer.

(2) From the thermo-gravimetric analysis, the addition of CNC improved the hydration degree of the cement paste. The mixture with 0.4% CNC showed the highest level of improvement. After 75 days of sulfuric acid immersion, the hydration degree was increased for the uncorroded part.

(3) CNC was found to enhance the unconfined compressive strength (UCS). The mixture with 0.4% CNC had the highest UCS, which can be attributed to reduced water absorption and enhanced cement hydration. The mixtures with CNC contents of less than 0.4% showed a positive UCS change after sulfuric acid immersion. Mixtures with higher amounts of CNC showed a negative UCS change.

(4) The mixture with 0.4% CNC showed the best potential in resisting sulfuric acid attack as it showed the lowest mass change and length change, and the highest UCS and ultrasonic pulse velocity (UPV) after 75 days of sulfuric acid immersion.

Chapter 7. Forecasting the deterioration of cement-based mixtures under sulfuric acid attack using support vector regression based on Bayesian optimization

This chapter has been submitted for peer review as **L. Wu**, C. Hu, W.V. Liu, (2020). Forecasting the deterioration of cement-based mixtures under sulfuric acid attack using support vector regression based on Bayesian optimization, *SN Applied Sciences*. © Springer. (under review)

7.1. Introduction

The sulfuric acid attack poses serious problems for cement-based sewer tunnels and could lead to significant service life reduction to the structures and a substantial financial cost for repair (Wu et al., 2019). To mitigate this sulfuric acid attack, much research has been carried out in seeking a more acid-resistant cement-based mixture. Previous studies (Chindaprasirt et al., 2004; Dinakar et al., 2008; Durning & Hicks, 1991; Ekolu et al., 2016; Hossain et al., 2016; Newman & Choo, 2003; Pavel & Jiří, 2016; Shetti & Das, 2015; Torii & Kawamura, 1994a) have proven that the addition of pozzolanic materials including fly ash, silica fume, and metakaolin can slow the deterioration by sulfuric acid attack. A large amount of data has been published regarding the deterioration of these mixtures exposed to sulfuric acid attack. However, these data are not comparable due to the difference in testing conditions in various studies. Thus, a new evaluation test is often carried out when a comparison of these mixtures is needed, which is time−consuming and labor−intensive. The immersion test often lasts for several months or even several years. In addition, the experimental investigation is discrete regarding the mixture design and testing conditions (pH of acids). Herein, many researchers have been trying to find alternative ways to evaluate acid resistance. One of the options is to predict the deterioration of concrete by empirical models or regression learning algorithm using a currently available database.

The first way to predict deterioration is to develop empirical equations for the prediction of the deterioration of mixtures under sulfuric acid attack. De Belie et al. (De Belie et al., 2004) developed a model to predict the degradation depth under sulfuric acid attack, considering the alkalinity and water absorption of the mixtures. A correlation coefficient of 0.84 was found between input parameters and the corrosion depth. More studies have been done to develop

empirical models for the deterioration prediction of samples subjected to sulfate attack (Kurtis et al., 2000; Lee et al., 2015; Marchand, 2002). However, these empirical models only included parameters about mixtures and ignored the effects of testings conditions on the deteriorations. This limits the application of current models to certain testing conditions. For instance, the empirical model published by Kurtis et al. (Kurtis et al., 2000) was developed to predict the deterioration of concrete specimens soaked in 2.1% sodium sulfate solution for 40 years, while the application of the model proposed by Lee et al. (Lee et al., 2015) was limited to concrete specimens exposed to 10% sodium sulfate solution and 10% magnesium sulfate solution for one year. When the testing conditions are changed, the accuracy of these models is unknown.

Another alternative way to forecast deterioration is through a machine learning algorithm such as artificial neural networks (ANN) and evolutionary polynomial regression (EPR). Using the data collected from their experimental tests, Hewayde et al. (Hewayde et al., 2007b) developed an ANN model for the prediction of compressive strength and mass change of 78 mixtures under a sulfuric acid attack. The ANN models showed reasonable accuracy in the prediction with an average absolute error (AAE) of 8.45% for mass change prediction and 4.85% for compressive strength prediction. Using the same database as Hewayde et al. (Hewayde et al., 2007b), Alani et al. (Alani & Faramarzi, 2014) proposed an EPR method to forecast the mass loss of concrete subject to sulfuric acid attack. Slightly higher accuracy was reported for the EPR method compared with the ANN model in mass change prediction. However, these models also failed to include the testing conditions in their studies. Only mixture design parameters were used as inputs in these two models.

Much research has reported that the testing conditions (e.g., acid concentration, reaction surface area, continuous wetting-drying cycles, immersion time, and surface to acid volume ratio) could

have a significant influence on concrete deterioration (Attiogbe & Rizkalla, 1988; Rombén, 1980; Wafa, 1994). For example, Chen et al. (Chen et al., 2018) found that immersion time is one of the main factors that affect the compressive strength of concrete after immersion. Through experimental observation, Attiogbe et al. (Attiogbe & Rizkalla, 1988) found that wetting-drying cycles increase the concrete deterioration degree. Rombén et al. (Rombén, 1980) stated that any testing conditions that would affect the acid supply would influence the deterioration of concrete. Herein, a prediction without considering the testing conditions could limit the application of the proposed model to certain testing conditions. Thus, there is an urgent need to develop a predictive model that incorporates these testing conditions.

With the rapid development of machine learning techniques, there are various algorithms available for the construction of such predictive models, such as ANN and EPR mentioned in the previous review. However, these ANN and EPR models have their shortcomings. For instance, ANN has a complex network structure with matrixes of weights and biases, which demands expensive computational time and memory (Kaviani & Sohn, 2020; Xin et al., 2020). In addition, due to the large number of weights, the ANNs are prone to overfitting which leads to poor generalization (Lawrence et al., 1997; Panchal et al., 2011). For the EPR methods, they were found to be too sensitive to outliers in a database. A single outlier in data could lead to a significant error in the prediction results (Wellmann et al., 2009). Thus, a model is needed to overcome these shortcomings.

In this study, the main aim is to develop a predictive model to forecast the deterioration of mortars under sulfuric acid attack incorporating both mixture design parameters and test conditions. Two Bayesian optimization-support vector regression (BO-SVR) models were constructed to predict mass change (model I) and residual compressive strength (model II) of mortar samples under a

sulfuric acid attack. The SVR algorithm was adopted because it was found to have a lower risk of overfitting (Moraes et al., 2013), and relatively low sensitivity to outliers due to the use of loss functions (Antonanzas et al., 2017). Furthermore, SVR models have excellent ability in searching global optimal solutions with a relatively small database (Gao & Song, 2013). Lastly, the SVR models are easy to construct because SVR models have fewer model variables (Kaytez et al., 2015; Pu et al., 2018). The BO technique was adopted to search the optimal hyperparameters for the SVR model because of its high accuracy and efficiency (Czarnecki et al., 2015). The input parameters included both mixture designs and testing conditions. The performance of the BO-SVR models was evaluated by prediction errors and a superiority test. This study has provided valuable insights into the deterioration prediction of mortars samples under different sulfuric acid immersion conditions.

7.2. Methodology

In this section, an SVR model optimized by the Bayesian algorithm is proposed to predict the mass change and compressive strength of mortar samples under a sulfuric acid attack. To assess the performance of the BO-SVR model, four other models were also constructed for comparison. Three SVR models optimized by different techniques (grid search (GS), random search (RS), and particle swarm optimization (PSO)) were constructed for comparison to assess the capability of BO technique in seeking the optimal hyperparameters of SVR. Then, the SVR models were compared with a traditional ANN model. All the models were verified using the *k*-fold cross-validation technique. The performance of each model was evaluated by four averaged indicators: the coefficient of determination R^2, the mean absolute error (MAE), the root mean square error (RMSE), and the mean absolute percent error (MAPE). The overall methodology is illustrated in Figure 7.1.

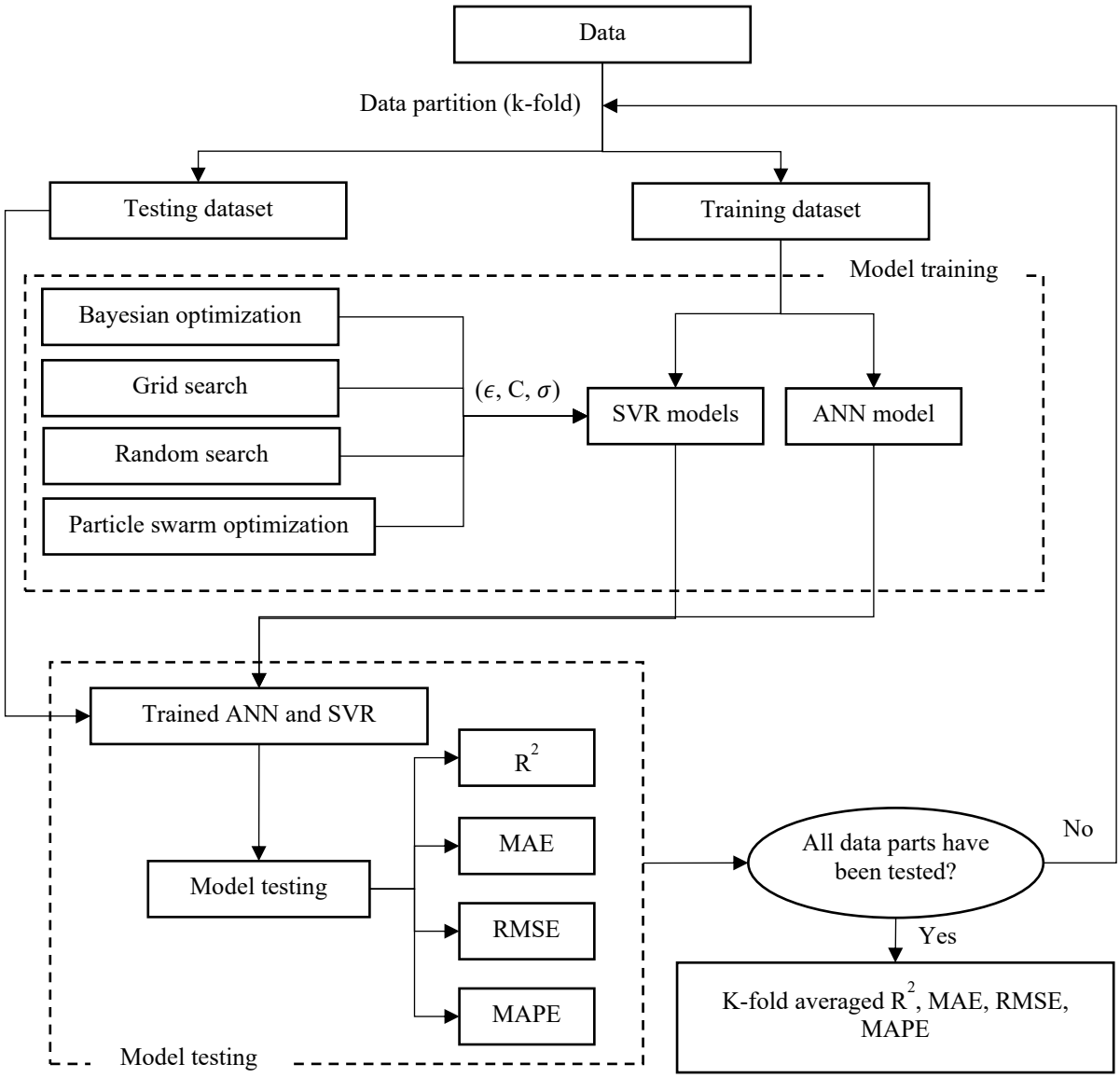

Figure 7.1. A flowchart showing the overall methodology

7.2.1. Support vector regression

The SVR algorithm (Cortes & Vapnik, 1995) is adopted in this study. The basic idea of SVR is to nonlinearly map the training dataset (input data and output data) into a high-dimensional feature space via a kernel function. A linear relationship between input data and output data can be found in this high-dimensional feature space to reflect the nonlinear relationship before mapping. This

linear function in the high-dimensional space is the SVR function. Supposing $T=\{(x_1,y_1), (x_2,y_2),\ldots,(x_n,y_n)\}$ is a training data set, where n is the sample number, $x_i \in R^n$ is the input vector, and $y_i \in R$ is the corresponding output. The SVR function can be written as follows:

$$f(x)=w^T x+b \tag{7-1}$$

where $f(x)$ is the predicted value, $w \in R^n$ indicates the slope of the function, and $b \in R$ is an offset scalar.

By introducing a tolerance ϵ and slack variables ξ_i, ξ_i^*, the SVR function can be written as an optimization problem:

$$\begin{aligned} &\textit{minimize} && \tfrac{1}{2} w^T w+C\textstyle\sum_{i=1}^{i=n}(\xi_i+\xi_i^*) \\ &\textit{s.t.} && y_i-f(x_i)\le\epsilon+\xi_i; \\ & && f(x_i)-y_i\le\epsilon+\xi_i^* \\ & && \xi_i,\xi_i^*\ge 0 \end{aligned} \tag{7-2}$$

In this optimization problem, an error of ϵ is allowed for each datapoint. In other words, a predicted $f(x_i)$ with an error smaller than ϵ means $f(x_i)$ is considered a correct prediction, and no penalty will be applied to the objective function. When an error is larger than ϵ, the extra error will be captured by the slack variables ξ_i, ξ_i^* and penalized in the objective function through a penalty factor C.

To solve this optimization problem, the optimization problem is often transformed into its dual form where the constraints are expressed by Lagrange multipliers (Kavaklioglu, 2011):

$$minimize \quad \frac{1}{2}\sum_{i=1}^{i=n}\sum_{j=1}^{n}(\alpha_i-\alpha_i^*)(\alpha_j-\alpha_j^*)x_i^T x_j+\epsilon\sum_{i=1}^{n}(\alpha_i+\alpha_i^*)-\sum_{i=1}^{n}y_i(\alpha_i-\alpha_i^*)$$

$$s.t. \quad \sum_{i=1}^{n}(\alpha_i+\alpha_i^*)=0;$$

$$0\le\alpha_i,\alpha_i^*\le C \tag{7-3}$$

And the SVR function can be rewritten as follows:

$$f(x)=\sum_{i=1}^{n}(\alpha_i^*-\alpha_i)\,K(x_i,x)+b \tag{7-4}$$

where α_i and α_i^* are the Lagrange multipliers. The support vector is the training vector with non-zero Lagrange multipliers. The dot product $x_i x$ is the kernel function $K(x_i,x_j)$.

Typically, there are three kernel functions available for the SVR modeling including radial basis function (RBF), polynomial kernel function, and sigmoid function. Since the RBF kernel function is capable of solving non-linear relationship problems and was reported to perform better than polynomial and sigmoid function (Hong et al., 2011; Huang et al., 2004), the RBF kernel $K(x,y)=exp(-\frac{(x-x_i)^2}{2\sigma^2})$ is adopted in this research. Variable σ is the width of the kernel function.

7.2.2. Implementation of Bayesian optimization in SVR model

The performance of non-linear SVR is highly dependent on the selection of hyperparameters (e.g., ϵ, C, and σ for RBF-based SVR) (Ito & Nakano, 2003; Kaneko & Funatsu, 2015; Laref et al., 2019; Smets et al., 2007). Careful tuning of these parameters is essential for the performance of the SVR model. Typical methods of hyperparameters optimization include GS, RS, and PSO. GS is to try every possible combination of hyperparameters until the stop criteria is met (Zhang et al.,

2014). The stop criteria could be that the pre-set max iteration step is reached, or all the possible combinations of hyperparameters have been tried. The combination of hyperparameters with the lowest objective function is then chosen as the hyperparameters for the SVR model. However, as this method searches all possible combinations of hyperparameters, it requires large computational time and memory (Bergstra & Bengio, 2012). RS is to find the optimal combination of hyperparameters by randomly choosing possible values of hyperparameters (Mantovani et al., 2015). RS is more efficient than GS in seeking hyperparameters as only part of the possible solutions is tried. However, the RS has a major drawback of high variance resulting from random trials of solutions. This makes the method difficult in reproducing results (Bergstra & Bengio, 2012). In PSO, positions and velocities are randomly assigned to a set of particles to seek the hyperparameters with the lowest objective function (Meng et al., 2014). It utilizes the information from previous iterations to update the positions and velocities of particles, which makes it efficient in hyperparameter optimization. However, it was found that PSO tends to provide local optimum and has a low convergence rate (Li et al., 2014). Compared with these methods, the BO technique was reported to provide higher accuracy and efficiency in finding the global optimal hyperparameters (Czarnecki et al., 2015). Thus, this research adopted the BO approach to find the optimal hyperparameters for the SVR models. The SVR models optimized with GS, RS and PSO were also established as the references to evaluate the performance of BO algorithm in hyperparameter optimization.

The implementation of BO-SVR model is presented in Figure 7.2 and described as follows:

Step 1: Data preparation: the input data in the dataset were first normalized to [0,1]. Then, the dataset is randomized and divided into five parts for the k-fold cross-validation of the model. When dividing the dataset into a training dataset and a testing dataset, random sampling may result in

biased consequences (Chou et al., 2010). It is likely that the high prediction accuracy of the randomly divided test dataset A cannot be reproduced from another randomly selected test dataset B. Thus, to minimize this bias, the *k*-fold cross-validation technique is employed in this study. The dataset is randomly divided into five parts; each part has the same proportion of the total dataset. The model will be run five times until all five parts of data have been used as a testing dataset.

Step 2: Model training: during the training process, the BO approach was adopted. A probabilistic distribution (statistical model) of the objective function will first be constructed through a Gaussian process. This probabilistic distribution describes the potential values of the objective function at different points. In this study, the objective function is to minimize the mean square error (MSE) between the observed values with the predicted values:

$$MSE = \frac{1}{n}\sum_{i=1}^{n}(y_i - y_i')^2 \quad (7\text{-}5)$$

where n is the number of the forecasting points, and y_i and y_i' are the actual and predicted values, respectively.

Then, a combination of hyperparameters will be selected based on an acquisition function. The acquisition function measures how much improvement will be made on the model to try a point (a combination of hyperparameters). The point with the highest expected improvement is picked as the next sample point. These selected hyperparameters are then applied to the objective function, and the probabilistic distribution is updated incorporating the new results. These steps are repeated until the stop criteria are met. At last, the output is the optimized combination of hyperparameters that will be used in the trained SVR model. Bayesian optimization makes full use of all the information from previous iterations to find the next data point. Herein, the BO is able to find the global optimal solution with relatively fewer iterations (Alade et al., 2019; Cheng et al., 2019).

The above-mentioned training process was carried out on the Matlab 2019a platform. The maximum iteration steps were set to 100 for mass change prediction and compressive strength prediction after running several trials.

Step 3: Model testing—test the model performance with the testing dataset. This will be discussed in Section 6.2.4.

Step 4: Use the next part of data as the testing dataset, and repeat steps 2 and 3 until every part has been used as the testing data.

The implementation of GS-SVR, RS-SVR and PSO-SVR followed similar steps described above except some differences in step 2. For GS, every possible combination of hyperparameters will be tried until the max iteration is reached. In order that a sufficient range of hyperparameters can be searched, the max iteration was set to a large number of 1000 for the GS-SVR model. For RS, the max iteration was set as 100 based on the results from several trials. The implementation of PSO-SVR followed a similar procedure described a relevant study by Meng et al.,(Meng et al., 2014). The random positions and velocities are first assigned to particles, then the training dataset is used to train the model and find the best particle positions with the lowest objective function. After that, the particle velocities and positions are updated for the next round of model training. The procedure is repeated until the max iteration step (200) is reached. The position with the lowest objective function will be adopted as the combination of hyperparameters for the model.

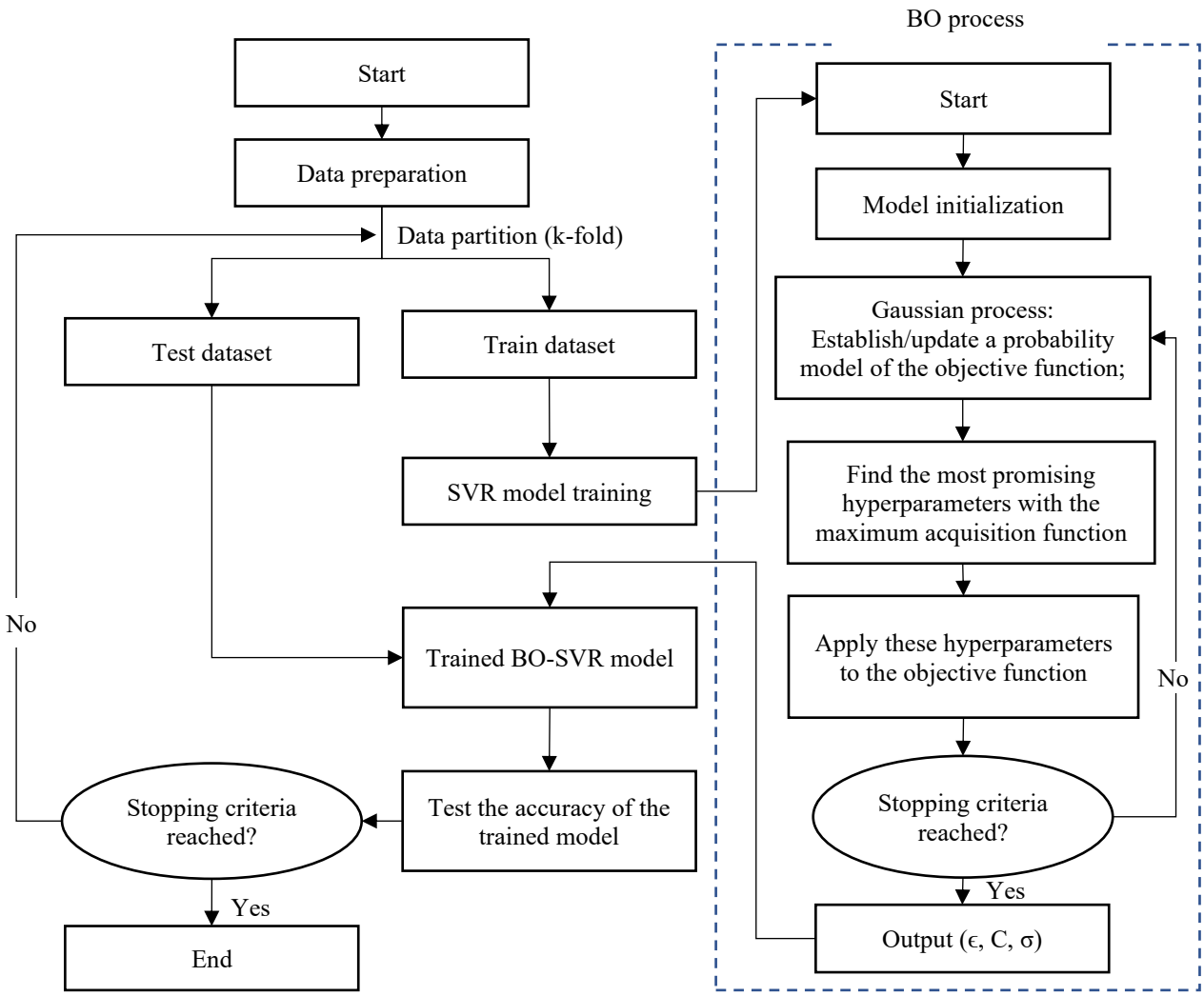

Figure 7.2. The flowchart of BO-SVR modeling

7.2.3. Development of artificial neural network

To provide a performance comparison, an ANN model was also constructed. Due to its strong ability in modeling complex and nonlinear relationships, ANN is one of the most commonly used machine learning methods for prediction problems of cement-based composites (Ling et al., 2019). This makes ANN a good reference in evaluating the performance of the BO-SVR model. ANN is a computational model that can mimic biological neural networks (Hammoudi et al., 2019). It consists of three layers: the input layer, the hidden layer, and the output layer. The input layer

receives the value of input factors that influence the outputs (Behnood & Golafshani, 2018). This layer has no activities during the computational process. The hidden layer adds non-linearity to the system via an activation function, and it carries the weights and biases describing the strength of the connection between linked neurons (Kramer, 1991). The output layer contains the ANN prediction values. During the training process, the weights and biases will be updated through backpropagation to minimize the error between the predicted results and the actual values.

To construct an ANN model, the selection of neuron number in the hidden layer is of great significance. More neurons in the hidden layer can reduce the error of the model but can also result in overfitting of the model (Hewayde et al., 2007b). If the number of neurons is small, underfitting may occur. In this study, the number of neurons was determined via Equation 7-6 below, which was proposed by Sheela et al. (Sheela & Deepa, 2013), because it produced the lowest MSE compared with other methods. In order to avoid overfitting, Bayesian regularization was adopted in this research due to its superior generalization capability (Doan & Liong, 2004).

$$N=(4n_1^2+3)/(n_1^2-8) \tag{7-6}$$

where N is the number of neurons in the hidden layer; n_1 denotes the number of input parameters.

Figure 7.3 shows the structures of ANN models for mass change and compressive strength predictions. For mass change prediction, there were 11 input parameters (6 about mixture design, and 5 about testing conditions), 5 neurons in the hidden layer, and one output parameter (mass change), while the ANN model for compressive strength prediction contained 12 input parameters (7 about mixture design/properties, and 5 about testing conditions), 5 neurons in the hidden layer, and one output parameter (compressive strength). The *k*-fold cross-validation technique was also adopted in the ANN modeling.

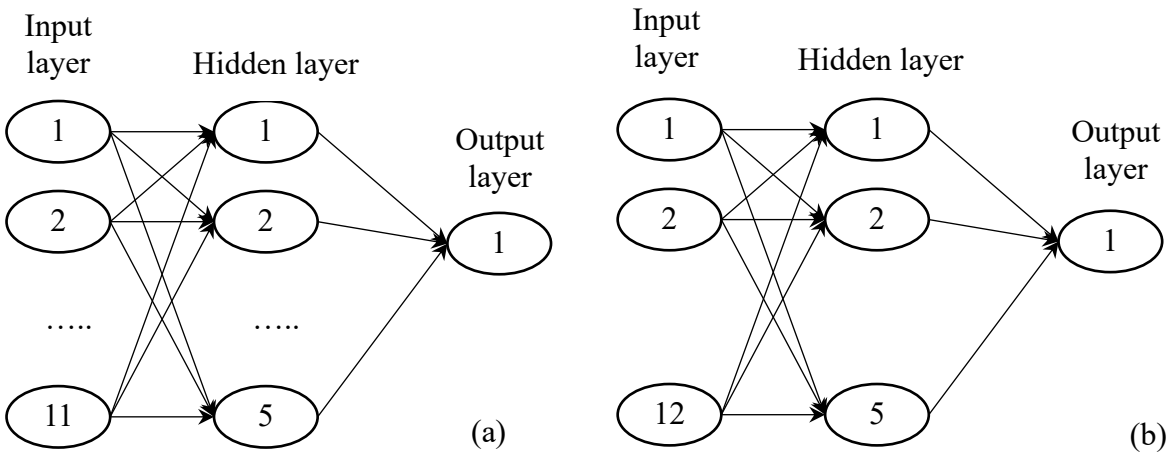

Figure 7.3. The structure of ANN models: a) mass change prediction; b) compressive strength prediction

7.2.4. Performance criteria

To assess the optimization performance of the BO technique, SVR models with three other optimization techniques were also constructed. These techniques include GS, RS, and PSO (Meng et al., 2014). The techniques were chosen because they have been frequently used as the optimization tools in machine learning and have provided good solutions in searching the hyperparameters (Bergstra & Bengio, 2012; Sonebi et al., 2016; Yaseen et al., 2018). This makes these optimization techniques good references. The modeling of the GS-SVR and RS-SVR models followed a similar procedure of BO-SVR, as described in Section 6.2.2. The PSO-SVR was established following a similar procedure described in the literature (Meng et al., 2014). In total, five predictive models were constructed. To evaluate the performance of these predictive models, four performance indicators were employed in this study, including the coefficient of determination R^2, the mean absolute error (MAE), the root mean square error (RMSE), and the mean absolute percent error (MAPE), which can be calculated as Equations 7-7~7-10. The MAE indicates the level of similarity between predicted and experimentally measured values; RMSE

represents the overall deviation between predicted and experimentally measured values; and MAPE can be considered as the relative error to the experimentally measured values (Cheng et al., 2019). The model with higher R^2 and lower MAE, RMSE, and MAPE can be regarded as having better performance in the prediction.

$$R^2 = \frac{\left(n\sum y_i y_i' - \sum y_i \sum y_i'\right)^2}{\left(n\sum y_i^2 - \sum y_i^2\right)\left(n\sum y_i'^2 - \left(\sum y_i'\right)^2\right)} \tag{7-7}$$

$$MAE = \frac{1}{n}\sum_{i=1}^{n} \left| y_i - y_i' \right| \tag{7-8}$$

$$RMSE = \sqrt{\frac{1}{n}\sum_{i=1}^{n} \left(y_i - y_i'\right)^2} \tag{7-9}$$

$$MAPE = \frac{100\%}{n}\sum_{i=1}^{n} \frac{\left| y_i - y_i' \right|}{\left| y_i \right|} \tag{7-10}$$

The overall performance of *k*-fold cross-validation was calculated by averaging each of the above-mentioned indicators of *k* individual folds:

$$A_{CV} = \frac{\sum_i^k P_i}{k} \tag{7-11}$$

where A_{CV} denotes the averaged value of the performance indicators for the *k*-fold cross-validation, and P_i is the value of the above-mentioned performance indicator for the i^{th} fold.

7.2.5. Test of superiority of model performance

A superiority test was carried out to verify if the proposed model performs significantly different from the other models. As a common method for multiple model comparison, the Friedman's test method was adopted in this study for the comparison between the five models (Hong et al., 2011). Friedman's test is a nonparametric method with a null hypothesis: the mean of forecasting errors

are the same for all models (López-Vázquez & Hochsztain, 2019). If the null hypothesis is rejected, it means the compared models perform significantly differently. To test this null hypothesis, the test statistic *FM* is calculated by Equation 7-12 (Xu et al., 2017). If the calculated FM is larger than the critical FM, it suggests that the null hypothesis of the Friedman's test is rejected. In this study, the Friedman's test will be carried out on the Matlab 2019a platform. The *FM* values will be calculated along with the p-value. The p-value is the probability of critical *FM*> calculated *FM*. A low p-value suggests that the null hypothesis of the Friedman's test is rejected, indicating a significant difference between compared models.

$$FM=\left[\frac{12}{N_F*k_F*(k_F+1)}\right]*\sum R_F^2-[3*N_F*(k_F+1)] \quad (7\text{-}12)$$

where N_F is the number of parameters used for performance evaluation; k_F is the number of models for comparison; R_F is the sum of the average rank of performance parameters for each model, which can be calculated by Equation 7-13 (Xu et al., 2017).

$$R_F=\frac{1}{N_F}\sum_{i=1}^{N_F} s_i \quad (7\text{-}13)$$

where s_i is the rank of the *i*th parameter for performance evaluation for each model.

7.3. Development of database

To predict the deterioration of mortar samples under sulfuric acid attack, data used in this study were obtained from experimental work in previous chapters (see Appendix 1 and 2). The input parameters include both mixture design and immersion conditions. These immersion conditions are: the pH of immersion acid, wetting-drying cycle, immersion ages, number of times acid was added, and ratios of acid volume to sample surface area. The mixture design parameters are: fly ash content, silica fume content, nano-silica content, CNC content, CAC content, and

geopolymers. The monitoring of deterioration of samples during immersion involves measuring the mass change and the residual compressive strength. In this study, two Bayesian-SVR models were constructed. Model I was constructed to predict mass change by considering abovementioned 11 input parameters (6 about mixture design, and 5 about testing conditions), while Model II was constructed to forecast the compressive strength, taking 12 input parameters into account (those parameters from Model I and the compressive strength after 28 days of curing). A total of 93 data points for the prediction of compressive strength and 244 data points for the prediction of mass change was collected (see Appendix 1 and 2).

7.3.1. Data preprocessing

The values of different input parameters may vary drastically in magnitude; this could affect the accuracy and efficiency of the model significantly because the parameters with a greater range may dominate the training process compared with parameters with a smaller range (Meng et al., 2014). Thus, the data collected for SVR modeling are normalized to [0,1] according to the following equation:

$$x' = \frac{x - x_{min}}{x_{max} - x_{min}} \tag{7-14}$$

where x' is the standardized data, x_{min} is the minimum value of the parameter, and x_{max} is the maximum value of the parameter.

7.3.2. Grey relational analysis

Since the selection of the input parameters has a great impact on the accuracy of the prediction performance, how close the selected input parameters are to the output parameters needs to be examined. In this study, the grey relational analysis was carried out after data normalization to

verify if the selected input parameters have a reasonably close relation with the output parameters. The grey relational analysis measures the closeness between one parameter and all the other parameters (Sun et al., 2018). In the grey relational analysis, the relevancy between two parameters is measured by the grey relational grade. The details for the calculation of the grey relational grades can found in the relevant literature(Chan & Tong, 2007) and (You et al., 2017). A higher grade represents that the input parameter is more closely related to the output parameter (Lai et al., 2012).

The calculated grey relational grades are listed in Table 7.1 and Table 7.2 for mass change prediction and compressive strength prediction, respectively. A higher grey relational grade (closer to 1) reflects a greater influence of the input parameter on the output parameter. It can be seen that the selected input parameters have a reasonably close relationship with the mass change and compressive strength. The grades ranged from 0.252 to 0.690 for inputs of mass change prediction and from 0.171 to 0.776 for inputs of compressive strength prediction.

Table 7.1. Grey relational grades between input factors with mass change

Input parameters	Grey relational grades to mass change
Geopolymer	0.689166
CAC content	0.690109
CNC content	0.686404
Fly ash content	0.689573
Silica fume content	0.674281
Nano-silica content	0.686983
Wet-dry cycle	0.604996
Ratio of sample surface to acid volume	0.688009
pH	0.614324
Time, day	0.2519
Acid addition times	0.48632

Table 7.2. Grey relational grades between input factors with compressive strength

Input parameters	Grey relational grades to compressive strength
Geopolymer	0.43565
CAC content	0.440422
CNC content	0.435376
Fly ash content	0.440716
Silica fume content	0.443132
Nano-silica content	0.435785
Wet-dry cycle	0.776117
Ratio of sample surface to acid volume	0.442449
pH	0.550196
Time, day	0.170955
Acid addition times	0.573986
Initial compressive strength	0.308181

7.4. Results and discussion

To assess the performance of the BO technique in searching for the optimal hyperparameters, SVR models with three other optimization techniques were also constructed for comparison in this study. These techniques included GS, RS, and PSO (Meng et al., 2014). Then, the SVR models were compared with the traditional ANN model. The five-fold cross-validation technique was applied to all five models. The performance of these models was evaluated and compared using the parameters in Section 6.2.5 (i.e., R^2, MAE, RMSE, MAPE). The above predictive models were independently applied in predicting mass change and compressive strength.

7.4.1. Prediction results of mass change

The mass change was predicted using five predictive models for mortars soaked in various sulfuric acid immersion conditions. Eleven input parameters were incorporated in the models, including 6 mixture design parameters and 5 parameters about immersion conditions. The five-fold cross-

validation technique was applied to test the accuracy of the model. The total of 244 data points was divided into five parts, with the sizes of each part being (48, 49, 49, 49, 49). One part of the data was used for testing the models, while the other four parts were fed to the models for the training process. For SVR models, the training process is to find the optimal hyperparameters (ϵ, C, σ). To compare the optimization performance of the four different techniques, Figure 7.4 illustrates the hyperparameter optimization process of each technique (data part 5 as testing data). The objective function (e.g., MSE) decreased with the increasing iteration number in all the optimization techniques. All the optimization processes converged before the set maximum iteration number. The objective function converged at iterations of around 50 with a value of 0.0454 for the BO technique, indicating an excellent efficiency in searching for the optimal hyperparameter for the SVR model. The results of the objective function and hypermeters after optimization (training process) are also listed in Table 7.3. The BO technique was able to find the hypermeters combination with the lowest objective function value, compared with other techniques. In short, the BO technique outperformed the other three techniques of SVR model optimization.

To compare the performance of BO-SVR with the four other predictive models in forecasting mass change, the five-fold average R^2, MAE, RMSE, and MAPE were calculated for each predictive model from the test data sets; the results are listed in Table 7.4. It can be seen from Table 7.4 that all of the models were able to predict the mass change with high accuracy. The minimum R^2 was obtained with the GS-SVR model having an R^2 of 0.9771. It can be seen from MAE and RMSE results that the performance of these models in mass change prediction was found in the order of BO-SVR > RS-SVR > ANN > GS-SVR > PSO-SVR. The ANN model showed an intermediate level of accuracy among the five models. It produced a prediction with R^2 of 0.9886, MAE of

0.1621%, and RMSE of 0.1200%. The highest accuracy was achieved with the BO-SVR model, with an R^2 of 0.9914. The BO-SVR was able to predict the mass change with small errors (MAE of 0.1471%, RMSE of 0.0804%). The excellent accuracy in predicting mass change is visually illustrated in Figure 7.5 for the BO-SVR model. For each experimentally measured mass change, there is a predicted value that is closely matching. However, the values of MAPE, which can be considered as relative errors to measured data, are noticeably large for all models, with values of 50.79%, 58.52%, 49.93%, 69.92%, and 44.30% for BO-SVR, GS-SVR, RS-SVR, PSO-SVR, and ANN, respectively. This is because, obtained from the experimental study, a large portion of the data points (mass change) was close to zero. The MAPE values would be significantly amplified as the output approaches zero (Tayman & Swanson, 1999). Thus, the MAPE was not considered the main evaluation parameter for mass change prediction.

A Friedman's test was also conducted to examine the superiority of BO-SVR model over the other four models. The calculated FM value was 10.93 with a p-value of 0.027. At the significance level of 0.05, as the p-value is lower than 0.05, it is concluded that there is a significant difference between BO-SVR and the other four models. Since the BO-SVR had the lowest errors, this significant difference suggests that the BO-SVR model performed considerably better than the other four models in predicting the mass change.

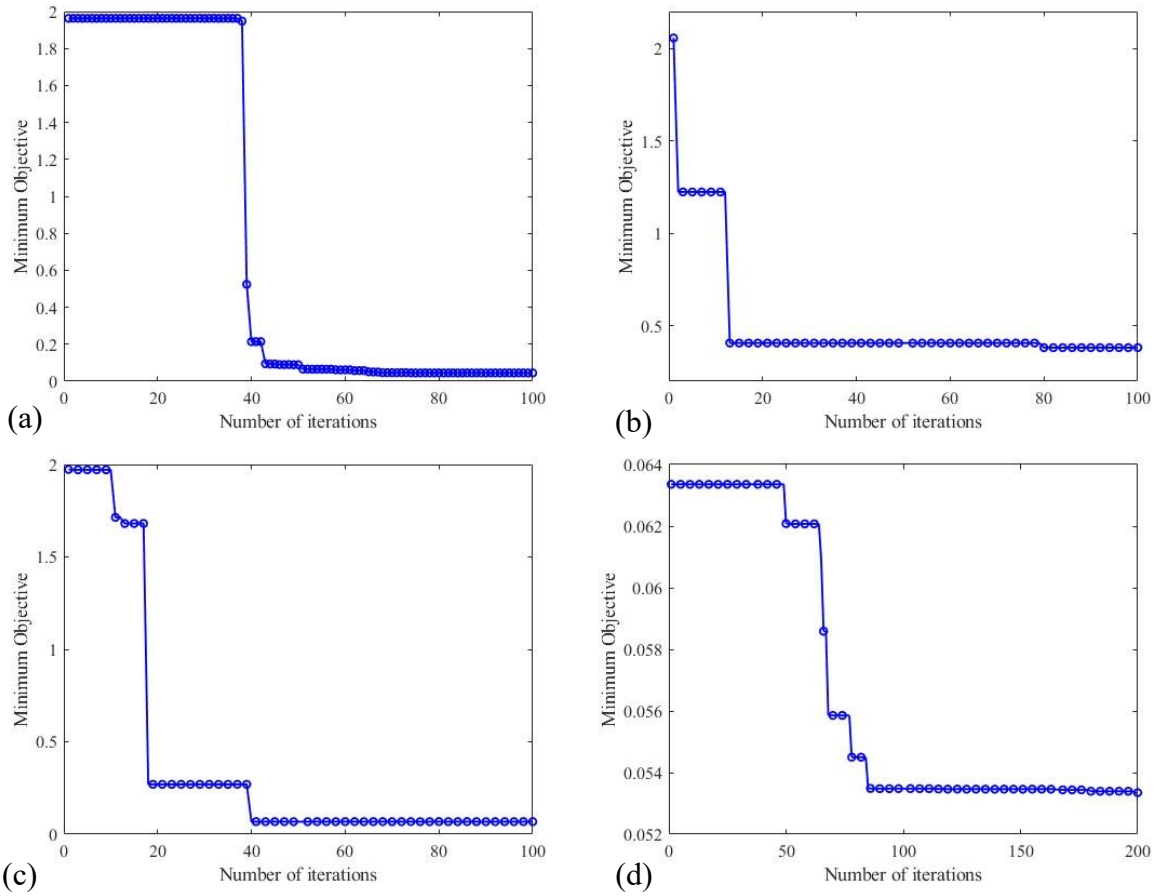

Figure 7.4. Optimization process in mass change prediction (data part 5 as testing data): a) BO-SVR; b) GS-SVR; c) RS-SVR; d) PSO-SVR

Table 7.3. Optimization results of each technique (data part 5 as testing data)

Optimization technique	Objective function value	(ϵ, C, σ)
BO	0.0454	(0.0017, 202.6242, 4.4972)
GS	0.3815	(0.0086, 46.4159, 2.1544)
RS	0.0679	(0.0059, 870.0991, 4.2942)
PSO	0.0530	(0.0913, 812.6573, 5.6815)

Table 7.4. Performance evaluation of different predictive models

Predictive techniques	Average R^2	Average MAE, %	Average RMSE, %	Average MAPE, %
BO-SVR	0.9914	0.1471	0.0804	50.79
GS-SVR	0.9771	0.1841	0.1433	58.52
RS-SVR	0.9868	0.1545	0.0835	49.93
PSO-SVR	0.9841	0.1855	0.1223	69.92
ANN	0.9886	0.1621	0.1200	44.30

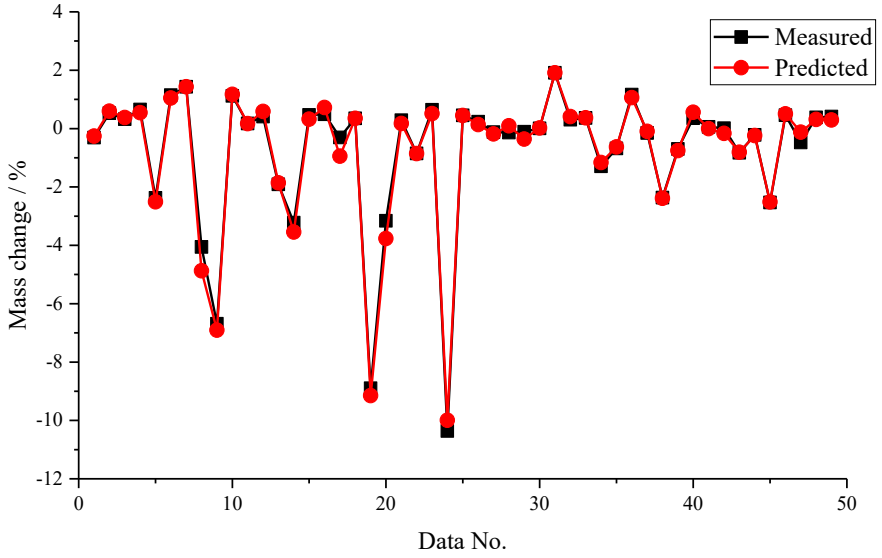

Figure 7.5. BO-SVR forecasting results of testing data part 5

7.4.2. Prediction results of compressive strength

For the prediction of residual compressive strength after immersion, twelve input parameters were included (i.e., those parameters in mass change prediction and compressive strength on the 28th day of curing). A total of 93 data points were used and divided into five parts with the sizes of (18, 19, 19, 19, 18) in the modeling. During the training process of SVR models, the optimal hyperparameters combinations were obtained by BO, GS, RS, and PSO techniques. The evolutions of the objective function (e.g., MSE) with iterations were plotted in Figure 7.6 for all SVR models. The optimization results of the training process are presented in Table 7.5. It can be seen from

Figure 7.6 that all the models converged before reaching the maximum iteration number. The BO and GS converged with relatively fewer iteration steps—about 20 iterations for BO and 5 iterations for RS. The GS and PSO found their optimal solution at iterations of 60 and 155, respectively. Compared with the other techniques, the BO technique obtained a hyperparameters combination of (0.7969, 299.8568 3.2164) with a low objective function value of 2.5161 (see Table 7.5).

To assess the performance of each model, the averaged R^2, MAE, RMSE, and MAPE were calculated. The results are listed in Table 7.6. Among these models, the ANN showed the lowest accuracy in predicting compressive strength, with R^2 of 0.6691, MAE of 2.4614 MPa, RMSE of 19.8146 MPa, and MAPE of 8.4614%. Following the ANN model, the PSO-SVR showed low accuracy in compressive strength prediction (R^2 of 0.7614, MAE of 2.4069 MPa, RMSE of 15.2562 MPa, and MAPE of 7.5155%). The BO-SVR demonstrated the best performance among the five predictive models. It showed a high R^2 of 0.8720 and only 5.7423% of MAPE. The BO-SVR forecasting results of data part 5 are also presented in Figure 7.7 to visually show the high accuracy in compressive strength prediction. The predicted values are closely matched with the experimentally measured values. The prediction accuracy was ranked as BO-SVR > RS-SVR > GS-SVR > PSO-SVR > ANN.

To ensure that the improvement in predicting accuracy is significant by the proposed BO-SVR model, a Friedman's test was carried to investigate the superiority of BO-SVR over the other four models in predicting the compressive strength. A p-value of 0.0039 was obtained, which indicates a significantly better performance of BO-SVR over the other four models.

Table 7.5. Optimization results of each technique (data part 5 as testing data)

Optimization technique	Objective function value	(ϵ, C, σ)
BO	2.5161	(0.7969, 299.8568 3.2164)
GS	2.8290	(0.0308, 10, 2.1544)
RS	2.5119	(0.0547, 362.3195, 2.3748)
PSO	10.39	(0.2557, 82.2266, 3.7792)

Table 7.6. Performance evaluation of different predictive models

Predictive techniques	Average R^2	Average MAE, MPa	Average RMSE, MPa	Average MAPE, %
BO-SVR	0.8720	1.7659	6.9268	5.7423
GS-SVR	0.7924	2.3798	11.8631	7.6802
RS-SVR	0.8048	2.2108	10.5025	7.4465
PSO-SVR	0.7614	2.4069	15.2562	7.5155
ANN	0.6691	2.4614	19.8146	8.4614

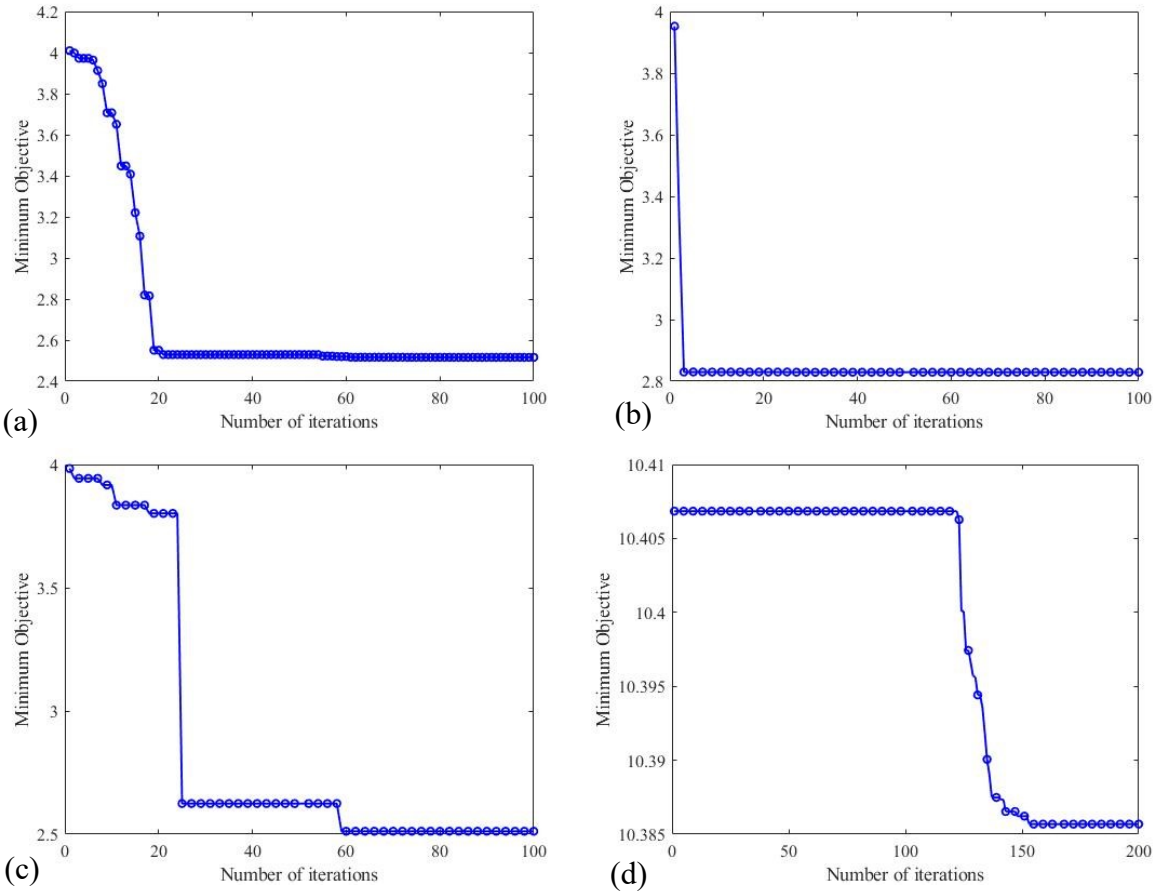

Figure 7.6. Optimization process in compressive strength prediction (data part 5 as testing data):

a) BO-SVR; b) GS-SVR; c) RS-SVR; d) PSO-SVR

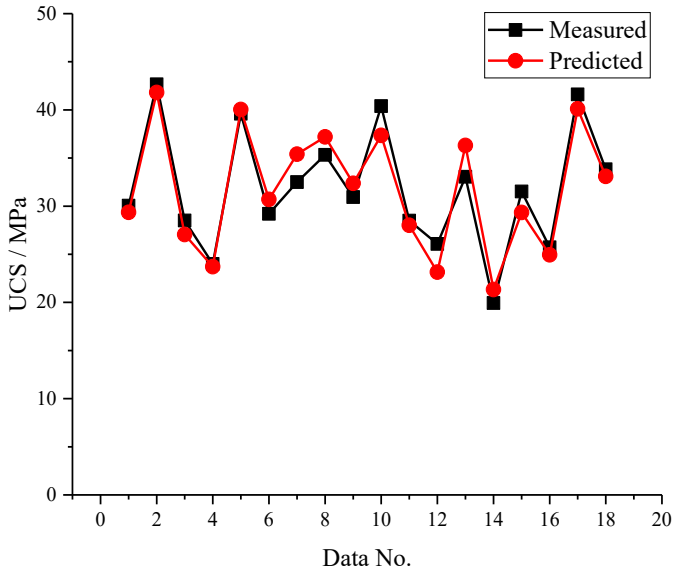

Figure 7.7. BO-SVR forecasting results of testing data part 5

7.4.3. Evaluation of the proposed model

The proposed BO-SVR model was able to predict the mass change and compressive strength of mortar samples with high accuracy. Among the four optimization techniques, the Bayesian algorithm outperformed the other three in both mass change prediction and compressive strength prediction. The Bayesian algorithm was able to find the best hyperparameters combination for SVR models that can result in the minimum value of the objective function. For example, a minimum value of the objective function of 0.0454 was achieved during the training process by the BO technique for mass change prediction, while the values of objective function were 0.3815, 0.0679, and 0.0530 for GS, RS, and PSO, respectively. Compared with the most commonly used ANN model, the Bayesian-optimized SVR provided a much better prediction on mass change and compressive strength of sulfuric acid immersed samples. For instance, the BO-SVR-predicted compressive strength had a *k*-fold averaged MAPE of 5.7423%, which is much smaller than 8.4614% from the ANN model.

Despite its excellent performance, the proposed BO-SVR model has its limitations in this study. Much work will be required to further the model. For example, although this model has considered many testing conditions as the input parameters (e.g., the pH of immersion acid, wetting-drying cycle, immersion ages, number of times of the acid addition, and ratios of acid volume to sample surface area), there are more conditions to incorporate. For instance, some studies accelerated the deterioration rate by brushing the samples (De Belie et al., 2004; Monteny et al., 2003), while sample brushing was not included as an input parameter in this model. Thus, more parameters, such as sample brushing and also immersion temperature (Mahmoodian & Alani, 2017), should be included in the model to better mimic the real conditions.

7.5. Conclusions

The objective of this study was to construct a support vector regression model with Bayesian optimization (BO-SVR) to predict the mass change and compressive strength of mortar samples under the sulfuric acid attack. The support vector regression model with Bayesian optimization was compared with four other predictive models. These models include grid search-support vector regression (GS-SVR), random search-support vector regression (RS-SVR), particle swarm optimization-support vector regression (PSO-SVR) and traditional artificial neural network (ANN). Five parameters of testing conditions and six mixture design parameters were used as input parameters. The database was collected from previous experimental work. In total, 93 data points were obtained for compressive strength prediction, and 244 data points were obtained for mass change prediction. The *k*-fold cross-validation technique was adopted to test the accuracy of the models. The performance of each model was evaluated by four parameters: the coefficient of determination R^2, the mean absolute error, the root mean square error and the mean absolute

percent error. Based on the evaluation of the predictive models, the following conclusions were drawn:

(1) The proposed BO-SVR model can predict the mass change and the compressive strength of mortar samples under the sulfuric acid attack with high accuracy.

(2) Compared with other optimization techniques, Bayesian optimization was efficient (with relatively fewer iterations) and provided better solutions in searching for the optimal hypermeters for the SVR model.

(3) Among all five models, the BO-SVR model showed the best performance in predicting mass change and compressive strength.

(4) The performance of models in mass change prediction was in the order of BO-SVR > RS-SVR > ANN > GS-SVR > PSO-SVR.

(5) The prediction accuracy was ranked as BO-SVR > RS-SVR > GS-SVR > PSO-SVR > ANN in compressive strength prediction.

Chapter 8. Conclusions and future work

The overall objective of this research is to systematically investigate the effects of three pozzolans (fly ash, metakaolin, and silica fume) in improving the acid resistance of cement-based materials. To achieve this objective, 28 mixtures have been evaluated in this thesis. The amount of deterioration reduction was calculated for all mixtures with respect to the deterioration of the reference mixture, and the results are summarized in Table 8.1. A ranking of improvement in acid resistance has been assigned to a mixture based on the deterioration reduction in each column. As shown in Table 8.1, the mixtures with pozzolans showed various levels of improvement in acid resistance. In general, the addition of fly ash and metakaolin significantly reduced the deteriorations (mass change and length change) of Portland cement-based mortars when the pH of immersion acids are relatively high (pH of 3.0), while the mixtures with low content of silica fume and nano-silica demonstrated good/excellent resistance to acids with low pHs (2.0 or 1.5). Furthermore, when the metakaolin was used to produce geopolymer mortars, the mixtures with calcium aluminate cement showed a moderate/good acid resistance regarding the length change. Additionally, the addition of cellulose nanocrystals was effective in reducing the deterioration for samples immersed in acids with a pH of 2.0. Among the mixtures investigated in this thesis, four of them showed the best performance, including the mixtures with 5% of silica fume, 1% and 1.5% of nano-silica, and 0.4% of cellulose nanocrystals.

Table 8.1. Summary of deterioration reduction with respect to the reference mixture

Category	Mixture ID	Reduction in mass change, %			Reduction in length change (pH2), %	Ranking of acid resistance
		pH1.5	pH2	pH3		
Silica fume	SF5	/	24.31	/	57.61	**Excellent/Excellent**
	SF10	/	-8.73	/	-3.57	Negative/Negative
	SF15	/	-20.91	/	-34.18	Negative/Negative
Nano-silica	NS0.5	/	9.38	/	16.96	Moderate/Good
	NS1	/	25.96	/	30.78	**Excellent/Excellent**
	NS1.5	/	20.86	/	11.74	**Excellent/Good**
	NS2	/	10.49	/	9.13	Good/Moderate
Cellulose nanocrystal	C0.2	/	9.38	/	34.24	Moderate/Excellent
	C0.4	/	12.16	/	35.98	**Good/Excellent**
	C1.0	/	9.27	/	6.65	Moderate/Moderate
	C1.5	/	-6.93	/	-3.65	Negative/Negative
Geopolymer	GM	/	-152.91	/	-74.43	Negative/Negative
	GMC5	/	-108.96	/	11.30	Negative/Good
	GMC10	/	-98.02	/	5.33	Negative/Moderate
Fly ash	FA5	2.62	/	69.32	/	Mild/Excellent
	FA10	2.67	/	54.88	/	Mild/Excellent
	FA20	3.56	/	161.24	/	Mild/Excellent
	FA30	-6.22	/	50.29	/	Negative/Excellent
Metakaolin	MK5	0.87	/	22.07	/	No/Excellent
	MK10	-1.58	/	-0.30	/	Negative/No
	MK20	-1.57	/	28.14	/	Negative/Excellent
	MK30	0.83	/	65.84	/	No/Excellent
Silica fume	SF5	8.76	/	131.26	/	Moderate/Excellent
	SF10	-3.06	/	77.40	/	Negative/Excellent
	SF20	-12.71	/	30.66	/	Negative/Excellent
	SF30	-6.31	/	27.95	/	Negative/Excellent

*Note: the ranking of each mixture was based on the author's subjective judgement: Excellent: deterioration reduction > 20%; Good: 10% < deterioration reduction < 20%; Moderate: 5% < deterioration reduction < 10%; Mild: 1% < deterioration reduction < 5%; No: -1% < deterioration reduction < 1%; Negative: deterioration reduction < -1%.

8.1. Conclusions

Based on the experimental results, the following conclusions were drawn:

1. The effects of three pozzolanic materials (fly ash, metakaolin, and silica fume) were investigated on improving the acid resistance of ordinary Portland cement mortars used for underground structures. The incorporation of these pozzolans was found to reasonably improve the acid resistance of ordinary Portland cement mortars regarding mass losses and changes in compressive strength. This provides a potential path for future recycling and repurposing mine waste.
2. The effectiveness of a nano pozzolan (nano-silica) and a normal pozzolan (silica fume) was compared on improving the acid resistance of ordinary Portland cement mortar. Mortars with normal pozzolan showed comparable performance than those with nano pozzolan in sulfuric acid environments. This suggests that it would be economically inefficient to use nano pozzolans.
3. One pozzolan (metakaolin) was used to produce acid-resistant geopolymers. It was found that the metakaolin-based geopolymer can provide high compressive strength and improved acid resistance when calcium aluminate cement was incorporated. This presents a potential way of recycling kaolinite in oil sands tailings in Canada.
4. As fibers are a common component in cement-based structures, a new fiber (cellulose nanocrystal) was innovatively introduced into ordinary Portland cement mortar to improve the acid resistance. This nanofiber was found to improve the compressive strength and the acid resistance of ordinary Portland cement mortar.
5. The effects of testing conditions and evaluation indicators on the evaluation of acid resistance were also investigated in this thesis. It was found that no single indicator was

able to describe the deterioration comprehensively. A combination of indicators is required in assessing the acid resistance of cement-based composites. In addition, the testing conditions were found to play an important role in acid resistance evaluation. These findings can provide a guideline in the standardization of the testing procedure.

6. A predictive model was established to forecast the deterioration (mass change and residual compressive strength) of mortars in sulfuric acid environments. The proposed Bayesian optimized-support vector regression was compared with the artificial neural network algorithm and verified through the k-fold cross-validation method. The proposed method was able to forecast mass change and residual compressive strength with high accuracy. This provides a new way of evaluating the acid resistance of cement-based materials.

8.2. Key contributions

This thesis brings significant contributions to both academia and industry:

1. The main contributions of this thesis are related to improving the acid resistance of cement-based materials used in underground structures under sulfuric acid attack. The sulfuric acid attack in underground structures (e.g., sewer tunnels and underground mining structures) are a serious problem that reduces service life, causes extremely high costs, and poses risks to individuals. The improved acid resistance of cementitious materials has substantial potential to increase the service life of cement-based structures, reduce the repair costs, and increase the safety of underground workers. Furthermore, the application of pozzolans in cement-based composites provides an innovative way of recycling and repurposing mine waste such as fly ash, metakaolin, and silica fume.
2. For the first time, the acid resistance was investigated for metakaolin-based geopolymers with calcium aluminate cement addition. This investigation offers a new option to enhance

the properties of metakaolin-based geopolymer. Moreover, the improved acid resistance of metakaolin-based geopolymer could potentially extend its application to structures under aggressive environments, and provides an innovative way of recycling and repurposing kaolinites from oil sands mining. In addition, as the production of geopolymers have significantly lower carbon dioxide emissions than that of ordinary Portland cement (OPC), the use of metakaolin-based geopolymer could reduce the emission of greenhouse gases.

3. For the first time, a green and sustainable nanofiber (cellulose nanocrystals) was introduced in the OPC system to improve the acid resistance. The addition of cellulose nanocrystals not only enhances the durability of cementitious composites in acidic environments but also benefits the forest industry economically as the cellulose nanocrystals are extracted from woods and plants.
4. This thesis investigated the effects of testing conditions and indicators of concrete deteriorations on the evaluation of acid resistance. This offers a guideline for the standardization of the test procedure and experimental design for future research works about acid resistance of cement-based materials.
5. This thesis investigated the mechanisms to improve the acid resistance of cement-based composites. This provides a guideline for the development of new products used in acidic environments.
6. Last but not least, a significant contribution is the prediction of deterioration of cement-based materials based on the mixture design and testing conditions. A predictive model was established to understand the experimental data in a continuous way and provide a preliminary predictive method that considers mixture design and testing conditions. The

incorporation of testing conditions in the predictive model offers a possibility of forecasting deterioration of a mixture under various exposure conditions.

8.3. Limitations and future work

Although the research in this thesis has provided a systematic investigation on the effects of pozzolans on the acid resistance of cement-based composites, there is still a need for continued investigation due to its limitations.

1. One limit of this research lies in difficulty in converting the improved acid resistance to the extended service life of the cement-based structures. The severity of sulfuric acid corrosion of cement-based structures is greatly controlled by the sulfuric acid supply in field conditions. However, the sulfuric acid supply varies greatly with time and space. For example, the microbially induced corrosion in a sewer system is greatly affected by temperature in sewer tunnels and hydraulic properties of water flow, both of which vary with time and locations (Wu et al., 2018). Owing to this great variation in field conditions, it is difficult to predict the extended service life of the cement-based structures from results tested with controlled laboratory testing conditions. In other words, the degree of improvement in acid resistance from laboratory tests cannot directly reflect how effective it is in field application. Hence, future research is suggested to focus on developing such models that can calculate the service life of structures in practice based on experimental results.
2. The testing method of acid resistance in this thesis does not take bacterial activities into considerations. For the microbially induced corrosion process, a simple acid immersion of samples cannot reflect the corrosion resistance of a mixture as some mixtures may inhibit

the growth of bacteria instead of improving the chemical acid resistance. A more systematic evaluation of mixtures under the bacterial environment is recommended for future research.

3. In this thesis, the acid resistance of metakaolin-based geopolymers was not investigated when only NaOH solution is used as the activator. The use of Na_2SiO_3 solution as one of the activators led to the generation of strätlingite (see Chapter 4) instead of participating in the geopolymerisation process. The elimination of Na_2SiO_3 solution in activators may provide an enhanced geopolymerisation process leading to improved acid resistance. In addition, the elimination of Na_2SiO_3 solution in activators can reduce the cost of geopolymer production as the Na_2SiO_3 solution occupies a large portion of the cost for geopolymer production. Thus, a study is recommended to investigate the acid resistance of metakaolin-based geopolymers with calcium aluminate cement addition, when no Na_2SiO_3 is added.
4. Despite its excellent performance, the proposed Bayesian optimized-support vector regression model has its limitations in this thesis. Much work will be required to further the model. For example, although this model has considered many testing conditions as the input parameters (e.g., the pH of immersion acid, wetting-drying cycle, immersion ages, number of times of the acid addition, and ratios of acid volume to sample surface area), there are more conditions to incorporate. For instance, some studies accelerated the deterioration rate by brushing the samples (De Belie et al., 2004; Monteny et al., 2003), while sample brushing was not included as an input parameter in this model. Thus, more parameters, such as sample brushing and immersion temperature (Mahmoodian & Alani, 2017), should be included in the model to better mimic the real conditions.

5. This thesis only investigates the acid resistance of binary blends of cement and pozzolans using full experimental design. Due to the differences in reactivity, compositions and particle sizes of pozzolans, the pozzolans perform differently in the ordinary Portland cement system. A ternary or quaternion blends of ordinary Portland cement, fly ash, metakaolin and silica fume may take advantages of each pozzolanic material and leads to a more acid-resistant mixture. Experimental design methods can be adopted to minimize the number of mixtures, including the orthogonal design and formula experiment design. A future study is recommended on this topic.
6. This thesis only investigates one grade of each pozzolanic material. For example, fly ash can be classified into Class C and Class F. This thesis only explores the potential of Class F fly ash, more work is recommended to compare the performance of different grades of pozzolans.
7. For underground structures, steel rebars are a common component to enhance their mechanical performance. The interaction between steel rebars and cement-mix is still unclear when the structures are subjected to sulfuric acid attack. More work is recommended on this topic.

References

Abbas, R., Khereby, M. A., Ghorab, H. Y., & Elkhoshkhany, N. (2020). Preparation of geopolymer concrete using Egyptian kaolin clay and the study of its environmental effects and economic cost. *Clean Technologies and Environmental Policy, 22*(3), 669-687.

Abbass, W., Khan, M. I., & Mourad, S. (2019). Experimentation and predictive models for properties of concrete added with active and inactive SiO2 fillers. *Materials, 12*(2), 299.

Abid, K., Gholami, R., Elochukwu, H., Mostofi, M., Bing, C. H., & Muktadir, G. (2018). A methodology to improve nanosilica based cements used in CO2 sequestration sites. *Petroleum, 4*(2), 198-208.

ACI Committee 201. (2001). *Guide to durable concrete*; ACI Committee 201.2R-01, Farmington Hills, MI.

ACI Committee 506. (2009). *Guide for specifying underground shotcrete*; ACI Committee 506, Farmington Hills, MI.

ACI Committee 506. (2016). *Guide to shotcrete*; ACI Committee 506, Farmington Hills, MI.

Æsøy, A., Østerhus, S. W., & Bentzen, G. (2002). Controlled treatment with nitrate in sewers to prevent concrete corrosion. *Water Science and Technology: Water Supply, 2*, 137-144.

Aggarwal, P., Singh, R. P., & Aggarwal, Y. (2015). Use of nano-silica in cement based materials—A review. *Cogent Engineering, 2*(1), 1078018.

Aggelakopoulou, E., Bakolas, A., & Moropoulou, A. (2011). Properties of lime–metakolin mortars for the restoration of historic masonries. *Applied Clay Science, 53*(1), 15-19.

Al-Akhras, N. M. (2006). Durability of metakaolin concrete to sulfate attack. *Cement and Concrete Research, 36*(9), 1727-1734.

al-Swaidani, A. M., Aliyan, S. D., & Adarnaly, N. (2016). Mechanical strength development of mortars containing volcanic scoria-based binders with different fineness. *Engineering Science and Technology, an International Journal, 19*(2), 970-979.

Al-Zeer, M. I., & MacKenzie, K. J. (2019). Fly ash-based geopolymers as sustainable bifunctional heterogeneous catalysts and their reactivity in Friedel-Crafts acylation reactions. *Catalysts, 9*(4), 372.

Alade, I. O., Rahman, M. A. A., & Saleh, T. A. (2019). Predicting the specific heat capacity of alumina/ethylene glycol nanofluids using support vector regression model optimized with Bayesian algorithm. *Solar Energy, 183*, 74-82.

Alanazi, H., Yang, M., Zhang, D., & Gao, Z. (2017). Early strength and durability of metakaolin-based geopolymer concrete. *Magazine of Concrete Research, 69*(1), 46-54.

Alani, A. M., & Faramarzi, A. (2014). An evolutionary approach to modelling concrete degradation due to sulphuric acid attack. *Applied Soft Computing, 24*, 985-993.

Alehyen, S., Zerzouri, M., ELalouani, M., Achouri, M., & Taibi, M. (2017). Porosity and fire resistance of fly ash based geopolymer. *Journal of Materials Environmental Sciences, 9*, 3676-3689.

Alexander, M., Bertron, A., & De Belie, N. (2013). *Performance of cement-based materials in aggressive aqueous environments* (Vol. 10): Springer.

Alexander, M., & Fourie, C. (2011). Performance of sewer pipe concrete mixtures with portland and calcium aluminate cements subject to mineral and biogenic acid attack. *Materials and Structures, 44*(1), 313-330.

Allahverdi, A., & Skvara, F. (2001). Nitric acid attack on hardened paste of geopolymeric cements, Part 2. *Ceramics Silikaty, 45*(4), 143-150.

Allahverdi, A., & Škvára, F. (2000). Acidic corrosion of hydrated cement based materials. Part 1.: Mechanism of the phenomenon. *Ceramics International, 44*(3), 114-120.

AMEC Earth & Environmental. (2006). *The beneficial use of waste*; Alberta Environment Alberta Environment, Calgary, CA.

Amin, M. (2016). *Performance of concrete with blended binders in sulfuric acid and ammonium sulphate solutions.* (Master of Science), The University of Manitoba,

Amin, M., & Bassuoni, M. T. (2017). Response of concrete with blended binders and nanoparticles to sulfuric acid attack. *Magazine of Concrete Research, 70*(12), 617-632.

Andrew, R. M. (2018). Global CO2 emissions from cement production, 1928–2017. *Earth System Science Data, 10*(4), 2213-2239.

Antonanzas, J., Urraca, R., Pernía-Espinoza, A., Aldama, A., Fernández-Jiménez, L. A., & Martínez-de-Pisón, F. J. (2017). *Single and blended models for day-ahead photovoltaic power forecasting.* Paper presented at the International Conference on Hybrid Artificial Intelligence Systems, Cham.

Apgar, D., & Witherspoon, J. (2008). *Minimization of odors and corrosion in collection systems*: Water Environment Research Foundation Alexandria, VA.

Ariffin, M., Bhutta, M., Hussin, M., Tahir, M. M., & Aziah, N. (2013). Sulfuric acid resistance of blended ash geopolymer concrete. *Construction and Building Materials, 43*, 80-86.

Armstrong, T. (2013). *An overview of global cement sector trends.* Paper presented at the FICEM-APCAC 30th Technical Congress. Lima, Peru.

Assi, L. N. (2017). *Cost and fuel usage optimization of activating solution based silica fume geopolymer concrete.* (Master of Science), University of South Carolina,

ASTM. (2011). *ASTM C404 - 11 Standard specification for aggregates for masonry grout*; ASTM International West Conshohocken, PA.

ASTM. (2013). *ASTM C642-13 Standard test method for density, absorption, and voids in hardened concrete*; ASTM International, West Conshohocken, PA. United States.

ASTM. (2014). *ASTM C136/C136M-14, Standard test method for sieve analysis of fine and coarse aggregates*; ASTM International West Conshohocken, PA. United States.

ASTM. (2015). *ASTM C143 / C143M-15a-Standard test method for slump of hydraulic-cement concrete*; ASTM International, West Conshohocken, PA. United States.

ASTM. (2016a). *ASTM C42 / C42M-16-Standard test method for obtaining and testing drilled cores and sawed beams of concrete*; ASTM International, West Conshohocken, PA. United States.

ASTM. (2016b). *ASTM C192 / C192M-16a-Standard practice for making and curing concrete test specimens in the laboratory*; ASTM International, West Conshohocken, PA. United States.

ASTM. (2016c). *ASTM C597-16 Standard test method for pulse velocity through concrete*; ASTM International, West Conshohocken, PA. United States.

ASTM. (2018). *ASTM C39/C39M-18 Standard test method for compressive strength of cylindrical concrete specimens*; ASTM International, West Conshohocken, PA. United States.

Atiş, C. D., Görür, E. B., Karahan, O., Bilim, C., İlkentapar, S., & Luga, E. (2015). Very high strength (120MPa) class F fly ash geopolymer mortar activated at different NaOH amount, heat curing temperature and heat curing duration. *Construction and Building Materials, 96*, 673-678.

Attiogbe, E. K., & Rizkalla, S. H. (1988). Response of concrete to sulfuric acid attack. *ACI Materials Journal, 85*(6), 481-488.

Aydın, A. C., Nasl, V. J., & Kotan, T. (2018). The synergic influence of nano-silica and carbon nano tube on self-compacting concrete. *Journal of Building Engineering, 20*, 467-475.

Aydın, S., Yazıcı, H., Yiğiter, H., & Baradan, B. (2007). Sulfuric acid resistance of high-volume fly ash concrete. *Building and Environment, 42*(2), 717-721.

Ayoub, G., Azar, N., Fadel, M. E., & Hamad, B. (2004). Assessment of hydrogen sulphide corrosion of cementitious sewer pipes: a case study. *Urban Water Journal, 1*(1), 39-53.

Babaee, M., Khan, M. S. H., & Castel, A. (2018). Passivity of embedded reinforcement in carbonated low-calcium fly ash-based geopolymer concrete. *Cement and Concrete Composites, 85*, 32-43.

Bahafid, S., Ghabezloo, S., Duc, M., Faure, P., & Sulem, J. (2017). Effect of the hydration temperature on the microstructure of Class G cement: C-S-H composition and density. *Cement and Concrete Research, 95*, 270-281.

Bai, T., Song, Z., Wang, H., Wu, Y., & Huang, W. (2019). Performance evaluation of metakaolin geopolymer modified by different solid wastes. *Journal of Cleaner Production, 226*, 114-121.

Bajpai, R., Choudhary, K., Srivastava, A., Sangwan, K. S., & Singh, M. (2020). Environmental impact assessment of fly ash and silica fume based geopolymer concrete. *Journal of Cleaner Production, 254*, 120147.

Bakharev, T. (2005). Resistance of geopolymer materials to acid attack. *Cement and Concrete Research, 35*(4), 658-670.

Bakharev, T., Sanjayan, J. G., & Cheng, Y. B. (2003). Resistance of alkali-activated slag concrete to acid attack. *Cement and Concrete Research, 33*(10), 1607-1611.

Balea, A., Blanco, A., & Negro, C. (2019). Nanocelluloses: natural-based materials for fiber-reinforced cement composites. A critical review. *Polymers, 11*(3), 518.

Bao, Y., Feng, D., Ma, N., Zhu, H., & Rabczuk, T. (2018). Experimental and numerical study on structural performance of reinforced concrete box sewer with localized extreme defect. *Underground Space, 3*(2), 166-179.

Barbhuiya, S., & Kumala, D. (2017). Behaviour of a sustainable concrete in acidic environment. *Sustainability, 9*(9), 1556.

Barnat-Hunek, D., Szymańska-Chargot, M., Jarosz-Hadam, M., & Łagód, G. (2019). Effect of cellulose nanofibrils and nanocrystals on physical properties of concrete. *Construction and Building Materials, 223*, 1-11.

Bassuoni, M. T., & Nehdi, M. L. (2007). Resistance of self-consolidating concrete to sulfuric acid attack with consecutive pH reduction. *Cement and Concrete Research, 37*(7), 1070-1084.

Behnood, A., & Golafshani, E. M. (2018). Predicting the compressive strength of silica fume concrete using hybrid artificial neural network with multi-objective grey wolves. *Journal of Cleaner Production, 202*, 54-64.

Bergstra, J., & Bengio, Y. (2012). Random search for hyper-parameter optimization. *The Journal of Machine Learning Research, 13*(1), 281-305.

Berodier, E., & Scrivener, K. (2014). Understanding the filler effect on the nucleation and growth of C-S-H. *Journal of the American Ceramic Society, 97*(12), 3764-3773.

Berra, M., Carassiti, F., Mangialardi, T., Paolini, A. E., & Sebastiani, M. (2012). Effects of nanosilica addition on workability and compressive strength of Portland cement pastes. *Construction and Building Materials, 35*, 666-675.

Bhogayata, A. C., & Arora, N. K. (2018). Impact strength, permeability and chemical resistance of concrete reinforced with metalized plastic waste fibers. *Construction and Building Materials, 161*, 254-266.

Biricik, H., & Sarier, N. (2014). Comparative study of the characteristics of nano silica-, silica fume-and fly ash-incorporated cement mortars. *Materials Research, 17*(3), 570-582.

Bock, E. (1961). On the solubility of anhydrous calcium sulphate and of gypsum in concentrated solutions of sodium chloride at 25 C, 30 C, 40 C, and 50 C. *Canadian Journal of Chemistry, 39*(9), 1746-1751.

Bouguermouh, K., Bouzidi, N., Mahtout, L., Pérez-Villarejo, L., & Martínez-Cartas, M. L. (2017). Effect of acid attack on microstructure and composition of metakaolin-based geopolymers: The role of alkaline activator. *Journal of Non-Crystalline Solids, 463*, 128-137.

Bowker, R. P., & Smith, J. M. (1985). *Odor and corrosion control in sanitary sewerage systems and treatment plants*; U.S. Environmental Protection Agency: Washington, DC, USA.

Breit, W. (2002). Säurewiderstand von Beton - acid resistance of concrete. *Beton, 52*(10), 505-510.

Brongers, M., Virmani, P., & Payer, J. (2002). *Drinking water and sewer systems in corrosion costs and preventative strategies in the United States*. United States Department of Transportation Federal Highway Administration,

Cadena, F., & Peters, R. W. (1988). Evaluation of chemical oxidizers for hydrogen sulfide control. *Water Pollution Control Federation, 60*, 1259-1263.

Caicedo-Ramirez, A. (2018). *Antimicrobial Aggregates for the In-Situ Control of Microbially Induced Concrete Corrosion.* University of Colorado at Boulder,

Cao, Y., Tian, N., Bahr, D., Zavattieri, P. D., Youngblood, J., Moon, R. J., & Weiss, J. (2016). The influence of cellulose nanocrystals on the microstructure of cement paste. *Cement and Concrete Composites, 74*, 164-173.

Cao, Y., Zavaterri, P., Youngblood, J., Moon, R., & Weiss, J. (2015). The influence of cellulose nanocrystal additions on the performance of cement paste. *Cement and Concrete Composites, 56*, 73-83.

Carette, G., & Malhotra, V. (1987). Characterization of Canadian fly ashes and their relative performance in concrete. *Canadian Journal of Civil Engineering, 14*(5), 667-682.

Chahal, N., Siddique, R., & Rajor, A. (2012). Influence of bacteria on the compressive strength, water absorption and rapid chloride permeability of fly ash concrete. *Construction and Building Materials, 28*(1), 351-356.

Chan, J. W. K., & Tong, T. K. L. (2007). Multi-criteria material selections and end-of-life product strategy: Grey relational analysis approach. *Materials & Design, 28*(5), 1539-1546.

Chang, Z.-T., Song, X.-J., Munn, R., & Marosszeky, M. (2005). Using limestone aggregates and different cements for enhancing resistance of concrete to sulphuric acid attack. *Cement and Concrete Research, 35*(8), 1486-1494.

Chatveera, B., Lertwattanaruk, P., & Makul, N. (2006). Effect of sludge water from ready-mixed concrete plant on properties and durability of concrete. *Cement and Concrete Composites, 28*(5), 441-450.

Chen, H., Qian, C., Liang, C., & Kang, W. J. P. o. (2018). An approach for predicting the compressive strength of cement-based materials exposed to sulfate attack. *PLoS One, 13*(1), e0191370.

Cheng-yi, H., & Feldman, R. F. (1985). Hydration reactions in portland cement-silica fume blends. *Cement and Concrete Research, 15*(4), 585-592.

Cheng, H., Ding, X., Zhou, W., & Ding, R. (2019). A hybrid electricity price forecasting model with Bayesian optimization for German energy exchange. *International Journal of Electrical Power & Energy Systems, 110*, 653-666.

Chindaprasirt, P., Homwuttiwong, S., & Sirivivatnanon, V. (2004). Influence of fly ash fineness on strength, drying shrinkage and sulfate resistance of blended cement mortar. *Cement and Concrete Research, 34*(7), 1087-1092.

Choi, S. K., Lee, S., Song, Y. K., & Moon, H. S. (2002). Leaching characteristics of selected Korean fly ashes and its implications for the groundwater composition near the ash disposal mound. *Fuel, 81*(8), 1083-1090.

Chou, J.-S., Chiu, C.-K., Farfoura, M., & Al-Taharwa, I. (2010). Optimizing the prediction accuracy of concrete compressive strength based on a comparison of data-mining techniques. *Journal of Computing in Civil Engineering, 25*(3), 242-253.

Churchill, P., & Elmer, D. (1999). Hydrogen sulfide odor control in wastewater collection systems. *Journal of New England Water Environment Association, 33*(1), 57-63.

City of Dallas. (2015). *Water and wastewater procedures and design manual*; Dallas water untilities, TX, USA.

City of Edmonton. (2015). *Design and construction standards*; Volume 3- Drainage: City of Edmonton, AB, CA.

City of Edmonton. (2016). *2016-2018 Business Plan*. Utility Services: City of Edmonton, AB, CA.

City of Kamloops. (2012). *Design criteria manual*; Development and Engineering Services Department-Engineering Development Section, Kamloops BC, CA.

City of London (Canada). (2015). *Design specifications & requirements manual*; The Corporation of the City of London, ON, CA.

City of San Diego. (2015). *Sewer design guide*; City of San Diego, CA, USA.

City of Saskatoon. (2017). *Design and development standards manual* Section Five-Sanitary sewer collection system: City of Saskatoon Sask, CA.

City of Toronto. (2009). *Design criteria for sewers and watermains*; Standards, Policies and Quality Assurance, District Engineering Services, ON, CA.

Clidence, D., & Shissler, D. (2008). Elimination of odor and hydrogen sulfide gas by superoxygenation of the bluebird force main in Laguna Beach, California. *Proceedings of the Water Environment Federation, 2008*(4), 815-825.

Cortes, C., & Vapnik, V. (1995). Support-vector networks. *Machine learning, 20*(3), 273-297.

CSA. (2000). *A23.4-16 - Precast concrete - Materials and construction*; CSA, Mississauga, Ontario, Canada.

CSA. (2013). *A3000-13 - Cementitious materials compendium*; CSA, Mississauga, Ontario, Canada.

CSA. (2014a). *A23.1-14/A23.2-14 - Concrete materials and methods of concrete construction / Test methods and standard practices for concrete*; CSA, Mississauga, Ontario, Canada.

CSA. (2014b). *A257.1-14 - Non-reinforced circular concrete culvert, storm drain, sewer pipe, and fittings*; CSA, Mississauga, Ontario, Canada.

CSA. (2014c). *A257.2-14 - Reinforced circular concrete culvert, storm drain, sewer pipe, and fittings*; CSA, Mississauga, Ontario, Canada.

Czarnecki, W. M., Podlewska, S., & Bojarski, A. J. (2015). Robust optimization of SVM hyperparameters in the classification of bioactive compounds. *Journal of Cheminformatics, 7*(1), 38.

Das, R., & Choudhury, I. (2013). Waste management in mining industry. *Indian Journal of Scientific Research, 4*(2), 139.

Davies, J. P., Clarke, B. A., Whiter, J. T., & Cunningham, R. J. (2001). Factors influencing the structural deterioration and collapse of rigid sewer pipes. *Urban Water, 3*(1), 73-89.

Davis, R. E. (1954). Pozzolanic materials-with special reference to their use in concrete pipe. *American Concrete Pipe Association, Technical Memo*.

De Belie, N., Monteny, J., Beeldens, A., Vincke, E., Van Gemert, D., & Verstraete, W. (2004). Experimental research and prediction of the effect of chemical and biogenic sulfuric acid on different types of commercially produced concrete sewer pipes. *Cement and Concrete Research, 34*(12), 2223-2236.

De Belie, N., Monteny, J., & Taerwe, L. (2002). Apparatus for accelerated degradation testing of concrete specimens. *Materials and Structures, 35*(7), 427-433.

De Spot, M., & Wojtarowicz, M. (2003). *Metakaolin study: Pre-feasibility review of the potential for developing metakaolin from oil sands operations for use in concrete*; Ecosmart™ Concrete: Vancouver, BC, Canada.

Demirboğa, R., & Gül, R. (2003). The effects of expanded perlite aggregate, silica fume and fly ash on the thermal conductivity of lightweight concrete. *Cement and Concrete Research, 33*(5), 723-727.

Diab, A. M., Elyamany, H. E., Elmoaty, A. E. M. A., & Sreh, M. M. (2019). Effect of nanomaterials additives on performance of concrete resistance against magnesium sulfate and acids. *Construction and Building Materials, 210*, 210-231.

Dietrich Stein, & Robert Stein. (2004). *Rehabilitation and maintenance of drains and sewers (e-book)*. In UNITRACC.com.

Dinakar, P., Babu, K. G., & Santhanam, M. (2008). Durability properties of high volume fly ash self compacting concretes. *Cement and Concrete Composites, 30*(10), 880-886.

Doan, C. D., & Liong, S.-y. (2004). *Generalization for multilayer neural network bayesian regularization or early stopping.* Paper presented at the Proceedings of the 2nd Asia Pacific Association of Hydrology and Water Resources Conference.

Dodson, V. H. (1990). Pozzolans and the Pozzolanic Reaction. In V. H. Dodson (Ed.), *Concrete Admixtures* (pp. 159-201). Boston, MA: Springer US.

Dousti, M. R., Boluk, Y., & Bindiganavile, V. (2019). The effect of cellulose nanocrystal (CNC) particles on the porosity and strength development in oil well cement paste. *Construction and Building Materials, 205*, 456-462.

Du, H., Du, S., & Liu, X. (2014). Durability performances of concrete with nano-silica. *Construction and Building Materials, 73*, 705-712.

Duan, P., Shui, Z., Chen, W., & Shen, C. (2013). Effects of metakaolin, silica fume and slag on pore structure, interfacial transition zone and compressive strength of concrete. *Construction and Building Materials, 44*, 1-6.

Dufresne, A. (2013). Nanocellulose: a new ageless bionanomaterial. *Materials Today, 16*(6), 220-227.

Dunster, A. M., Parsonage, J. R., & Thomas, M. J. K. (1993). The pozzolanic reaction of metakaolinite and its effects on Portland cement hydration. *Journal of Materials Science, 28*(5), 1345-1350.

Durning, T. A., & Hicks, M. C. (1991). Using microsilica to increase concrete's resistance to aggressive chemicals. *Concrete international, 13*(3), 42-48.

Duxson, P., Fernández-Jiménez, A., Provis, J. L., Lukey, G. C., Palomo, A., & van Deventer, J. S. (2007). Geopolymer technology: the current state of the art. *Journal of Materials Science, 42*(9), 2917-2933.

Dyer, T. (2017). Influence of cement type on resistance to attack from two carboxylic acids. *Cement and Concrete Composites, 83*, 20-35.

Ehrich, S., Helard, L., Letourneux, R., Willocq, J., & Bock, E. (1999). Biogenic and chemical sulfuric acid corrosion of mortars. *Journal of Materials in Civil Engineering, 11*(4), 340-344.

Ekolu, S. O., Diop, S., Azene, F., & Mkhize, N. (2016). Disintegration of concrete construction induced by acid mine drainage attack. *Journal of the South African Institution of Civil Engineering, 58*(1), 34-42.

Erbektas, A. R., Isgor, O. B., & Weiss, W. J. (2019). An accelerated testing protocol for assessing microbially induced concrete deterioration during the bacterial attachment phase. *Cement and Concrete Composites, 104*, 103339.

Ercikdi, B., Kesimal, A., Cihangir, F., Deveci, H., & Alp, İ. (2009). Cemented paste backfill of sulphide-rich tailings: Importance of binder type and dosage. *Cement and Concrete Composites, 31*(4), 268-274.

Ergüler, G. K. (2015). Investigation the applicability of eggshell for the treatment of a contaminated mining site. *Minerals Engineering, 76*, 10-19.

Faisal, M., & Muhammad, K. (2016). Synthesis and characterization of geopolymer from bagasse bottom ash, waste of sugar industries and naturally available china clay. *Journal of Cleaner Production, 129*, 491-495.

Fan, Y., Zhang, S., Wang, Q., & Shah, S. P. (2016). The effects of nano-calcined kaolinite clay on cement mortar exposed to acid deposits. *Construction and Building Materials, 102*, 486-495.

Fan, Y. F., Hu, Z. Q., Zhang, Y. Z., & Liu, J. L. (2010). Deterioration of compressive property of concrete under simulated acid rain environment. *Construction and Building Materials, 24*(10), 1975-1983.

Feldman, R. F. (1977). Non-destructive testing of concrete. *Canadian Building Digest, 187*, 4.

Feng, J., Sun, J., & Yan, P. (2018). The influence of ground fly ash on cement hydration and mechanical property of mortar. *Advances in Civil Engineering, 2018*, 4023178.

Fernández-Jiménez, A., Palomo, A., Vazquez, T., Vallepu, R., Terai, T., & Ikeda, K. (2008). Alkaline activation of blends of metakaolin and calcium aluminate. *Journal of the American Ceramic Society, 91*(4), 1231-1236.

Fernández-Jiménez, A., Vázquez, T., & Palomo, A. (2011). Effect of sodium silicate on calcium aluminate cement hydration in highly alkaline media: a microstructural characterization. *Journal of the American Ceramic Society, 94*(4), 1297-1303.

Fernando, P.-T., & Said, J. (2011). Resistance to acid attack, abrasion and leaching behavior of alkali-activated mine waste binders. *Materials and Structures, 44*(2), 487-498.

Firer, D., Friedler, E., & Lahav, O. (2008). Control of sulfide in sewer systems by dosage of iron salts: comparison between theoretical and experimental results, and practical implications. *Science of the total environment, 392*(1), 145-156.

Forood, T. I., Redaelli, E., Lollini, F., Li, W., & Bertolini, L. (2016). Effects of nanosilica on compressive strength and durability properties of concrete with different water to binder ratios. *Advances in Materials Science and Engineering, 2016*, 8453567.

Fraay, A. L. A., Bijen, J. M., & de Haan, Y. M. (1989). The reaction of fly ash in concrete a critical examination. *Cement and Concrete Research, 19*(2), 235-246.

Freed, W. W. (2000). Reinforced concrete containing antimicrobial-enhanced fibers. Google Patents WO 1995006086 A3.

Fu, T., Montes, F., Suraneni, P., Youngblood, J., & Weiss, J. (2017). The influence of cellulose nanocrystals on the hydration and flexural strength of Portland cement pastes. *Polymers, 9*(9), 424.

Ganigue, R., Gutierrez, O., Rootsey, R., & Yuan, Z. (2011). Chemical dosing for sulfide control in Australia: an industry survey. *Water Research, 45*(19), 6564-6574.

Gao, T., Shen, L., Shen, M., Liu, L., & Chen, F. (2016). Analysis of material flow and consumption in cement production process. *Journal of Cleaner Production, 112*, 553-565.

Gao, X. X., Michaud, P., Joussein, E., & Rossignol, S. (2013). Behavior of metakaolin-based potassium geopolymers in acidic solutions. *Journal of Non-Crystalline Solids, 380*, 95-102.

Gao, Y., & Song, Z. (2013). *Time series prediction model of concrete corrosion in sulfuric based on SVM.* Paper presented at the 2013 International Conference on Computer Sciences and Applications, Wuhan, China.

Goncalves, J., El-Bakkari, M., Boluk, Y., & Bindiganavile, V. (2019). Cellulose nanofibres (CNF) for sulphate resistance in cement based systems. *Cement and Concrete Composites, 99*, 100-111.

Gopalan, M., & Haque, M. (1986). Strength development of fly ash concretes. *Materials and Structures, 19*(1), 33-37.

Government of the Hong Kong-Special Administrative Region. (2013). *Sewerage manual*; Key Planning Issues and Gravity Collection System: Drainage Services Department, Hongkong, China.

Grandclerc, A., Dangla, P., Gueguen-Minerbe, M., & Chaussadent, T. (2018). Modelling of the sulfuric acid attack on different types of cementitious materials. *Cement and Concrete Research, 105*, 126-133.

Grengg, C. (2018). *Microbial induced acid corrosion in sewer environments.* (Doctor of Philosophy), Graz University of Technology,

Grengg, C., Mittermayr, F., Baldermann, A., Böttcher, M. E., Leis, A., Koraimann, G., . . . Dietzel, M. (2015). Microbiologically induced concrete corrosion: A case study from a combined sewer network. *Cement and Concrete Research, 77*, 16-25.

Grengg, C., Mittermayr, F., Ukrainczyk, N., Koraimann, G., Kienesberger, S., & Dietzel, M. (2018). Advances in concrete materials for sewer systems affected by microbial induced concrete corrosion: A review. *Water Research, 134*, 341-352.

Gruyaert, E., Van den Heede, P., Maes, M., & De Belie, N. (2012). Investigation of the influence of blast-furnace slag on the resistance of concrete against organic acid or sulphate attack by means of accelerated degradation tests. *Cement and Concrete Research, 42*(1), 173-185.

Gu, L., Bennett, T., & Visintin, P. (2019). Sulphuric acid exposure of conventional concrete and alkali-activated concrete: Assessment of test methodologies. *Construction and Building Materials, 197*, 681-692.

Guo, X., Shi, H., & Dick, W. A. (2010). Compressive strength and microstructural characteristics of class C fly ash geopolymer. *Cement and Concrete Composites, 32*(2), 142-147.

Gutberlet, T., Hilbig, H., & Beddoe, R. (2015). Acid attack on hydrated cement—Effect of mineral acids on the degradation process. *Cement and Concrete Research, 74*, 35-43.

Gutiérrez-Padilla, M. G. D., Bielefeldt, A., Ovtchinnikov, S., Hernandez, M., & Silverstein, J. (2010). Biogenic sulfuric acid attack on different types of commercially produced concrete sewer pipes. *Cement and Concrete Research, 40*(2), 293-301.

Gutierrez, O., Mohanakrishnan, J., Sharma, K. R., Meyer, R. L., Keller, J., & Yuan, Z. (2008). Evaluation of oxygen injection as a means of controlling sulfide production in a sewer system. *Water Research, 42*(17), 4549-4561.

Hammoudi, A., Moussaceb, K., Belebchouche, C., & Dahmoune, F. (2019). Comparison of artificial neural network (ANN) and response surface methodology (RSM) prediction in compressive strength of recycled concrete aggregates. *Construction and Building Materials, 209*, 425-436.

Haynes, R. J. (2009). Reclamation and revegetation of fly ash disposal sites – Challenges and research needs. *Journal of Environmental Management, 90*(1), 43-53.

Hendi, A., Rahmani, H., Mostofinejad, D., Tavakolinia, A., & Khosravi, M. (2017). Simultaneous effects of microsilica and nanosilica on self-consolidating concrete in a sulfuric acid medium. *Construction and Building Materials, 152*, 192-205.

Hewayde, E., Allouche, E., & Nakhla, G. (2003). Experimental investigations of the effect of selected admixtures on the resistance of concrete to sulfuric acid attack. In *New Pipeline Technologies, Security, and Safety* (pp. 504-513).

Hewayde, E., Nehdi, M., Allouche, E., & Nakhla, G. (2006). Effect of geopolymer cement on microstructure, compressive strength and sulphuric acid resistance of concrete. *Magazine of Concrete Research, 58*(5), 321-331.

Hewayde, E., Nehdi, M., Allouche, E., & Nakhla, G. (2007a). Effect of Mixture Design Parameters and Wetting-Drying Cycles on Resistance of Concrete to Sulfuric Acid Attack. *Journal of Materials in Civil Engineering, 19*(2), 155-163.

Hewayde, E., Nehdi, M., Allouche, E., & Nakhla, G. (2007b). Neural network prediction of concrete degradation by sulphuric acid attack. *Structure Infrastructure Engineering, 3*(1), 17-27.

Hewayde, E., Nehdi, M. L., Allouche, E., & Nakhla, G. (2007c). Using concrete admixtures for sulphuric acid resistance. *Construction Materials, 160*(1), 25-35.

Hewayde, E., Nehdi, M. L., Allouche, E., & Nakhla, G. (2007d). Using concrete admixtures for sulphuric acid resistance. *Proceedings of the Institution of Civil Engineers-Construction Materials, 160*(1), 25-35.

Hewayde, E. H. (2005). *Investigation on degradation of concrete sewer pipes by sulfuric acid attack.* (Ph.D.), The University of Western Ontario (Canada), Ann Arbor.

Høien, A. H., Nilsen, B., & Olsson, R. (2019). Main aspects of deformation and rock support in Norwegian road tunnels. *Tunnelling and Underground Space Technology, 86*, 262-278.

Hong, W.-C., Dong, Y., Lai, C.-Y., Chen, L.-Y., & Wei, S.-Y. (2011). SVR with hybrid chaotic immune algorithm for seasonal load demand forecasting. *Energies, 4*(6), 960-977.

Hossain, M. M., Karim, M. R., Hasan, M., Hossain, M. K., & Zain, M. F. M. (2016). Durability of mortar and concrete made up of pozzolans as a partial replacement of cement: A review. *Construction and Building Materials, 116*, 128-140.

House, M. W. (2013). *Using biological and physico-chemical test methods to assess the role of concrete mixture design in resistance to microbially induced corrosion.* (Master of Science), Purdue University, West Lafayette, Indiana.

House, M. W., & Weiss, W. J. (2014). *Review of microbially induced corrosion and comments on needs related to testing procedures.* Paper presented at the 4th International Conference on the Durability of Concrete Structures, ICDCS 2014, West Lafayette, IN.

Huang, G., Pudasainee, D., Gupta, R., & Liu, W. V. (2019). Hydration reaction and strength development of calcium sulfoaluminate cement-based mortar cured at cold temperatures. *Construction and Building Materials, 224*, 493-503.

Huang, Z., Chen, H., Hsu, C.-J., Chen, W.-H., & Wu, S. (2004). Credit rating analysis with support vector machines and neural networks: a market comparative study. *Decision Support Systems, 37*(4), 543-558.

Huber, B., Hilbig, H., Drewes, J. E., & Müller, E. (2017). Evaluation of concrete corrosion after short- and long-term exposure to chemically and microbially generated sulfuric acid. *Cement and Concrete Research, 94*, 36-48.

Huseyin, S., Mohammed, M., Mohammed, S., & Ibrabimm, A. (1987). Case study of deterioration of concrete in sewage environment in an arabian gulf country. *Durability of building materials, 5*(2), 145-154.

Idriss, A., Negi, S., Jofriet, J., & Hayward, G. (2001). Effect of hydrogen sulphide emissions on cement mortar specimens. *Canadian Biosystems Engineering, 43*, 5.

Islander, R. L., Devinny, J. S., Mansfeld, F., Postyn, A., & Shih, H. (1991). Microbial ecology of crown corrosion in sewers. *Journal of Environmental Engineering, 117*(6), 751-770.

Israel, D., Macphee, D. E., & Lachowski, E. E. (1997). Acid attack on pore-reduced cements. *Journal of Materials Science, 32*(15), 4109-4116.

Ito, K., & Nakano, R. (2003, 20-24 July). *Optimizing Support Vector regression hyperparameters based on cross-validation.* Paper presented at the Proceedings of the International Joint Conference on Neural Networks, Portland, OR, USA.

Jackson, M. D., Landis, E. N., Brune, P. F., Vitti, M., Chen, H., Li, Q., . . . Ingraffea, A. R. (2014). Mechanical resilience and cementitious processes in Imperial Roman architectural mortar. *Proceedings of the National Academy of Sciences, 111*(52), 18484-18489.

Jalal, M., Pouladkhan, A., Harandi, O. F., & Jafari, D. (2015). Comparative study on effects of Class F fly ash, nano silica and silica fume on properties of high performance self compacting concrete. *Construction and Building Materials, 94*, 90-104.

James, J. (2003). Controlling sewer crown corrosion using the crown spray process with magnesium hydroxide. *Proceedings of the Water Environment Federation, 2003*(3), 259-268.

Janfeshan Araghi, H., Nikbin, I. M., Rahimi Reskati, S., Rahmani, E., & Allahyari, H. (2015). An experimental investigation on the erosion resistance of concrete containing various PET particles percentages against sulfuric acid attack. *Construction and Building Materials, 77*, 461-471.

Jenkins, S. H. (2013). *Eighth International Conference on Water Pollution Research: Proceedings of the 8th International Conference, Sydney, Australia, 1976*: Elsevier.

Jensen, H. S. (2009). *Hydrogen sulfide induced concrete corrosion of sewer networks.* (Doctor of Philosophy), Aalborg University,

Jeon, I. K., Qudoos, A., Jakhrani, S. H., Kim, H. G., & Ryou, J.-S. (2020). Investigation of sulfuric acid attack upon cement mortars containing silicon carbide powder. *Powder Technology, 359*, 181-189.

Jerlin Regin, J., Vincent, P., & Ganapathy, C. (2017). Effect of mineral admixtures on mechanical properties and chemical resistance of lightweight coconut shell concrete. *Arabian Journal for Science and Engineering, 42*(3), 957-971.

Jiang, G., Gutierrez, O., Sharma, K. R., Keller, J., & Yuan, Z. (2011a). Optimization of intermittent, simultaneous dosage of nitrite and hydrochloric acid to control sulfide and methane productions in sewers. *Water Research, 45*(18), 6163-6172.

Jiang, G., Gutierrez, O., & Yuan, Z. (2011b). The strong biocidal effect of free nitrous acid on anaerobic sewer biofilms. *Water Research, 45*(12), 3735-3743.

Jiang, G., Keller, J., Bond, P. L., & Yuan, Z. (2016). Predicting concrete corrosion of sewers using artificial neural network. *Water Research, 92*, 52-60.

Jiang, G., Wightman, E., Donose, B. C., Yuan, Z., Bond, P. L., & Keller, J. (2014). The role of iron in sulfide induced corrosion of sewer concrete. *Water Research, 49*, 166-174.

Jones, S. N., & Cetin, B. (2017). Remediation of acid mine drainages with recycled concrete aggregates. In *Geotechnical Frontiers 2017* (pp. 450-458).

Joorabchian, S. M. (2010). *Durability of concrete exposed to sulfuric acid attack.* (Master of Applied Science), Ryerson University, Toronto, Ontario, Canada.

Joseph, A. P., Keller, J., Bustamante, H., & Bond, P. L. (2012). Surface neutralization and H2S oxidation at early stages of sewer corrosion: influence of temperature, relative humidity and H2S concentration. *Water Research, 46*(13), 4235-4245.

Joshi, R. (1973). Pozzolanic activity in synthetic fly ashes: I, experimental production and characterization. *American Ceramic Society Bulletin, 52*.

Kadri, E.-H., Kenai, S., Ezziane, K., Siddique, R., & De Schutter, G. (2011). Influence of metakaolin and silica fume on the heat of hydration and compressive strength development of mortar. *Applied Clay Science, 53*(4), 704-708.

Kaiser, P. K., Amann, F., & Steiner, W. (2010). *How highly stressed brittle rock failure impacts tunnel design.* Paper presented at the ISRM International Symposium-EUROCK 2010.

Kaneko, H., & Funatsu, K. (2015). Fast optimization of hyperparameters for support vector regression models with highly predictive ability. *Chemometrics and Intelligent Laboratory Systems, 142*, 64-69.

Kani, E. N., Allahverdi, A., & Provis, J. L. (2017). Calorimetric study of geopolymer binders based on natural pozzolan. *Journal of Thermal Analysis Calorimetry, 127*(3), 2181-2190.

Kannan, V., & Ganesan, K. (2014). Chloride and chemical resistance of self compacting concrete containing rice husk ash and metakaolin. *Construction and Building Materials, 51*, 225-234.

Karatas, M., Dener, M., Mohabbi, M., & Benli, A. (2019). A study on the compressive strength and microstructure characteristic of alkali-activated metakaolin cement. *Matéria, 24*(4).

Karthik, A., Sudalaimani, K., Vijayakumar, C., & Saravanakumar, S. (2019). Effect of bio-additives on physico-chemical properties of fly ash-ground granulated blast furnace slag based self cured geopolymer mortars. *Journal of Hazardous Materials, 361*, 56-63.

Karthik, A., Sudalaimani, K., & Vijayakumar, C. T. (2017). Durability study on coal fly ash-blast furnace slag geopolymer concretes with bio-additives. *Ceramics International, 43*(15), 11935-11943.

Kaufmann, J. (2014). *Durability performance of fiber reinforced shotcrete in aggressive environment.* Paper presented at the World Tunnelling Congress, Foz do Iguaçu, Brazil.

Kavaklioglu, K. (2011). Modeling and prediction of Turkey's electricity consumption using Support Vector Regression. *Applied Energy, 88*(1), 368-375.

Kaviani, S., & Sohn, I. (2020). Influence of random topology in artificial neural networks: A survey. *ICT Express*.

Kaytez, F., Taplamacioglu, M. C., Cam, E., & Hardalac, F. (2015). Forecasting electricity consumption: A comparison of regression analysis, neural networks and least squares support vector machines. *International Journal of Electrical Power & Energy Systems, 67*, 431-438.

Kefeni, K. K., & Mamba, B. B. (2020). Evaluation of charcoal ash nanoparticles pollutant removal capacity from acid mine drainage rich in iron and sulfate. *Journal of Cleaner Production, 251*, 119720.

Khalafi, L., Kashani, S., & Karimi, J. (2015). Molecular recognition: detection of colorless compounds based on color change. *Journal of Chemical Education, 93*(2), 376-379.

Khaloo, A., Mobini, M. H., & Hosseini, P. (2016). Influence of different types of nano-SiO2 particles on properties of high-performance concrete. *Construction and Building Materials, 113*, 188-201.

Khan, H. A., Castel, A., Khan, M. S. H., & Mahmood, A. H. (2019). Durability of calcium aluminate and sulphate resistant Portland cement based mortars in aggressive sewer environment and sulphuric acid. *Cement and Concrete Research, 124*, 105852.

Khan, M. A. (2015). Chapter 10 - Alternative ABC methods and funding justification. In M. A. Khan (Ed.), *Accelerated Bridge Construction* (pp. 443-488). Boston: Butterworth-Heinemann.

Khatib, J. M. (2008). Performance of self-compacting concrete containing fly ash. *Construction and Building Materials, 22*(9), 1963-1971.

Khatib, J. M., & Clay, R. M. (2004). Absorption characteristics of metakaolin concrete. *Cement and Concrete Research, 34*(1), 19-29.

Khatib, J. M., & Hibbert, J. J. (2005). Selected engineering properties of concrete incorporating slag and metakaolin. *Construction and Building Materials, 19*(6), 460-472.

Kim, H., Swamy, K. K., Kwon, N., Kim, Y., Park, S., & Yoon, J. (2017). Colorimetric detection of thiophenol based on a phenolphthalein derivative and its application as a molecular logic gate. *ChemPhysChem, 18*(13), 1752-1754.

Klassen, A. (2013). Sewer-system fix is costly. Retrieved from Available online http://www.kamloopsthisweek.com/sewer-system-fix-is-costly/ (accessed on May 2017)

Koenig, A., & Dehn, F. (2016). Main considerations for the determination and evaluation of the acid resistance of cementitious materials. *Materials and Structures/Materiaux et Constructions, 49*(5), 1693-1703.

Kong, D., Du, X., Wei, S., Zhang, H., Yang, Y., & Shah, S. P. (2012). Influence of nano-silica agglomeration on microstructure and properties of the hardened cement-based materials. *Construction and Building Materials, 37*, 707-715.

Korucu, H., Şimşek, B., Uygunoğlu, T., Güvenç, A. B., & Yartaşı, A. (2019). Statistical approach to carbon based materials reinforced cementitious composites: Mechanical, thermal, electrical and sulfuric acid resistance properties. *Composites Part B: Engineering, 171*, 347-360.

Kramer, M. A. (1991). Nonlinear principal component analysis using autoassociative neural networks. *AIChE Journal, 37*(2), 233-243.

Kristiawan, S., & Tyas, G. (2016). *Degradation of self-compacting concrete (SCC) due to sulfuric acid attack: Experiment investigation on the effect of high volume fly ash content.* Paper presented at the IOP Conference Series: Materials Science and Engineering.

Kuliczkowska, E. (2016). The interaction between road traffic safety and the condition of sewers laid under roads. *Transportation Research Part D: Transport and Environment, 48*, 203-213.

Kurt W. Koehn. (1994). *Methods and benefits of spincasting cements on corrugated metal pipes*; C. K. Masonry Co., Inc.: Nashville, TN, USA.

Kurtis, K. E., Monteiro, P. J., & Madanat, S. M. (2000). Empirical models to predict concrete expansion caused by sulfate attack. *ACI Materials Journal, 97*(2), 156-161.

L'Hôpital, E., Lothenbach, B., Scrivener, K., & Kulik, D. (2016). Alkali uptake in calcium alumina silicate hydrate (CASH). *Cement and Concrete Research, 85*, 122-136.

Lahoti, M., Narang, P., Tan, K. H., & Yang, E.-H. (2017). Mix design factors and strength prediction of metakaolin-based geopolymer. *Ceramics International, 43*(14), 11433-11441.

Lai, W.-C., Chang, T.-P., Wang, J.-J., Kan, C.-W., & Chen, W.-W. (2012). An evaluation of Mahalanobis Distance and grey relational analysis for crack pattern in concrete structures. *Computational Materials Science, 65*, 115-121.

Laref, R., Losson, E., Sava, A., & Siadat, M. (2019). On the optimization of the support vector machine regression hyperparameters setting for gas sensors array applications. *Chemometrics and Intelligent Laboratory Systems, 184*, 22-27.

Larsen, T. A., Udert, K. M., & Lienert, J. (2013). *Source separation and decentralization for wastewater management*: Iwa Publishing.

Lawrence, S., Giles, C. L., & Tsoi, A. C. (1997). *Lessons in neural network training: Overfitting may be harder than expected.* Paper presented at the AAAI/IAAI.

Lee, K.-M., Bae, S.-H., Park, J.-I., & Kwon, S.-O. (2015). Mass change prediction model of concrete subjected to sulfate attack. *Mathematical Problems in Engineering, 2015*, 298918.

Leslie, J., & Cheesman, W. (1949). An ultrasonic method of studying deterioration and cracking in concrete structures. *Journal of the American Concrete Institute, 21*(1), 17-36.

Li, G. (2004). Properties of high-volume fly ash concrete incorporating nano-SiO2. *Cement and Concrete Research, 34*(6), 1043-1049.

Li, H., Yan, D., Chen, G., Xu, S., Liu, J., & Hu, Y. (2016). Porosity, pore size distribution and chloride permeability of shotcrete modified with nano particles at early age. *Journal of Wuhan University of Technology-Mater. Sci. Ed., 31*(3), 582-589.

Li, M., Du, W., & Nian, F. (2014). An Adaptive Particle Swarm Optimization Algorithm Based on Directed Weighted Complex Network. *Mathematical Problems in Engineering, 2014*, 434972.

Li, X., O'Moore, L., Song, Y., Bond, P. L., Yuan, Z., Wilkie, S., . . . Jiang, G. (2019). The rapid chemically induced corrosion of concrete sewers at high H2S concentration. *Water Research, 162*, 95-104.

Li, Z., & Li, S. (2018). Carbonation resistance of fly ash and blast furnace slag based geopolymer concrete. *Construction and Building Materials, 163*, 668-680.

Lieser, M., & Stek, C. (2010). Composites and the future of society: preventing a legacy of costly corrosion with modern materials. *Composites the Future of Society*, 1-10.

Lim, S., & Mondal, P. (2015). Effects of incorporating nanosilica on carbonation of cement paste. *Journal of Materials Science, 50*(10), 3531-3540.

Lin-ping, W., Guang-ping, H., Chao-shi, H., & Wei Victor, L. Effects of cellulose nanocrystals on improving the acid resistance of cementitious composites in mining. *International Journal of Minerals, Metallurgy and Materials*.

Ling, H., Qian, C., Kang, W., Liang, C., & Chen, H. (2019). Combination of support vector machine and K-fold cross validation to predict compressive strength of concrete in marine environment. *Construction and Building Materials, 206*, 355-363.

López-Vázquez, C., & Hochsztain, E. (2019). Extended and updated tables for the Friedman rank test. *Communications in Statistics, 48*(2), 268-281.

Macías, A., Goni, S., & Madrid, J. (1999). Limitations of Köch-Steinegger test to evaluate the durability of cement pastes in acid medium. *Cement and Concrete Research, 29*(12), 2005-2009.

Madandoust, R., & Mousavi, S. Y. (2012). Fresh and hardened properties of self-compacting concrete containing metakaolin. *Construction and Building Materials, 35*, 752-760.

Madavarapu, S. B. (2014). *FTIR analysis of alkali activated slag and fly ash using deconvolution techniques.* (Master of Science), Arizona State University Tempe, AZ, United States,

Mahdikhani, M., Bamshad, O., & Fallah Shirvani, M. (2018). Mechanical properties and durability of concrete specimens containing nano silica in sulfuric acid rain condition. *Construction and Building Materials, 167*, 929-935.

Mahmoodian, M., & Alani, A. M. (2017). Effect of temperature and acidity of sulfuric acid on concrete properties. *Journal of Materials in Civil Engineering, 29*(10), 04017154.

Mahmoud, M., & Bassuoni, M. (2020). Response of concrete to incremental aggression of sulfuric acid. *Journal of Testing and Evaluation, 48*(4), 19.

Makhloufi, Z., Bederina, M., Bouhicha, M., & Kadri, E.-H. (2014). Effect of mineral admixtures on resistance to sulfuric acid solution of mortars with quaternary binders. *Physics Procedia, 55*, 329-335.

Mantovani, R. G., Rossi, A. L., Vanschoren, J., Bischl, B., & De Carvalho, A. C. (2015). *Effectiveness of random search in SVM hyper-parameter tuning.* Paper presented at the 2015 International Joint Conference on Neural Networks (IJCNN).

Marchand, J., Odler, I., Skalny, J.,. (2002). *Sulfate attack on concrete*. London: CRC Press.

Mardani-Aghabaglou, A., İnan Sezer, G., & Ramyar, K. (2014). Comparison of fly ash, silica fume and metakaolin from mechanical properties and durability performance of mortar mixtures view point. *Construction and Building Materials, 70*(Supplement C), 17-25.

Mazlan, D., Din, M. M., Tokoro, C., & Ibrahim, I. (2016). Cellulose nanocrystals addition effects on cement mortar matrix properties. *International Journal of Advances in Mechanical and Civil Engineering, 3*, 44-48.

McAlpine, G., & Anderson, B. (2005). Structural Rehabilitation of Cast-In-Place Concrete Sewers. In *Pipelines 2005: Optimizing Pipeline Design, Operations, and Maintenance in Today's Economy* (pp. 510-522).

Medpelli, D. (2015). *New nanostructured aluminosilicates from geopolymer chemistry.* (Doctor of Philosophy), Arizona State University,

Mehta, P. (1985). Studies on chemical resistance of low water/cement ratio concretes. *Cement and Concrete Research, 15*(6), 969-978.

Mehta, P. K. (1977). Properties of blended cements made from rice husk ash. *Journal of American Concrete Institute, 74*(9), 440-442.

Mehta, P. K., & Monteiro, P. J. (2014). *Concrete microstructure, properties and materials*. New York: McGraw-Hill Education.

Meng, Q., Ma, X., & Zhou, Y. (2014). Forecasting of coal seam gas content by using support vector regression based on particle swarm optimization. *Journal of Natural Gas Science and Engineering, 21*, 71-78.

Mignon, A., Vermeulen, J., Snoeck, D., Dubruel, P., Van Vlierberghe, S., & De Belie, N. (2017). Mechanical and self-healing properties of cementitious materials with pH-responsive semi-synthetic superabsorbent polymers. *Materials and Structures, 50*(6), 238.

Miller, S. A., John, V. M., Pacca, S. A., & Horvath, A. (2018). Carbon dioxide reduction potential in the global cement industry by 2050. *Cement and Concrete Research, 114*, 115-124.

Mohanakrishnan, J., Gutierrez, O., Meyer, R. L., & Yuan, Z. (2008). Nitrite effectively inhibits sulfide and methane production in a laboratory scale sewer reactor. *Water Research, 42*(14), 3961-3971.

Mohanakrishnan, J., Gutierrez, O., Sharma, K. R., Guisasola, A., Werner, U., Meyer, R. L., . . . Yuan, Z. (2009). Impact of nitrate addition on biofilm properties and activities in rising main sewers. *Water Research, 43*(17), 4225-4237.

Monteny, J., De Belie, N., & Taerwe, L. (2003). Resistance of different types of concrete mixtures to sulfuric acid. *Materials and Structures, 36*(4), 242-249.

Moraes, R., Valiati, J. F., & Gavião Neto, W. P. (2013). Document-level sentiment classification: An empirical comparison between SVM and ANN. *Expert Systems with Applications, 40*(2), 621-633.

Mori, T., Nonaka, T., Tazaki, K., Koga, M., Hikosaka, Y., & Noda, S. (1992). Interactions of nutrients, moisture and pH on microbial corrosion of concrete sewer pipes. *Water Research, 26*(1), 29-37.

Morrison, R., Sangster, T., Downey, D., Matthews, J., Condit, W., Sinha, S., . . . Sterling, R. (2013). *State of technology for rehabilitation of water distribution systems*; EPA/600/R-13/036

Nath, S. K., Maitra, S., Mukherjee, S., & Kumar, S. (2016). Microstructural and morphological evolution of fly ash based geopolymers. *Construction and Building Materials, 111*, 758-765.

Nematzadeh, M., & Fallah-Valukolaee, S. (2017). Erosion resistance of high-strength concrete containing forta-ferro fibers against sulfuric acid attack with an optimum design. *Construction and Building Materials, 154*, 675-686.

Neville, A. (1995). Chloride attack of reinforced concrete: an overview. *Materials and Structures, 28*(2), 63-70.

Newman, J., & Choo, B. S. (2003). *Advanced concrete technology 3: processes*. Oxford, UK: Butterworth-Heinemann.

Norman E. (2016). *Manhole rehabilitation: delivering on the design with proper installation practices and related quality assurance testing*. Paper presented at the North American Society for Trenchless Technology (NASTT) NASTT's 2016 No-Dig Show, Dallas, Texas, USA

Okun, D. A., Wang, L. K., & Shammas, N. K. (2010). *Water supply and distribution and wastewater collection*: John Wiley and Sons.

Ondrejka Harbulakova, V., Estokova, A., & Kovalcikova, M. (2017). Correlation analysis between different types of corrosion of concrete containing sulfate resisting cement. *Environments, 4*(3), 44.

Oualit, M., Jauberthie, R., Rendell, F., Mélinge, Y., & Abadlia, M. T. (2012). External corrosion to concrete sewers: a case study. *Urban Water Journal, 9*(6), 429-434.

Ozer, I., & Soyer-Uzun, S. (2015). Relations between the structural characteristics and compressive strength in metakaolin based geopolymers with different molar Si/Al ratios. *Ceramics International, 41*(8), 10192-10198.

Pacewska, B., Nowacka, M., Wilińska, I., Kubissa, W., & Antonovich, V. (2011). Studies on the influence of spent FCC catalyst on hydration of calcium aluminate cements at ambient temperature. *Journal of Thermal Analysis Calorimetry, 105*(1), 129-140.

Pacheco-Torgal, F., & Jalali, S. (2009). Sulphuric acid resistance of plain, polymer modified, and fly ash cement concretes. *Construction and Building Materials, 23*(12), 3485-3491.

Palomo, A., Blanco-Varela, M. T., Granizo, M. L., Puertas, F., Vazquez, T., & Grutzeck, M. W. (1999). Chemical stability of cementitious materials based on metakaolin. *Cement and Concrete Research, 29*(7), 997-1004.

Panchal, G., Ganatra, A., Shah, P., & Panchal, D. (2011). Determination of over-learning and over-fitting problem in back propagation neural network. *International Journal of Soft Computing, 2*(2), 40-51.

Papadakis, V. G. (1999). Effect of fly ash on Portland cement systems: Part I. Low-calcium fly ash. *Cement and Concrete Research, 29*(11), 1727-1736.

Papadakis, V. G., Vayenas, C. G., & Fardis, M. N. (1991). Physical and chemical characteristics affecting the durability of concrete. *Materials Journal, 88*(2), 186-196.

Parande, A., Ramsamy, P., Ethirajan, S., Rao, C., & Palanisamy, N. (2006). Deterioration of reinforced concrete in sewer environments. *Proceedings of the Institution of Civil Engineers-Municipal Engineer, 159*(1), 11-20.

Park, S.-K., Kim, J.-H. J., Nam, J.-W., Phan, H. D., & Kim, J.-K. (2009). Development of anti-fungal mortar and concrete using Zeolite and Zeocarbon microcapsules. *Cement and Concrete Composites, 31*(7), 447-453.

Pasupathy, K., Berndt, M., Castel, A., Sanjayan, J., & Pathmanathan, R. (2016). Carbonation of a blended slag-fly ash geopolymer concrete in field conditions after 8years. *Construction and Building Materials, 125*, 661-669.

Pavel, R., & Jiří, T. (2016). Resistance of concrete with metakaolin addition to acid environment. *Key Engineering Materials, 677*, 144-149.

Pelisser, F., Gleize, P. J. P., & Mikowski, A. (2012). Effect of the Ca/Si molar ratio on the micro/nanomechanical properties of synthetic C-S-H measured by nanoindentation. *The Journal of Physical Chemistry C, 116*(32), 17219-17227.

Perná, I., & Hanzlíček, T. (2016). The setting time of a clay-slag geopolymer matrix: the influence of blast-furnace-slag addition and the mixing method. *Journal of Cleaner Production, 112*, 1150-1155.

Pietersen, H. S., Fraay, A. L., & Bijen, J. M. (1989). Reactivity of fly ash at high pH. *MRS Online Proceedings Library Archive, 178*, 139.

Pomeroy, R., & Bowlus, F. D. (1946). Progress report on sulfide control research. *Sewage works journal, 18*(4), 597-640.

Poon, C. S., Kou, S. C., & Lam, L. (2006). Compressive strength, chloride diffusivity and pore structure of high performance metakaolin and silica fume concrete. *Construction and Building Materials, 20*(10), 858-865.

Portland Cement Association. (2002). Concrete information: Types and causes of concrete deterioration. *PCA R&D Serial*(2617).

Pouhet, R., & Cyr, M. (2016). Carbonation in the pore solution of metakaolin-based geopolymer. *Cement and Concrete Research, 88*, 227-235.

Pu, Y., Apel, D. B., Wang, C., & Wilson, B. (2018). Evaluation of burst liability in kimberlite using support vector machine. *Acta Geophysica, 66*(5), 973-982.

Quercia Bianchi, G. (2014). *Application of nano-silica in concrete.* (Doctor of Philosophy), Technische Universiteit Eindhoven, Eindhoven.

Quercia, G., Spiesz, P., Hüsken, G., & Brouwers, H. (2014). SCC modification by use of amorphous nano-silica. *Cement and Concrete Composites, 45*, 69-81.

Rahmani, H., Ramazanianpour, A., Parhizkar, T., & Hillemeier, B. (2009). *Contradictory effects of silica fume concretes in sulfuric acid environments*. Paper presented at the 3rd International Conference on Concrete and Development, Tehran, Iran.

Rahmani, H., & Ramzanianpour, A. (2008). Effect of silica fume and natural pozzolanas on sulfuric acid resistance of dense concretes. *Asian Journal of Civil Engineering (Building and Housing), 9*(3), 303-319.

Read, G. F., & Vickridge, I. G. (1997). 4 - Planning sewerage rehabilitation and maintenance. In G. F. Read & I. G. Vickridge (Eds.), *Sewers* (pp. 69-83). London: Butterworth-Heinemann.

Reardon, E. J. (1990). An ion interaction model for the determination of chemical equilibria in cement/water systems. *Cement and Concrete Research, 20*(2), 175-192.

Richardson, I. G. (1999). The nature of C-S-H in hardened cements. *Cement and Concrete Research, 29*(8), 1131-1147.

Rombén, L. (1980). *Aspects on testing methods for acid attacks on concrete-further experiments*; Swedish Cement and Concrete Research Institute: Sweden.

Rootsey, R., Melchers, R., Stuetz, R., Keller, J., & Yuan, Z. (2012). *Taking control of odours and corrosion in sewers.* Paper presented at the Australia's National Water Conference and Exhibition (OzWater 2012), Sydney, AU.

Rovnaník, P., Rovnaníková, P., Vyšvařil, M., Grzeszczyk, S., & Janowska-Renkas, E. (2018). Rheological properties and microstructure of binary waste red brick powder/metakaolin geopolymer. *Construction and Building Materials, 188*, 924-933.

Rowles, M., & O'connor, B. (2003). Chemical optimisation of the compressive strength of aluminosilicate geopolymers synthesised by sodium silicate activation of metakaolinite. *Journal of Materials Chemistry, 13*(5), 1161-1165.

Roy, D. M., Arjunan, P., & Silsbee, M. R. (2001). Effect of silica fume, metakaolin, and low-calcium fly ash on chemical resistance of concrete. *Cement and Concrete Research, 31*(12), 1809-1813.

Rupasinghe, M., San Nicolas, R., Mendis, P., Sofi, M., & Ngo, T. (2017). Investigation of strength and hydration characteristics in nano-silica incorporated cement paste. *Cement and Concrete Composites, 80*, 17-30.

Sabir, B. B., Wild, S., & Bai, J. (2001). Metakaolin and calcined clays as pozzolans for concrete: a review. *Cement and Concrete Composites, 23*(6), 441-454.

Sadrmomtazi, A., Fasihi, A., Balalaei, F., & Haghi, A. (2009). *Investigation of mechanical and physical properties of mortars containing silica fume and nano-SiO2.* Paper presented at the Proceedings of the Third International Conference on Concrete and Development, Tehran, Iran.

Said-Mansour, M., Kadri, E.-H., Kenai, S., Ghrici, M., & Bennaceur, R. (2011). Influence of calcined kaolin on mortar properties. *Construction and Building Materials, 25*(5), 2275-2282.

Salesi, S., & Cosma, G. (2017, 21-23 Oct. 2017). *A novel extended binary cuckoo search algorithm for feature selection.* Paper presented at the 2017 2nd International Conference on Knowledge Engineering and Applications (ICKEA).

Sand, W. (1987). Biotest system for rapid evaluation of concrete resitance to sulfur-oxidizing bacteria. *Materials Performance, 26*(3), 14-17.

Sargent, P. (2015). The development of alkali-activated mixtures for soil stabilisation. In *Handbook of alkali-activated cements, mortars and concretes* (pp. 555-604): Elsevier.

Schrader, E. K., & Kaden, R. A. (1987). Durability of shotcrete. *Special Publication, 100*, 1071-1102.

Scrivener, K. L., & Capmas, A. (1998). 13 - Calcium aluminate cements. In P. C. Hewlett (Ed.), *Lea's Chemistry of Cement and Concrete (Fourth Edition)* (pp. 713-782). Oxford: Butterworth-Heinemann.

Senhadji, Y., Escadeillas, G., Mouli, M., Khelafi, H., & Benosman. (2014). Influence of natural pozzolan, silica fume and limestone fine on strength, acid resistance and microstructure of mortar. *Powder Technology, 254*, 314-323.

Sheela, K. G., & Deepa, S. N. (2013). Review on methods to fix number of hidden neurons in neural networks. *Mathematical Problems in Engineering, 2013*, 425740.

Shetti, A. P., & Das, B. B. (2015). Acid, alkali and chloride resistance of early age cured silica fume concrete. In *Advances in Structural Engineering: Materials, Volume Three* (pp. 1849-1862): Springer India.

Shi, C., & Stegemann, J. (2000). Acid corrosion resistance of different cementing materials. *Cement and Concrete Research, 30*(5), 803-808.

Shih, J.-Y., Chang, T.-P., & Hsiao, T.-C. (2006). Effect of nanosilica on characterization of Portland cement composite. *Materials Science and Engineering: A, 424*(1), 266-274.

Shing, C. K., Wu, C. L., Chen, J. W., Yuen, C. S., & Tsui, R. Y. (2012). A review on protection of concrete for sewage installations and an accelerated test on protection systems. *HKIE Transactions, 19*(3), 8-16.

Siad, H., Lachemi, M., Sahmaran, M., & Hossain, K. M. A. (2016). Effect of glass powder on sulfuric acid resistance of cementitious materials. *Construction and Building Materials, 113*, 163-173.

Siddique, R. (2011). Utilization of silica fume in concrete: Review of hardened properties. *Resources, Conservation and Recycling, 55*(11), 923-932.

Siddique, R., & Khan, M. I. (2011). *Supplementary cementing materials*: Springer Science & Business Media.

Singapore. (2004). *Code of Practice* Sewerage and Sanitary Works Water Reclamation (Network) Department, Singapore.

Singh, B., Ishwarya, G., Gupta, M., & Bhattacharyya, S. (2015). Geopolymer concrete: A review of some recent developments. *Construction and Building Materials, 85*, 78-90.

Singh, M., & Siddique, R. (2015). Properties of concrete containing high volumes of coal bottom ash as fine aggregate. *Journal of Cleaner Production, 91*, 269-278.

Sivakugan, N., Veenstra, R., & Naguleswaran, N. (2015). Underground mine backfilling in Australia using paste fills and hydraulic fills. *International Journal of Geosynthetics and Ground Engineering, 1*(2), 18.

Smets, K., Verdonk, B., & Jordaan, E. M. (2007, 12-17 Aug. 2007). *Evaluation of performance measures for SVR hyperparameter selection.* Paper presented at the 2007 International Joint Conference on Neural Networks, Orlando, Florida, USA.

Sonebi, M., Cevik, A., Grünewald, S., & Walraven, J. (2016). Modelling the fresh properties of self-compacting concrete using support vector machine approach. *Construction and Building Materials, 106*, 55-64.

Song, X., Marosszeky, M., Brungs, M., & Chang, Z.-T. (2005). *Response of geopolymer concrete to sulphuric acid attack.* Paper presented at the Proceedings of World Congress Geopolymer.

Stantec Consulting Ltd. (2015). *151 Street and 99 Avenue sanitary trunk conceptual design report*. Drainage Services. The City of Edmonton.

Stolte, E. (2015). Major Edmonton sewer trunk line hanging on by "ribs and lagging". *Edmonton Journal*. Retrieved from Available online: http://edmontonjournal.com/news/local-news/major-edmonton-sewer-trunk-line-hanging-on-by-ribs-and-lagging (accessed on May 2017)

Sturm, P., Gluth, G., Jäger, C., Brouwers, H., & Kühne, H.-C. (2018). Sulfuric acid resistance of one-part alkali-activated mortars. *Cement Concrete Research, 109*, 54-63.

Subcommittee on paints and protective coatings. (1969). *Paints and protective coatings for wastewater treatment facilities*. W. P. C. Federation: Washington, DC,.

Sublette, K. L., Kolhatkar, R., & Raterman, K. (1998). Technological aspects of the microbial treatment of sulfide-rich wastewaters: a case study. *Biodegradation, 9*(3), 259-271.

Sun, G., Guan, X., Yi, X., & Zhou, Z. (2018). Grey relational analysis between hesitant fuzzy sets with applications to pattern recognition. *Expert Systems with Applications, 92*, 521-532.

Sun, J., Pikaar, I., Sharma, K. R., Keller, J., & Yuan, Z. (2015). Feasibility of sulfide control in sewers by reuse of iron rich drinking water treatment sludge. *Water Research, 71*, 150-159.

Sun, X. (2015). *Improving the understanding of concrete sewer corrosion through investigations of the gaseous hydrogen sulfide uptake and transformation processes in the corrosion layer.* (Ph.D.), The University of Queensland,

Sun, X., Jiang, G., Chiu, T. H., Zhou, M., Keller, J., & Bond, P. L. (2016). Effects of surface washing on the mitigation of concrete corrosion under sewer conditions. *Cement and Concrete Composites, 68*, 88-95.

Supit, S. W. M., & Shaikh, F. U. A. (2015). Durability properties of high volume fly ash concrete containing nano-silica. *Materials and Structures, 48*(8), 2431-2445.

Tajuelo Rodriguez, E., Garbev, K., Merz, D., Black, L., & Richardson, I. G. (2017). Thermal stability of C-S-H phases and applicability of Richardson and Groves' and Richardson C-(A)-S-H(I) models to synthetic C-S-H. *Cement and Concrete Research, 93*, 45-56.

Tamimi, A. (1997). High-performance concrete mix for an optimum protection in acidic conditions. *Materials and Structures, 30*(3), 188-191.

Tariq, A., & Yanful, E. K. (2013). A review of binders used in cemented paste tailings for underground and surface disposal practices. *Journal of Environmental Management, 131*, 138-149.

Tayman, J., & Swanson, D. A. (1999). On the validity of MAPE as a measure of population forecast accuracy. *Population Research and Policy Review, 18*(4), 299-322.

Thomas, M. (2007). *Optimizing the use of fly ash in concrete* (Vol. 5420). Skokie, IL: Portland Cement Association

Tiffo, E., Mbah, J. B. B., Belibi, P. D. B., Djobo, J. N. Y., & Elimbi, A. (2020). Physical and mechanical properties of unheated and heated kaolin based-geopolymers with partial replacement of aluminium hydroxide. *Materials Chemistry and Physics, 239*, 122103.

Tokyay, M. (2016). *Cement and concrete mineral admixtures*. Boca Raton, Florida: CRC Press.

Torii, K., & Kawamura, M. (1994a). Effects of fly ash and silica fume on the resistance of mortar to sulfuric acid and sulfate attack. *Cement and Concrete Research, 24*(2), 361-370.

Torii, K., & Kawamura, M. (1994b). Pore structure and chloride ion permeability of mortars containing silica fume. *Cement and Concrete Composites, 16*(4), 279-286.

Tsubone, K., Yamaguchi, Y., Ogawa, Y., & Kawai, K. (2016) Deterioration of concrete immersed in sulfuric acid for a long term. In*: Vol. 711. 8th International Conference on Concrete under Severe Conditions - Environment and Loading, CONSEC 2016* (pp. 659-664): Trans Tech Publications Ltd.

U.S. Environmental Protection Agency. (1991). *Hydrogen sulfide corrosion in wastewater collection and treatment systems*; Environmental Protection Agency: Environmental Protection Agency, Washington, DC.

US Environmental Protection Agency. (1985). *Design manual, odor and corrosion control in sanitary sewerage systems and treatment plants*. U.S EPA.

Vafaei, M., & Allahverdi, A. (2016). Influence of calcium aluminate cement on geopolymerization of natural pozzolan. *Construction and Building Materials, 114*, 290-296.

Vafaei, M., & Allahverdi, A. (2018). Acid-resistant geopolymer based on fly ash–calcium aluminate cement. *Journal of Materials in Civil Engineering, 30*(7), 04018143.

Vafaei, M., Allahverdi, A., Dong, P., & Bassim, N. (2018). Acid attack on geopolymer cement mortar based on waste-glass powder and calcium aluminate cement at mild concentration. *Construction and Building Materials, 193*, 363-372.

Valipour, M., Pargar, F., Shekarchi, M., & Khani, S. (2013). Comparing a natural pozzolan, zeolite, to metakaolin and silica fume in terms of their effect on the durability characteristics of concrete: A laboratory study. *Construction and Building Materials, 41*, 879-888.

Valix, M., Zamri, D., Mineyama, H., Cheung, W. H., Shi, J., & Bustamante, H. (2012). Microbiologically induced corrosion of concrete and protective coatings in gravity sewers. *Chinese Journal of Chemical Engineering, 20*(3), 433-438.

Vélez-Pérez, L. S., Ramirez-Nava, J., Hernández-Flores, G., Talavera-Mendoza, O., Escamilla-Alvarado, C., Poggi-Varaldo, H. M., . . . López-Díaz, J. A. (2020). Industrial acid mine drainage and municipal wastewater co-treatment by dual-chamber microbial fuel cells. *International Journal of Hydrogen Energy, 45*(26), 13757-13766.

Villaquirán-Caicedo, M. A. (2019). Studying different silica sources for preparation of alternative waterglass used in preparation of binary geopolymer binders from metakaolin/boiler slag. *Construction and Building Materials, 227*, 116621.

Voldsund, M., Gardarsdottir, S. O., De Lena, E., Pérez-Calvo, J.-F., Jamali, A., Berstad, D., . . . Anantharaman, R. (2019). Comparison of technologies for CO2 capture from cement production—Part 1: Technical evaluation. *Energies, 12*(3), 559.

Vollertsen, J., Nielsen, A. H., Jensen, H. S., Wium-Andersen, T., & Hvitved-Jacobsen, T. (2008). Corrosion of concrete sewers—The kinetics of hydrogen sulfide oxidation. *Science of the total environment, 394*(1), 162-170.

Wafa, F. (1994). Accelerated sulfate attack on concrete in a hot climate. *Cement, Concrete and Aggregates, 16*(1), 31-35.

Wan, Q., Rao, F., Song, S., García, R. E., Estrella, R. M., Patiño, C. L., & Zhang, Y. (2017). Geopolymerization reaction, microstructure and simulation of metakaolin-based geopolymers at extended Si/Al ratios. *Cement and Concrete Composites, 79*, 45-52.

Wang, J., Niu, D., Ding, S., Mi, Z., & Luo, D. (2015). Microstructure, permeability and mechanical properties of accelerated shotcrete at different curing age. *Construction and Building Materials, 78*, 203-216.

Wang, Y., Liu, X., Zhang, W., Li, Z., Zhang, Y., Li, Y., & Ren, Y. (2020). Effects of Si/Al ratio on the efflorescence and properties of fly ash based geopolymer. *Journal of Cleaner Production, 244*, 118852.

Water Environment Federation. (2009). *Existing sewer evaluation and rehabilitation: WEF manual of practice* (3rd ed.). New York: WEF Press: Water Environment Federation Alexandria, Virginia, USA.

Watt, J., & Thorne, D. (1965). Composition and pozzolanic properties of pulverised fuel ashes. I. Composition of fly ashes from some British power stations and properties of their component particles. *Journal of Chemical Technology and Biotechnology, 15*(12), 585-594.

Wellmann, R., Harmand, P., & Müller, C. H. (2009). Distribution-free tests for polynomial regression based on simplicial depth. *Journal of Multivariate Analysis, 100*(4), 622-635.

Wells, T., Melchers, R., Joseph, A., Bond, P., Vitanage, D., Bustamante, H., . . . Evans, T. (2012). *A collaborative investigation of the microbial corrosion of concrete sewer pipe in Australia.* Paper presented at the Proceedings of OzWater-12 Australia's National Water Conference and Exhibition.

Wells, T., & Melchers, R. E. (2014). An observation-based model for corrosion of concrete sewers under aggressive conditions. *Cement and Concrete Research, 61-62*, 1-10.

Wells, T., Melchers, R. E., & Bond, P. (2009). *Factors involved in the long term corrosion of concrete sewers*. Paper presented at the Australasian corrosion association proceedings of corrosion and prevention, Coffs Harbour, Australia.

Wild, S., Khatib, J. M., & Jones, A. (1996). Relative strength, pozzolanic activity and cement hydration in superplasticised metakaolin concrete. *Cement and Concrete Research, 26*(10), 1537-1544.

Wild, S., Sabir, B. B., & Khatib, J. M. (1995). Factors influencing strength development of concrete containing silica fume. *Cement and Concrete Research, 25*(7), 1567-1580.

Wodetzki, B., & Kaakaty, C. (2013). Iron - The optimal solution for odor and corrosion. *Proceedings of the Water Environment Federation, 2013*(10), 5467-5472.

Wong, H. S., & Abdul Razak, H. (2005). Efficiency of calcined kaolin and silica fume as cement replacement material for strength performance. *Cement and Concrete Research, 35*(4), 696-702.

Worrell, E., Price, L., Martin, N., Hendriks, C., & Meida, L. O. (2001). Carbon dioxide emissions from the global cement industry. *Annual Review of Energy and the Environment, 26*(1), 303-329.

Wu, L., Hu, C., & Liu, W. (2018). The sustainability of concrete in sewer tunnel—A narrative review of acid corrosion in the City of Edmonton, Canada. *Sustainability, 10*(2), 517.

Wu, L., Hu, C., & Liu, W. V. (2019). Effects of pozzolans on acid resistance of shotcrete for sewer tunnel rehabilitation. *Journal of Sustainable Cement-Based Materials, 8*(1), 55-77.

Wu, Z., Shi, C., Khayat, K. H., & Wan, S. (2016). Effects of different nanomaterials on hardening and performance of ultra-high strength concrete (UHSC). *Cement and Concrete Composites, 70*, 24-34.

Xiao, J., Qu, W., Li, W., & Zhu, P. (2016). Investigation on effect of aggregate on three non-destructive testing properties of concrete subjected to sulfuric acid attack. *Construction and Building Materials, 115*, 486-495.

Xin, R., Zhang, J., & Shao, Y. (2020). Complex network classification with convolutional neural network. *Tsinghua Science and Technology, 25*(4), 447-457.

Xu, J., Shan, G., Amei, A., Zhao, J., Young, D., & Clark, S. (2017). A modified Friedman test for randomized complete block designs. *Communications in Statistics, 46*(2), 1508-1519.

Yajun, J., & Cahyadi, J. H. (2004). Simulation of silica fume blended cement hydration. *Materials and Structures, 37*(6), 397-404.

Yajuun, J., & Cahyadi, J. (2002). Investigation on microstructure of silica fume cement pastes. *WIT Transactions on the Built Environment, 59*, 9.

Yang, C., & Wang, Z. (2005). Surface pre-grouting and freezing for shaft sinking in aquifer formations. *Mine Water and the Environment, 24*(4), 209-212.

Yang, Y., Ji, T., Lin, X., Chen, C., & Yang, Z. (2018). Biogenic sulfuric acid corrosion resistance of new artificial reef concrete. *Construction and Building Materials, 158*, 33-41.

Yang, Y. T., & Ji, H. G. (2012). The corrosion of concrete shaft lining of mine and its related research progress. *Applied Mechanics and Materials, 226*, 976-979.

Yaseen, Z. M., Tran, M. T., Kim, S., Bakhshpoori, T., & Deo, R. C. (2018). Shear strength prediction of steel fiber reinforced concrete beam using hybrid intelligence models: A new approach. *Engineering Structures, 177*, 244-255.

Yin, S., Shao, Y., Wu, A., Rao, Y., & Chen, X. (2017). *Deformation behaviors of cemented backfill using sulphide-content tailings*. Paper presented at the Proceedings of the 20th International Seminar on Paste and Thickened Tailings, Beijing.

Yin, S., Shao, Y., Wu, A., Wang, Z., & Yang, L. (2020). Assessment of expansion and strength properties of sulfidic cemented paste backfill cored from deep underground stopes. *Construction and Building Materials, 230*, 116983.

You, M.-L., Shu, C.-M., Chen, W.-T., & Shyu, M.-L. (2017). Analysis of cardinal grey relational grade and grey entropy on achievement of air pollution reduction by evaluating air quality trend in Japan. *Journal of Cleaner Production, 142*, 3883-3889.

Yu, H., Wu, L., Liu, W. V., & Pourrahimian, Y. (2018). Effects of fibers on expansive shotcrete mixtures consisting of calcium sulfoaluminate cement, ordinary Portland cement, and calcium sulfate. *Journal of Rock Mechanics and Geotechnical Engineering, 10*(2), 212-221.

Yuan, H., Dangla, P., Chatellier, P., & Chaussadent, T. (2013). Degradation modelling of concrete submitted to sulfuric acid attack. *Cement and Concrete Research, 53*, 267-277.

Yuan, H., Dangla, P., Chatellier, P., & Chaussadent, T. (2015). Degradation modeling of concrete submitted to biogenic acid attack. *Cement and Concrete Research, 70*, 29-38.

Zhang, H., Chen, L., Qu, Y., Zhao, G., & Guo, Z. (2014). Support Vector Regression Based on Grid-Search Method for Short-Term Wind Power Forecasting. *Journal of Applied Mathematics, 2014*, 835791.

Zhang, L., Keller, J., & Yuan, Z. (2009). Inhibition of sulfate-reducing and methanogenic activities of anaerobic sewer biofilms by ferric iron dosing. *Water Research, 43*(17), 4123-4132.

Zhang, M.-H., Islam, J., & Peethamparan, S. (2012). Use of nano-silica to increase early strength and reduce setting time of concretes with high volumes of slag. *Cement and Concrete Composites, 34*(5), 650-662.

Zhang, M., Zhao, M., Zhang, G., Mann, D., Lumsden, K., & Tao, M. (2016). Durability of red mud-fly ash based geopolymer and leaching behavior of heavy metals in sulfuric acid solutions and deionized water. *Construction and Building Materials, 124*, 373-382.

Zhang, S., Li, V. C., & Ye, G. (2020). Micromechanics-guided development of a slag/fly ash-based strain-hardening geopolymer composite (SHGC). *Cement and Concrete Composites, 109*, 103510.

Zhang, S., & Zong, L. (2014). Evaluation of relationship between water absorption and durability of concrete materials. *Advances in Materials Science and Engineering, 2014*, 650373.

Zhang, Y., Sun, W., & Li, Z. (2008). Infrared spectroscopy study of structural nature of geopolymeric products. *Journal of Wuhan University of Technology-Mater. Sci. Ed., 23*(4), 522-527.

Zhao, J. Q. (1998). *Trunk sewers in Canada.* Paper presented at the 1998 APWA International Public Works Congress Seminar Series, American Public Works Association Las Vegas, CA, United States.

Zhao, J. Q., & Rajani, B. (2002). *Construction and rehabilitation costs for buried pipe with a focus on trenchless technologies*; NRC, Institute for Research in Construction: Ottawa, Canada.

Zhao, X., Liu, C., Wang, L., Zuo, L., Zhu, Q., & Ma, W. (2019). Physical and mechanical properties and micro characteristics of fly ash-based geopolymers incorporating soda residue. *Cement and Concrete Composites, 98*, 125-136.

Zivica, V., & Bajza, A. (2001). Acidic attack of cement based materials - A review. Part 1. Principle of acidic attack. *Construction and Building Materials, 15*(8), 331-340.

Appendix

Appendix 1. Data of mass change used for predictive modeling

No.	Geopolymer	CAC content, %	CNC content, %	Fly ash content, %	Silica fume content, %	Nano-silica content, %	Wet-dry cycle	Ratio of sample surface to acid volume	pH	Time, day	Acid addition times	Mass change, %
1	0	0	0	0	0	0	3	0.26201	1.5	21	9	-0.1113
2	0	0	0	0.05	0	0	3	0.26201	1.5	21	9	-0.1227
3	0	0	0	0.1	0	0	3	0.26201	1.5	21	9	-0.1357
4	0	0	0	0.2	0	0	3	0.26201	1.5	21	9	-0.028
5	0	0	0	0.3	0	0	3	0.26201	1.5	21	9	-0.176
6	0	0	0	0	0	0	5	0.26201	1.5	35	11	-0.2485
7	0	0	0	0.05	0	0	5	0.26201	1.5	35	11	-0.2744
8	0	0	0	0.1	0	0	5	0.26201	1.5	35	11	-0.2694
9	0	0	0	0.2	0	0	5	0.26201	1.5	35	11	-0.1299
10	0	0	0	0.3	0	0	5	0.26201	1.5	35	11	-0.3202
11	0	0	0	0	0	0	8	0.26201	1.5	56	14	-0.8392
12	0	0	0	0.05	0	0	8	0.26201	1.5	56	14	-0.8519
13	0	0	0	0.1	0	0	8	0.26201	1.5	56	14	-0.8268
14	0	0	0	0.2	0	0	8	0.26201	1.5	56	14	-0.6345
15	0	0	0	0.3	0	0	8	0.26201	1.5	56	14	-0.9362
16	0	0	0	0.05	0	0	3	0.11884	1.5	21	9	0.46866
17	0	0	0	0.1	0	0	3	0.11884	1.5	21	9	0.436
18	0	0	0	0.2	0	0	3	0.11884	1.5	21	9	0.64121
19	0	0	0	0.3	0	0	3	0.11884	1.5	21	9	0.44875

No.	Geopolymer	CAC content, %	CNC content, %	Fly ash content, %	Silica fume content, %	Nano-silica content, %	Wet-dry cycle	Ratio of sample surface to acid volume	pH	Time, day	Acid addition times	Mass change, %
20	0	0	0	0.05	0	0	3	0.11884	3	21	9	-0.2609
21	0	0	0	0.1	0	0	3	0.11884	3	21	9	-0.252
22	0	0	0	0.2	0	0	3	0.11884	3	21	9	-0.256
23	0	0	0	0.3	0	0	3	0.11884	3	21	9	-0.2041
24	0	0	0	0	0	0	5	0.26201	3	35	11	-0.2132
25	0	0	0	0.05	0	0	5	0.11884	3	35	11	-0.1716
26	0	0	0	0.1	0	0	5	0.11884	3	35	11	-0.1783
27	0	0	0	0.2	0	0	5	0.11884	3	35	11	-0.1647
28	0	0	0	0.3	0	0	5	0.11884	3	35	11	-0.1242
29	0	0	0	0	0	0	8	0.26201	3	56	14	-0.1883
30	0	0	0	0.05	0	0	8	0.11884	3	56	14	-0.0893
31	0	0	0	0.1	0	0	8	0.11884	3	56	14	-0.0744
32	0	0	0	0.2	0	0	8	0.11884	3	56	14	-0.0507
33	0	0	0	0.3	0	0	8	0.11884	3	56	14	-0.0206
34	0	0	0	0.05	0	0	3	0.11884	3	21	9	-0.2474
35	0	0	0	0.1	0	0	3	0.11884	3	21	9	-0.2668
36	0	0	0	0.2	0	0	3	0.11884	3	21	9	-0.0987
37	0	0	0	0.3	0	0	3	0.11884	3	21	9	-0.2706
38	0	0	0	0.05	0	0	5	0.11884	3	35	11	-0.1483
39	0	0	0	0.1	0	0	5	0.11884	3	35	11	-0.1691
40	0	0	0	0.2	0	0	5	0.11884	3	35	11	0.01223
41	0	0	0	0.3	0	0	5	0.11884	3	35	11	-0.1521
42	0	0	0	0	0	0	7	0.26201	3	49	13	-0.4772

No.	Geopolymer	CAC content, %	CNC content, %	Fly ash content, %	Silica fume content, %	Nano-silica content, %	Wet-dry cycle	Ratio of sample surface to acid volume	pH	Time, day	Acid addition times	Mass change, %
43	0	0	0	0.05	0	0	7	0.11884	3	49	13	-0.1391
44	0	0	0	0.1	0	0	7	0.11884	3	49	13	-0.1828
45	0	0	0	0.2	0	0	7	0.11884	3	49	13	0.01459
46	0	0	0	0.3	0	0	7	0.11884	3	49	13	-0.1497
47	0	0	0	0	0	0	9	0.26201	3	63	15	-0.4787
48	0	0	0	0.05	0	0	9	0.11884	3	63	15	-0.1069
49	0	0	0	0.1	0	0	9	0.11884	3	63	15	-0.1477
50	0	0	0	0.2	0	0	9	0.11884	3	63	15	0.05884
51	0	0	0	0.3	0	0	9	0.11884	3	63	15	-0.1248
52	0	0	0	0	0	0	11	0.26201	3	77	17	-0.4107
53	0	0	0	0.05	0	0	11	0.11884	3	77	17	-0.047
54	0	0	0	0.1	0	0	11	0.11884	3	77	17	-0.098
55	0	0	0	0.2	0	0	11	0.11884	3	77	17	0.12399
56	0	0	0	0.3	0	0	11	0.11884	3	77	17	-0.0568
57	0	0	0	0	0	0	13	0.26201	3	91	19	-0.3027
58	0	0	0	0.05	0	0	13	0.11884	3	91	19	-0.0922
59	0	0	0	0.1	0	0	13	0.11884	3	91	19	-0.1366
60	0	0	0	0.2	0	0	13	0.11884	3	91	19	0.18653
61	0	0	0	0.3	0	0	13	0.11884	3	91	19	-0.1509
62	0	0	0	0	0	0	3	0.26201	6.5	21	9	0.27487
63	0	0	0	0.05	0	0	3	0.26201	6.5	21	9	0.45321
64	0	0	0	0.1	0	0	3	0.26201	6.5	21	9	0.49602
65	0	0	0	0.2	0	0	3	0.26201	6.5	21	9	0.38124

No.	Geopolymer	CAC content, %	CNC content, %	Fly ash content, %	Silica fume content, %	Nano-silica content, %	Wet-dry cycle	Ratio of sample surface to acid volume	pH	Time, day	Acid addition times	Mass change, %
66	0	0	0	0.3	0	0	3	0.26201	6.5	21	9	0.3436
67	0	0	0	0	0	0	5	0.26201	6.5	35	11	0.32172
68	0	0	0	0.05	0	0	5	0.26201	6.5	35	11	0.52473
69	0	0	0	0.1	0	0	5	0.26201	6.5	35	11	0.56339
70	0	0	0	0.2	0	0	5	0.26201	6.5	35	11	0.45627
71	0	0	0	0.3	0	0	5	0.26201	6.5	35	11	0.42245
72	0	0	0	0	0	0	8	0.26201	6.5	56	14	0.38497
73	0	0	0	0.05	0	0	8	0.26201	6.5	56	14	0.62974
74	0	0	0	0.1	0	0	8	0.26201	6.5	56	14	0.65037
75	0	0	0	0.2	0	0	8	0.26201	6.5	56	14	0.5491
76	0	0	0	0.3	0	0	8	0.26201	6.5	56	14	0.52787
77	0	0	0	0.05	0	0	3	0.11884	6.5	21	9	-0.2546
78	0	0	0	0.1	0	0	3	0.11884	6.5	21	9	-0.1657
79	0	0	0	0.2	0	0	3	0.11884	6.5	21	9	-0.106
80	0	0	0	0.3	0	0	3	0.11884	6.5	21	9	0.10038
81	0	0	0	0	0	0	5	0.26201	6.5	35	11	0.15877
82	0	0	0	0.05	0	0	5	0.11884	6.5	35	11	-0.1076
83	0	0	0	0.1	0	0	5	0.11884	6.5	35	11	0.01278
84	0	0	0	0.2	0	0	5	0.11884	6.5	35	11	0.07934
85	0	0	0	0.3	0	0	5	0.11884	6.5	35	11	0.29516
86	0	0	0	0	0	0	7	0.26201	6.5	49	13	0.28057
87	0	0	0	0.05	0	0	7	0.11884	6.5	49	13	0.0085
88	0	0	0	0.1	0	0	7	0.11884	6.5	49	13	0.09691

No.	Geopolymer	CAC content, %	CNC content, %	Fly ash content, %	Silica fume content, %	Nano-silica content, %	Wet-dry cycle	Ratio of sample surface to acid volume	pH	Time, day	Acid addition times	Mass change, %
89	0	0	0	0.2	0	0	7	0.11884	6.5	49	13	0.16155
90	0	0	0	0.3	0	0	7	0.11884	6.5	49	13	0.35276
91	0	0	0	0	0	0	9	0.26201	6.5	63	15	0.33559
92	0	0	0	0.05	0	0	9	0.11884	6.5	63	15	0.09209
93	0	0	0	0.1	0	0	9	0.11884	6.5	63	15	0.17407
94	0	0	0	0.2	0	0	9	0.11884	6.5	63	15	0.21342
95	0	0	0	0.3	0	0	9	0.11884	6.5	63	15	0.38666
96	0	0	0	0	0	0	11	0.26201	6.5	77	17	0.41738
97	0	0	0	0.05	0	0	11	0.11884	6.5	77	17	0.26232
98	0	0	0	0.1	0	0	11	0.11884	6.5	77	17	0.34856
99	0	0	0	0.2	0	0	11	0.11884	6.5	77	17	0.37263
100	0	0	0	0.3	0	0	11	0.11884	6.5	77	17	0.5735
101	0	0	0	0	0	0	13	0.26201	6.5	91	19	0.46222
102	0	0	0	0.05	0	0	13	0.11884	6.5	91	19	0.26519
103	0	0	0	0.1	0	0	13	0.11884	6.5	91	19	0.30249
104	0	0	0	0.2	0	0	13	0.11884	6.5	91	19	0.35743
105	0	0	0	0.3	0	0	13	0.11884	6.5	91	19	0.59122
106	0	0	0	0	0	0	3	0.26201	4.5	21	9	0.27103
107	0	0	0	0.05	0	0	3	0.26201	4.5	21	9	0.38128
108	0	0	0	0.1	0	0	3	0.26201	4.5	21	9	0.32278
109	0	0	0	0.2	0	0	3	0.26201	4.5	21	9	0.26424
110	0	0	0	0.3	0	0	3	0.26201	4.5	21	9	0.28369
111	0	0	0	0	0	0	5	0.26201	4.5	35	11	0.31698

No.	Geopolymer	CAC content, %	CNC content, %	Fly ash content, %	Silica fume content, %	Nano-silica content, %	Wet-dry cycle	Ratio of sample surface to acid volume	pH	Time, day	Acid addition times	Mass change, %
112	0	0	0	0.05	0	0	5	0.26201	4.5	35	11	0.41658
113	0	0	0	0.1	0	0	5	0.26201	4.5	35	11	0.35734
114	0	0	0	0.2	0	0	5	0.26201	4.5	35	11	0.30298
115	0	0	0	0.3	0	0	5	0.26201	4.5	35	11	0.30785
116	0	0	0	0	0	0	7	0.26201	4.5	49	13	0.34969
117	0	0	0	0.05	0	0	7	0.26201	4.5	49	13	0.44011
118	0	0	0	0.1	0	0	7	0.26201	4.5	49	13	0.39975
119	0	0	0	0.2	0	0	7	0.26201	4.5	49	13	0.35645
120	0	0	0	0.3	0	0	7	0.26201	4.5	49	13	0.36631
121	0	0	0	0	0	0	9	0.26201	4.5	63	15	0.30296
122	0	0	0	0.05	0	0	9	0.26201	4.5	63	15	0.38598
123	0	0	0	0.1	0	0	9	0.26201	4.5	63	15	0.36676
124	0	0	0	0.2	0	0	9	0.26201	4.5	63	15	0.32855
125	0	0	0	0.3	0	0	9	0.26201	4.5	63	15	0.33669
126	0	0	0	0	0	0	3	0.20315	1.5	21	9	-0.5533
127	0	0	0	0.05	0	0	3	0.20315	1.5	21	9	-0.3738
128	0	0	0	0.1	0	0	3	0.20315	1.5	21	9	-0.3099
129	0	0	0	0.2	0	0	3	0.20315	1.5	21	9	-0.1759
130	0	0	0	0.3	0	0	3	0.20315	1.5	21	9	-0.2159
131	0	0	0	0	0	0	5	0.20315	1.5	35	11	-0.9122
132	0	0	0	0.05	0	0	5	0.20315	1.5	35	11	-0.7253
133	0	0	0	0.1	0	0	5	0.20315	1.5	35	11	-0.682
134	0	0	0	0.2	0	0	5	0.20315	1.5	35	11	-0.479

No.	Geopolymer	CAC content, %	CNC content, %	Fly ash content, %	Silica fume content, %	Nano-silica content, %	Wet-dry cycle	Ratio of sample surface to acid volume	pH	Time, day	Acid addition times	Mass change, %
135	0	0	0	0.3	0	0	5	0.20315	1.5	35	11	-0.5769
136	0	0	0	0	0	0	7	0.20315	1.5	49	13	-1.4083
137	0	0	0	0.05	0	0	7	0.20315	1.5	49	13	-1.2875
138	0	0	0	0.1	0	0	7	0.20315	1.5	49	13	-1.2122
139	0	0	0	0.2	0	0	7	0.20315	1.5	49	13	-1.1345
140	0	0	0	0.3	0	0	7	0.20315	1.5	49	13	-1.292
141	0	0	0	0	0	0	9	0.20315	1.5	63	15	-2.04
142	0	0	0	0.05	0	0	9	0.20315	1.5	63	15	-2.0228
143	0	0	0	0.1	0	0	9	0.20315	1.5	63	15	-1.9103
144	0	0	0	0.2	0	0	9	0.20315	1.5	63	15	-1.9081
145	0	0	0	0.3	0	0	9	0.20315	1.5	63	15	-2.15
146	0	0	0	0	0	0	11	0.20315	1.5	77	17	-2.587
147	0	0	0	0.05	0	0	11	0.20315	1.5	77	17	-2.5374
148	0	0	0	0.1	0	0	11	0.20315	1.5	77	17	-2.3844
149	0	0	0	0.2	0	0	11	0.20315	1.5	77	17	-2.3771
150	0	0	0	0.3	0	0	11	0.20315	1.5	77	17	-2.7044
151	0	0	0	0	0	0	13	0.20315	1.5	91	19	-3.2374
152	0	0	0	0.05	0	0	13	0.20315	1.5	91	19	-3.1527
153	0	0	0	0.1	0	0	13	0.20315	1.5	91	19	-3.1508
154	0	0	0	0.2	0	0	13	0.20315	1.5	91	19	-3.1221
155	0	0	0	0.3	0	0	13	0.20315	1.5	91	19	-3.439
156	0	0	0	0.05	0	0	5	0.56589	1.5	88	6	-1.0577
157	0	0	0	0.1	0	0	5	0.56589	1.5	88	6	-0.942

No.	Geopolymer	CAC content, %	CNC content, %	Fly ash content, %	Silica fume content, %	Nano-silica content, %	Wet-dry cycle	Ratio of sample surface to acid volume	pH	Time, day	Acid addition times	Mass change, %
158	0	0	0	0.2	0	0	5	0.56589	1.5	88	6	-0.6972
159	0	0	0	0.3	0	0	5	0.56589	1.5	88	6	-0.6624
160	0	0	0	0	0	0	12	0.37726	2	42	12	-2.5307
161	0	0	0	0.05	0	0	12	0.37726	2	42	12	-2.4511
162	0	0	0	0.1	0	0	12	0.37726	2	42	12	-2.3659
163	0	0	0	0.2	0	0	12	0.37726	2	42	12	-2.2051
164	0	0	0	0.3	0	0	12	0.37726	2	42	12	-2.2578
165	0	0	0	0	0	0	12	0.45271	2	42	16	-3.2676
166	0	0	0	0.05	0	0	12	0.45271	2	42	16	-3.2237
167	0	0	0	0.1	0	0	12	0.45271	2	42	16	-3.1584
168	0	0	0	0.2	0	0	12	0.45271	2	42	16	-3.9983
169	0	0	0	0.3	0	0	12	0.45271	2	42	16	-3.925
170	0	0	0	0	0	0	1	0.2	2	15	3	0.045527
171	0	0	0	0	5	0	1	0.2	2	15	3	0.269511
172	0	0	0	0	10	0	1	0.2	2	15	3	0.143923
173	0	0	0	0	15	0	1	0.2	2	15	3	0.074145
174	0	0	0	0	0	0	2	0.2	2	30	6	0.412122
175	0	0	0	0	5	0	2	0.2	2	30	6	0.890305
176	0	0	0	0	10	0	2	0.2	2	30	6	0.678828
177	0	0	0	0	15	0	2	0.2	2	30	6	0.613871
178	0	0	0	0	0	0	3	0.2	2	45	9	0.852683
179	0	0	0	0	5	0	3	0.2	2	45	9	1.120376
180	0	0	0	0	10	0	3	0.2	2	45	9	0.879956

No.	Geopolymer	CAC content, %	CNC content, %	Fly ash content, %	Silica fume content, %	Nano-silica content, %	Wet-dry cycle	Ratio of sample surface to acid volume	pH	Time, day	Acid addition times	Mass change, %
181	0	0	0	0	15	0	3	0.2	2	45	9	0.762704
182	0	0	0	0	0	0	4	0.2	2	60	12	1.095098
183	0	0	0	0	5	0	4	0.2	2	60	12	1.411189
184	0	0	0	0	10	0	4	0.2	2	60	12	1.079022
185	0	0	0	0	15	0	4	0.2	2	60	12	0.943931
186	0	0	0	0	0	0	5	0.2	2	75	15	1.383422
187	0	0	0	0	5	0	5	0.2	2	75	15	1.565084
188	0	0	0	0	10	0	5	0.2	2	75	15	1.254122
189	0	0	0	0	15	0	5	0.2	2	75	15	1.124421
190	0	0	0	0	0	0.5	1	0.2	2	15	3	-0.29905
191	0	0	0	0	0	1	1	0.2	2	15	3	-0.30833
192	0	0	0	0	0	1.5	1	0.2	2	15	3	-0.17926
193	0	0	0	0	0	2	1	0.2	2	15	3	-0.14352
194	0	0	0	0	0	0.5	2	0.2	2	30	6	0.23217
195	0	0	0	0	0	1	2	0.2	2	30	6	0.2363
196	0	0	0	0	0	1.5	2	0.2	2	30	6	0.386271
197	0	0	0	0	0	2	2	0.2	2	30	6	0.422751
198	0	0	0	0	0	0.5	3	0.2	2	45	9	0.247531
199	0	0	0	0	0	1	3	0.2	2	45	9	0.288615
200	0	0	0	0	0	1.5	3	0.2	2	45	9	0.41071
201	0	0	0	0	0	2	3	0.2	2	45	9	0.476811
202	0	0	0	0	0	0.5	4	0.2	2	60	12	0.487964
203	0	0	0	0	0	1	4	0.2	2	60	12	0.528827

No.	Geopolymer	CAC content, %	CNC content, %	Fly ash content, %	Silica fume content, %	Nano-silica content, %	Wet-dry cycle	Ratio of sample surface to acid volume	pH	Time, day	Acid addition times	Mass change, %
204	0	0	0	0	0	1.5	4	0.2	2	60	12	0.642186
205	0	0	0	0	0	2	4	0.2	2	60	12	0.707662
206	0	0	0	0	0	0.5	5	0.2	2	75	15	0.835087
207	0	0	0	0	0	1	5	0.2	2	75	15	0.858344
208	0	0	0	0	0	1.5	5	0.2	2	75	15	0.983625
209	0	0	0	0	0	2	5	0.2	2	75	15	1.163166
210	0	0	0.2	0	0	0	1	0.2	2	15	3	0.234216
211	0	0	0.4	0	0	0	1	0.2	2	15	3	0.241877
212	0	0	1	0	0	0	1	0.2	2	15	3	0.469661
213	0	0	1.5	0	0	0	1	0.2	2	15	3	0.353606
214	0	0	0.2	0	0	0	2	0.2	2	30	6	0.828925
215	0	0	0.4	0	0	0	2	0.2	2	30	6	0.861564
216	0	0	1	0	0	0	2	0.2	2	30	6	1.142945
217	0	0	1.5	0	0	0	2	0.2	2	30	6	1.128832
218	0	0	0.2	0	0	0	3	0.2	2	45	9	1.095936
219	0	0	0.4	0	0	0	3	0.2	2	45	9	1.105681
220	0	0	1	0	0	0	3	0.2	2	45	9	1.394154
221	0	0	1.5	0	0	0	3	0.2	2	45	9	1.352532
222	0	0	0.2	0	0	0	4	0.2	2	60	12	1.357651
223	0	0	0.4	0	0	0	4	0.2	2	60	12	1.433145
224	0	0	1	0	0	0	4	0.2	2	60	12	1.739422
225	0	0	1.5	0	0	0	4	0.2	2	60	12	1.706603
226	0	0	0.2	0	0	0	5	0.2	2	75	15	1.576877

No.	Geopolymer	CAC content, %	CNC content, %	Fly ash content, %	Silica fume content, %	Nano-silica content, %	Wet-dry cycle	Ratio of sample surface to acid volume	pH	Time, day	Acid addition times	Mass change, %
227	0	0	0.4	0	0	0	5	0.2	2	75	15	1.650978
228	0	0	1	0	0	0	5	0.2	2	75	15	1.946807
229	0	0	1.5	0	0	0	5	0.2	2	75	15	1.911857
230	1	0	0	0	0	0	1	0.2	2	15	3	-5.15793
231	1	5	0	0	0	5	1	0.2	2	15	3	-4.05466
232	1	10	0	0	0	10	1	0.2	2	15	3	-3.94767
233	1	0	0	0	0	0	2	0.2	2	30	6	-7.68951
234	1	5	0	0	0	5	2	0.2	2	30	6	-6.68887
235	1	10	0	0	0	10	2	0.2	2	30	6	-6.10086
236	1	0	0	0	0	0	3	0.2	2	45	9	-10.9064
237	1	5	0	0	0	5	3	0.2	2	45	9	-8.89984
238	1	10	0	0	0	10	3	0.2	2	45	9	-8.27919
239	1	0	0	0	0	0	4	0.2	2	60	12	-13.1844
240	1	5	0	0	0	5	4	0.2	2	60	12	-10.8488
241	1	10	0	0	0	10	4	0.2	2	60	12	-10.3624
242	1	0	0	0	0	0	5	0.2	2	75	15	-13.8722
243	1	5	0	0	0	5	5	0.2	2	75	15	-11.457
244	1	10	0	0	0	10	5	0.2	2	75	15	-10.8559

Appendix 2. Data of UCS used for SVR modeling

No.	Geopolymer	CAC content, %	CNC content, %	Silica fume content, %	Nano-silica content, %	Fly ash content, %	Wet-dry cycle	Time, day	Acid addition times	Ratio of sample surface to acid volume	Initial UCS	pH	UCS
1	0	0	0	0	0	0	2	7	6	0.11884	28.6369	1.5	29.9134
2	0	0	0	0	0	0.05	2	7	6	0.11884	21.0106	1.5	31.1338
3	0	0	0	0	0	0.1	2	7	6	0.11884	20.8408	1.5	27.3461
4	0	0	0	0	0	0.2	2	7	6	0.11884	21.6815	1.5	23.4225
5	0	0	0	0	0	0.3	2	7	6	0.11884	15.8302	1.5	19.448
6	0	0	0	0	0	0	4	21	9	0.26201	28.6369	1.5	27.8556
7	0	0	0	0	0	0.05	4	21	9	0.11884	21.0106	1.5	29.905
8	0	0	0	0	0	0.1	4	21	9	0.11884	20.8408	1.5	25.9703
9	0	0	0	0	0	0.2	4	21	9	0.11884	21.6815	1.5	24
10	0	0	0	0	0	0.3	4	21	9	0.11884	15.8302	1.5	26.0722
11	0	0	0	0	0	0	9	56	14	0.26201	28.6369	1.5	31.2357
12	0	0	0	0	0	0.05	9	56	14	0.26201	21.0106	1.5	30.9469
13	0	0	0	0	0	0.1	9	56	14	0.26201	20.8408	1.5	33.3649
14	0	0	0	0	0	0.2	9	56	14	0.26201	21.6815	1.5	33.8344
15	0	0	0	0	0	0.3	9	56	14	0.26201	15.8302	1.5	31.3455
16	0	0	0	0	0	0	14	91	19	0.20315	28.6369	1.5	29.1975
17	0	0	0	0	0	0.05	14	91	19	0.20315	21.0106	1.5	28.5011
18	0	0	0	0	0	0.1	14	91	19	0.20315	20.8408	1.5	25.5541
19	0	0	0	0	0	0.2	14	91	19	0.20315	21.6815	1.5	23.2612
20	0	0	0	0	0	0.3	14	91	19	0.20315	15.8302	1.5	17.421
21	0	0	0	0	0	0	2	7	6	0.26201	28.6369	3	31.5244

No.	Geopolymer	CAC content, %	CNC content, %	Silica fume content, %	Nano-silica content, %	Fly ash content, %	Wet-dry cycle	Time, day	Acid addition times	Ratio of sample surface to acid volume	Initial UCS	pH	UCS
22	0	0	0	0	0	0.05	2	7	6	0.11884	21.0106	3	29.1465
23	0	0	0	0	0	0.1	2	7	6	0.11884	20.8408	3	27.6836
24	0	0	0	0	0	0.2	2	7	6	0.11884	21.6815	3	22.896
25	0	0	0	0	0	0.3	2	7	6	0.11884	15.8302	3	19.9406
26	0	0	0	0	0	0	4	21	9	0.26201	28.6369	3	31.7282
27	0	0	0	0	0	0.05	4	21	9	0.11884	21.0106	3	32.4586
28	0	0	0	0	0	0.1	4	21	9	0.11884	20.8408	3	29.0276
29	0	0	0	0	0	0.2	4	21	9	0.11884	21.6815	3	28.5128
30	0	0	0	0	0	0.3	4	21	9	0.11884	15.8302	3	27.1338
31	0	0	0	0	0	0	9	56	14	0.26201	28.6369	3	33.1432
32	0	0	0	0	0	0.05	9	56	14	0.11884	21.0106	3	32.4926
33	0	0	0	0	0	0.1	9	56	14	0.11884	20.8408	3	34.1571
34	0	0	0	0	0	0.2	9	56	14	0.11884	21.6815	3	33.7155
35	0	0	0	0	0	0.3	9	56	14	0.11884	15.8302	3	33.2059
36	0	0	0	0	0	0	14	91	19	0.26201	28.6369	3	34.4459
37	0	0	0	0	0	0.05	14	91	19	0.11884	21.0106	3	35.3291
38	0	0	0	0	0	0.1	14	91	19	0.11884	20.8408	3	36.8238
39	0	0	0	0	0	0.2	14	91	19	0.11884	21.6815	3	32.6115
40	0	0	0	0	0	0.3	14	91	19	0.11884	15.8302	3	23.414
41	0	0	0	0	0	0	2	7	6	0.26201	28.6369	6.5	29.3758
42	0	0	0	0	0	0.05	2	7	6	0.11884	21.0106	6.5	25.189
43	0	0	0	0	0	0.1	2	7	6	0.11884	20.8408	6.5	23.9321
44	0	0	0	0	0	0.2	2	7	6	0.11884	21.6815	6.5	21.5202

No.	Geopolymer	CAC content, %	CNC content, %	Silica fume content, %	Nano-silica content, %	Fly ash content, %	Wet-dry cycle	Time, day	Acid addition times	Ratio of sample surface to acid volume	Initial UCS	pH	UCS
45	0	0	0	0	0	0.3	2	7	6	0.11884	15.8302	6.5	18.8705
46	0	0	0	0	0	0	4	21	9	0.26201	28.6369	6.5	30.7261
47	0	0	0	0	0	0.05	4	21	9	0.11884	21.0106	6.5	27.414
48	0	0	0	0	0	0.1	4	21	9	0.11884	20.8408	6.5	27.3434
49	0	0	0	0	0	0.2	4	21	9	0.11884	21.6815	6.5	25.7155
50	0	0	0	0	0	0.3	4	21	9	0.11884	15.8302	6.5	23.1507
51	0	0	0	0	0	0	9	56	14	0.26201	28.6369	6.5	33.5032
52	0	0	0	0	0	0.05	9	56	14	0.26201	21.0106	6.5	28.1444
53	0	0	0	0	0	0.1	9	56	14	0.26201	20.8408	6.5	30.0565
54	0	0	0	0	0	0.2	9	56	14	0.26201	21.6815	6.5	31.1592
55	0	0	0	0	0	0.3	9	56	14	0.26201	15.8302	6.5	32.9851
56	0	0	0	0	0	0	14	91	19	0.26201	28.6369	6.5	35.5862
57	0	0	0	0	0	0.05	14	91	19	0.11884	21.0106	6.5	32.7643
58	0	0	0	0	0	0.1	14	91	19	0.11884	20.8408	6.5	35.2866
59	0	0	0	0	0	0.2	14	91	19	0.11884	21.6815	6.5	33.0446
60	0	0	0	0	0	0.3	14	91	19	0.11884	15.8302	6.5	31.3885
61	0	0	0	0	0	0	14	91	19	0.26201	28.6369	4.5	34.8365
62	0	0	0	0	0	0.05	14	91	19	0.26201	21.0106	4.5	36.3822
63	0	0	0	0	0	0.1	14	91	19	0.26201	20.8408	4.5	35.465
64	0	0	0	0	0	0.2	14	91	19	0.26201	21.6815	4.5	39.1083
65	0	0	0	0	0	0.3	14	91	19	0.26201	15.8302	4.5	34.5478
66	0	0	0	0	0	0.05	5	88	6	0.56589	21.6111	1.5	38.1496
67	0	0	0	0	0	0.1	5	88	6	0.56589	21.2376	1.5	39.6024

No.	Geopolymer	CAC content, %	CNC content, %	Silica fume content, %	Nano-silica content, %	Fly ash content, %	Wet-dry cycle	Time, day	Acid addition times	Ratio of sample surface to acid volume	Initial UCS	pH	UCS
68	0	0	0	0	0	0.2	5	88	6	0.56589	22.426	1.5	41.1004
69	0	0	0	0	0	0.3	5	88	6	0.56589	20.3209	1.5	41.797
70	0	0	0	0	0	0	12	42	12	0.37726	28.6369	2	34.6404
71	0	0	0	0	0	0.05	12	42	12	0.37726	21.0106	2	39.9346
72	0	0	0	0	0	0.1	12	42	12	0.37726	20.8408	2	41.314
73	0	0	0	0	0	0.2	12	42	12	0.37726	21.6815	2	42.7581
74	0	0	0	0	0	0.3	12	42	12	0.37726	15.8302	2	40.1963
75	0	0	0	0	0	0	12	42	16	0.45271	28.6369	2	36.3851
76	0	0	0	0	0	0.05	12	42	16	0.45271	21.0106	2	42.6512
77	0	0	0	0	0	0.1	12	42	16	0.45271	20.8408	2	44.442
78	0	0	0	0	0	0.2	12	42	16	0.45271	21.6815	2	46.6266
79	0	0	0	0	0	0.3	12	42	16	0.45271	15.8302	2	44.3555
80	1	0	0	0	0	0	5	75	15	0.2	56.5080	2	19.4047
81	1	5	0	0	0	0	5	75	15	0.2	47.3659	2	35.1424
82	1	10	0	0	0	0	5	75	15	0.2	40.4647	2	30.9661
83	0	0	0.2	0	0	0	5	75	15	0.2	38.3765	2	43.8516
84	0	0	0.4	0	0	0	5	75	15	0.2	43.5460	2	46.5000
85	0	0	1	0	0	0	5	75	15	0.2	42.9094	2	41.6107
86	0	0	1.5	0	0	0	5	75	15	0.2	43.0877	2	41.4324
87	0	0	0	5	0	0	5	75	15	0.2	44.5647	2	41.0759
88	0	0	0	10	0	0	5	75	15	0.2	52.6627	2	46.4746
89	0	0	0	15	0	0	5	75	15	0.2	48.8938	2	40.3119
90	0	0	0	0	0.5	0	5	75	15	0.2	36.8741	2	41.8398

No.	Geopolymer	CAC content, %	CNC content, %	Silica fume content, %	Nano-silica content, %	Fly ash content, %	Wet-dry cycle	Time, day	Acid addition times	Ratio of sample surface to acid volume	Initial UCS	pH	UCS
91	0	0	0	0	1	0	5	75	15	0.2	40.1591	2	42.0181
92	0	0	0	0	1.5	0	5	75	15	0.2	37.6380	2	41.7634
93	0	0	0	0	2	0	5	75	15	0.2	35.5244	2	40.3883

Appendix 3 Matlab codes for SVR modeling

Main function of SVR modeling

```
clc;
clear;
close all;

load ('Data.mat'); %load database
a=size(Data,1);
b=size(Data,2);

rand_num=randperm(a);
Data1=Data(rand_num,:);%randomize database

%seperate input and output data
X=Data1(:,1:b-1);
Y=Data1(:,b);

%data partition
k=5;
c=cvpartition(Y,'KFold',k);
pstart=1;
pend=0;

%define performance parameters
R2=zeros(k,1);
MAE=zeros(k,1);
RMSE=zeros(k,1);
MAPE=zeros(k,1);

%define hyperparameters of SVR
ep=zeros(k,1);
box=zeros(k,1);
kscale=zeros(k,1);

%k-fold model training and testing
for i =1:k
    %database devided into training dataset and testing dataset
    pend=pend+c.TestSize(i);
    testX=X([pstart:pend],:);
    testY(1:c.TestSize(i),i)=Y([pstart:pend],:);
    trainX=X;
    trainX([pstart:pend],:)=[];
    trainY=Y;
    trainY(pstart:pend)=[];

    %PSO optimization
    [Ep,C,ks]=PSO_5FOLD(trainX,trainY);

    %verification
    MdlStd=fitrsvm(trainX,trainY,'KernelFunction','rbf',...
       'BoxConstraint',C,'Epsilon',Ep,'KernelScale',ks,'Standardize',true); %
model training
```

```
    prdct_label(1:c.TestSize(i),i)=predict(MdlStd,testX); %prediction using
testing dataset

    %record optimal hyperparameters
    ep(i,1)=MdlStd.Epsilon;
    box(i,1)=MdlStd.BoxConstraints(1,1);
    kscale(i,1)=MdlStd.KernelParameters.Scale;

    pstart=pstart+c.TestSize(i);


end

% calculate the performance evaluation parameters
for i=1:k
mae=0;
mse=0;
mape=0;
a_teste=size(testY(:,i),1);
teste=testY(:,i);
for n=1:a_teste
    if teste(n,:)==0
        teste(n,:)=[];
    end
end

a_teste=size(teste(:,1),1);

r1=0; r2=0; r3=0; r4=0; r5=0; r6=0; r7=0;

for j=1:a_teste
    r1=r1+testY(j,i)*prdct_label(j,i);
    r2=r2+testY(j,i);
    r3=r3+prdct_label(j,i);
    r4=r4+testY(j,i)^2;
    r5=r5+testY(j,i);
    r6=r6+prdct_label(j,i)^2;
    r7=r7+prdct_label(j,i);

    mae=mae+abs(testY(j,i)-prdct_label(j,i));
    mse=mse+(testY(j,i)-prdct_label(j,i))^2;
    mape=mape+abs(testY(j,i)-prdct_label(j,i))/abs(testY(j,i));
end
MAE(i,1)=mae/a_teste;
RMSE(i,1)=mse/a_teste;
MAPE(i,1)=mape/a_teste;
R2(i,1)=(a_teste*r1-r2*r3)^2/((a_teste*r4-r5^2)*(a_teste*r6-r7^2));

end

testY_1=testY(:,1);
testY_2=testY(:,2);
testY_3=testY(:,3);
testY_4=testY(:,4);
testY_5=testY(:,5);
```

```
testpy_1=prdct_label(:,1);
testpy_2=prdct_label(:,2);
testpy_3=prdct_label(:,3);
testpy_4=prdct_label(:,4);
testpy_5=prdct_label(:,5);

i2=min(MAE);
i3=min(RMSE);
i4=min(MAPE);

a2=max(MAE);
a3=max(RMSE);
a4=max(MAPE);

m2=mean(MAE);
m3=mean(RMSE);
m4=mean(MAPE);

i1=min(R2);
a1=max(R2);
m1=mean(R2);
```

Main function for PSO optimization (modified from the codes developed by Sadegh Salesi and Georgina Cosma (Salesi & Cosma, 2017)):

```
function [Ep,C,ks]=PSO_5FOLD(X,Y) % Epsilon: nu,  BC box constraint: C,
kernel scale:sigma


nVar=3; % number of unknown variables
Varsize=[1 nVar];  %matrix size of decision variables
lb=[1e-3,1e-6,1e-5];   % lower bound of decision variables: C epsilon kernel
scale;
ub=[1e3,0.999,9.9999];  % upper bound of decision variables: C epsilon kernel
scale;

%--------------%%parameters of pso---------
maxiter=200;
popsize=20; % population size
w=1; %inertia cofficient
wdamp=0.9; %damp ratio of inertia cofficient
c1=2; %personal acceleration coefficient
c2=2;  %social acceleration coefficient

%---------------%%initialization-------------
emp.position=[];
emp.fitness=[];
emp.velocity=[];
emp.best.position=[];
emp.best.fitness=[];

%create population array
particle=repmat(emp,popsize,1);

%initialize global best
Globalbest.fitness=inf; % worst value for minimization problem

%%for j=1:a_test
%initialize population members
  for i=1:popsize
    %generate random solution
    particle(i).position=lb+rand(1,nVar).*(ub-lb);

    %initialize velocity
    particle(i).velocity=zeros(Varsize);

    % evaluation
    [particle(i).fitness]=SVR_5FOLD(X,Y,particle(i).position);

    %update the personal best
    particle(i).best.position=particle(i).position;
    particle(i).best.fitness=particle(i).fitness;

    %update global best
```

```
    if particle(i).best.fitness<Globalbest.fitness
       Globalbest=particle(i).best;
    end

  end

%array to hold best fitness value on each iteration
Bestfitness=zeros(maxiter,1);

%-----------------%main loop of pso-----------------


  for it=1:maxiter

    for i=1:popsize

        %update velocity
        particle(i).velocity=w*particle(i).velocity...
            +c1*rand(Varsize).*(particle(i).best.position-
particle(i).position)...
            +c2*rand(Varsize).*(Globalbest.position-particle(i).position);

        %update position
        particle(i).velocity=min(particle(i).velocity,0.01);
        particle(i).velocity=max(particle(i).velocity,-0.01);

        particle(i).position=particle(i).position+particle(i).velocity;

        if particle(i).position(2)<0
            break;
        end

        %evaluation
        particle(i).fitness=SVR_5FOLD(X,Y,particle(i).position);

        %update personal best
        if particle(i).fitness<particle(i).best.fitness
            particle(i).best.position=particle(i).position;
            particle(i).best.fitness=particle(i).fitness;

                %update global best
                if particle(i).best.fitness<Globalbest.fitness
                    Globalbest=particle(i).best;
                end

        end

    end

    %store the best fitness value
    Bestfitness(it)=Globalbest.fitness;

    %display iteration information
```

```
    disp(['Iteration' num2str(it) ':best fitness='
num2str(Bestfitness(it))]);

    %damping inertia coefficient
    w=w*wdamp;

  end

%-----------%results-----------------

figure;

siz=size(Bestfitness,1);
clf;
line_fewer_markers(1:siz,Bestfitness,50,'b-o',"linewidth", 1.4,...
'MarkerSize',5)
xlabel('Number of iterations')
ylabel('Minimum Objective')
set(gca,'FontSize',12,'FontName','Times New Roman')
set(gca,'Box','on');

Ep=Globalbest.position(2);
C=Globalbest.position(1);
ks=Globalbest.position(3);

end
```

Main function of 5-fold cross validation:

```
function [fitness]=SVR_5FOLD(X,Y,Z) % Epsilon: nu,  BC box constraint: C,
kernel scale:sigma

   % parameter definition
    k=5;
    c=cvpartition(Y,'KFold',k);
    pstart=1;
    pend=0;
    MSE=zeros(1,k);

%model training and testing
  for i =1:k

    %divide database into training and testing datasets
    pend=pend+c.TestSize(i);
    testX=X([pstart:pend],:);
    testY=Y([pstart:pend],:);
    trainX=X;
    trainX([pstart:pend],:)=[];
    trainY=Y;
    trainY(pstart:pend)=[];
    model=fitrsvm(trainX,trainY,'KernelFunction','rbf',
'BoxConstraint',Z(1),'Epsilon',Z(2),'KernelScale',Z(3),'Standardize',true); %
model training
    prdct_label= predict(model,testX); %predicting with testing dataset
    %yfit=predict(model,trainX);

    pstart=pstart+c.TestSize(i);

    %calculating MSE
    a=size(testY,1);
    sum=0;
    for j=1:a
        sum=sum+(testY(j)-prdct_label(j))^2;
    end

    MSE(i)=sum/a;

  end

 fitness=mean(MSE);

end
```

Main function of artificial neural network prediction:

```
clc;
clear;
close all;

load ('Data.mat'); %load database

%seperate input data and output data
a=size(Data,1);
b=size(Data,2);
rand_num=randperm(a);
Data1=Data(rand_num,:);
X=Data1(:,1:b-1);
Y=Data1(:,b);

%data partition
k=5;
a_test=ceil(a*1/k);
c=cvpartition(Y,'KFold',k);
pstart=1;
pend=0;

%parameter definition
prdct_label=zeros(a_test,k);
testY=zeros(a_test,k);
ep=zeros(k,1);
C=zeros(k,1);
kscale=zeros(k,1);

% model training and testing
  for i =1:k

    %divide database into training and testing datasets
    pend=pend+c.TestSize(i);
    testX=X([pstart:pend],:);
    testY(1:c.TestSize(i),i)=Y([pstart:pend],:);
    trainX=X;
    trainX([pstart:pend],:)=[];
    trainY=Y;
    trainY(pstart:pend)=[];

    trainX=transpose(trainX);
    trainY=transpose(trainY);

    %neural network construction
    net = feedforwardnet(6,'trainbr');
    net=train(net,trainX,trainY);
    %view(net)
    prdct_label(1:c.TestSize(i),i)=transpose(net(transpose(testX))); %predict
with testing dataset


    pstart=pstart+c.TestSize(i);
```

```
[fit2,gof2]=fit(testY(1:c.TestSize(i),i),prdct_label(1:c.TestSize(i),i),'poly
1')

  end

%calculation of performance evaluation parameters
for i=1:k
mae=0;
mse=0;
mape=0;
a_teste=size(testY(:,i),1);
teste=testY(:,i);
for n=1:a_teste
    if teste(n,:)==0;
        teste(n,:)=[];
    end
end

a_teste=size(teste(:,1),1);

r1=0; r2=0; r3=0; r4=0; r5=0; r6=0; r7=0;

for j=1:a_teste
    r1=r1+testY(j,i)*prdct_label(j,i);
    r2=r2+testY(j,i);
    r3=r3+prdct_label(j,i);
    r4=r4+testY(j,i)^2;
    r5=r5+testY(j,i);
    r6=r6+prdct_label(j,i)^2;
    r7=r7+prdct_label(j,i);

    mae=mae+abs(testY(j,i)-prdct_label(j,i));
    mse=mse+(testY(j,i)-prdct_label(j,i))^2;
    mape=mape+abs(testY(j,i)-prdct_label(j,i))/abs(testY(j,i));
end
MAE(i,1)=mae/a_teste;
RMSE(i,1)=mse/a_teste;
MAPE(i,1)=mape/a_teste;
R2(i,1)=(a_teste*r1-r2*r3)^2/((a_teste*r4-r5^2)*(a_teste*r6-r7^2));

end


testY_1=testY(:,1);
testY_2=testY(:,2);
testY_3=testY(:,3);
testY_4=testY(:,4);
testY_5=testY(:,5);

testpy_1=prdct_label(:,1);
testpy_2=prdct_label(:,2);
testpy_3=prdct_label(:,3);
testpy_4=prdct_label(:,4);
testpy_5=prdct_label(:,5);
```

```
i2=min(MAE)
i3=min(RMSE)
i4=min(MAPE)

a2=max(MAE)
a3=max(RMSE)
a4=max(MAPE)

m2=mean(MAE)
m3=mean(RMSE)
m4=mean(MAPE)

i1=min(R2)
a1=max(R2)
m1=mean(R2)
```